# From Stable Radicals to Thermally Robust High-Spin Diradicals and Triradicals.

Chan Shu, <sup>†</sup> Zhimin Yang, <sup>,⊥</sup> and Andrzej Rajca\*

Department of Chemistry, University of Nebraska, Lincoln, Nebraska 68588-0304, USA

#### **Abstract**

Stable radicals and thermally robust high-spin di- and triradicals have emerged as important organic materials due to their promising applications in diverse fields. New fundamental properties, such as SOMO/HOMO inversion of orbital energies, are explored for the design of new stable radicals, including highly luminescent ones with good photostability. A relation with the singlet triplet energy gap in the corresponding diradicals is proposed. Thermally robust high-spin di- and triradicals, with energy gaps that are comparable to or greater than a thermal energy at room temperature, are more challenging to synthesize but more rewarding. We summarize a number of high-spin di- and triradicals, based on nitronyl nitroxides that provide a relation between the experimental pairwise exchange coupling constant J/k in the high-spin species vs. experimental hyperfine coupling constants in the corresponding monoradicals. This relation allows us to identify outliers, which may correspond to radicals where J/k is not measured with sufficient accuracy. Double helical high-spin diradicals, in which spin density is delocalized over the chiral  $\pi$ -system, have been barely explored, with the sole example of such high-spin diradical possessing alternant  $\pi$ -system with Kekulé resonance form. Finally, we discuss a high-spin diradical with electrical conductivity and derivatives of triangulene diradicals.

## **Table of Content**

- 1. Introduction
- 2. Persistent and Stable Monoradicals as Spin Centers
  - 2.1. Carbon-centered monoradicals
  - 2.2. Nitrogen-centered monoradicals
  - 2.3. Nitrogen, oxygen-, oxygen-, and nitrogen, sulfur-centered monoradicals
- 3. Radicals and Radical Ions with SOMO-HOMO Inversion (SHI)
  - 3.1. General overview
  - 3.2. Radicals and radical ions embedded in helical  $\pi$ -systems
  - 3.3. Is there a relation between the SOMO-HOMO electron energy difference (SHI) in monoradicals (ions) and singlet-triplet energy gap ( $\Delta E_{ST}$ ) in diradicals (ions)?
- 4. High-Spin Di- and Tri-Radicals
  - 4.1. Design rules for high-spin di- and polyradicals
  - 4.2. Magnetic characterization of diradicals and triradicals
    - 4.2.1. EPR spectroscopy
    - 4.2.2. SQUID magnetometry
  - 4.3. High-spin di- and triradicals based on nitronyl nitroxide (NN)
    - 4.3.1. Synthetic routes to high-spin nitronyl nitroxide-based radicals
    - 4.3.2. High-spin nitronyl nitroxide-based neutral di- and triradicals
    - 4.3.3. High-spin nitronyl nitroxide-based diradical anions
    - 4.3.4. High-spin nitronyl nitroxide-based di- and triradical cations
    - 4.3.5. The relation between the hyperfine coupling constant in monoradicals and pairwise exchange coupling constant J/k in NN-based diradicals and triradicals.
  - 4.4. High-spin diradicals with Kekulé resonance structures rule breakers?
  - 4.5. High-spin Blatter-based diradical as electrical conductor rule breaker?
  - 4.6 High-spin triangulene diradicals.

# 1. Introduction

Persistent organic radicals have been known for well over a century. While they contributed to the rich history of organic chemistry, more recently they emerged as important class of organic materials and biomaterials that are under intense investigations for a wide range of applications. Applications will of course be facilitated with emergence of not only stable radicals but also, thermally robust, with highly tunable structures. Not surprisingly, they are the subject of many recent reviews, for example, refs 7-16.

When we refer to a radical or polyradical as stable, we will start with the classic guideline given by Ingold:  $^{17}$  "The word stable should only be used to describe a radical so persistent and so unreactive to air, moisture, etc., under ambient conditions that the pure radical can be handled and stored in the lab with no more precautions than would be used for the majority of commercially available organic chemicals." We propose to augment this definition by adding designations of "thermally robust" and "thermally ultra-robust" concerning solid radicals under inert atmosphere; the "thermally ultra-robust" radicals are those with the thermogravimetric analysis (TGA) onset of decomposition temperature ( $T_d$ ) above 250 °C, and the "thermally robust" radicals are those with  $T_d$  above 150 °C, where  $T_d$  corresponds to the mass loss of 1%. TGA-based definitions of thermal robustness are especially relevant to applications of open-shell molecules as organic materials that frequently require preparation of stable thin films via evaporation (sublimation).

Ingold's definition of persistent radical is less practical;<sup>17</sup> in this review, we will refer to persistent radical as such that can be handled without significant decomposition under either inert atmosphere or on air in fluid solution at specified temperature, ideally at room temperature or above.

As mentioned above some radicals are used as biomaterials – especially in biomedicine and biophysics. Because *in vivo* or in live cells most radicals typically undergo rapid one-electron reduction by antioxidants or enzymes, persistence of the radical in this situation will be decided by rates of these

reductive processes.

We will start with an overview of selected stable or persistent monoradicals, focused on new properties and applications in biomedicine, biophysics, and organic materials (Section 2). New fundamental properties such as SOMO/HOMO inversion (SHI) of orbital energies are being uncovered and explored for the design of new stable radicals, including highly luminescent ones with good photostability. For a subset of twelve SOMO/HOMO inverted monoradicals, a relation with the singlet triplet energy gap ( $\Delta E_{ST}$ ) in the corresponding diradicals is proposed as discussed in Section 3.

Section 4 will focus on high-spin di- and triradicals. High-spin di- and triradicals, with nearly planar  $\pi$ -systems, thermal robustness, and low-spin high-spin energy gaps that are comparable to or greater than the thermal energy at room temperature, are more challenging to synthesize but they may be more rewarding. Such di- and triradicals possess relatively large populations of the high-spin states at room temperature and their properties related to paramagnetism scale with the factor of S(S+1), where the total spin quantum number S corresponds to the high-spin ground state. This implies scaling with approximately  $n^2$ , where n is the number of "unpaired" electrons, for many properties including relaxivity of MRI contrast agents, dynamic nuclear polarization (DNP), assuming that other controlling factors can be optimized too. Such di- and triradicals form interesting thin films that may be prepared via evaporation, thus facilitating their potential applications in electronics and spintronics. One example of such high–spin diradicals, so far, is a good electrical conductor – contrary to expectations. For about a dozen of high-spin di- and triradicals, based on nitronyl nitroxides, a relation between the experimental pairwise exchange coupling constant J/k (equal to the half of the singlet triplet energy gap in a diradical) in the high-spin species vs. experimental hyperfine coupling constants in the corresponding monoradicals is established. Such a relation allows us to identify outliers, which may correspond to radicals where J/k is not measured with sufficient accuracy, e.g., because of the large magnitude. Double helical (or helical) high-spin di- and polyradicals, in which spin density is delocalized over the chiral  $\pi$ -system, have been barely explored, with only one example of such highspin diradical, which also possesses alternant  $\pi$ -system with Kekulé resonance form. Finally, we discuss recent progress in studies of derivatives of triangulene and aza-triangulene diradicals with large  $\Delta E_{\rm ST}$ .

#### 2. Persistent and Stable Monoradicals as Spin Centers

Examples of notable C-, N-, O-, N,O-, and N,S-centered neutral monoradicals are described in the next three sub-sections and in Figures 1-5.

## 2.1. Carbon-centered monoradicals

We note that all radicals in Figure 1 are stabilized to some degree by delocalization and steric shielding of unpaired electron, i.e., atoms with large spin densities. The carbon-based radicals are the ones of most historical importance, and the triphenylmethyl (Gomberg's radical) is considered the first room temperature persistent organic radical; it is a seminal discovery in organic chemistry (Figure 1).  $^{1.2.6}$  The triphenylmethyl radical reacts with oxygen and under inert atmosphere, it is in equilibrium (association constant,  $K_{assoc} \approx 3 \times 10^3 \,\mathrm{M}^{-1}$  at 293 K) $^{18}$  with its C-C bonded dimer ( $\sigma$ -dimer) in solution. The correct structure for the  $\sigma$ -dimer, which was originally proposed by Jacobsen in 1905, $^{19}$  was established by NMR spectroscopy in 1978. $^{20.21}$  Substitution at the *para*-positions, leads to monomeric triarylmethyls, e.g., 4,4',4"-tris(*tert*-butylphenyl)methyl. $^{22}$  Sterically hindered derivatives of triphenylmethyl were engineered into very high-spin polyradicals, $^{23.31}$  including the first organic polymer with magnetic ordering, $^{32}$  which were found to be persistent at low temperatures in solution, while the most sterically shielded diradicals could be either isolated or handled at room temperature under inert atmosphere. $^{33.35}$ 

Chlorinated derivatives of triphenylmethyl, such as perchlorotriphenylmethyl (**PTM**)<sup>36-39</sup> or tris(2,4,6-trichlorophenyl)methyl (**TTM**),<sup>40,41</sup> are thermally ultra-robust. They show neither dimerization nor reactivity toward oxygen in both solution or solid state, and do not decompose in the

solid state until heated to ~300 °C. This extraordinary stability is associated with the steric shielding of *ortho*-chlorines. <sup>42</sup> **PTM** was used for the design of high-spin diradical and triradical. <sup>43-45</sup> Both **PTM** and **TTM**, functionalized with electron donating  $\pi$ -systems, led to the discovery of efficient doublet state light emitters, including high efficiency organic light emitting diodes (OLEDs). Because photostability of such radicals may be associated with SOMO/HOMO energy level inversion, they are discussed in more detail in Section 3.

Another class of highly persistent triarylmethyls is illustrated by the structure of Finland trityl (FT) radical and its more hydrophilic version Ox-063. 46-48 Analogous to PTM or TTM, here the persistence is attained by severe out-of-plane twisting of the ortho-substituted aryl rings. Both radicals are monomeric and persistent at ambient conditions, and especially Ox-063 and Ox-063-d<sub>24</sub> are well soluble in water, biocompatible and lacking of interactions with blood albumin. 49 Because of negligible hyperfine couplings and the g-values that are close to that of the free electron, derivatives of both FT and Ox radicals feature relatively narrow electron paramagnetic resonance (EPR) lines and possess relatively long electron spin relaxation times ( $T_{\rm m}$  and  $T_{\rm 1}$ ).<sup>50</sup> Their derivatives found applications as dynamic nuclear polarization (DNP) agents in NMR,51-54 and as oxygen and pH sensors in biomedicine,<sup>55</sup> as spin labels in biophysics, e.g., derivatives of FT or Ox-063-d<sub>24</sub> for EPR distance measurements,<sup>56-62</sup> especially at up to 150 K in cell<sup>60,61</sup> and at room temperature in vitro.<sup>56-58</sup> <sup>13</sup>Clabeled (at center C) Ox-063-d<sub>24</sub> and its derivatives possess enhanced anisotropy of the hyperfine coupling providing relatively wide EPR spectrum that is also sensitive to molecular tumbling; 63 this allows for applications such as viscosity sensors in biomedicine<sup>49</sup> and spin labels for distance measurements using widely available double electron-electron resonance (DEER) spectroscopy.<sup>62</sup>

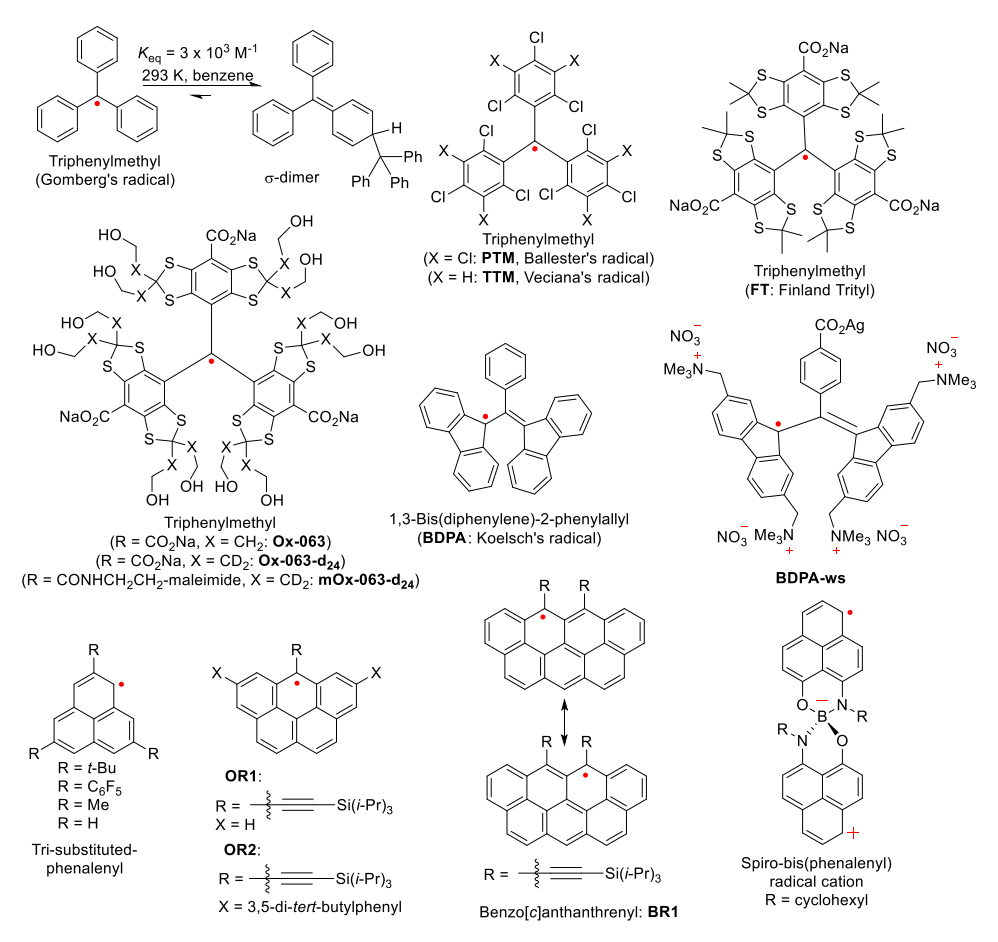


Figure 1. Examples of persistent and stable C-centered organic radicals.

Koelsch's radical, 1,3-bisdiphenylene-2-phenylallyl (BDPA), is also historically unique as it was the first carbon-based radical to display no significant reactivity toward oxygen; at the time, this was so unprecedented that the original Koelsch's manuscript was rejected in 1930's and forgotten for nearly 30 years.<sup>64</sup> Recent studies showed that BDPA and its derivatives, including TEMPO-based biradicals, are not as stable as previously thought, e.g., 5 mM BDPA decomposes in DMSO at room temperature with the initial half-life of the order of 1 day, most likely via σ-dimer formation.<sup>65</sup> For the solid BDPA, no decomposition was detected after 2 weeks under vacuum; however, under air, a half-life of the order of 10 days was found.<sup>65</sup> Nevertheless, such persistence is sufficient for the use of BDPA, including its water soluble derivative derivatives, as DNP agents in NMR.<sup>69,70</sup> Recently, more persistent water soluble derivative of BDPA, such as BDPA-ws (Figure 1) was synthesized<sup>71</sup> and studied as DNP agent.<sup>72</sup>

Phenalenyl-based radicals are fundamentally interesting and may be viewed as open-shell

graphene fragments.<sup>9,73</sup> While parent phenalenyl radical (R = H, Figure 1) exists predominantly as diamagnetic  $\sigma$ -dimer, <sup>9</sup> 2,5,8-tri-tert-butylphenalenyl radical forms a centrosymmetric  $\pi$ -dimer in the crystalline state with  $\Delta E_{\rm ST} = -4$  kcal mol<sup>-1</sup> and is reactive toward oxygen.<sup>74</sup> Based on studies by Kochi group, in dichloromethane solution,  $K_{\rm assoc} = 0.2~{\rm M}^{-1}$  at 298 K for the  $\pi$ -dimer was determined by both EPR and UV-vis-NIR spectroscopy but a much larger  $K_{\rm assoc} = 70 - 90~{\rm M}^{-1}$  at 298 K was found for  $\pi$ pimer (radical plus cation); however, enthalpy of association  $\Delta H_{\rm assoc} = -9 \text{ kcal mol}^{-1}$  for the  $\pi$ -dimer was larger than  $\Delta H_{\rm assoc} = -7$  kcal mol<sup>-1</sup> for the  $\pi$ -pimer, with a more negative  $\Delta S_{\rm assoc}$  for the  $\pi$ -dimer. In contrast, R = Me derivative formed two distinct  $\sigma$ -dimers and one  $\pi$ -dimer (all diamagnetic).<sup>77</sup> Kubo and co-workers determined that tri-substituted-phenalenyl with R = perfluorophenyl ( $C_6F_5$ ) can form either  $\sigma$ -dimer or one-dimensional  $\pi$ -stack in the crystalline state. Although, based on the X-ray structure at 10 K,  $\pi$ -stacks are relatively spin-insulated with a perfectly equidistant phenalenyl moieties with a somewhat elongated plane-to-plane distance of 3.503 Å, the magnetic susceptibility data could not be reasonably fit to a uniform 1-dimensional  $S = \frac{1}{2}$  antiferromagnetic Heisenberg chain. <sup>79</sup> DFT computations predict greater thermodynamic stability for  $\sigma$ - vs.  $\pi$ -dimers, even for derivatives of phenalenyls, for which only  $\pi$ -dimers were isolated; 80 this phenomenon may be ascribed to kinetic control of dimerization or solvent effects (vide: dicyanomethyl radicals), or inherent deficiency of DFT as outlined in ref 75.

Sterically shielded dibenzo-fused derivatives of phenalenyl **OR1** and **OR2** (Figure 1) were reported to form  $\pi$ -dimers, with  $K_{\rm assoc} = 6 - 21$  M<sup>-1</sup> (at 298 K) and  $\Delta E_{\rm ST} \approx (-2) - (-3)$  kcal mol<sup>-1</sup> in toluene. The reported  $K_{\rm assoc}$  (and underlying thermodynamic parameters, e.g.,  $\Delta H_{\rm assoc}$ ) were widely different, based on UV-vis-NIR vs. EPR spectra, in contrast to those for  $\pi$ -dimer of 2,5,8-tri-*tert*-butylphenalenyl radical reported by Kochi. Most likely these authors failed to do properly quantitative EPR spectroscopy (Section 4.2.1). These radicals may be viewed as air stable, with half-live in air saturated solutions of 7 – 34 days, and presumably, less associated than  $\sigma$ -dimer forming

Gomberg triarylmethyl. Crystalline **OR1** was an insulator with room temperature conductivity,  $\sigma_{RT} < 10^{-10} \text{ S cm}^{-1}$ , and the average intermolecular distance of 3.29 Å was found within  $\pi$ -dimer.<sup>81</sup>

Even more benzo-fused derivative of phenalenyl, i.e., benzo[c]anthanthrenyl radical derivative, **BR1** (Figure 1),<sup>82</sup> crystallized as a slipped 1D chain with equidistant average  $\pi$ – $\pi$  contacts of 3.565 Å along the stacking direction. However, fit of magnetic susceptibility data to 1-dimensional  $S = \frac{1}{2}$  antiferromagnetic Heisenberg chain was overparametrized and thus unreliable. Also, room temperature conductivity.  $\sigma_{RT} \approx 2.5 \times 10^{-9}$  S cm<sup>-1</sup>, indicated that the material was practically an insulator.<sup>82</sup>

Haddon and coworkers reported spiro-bis(phenalenyl) derivatives, which correspond to spiroconjugated radical cations (R = alkyl) and are mostly isolable as stable monomeric crystalline solids. <sup>83-86</sup> Because of formal negative charge on boron, these compounds may be viewed as "neutral" (actually zwitterionic) radicals. While the R = n-hexyl derivative was reported as the first phenalenyl-based neutral radical molecular conductor, the room temperature conductivity,  $\sigma_{RT} = 0.05$  S cm<sup>-1</sup>, was low and activation energy to the charge transfer,  $E_a = 0.13$  eV, was large. <sup>83</sup> Better optimized, in terms of crystal packing, the R = cyclohexyl derivative possessed a good electrical conductivity  $\sigma_{RT} = 0.3$  S cm<sup>-1</sup> and low charge transfer  $E_a = 0.05$  eV. <sup>84</sup> Interestingly, R = benzyl derivative forms a uniform one-dimensional  $S = \frac{1}{2}$  antiferromagnetic Heisenberg chain (J/k = -75 K), with closest C---C contacts of 3.47 and 3.58 Å along the stacking direction; the material had  $\sigma_{RT} = 1.4 \times 10^{-3}$  S cm<sup>-1</sup> with a relatively large  $E_a = 0.2$  eV. <sup>85</sup> In contrast, a benzannulated spiro-bis(phenalenyl) derivative with R = benzyl showed complex temperature dependent interconversion between σ-dimer and stacked π-chain radical in the crystals. <sup>86</sup>

Dicyanoarylmethyl radicals were initially studied as reactive intermediates. In 1966, Hartzler<sup>87</sup> reported that 1,2-diaryl-1,1,2,2-tetracycanoethane (R = H) in chloroform-d underwent rearrangement to the aromatized  $\sigma$ -dimer of dicycanoarylmethyl radical (R = H) (Figure 2), after overnight at ambient temperature. Although Hartzler could not detect EPR spectrum for the radical, including its R = NO<sub>2</sub>

derivative,<sup>87</sup> de Jongh could obtain a resolved EPR spectrum for the R = CH<sub>3</sub> radical and to determine, by NMR line broadening, the rate constant,  $k_{diss} = 20 \text{ s}^{-1}$  at 373 K, as well as the activation parameters ( $\Delta H_{act} = 26 \text{ kcal mol}^{-1}$  and  $\Delta S_{act} = +13 \text{ cal mol}^{-1} \text{ K}^{-1}$ ) for the dissociation of 1,2-diaryl-1,1,2,2-tetracycanoethane (R = CH<sub>3</sub>) into the radicals in the 353 – 393 K range (Figure 2).<sup>88</sup>

More recently multiple groups, including especially those of Winter and Seki, recognized potential of air and thermally stable dicyanoarylmethyl radicals co-existing with their  $\sigma$ -dimers and/or  $\pi$ -dimers (Figure 2). 89-100,102

Figure 2. Examples of dicyanoarylmethyl radicals.

In 2016, Seki synthesized self-assembling biradicals, in which either triphenylamine or carbazole was substituted with dicyano radicals, based on dicyanoarylmethyls. The self-assembly created cyclic oligomers which showed thermochromic and mechanochromic properties due to generation of radicals by C–C bond cleavage ( $\sigma$ -dimers). Winter measured association constants for formation of  $\sigma$ -dimers of *para*-mono-substituted dicyanophenylmethyl radicals,  $K_{assoc} = 10^5 - 10^8$  M<sup>-1</sup> and found that they decrease for electron donating substituents, giving linear Hammett plots. In 2017, Seki demonstrated the first example of dicycanoarylmethyl radical (with the julolidine skeleton) forming  $\pi$ -dimer (in toluene solution). Winter have shown that for some radicals greater solvent polarity, which is associated with increased electron spin delocalization, leads to preferential  $\pi$ -dimer formation (Figure 2). While several factors were considered to determine the mode of dimerization ( $\sigma$ - or  $\pi$ -dimer), Seki demonstrated to determine the mode of dimerization ( $\sigma$ - or  $\pi$ -dimer), Seki demonstrated to determine the mode of dimerization ( $\sigma$ - or  $\pi$ -dimer), Seki demonstrated to determine the mode of dimerization ( $\sigma$ - or  $\sigma$ -dimer), Seki demonstrated to determine the mode of dimerization ( $\sigma$ - or  $\sigma$ -dimer), Seki demonstrated to determine the mode of dimerization ( $\sigma$ - or  $\sigma$ -dimer), Seki demonstrated to determine the mode of dimerization ( $\sigma$ - or  $\sigma$ -dimer), Seki demonstrated to determine the mode of dimerization ( $\sigma$ - or  $\sigma$ -dimer), Seki demonstrated to determine the mode of dimerization ( $\sigma$ - or  $\sigma$ -dimer), Seki demonstrated to determine the mode of dimerization ( $\sigma$ - or  $\sigma$ -dimer), Seki demonstrated to determine the mode of dimerization ( $\sigma$ - or  $\sigma$ -dimer), Seki demonstrated to determine the mode of dimerization ( $\sigma$ - or  $\sigma$ -dimer), Seki demonstrated to determine the mode of dimerization ( $\sigma$ - or  $\sigma$ -dimer), Seki demonstrated to determine the mode of dimerization ( $\sigma$ - or  $\sigma$ -dimerization).

Seki studied another radical, **O2DP** (Figure 2), which possesses modified julolidine skeleton, and it forms  $\sigma$ -dimer at low temperature in toluene. Notably, the **O2DP** radical possesses a strong NIR absorption at  $\lambda_{max} = 1059$  nm, with a wide optical window in the visible region and a relatively small dimerization enthalpy,  $\Delta H_{assoc} \approx -10$  kcal mol<sup>-1</sup>.97 Winter suggested that antiaromaticity relief within planarized electron donating group of dicyanoarylmethyl radicals (e.g., analogous to **O2DP**, Figure 2) may stabilize their zwitterionic resonance form, thus leading to overall improvement in radical stability.98 In addition, Osuka and coworkers demonstrated monomeric (even at low temperatures) stable dicyanoarylmethyl radical in solution by appending dicyanomethyl radical to B<sup>III</sup>—subporphyrin.99 Finally, based on discovery of Malishewski that oxidation power of tetracyanoquinodimethane (TCNQ) can be increased dramatically by coordination of cyano groups by a strong Lewis acid such as B(C<sub>6</sub>F<sub>5</sub>)<sub>3</sub>, <sup>101</sup> the analogous coordination approach led to increased dissociation of  $\sigma$ -dimer of dicyanoarylmethyl radical, perhaps due to better stabilization of the radical by capto-dative effect. <sup>102</sup>

## 2.2. Nitrogen-centered monoradicals

Aminyl radicals have long history as reactive intermediates, <sup>103,104</sup> including in organic synthesis <sup>105,106</sup> and biochemistry. <sup>107</sup> Only 1,3,6,8-tetra-*tert*-butylcarbazyl, **TTBC** (Figure 3), and perchlorodiphenylaminyl are historically known to be persistent at ambient conditions. <sup>108,109</sup> More recently, alkyl-aryl and diaryl aminyl radicals were employed as building blocks for high-spin di-, tri-, and tetraradicals with low- and high-spin energy gaps of up to about 10 kcal mol<sup>-1</sup> and with half-lives of up to 6 h at room temperature in a fluid 2-methyltetrahydrofuran solutions; <sup>110-115</sup> also, highly resonance stabilized and sterically shielded high-spin aminyl triradical was reported by Shimizu and Osuka. <sup>116</sup> Derivatives of carbazole radical cations were also incorporated into polymers, for which triplet ground states were detected. <sup>117</sup>

PEGylated derivatives of TTBC were reported. 118,119 At 295 K in acetone, PEGC (Figure 3) has

a half-life,  $\tau_{1/2} = 48$  s, compared to  $\tau_{1/2} = 2.3$  h for its octa-deuterated isotopomer, which corresponds to an extraordinary large kinetic isotopic effect,  $k_{\rm H}/k_{\rm D} \approx 150$  at room temperature. While large values of  $k_{\rm H}/k_{\rm D}$  and unusual activation parameters are consistent with quantum mechanical tunneling, the Arrhenius and Eyring plots are linear over a wide temperature range of 116 K. Notably, constitutional isomer of **PEGC**, in which positions of *tert*-alkyl substituents are inverted, is much more persistent with  $\tau_{1/2} = 49$  h in acetone at 295 K. 119

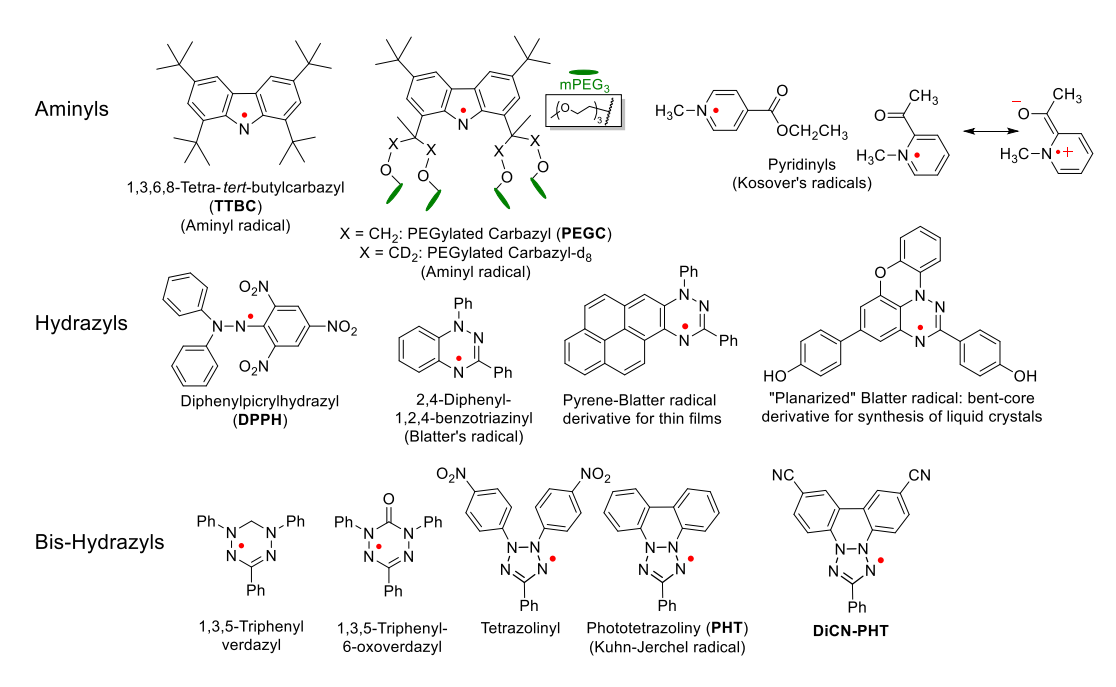


Figure 3. Examples of persistent and stable N-centered radicals.

Pyridinyl radicals were discovered by Kosower and co-workers in 1960's. <sup>120-122</sup> Their unusual persistence at room temperature (under inert atmosphere) is associated with a favorable zwitterionic resonance form (Figure 3). Both pyridinyls in Figure 3 are about 95% monomeric at room temperature and in equilibria with their σ-dimers; they can be purified by distillation under vacuum. <sup>122</sup> In addition, 2,4,6-triphenyl-substituted pyridinyl radical was demonstrated to be monomeric; <sup>123</sup> Kubo, Matsumoto, and co-workers used 2,6-diphenyl pyridinyl as building block for high-spin diradical, persistent at room temperature. <sup>124</sup>

Hydrazyl-based radicals, [R<sub>2</sub>NNR]\* (R = aryl) are typically persistent at ambient conditions. For example, **DPPH** is commonly used as an EPR reference; it possesses a good stability, as it is

monomeric and stable in the solid state on air, and can be heated to ~80 °C in solution before decomposing. DPPH is practically an insulator with single crystal conductivity,  $\sigma_{RT} \approx 10^{-10} \text{ S}$  cm<sup>-1</sup> at room temperature ( $E_a = 1.5 \text{ eV}$ ). We note that thin films of DPPH, prepared by sublimation under vacuum ( $p = 10^{-6}$  Torr), are very air-sensitive. 127

Annulated hydrazyls such as Blatter's radical<sup>129</sup> possess even better stability due to enforced orbital overlap leading to enhanced resonance stabilization. For instance, a derivative of Blatter's radical can be refluxed in chlorobenzene (bp 131 °C) without decomposition and can be heated in the solid phase to ~270 °C before decomposition begins. <sup>130</sup> Numerous derivatives of Blatter's radical have been recently prepared and their interesting properties studied; <sup>131-146</sup> this includes DNP agents for NMR spectroscopy, <sup>136</sup> the magnetically ordered thin film of Pyrene-Blatter on SiO<sub>2</sub>/Si substrate that is stable at ambient conditions, <sup>137-140</sup> self-assembled films of Blatter radical on Au, <sup>141</sup> paramagnetic liquid crystals of "planarized" Blatter, <sup>142,143</sup> batteries, <sup>144</sup> and potential molecular qubits. <sup>145,146</sup>

Derivatives of Blatter radical are important building blocks for thermally robust and ultra-robust high-spin di- and triradicals (Sections 4.3 and 4.5). 147-150

Bishydrazyl radicals,<sup>151</sup> such as verdazyl and 6-oxoverdazyl, are also extraordinarily stable because their spin density can delocalize over two hydrazyl moieties. Carbazole substituted derivative of verdazyl was found to be luminescent with quantum yield of fluorescence at room temperature of about 8%.<sup>152</sup> Derivatives of 1,3,5-triphenyl-6-oxoverdazyls were used as building blocks for thermally robust high-spin di- and triradicals; however, their low-spin high-spin energy gaps were rather low (Section 4.3).<sup>153,154</sup>

Another family of bishydrazyl radicals,<sup>151</sup> such as tetrazolinyl<sup>155</sup> and Kuhn-Jerchel radical (phototetrazolinyl, **PHT**), have a long history<sup>156-158</sup> but their thermal robustness and other properties were explored only recently.<sup>159-161</sup> For example, dicyano-substituted derivative of phototetrazolinyl (**DiCN-PHT**) is found to be stable under inert atmosphere up to 260+ °C (polycrystalline) and, in

benzene solution at room temperature, its estimated half-life is a few months. <sup>161</sup> In polycrystalline **DiCN-PHT**, uniform one-dimensional  $S = \frac{1}{2}$  antiferromagnetic Heisenberg chains (J/k = -22 K) are formed. <sup>161</sup> Upon controlled evaporation on SiO<sub>2</sub>/Si substrate under ultra-high vacuum, <sup>139</sup> **DiCN-PHT** forms nanoneedle assemblies. <sup>161</sup> The stability of this planar radical is unusual because of relatively large spin densities at the *ortho*- (and *para*-) positions with respect to the nitrogens of the tetrazolinyl moiety, as indicated by hyperfine coupling constant,  $A(^{1}H) = 5.8$  MHz, which is greater by a factor of 3 than that in 1,3,5-triphenyl-6-oxoverdazyl radical (Section 4.3). <sup>161</sup>

## 2.3. Nitrogen, oxygen-, and nitrogen, sulfur-centered monoradicals

Piperidine nitroxides, such as 2,2,6,6-tetramethylpiperidine-1-oxyl (TEMPO) or 4-hydroxy-TEMPO (TEMPOL), are well-known stable organic radicals, which were pioneered by Rosantzev (Figure 4). 162,163 Various TEMPO derivatives are heavily utilized in various applications, such as oxidation catalysts in organic synthesis, 164 polymerization mediators, 164 and DNP agents for NMR spectroscopy. 166,167 TEMPOL (and its derivatives) was explored for multiple biomedical applications, based on its ability to modify oxidative stress and report (or alter) the redox status of tissues; e.g., as reporters of redox status in cancer or as protectors against ionizing radiation, 168,169 TEMPO (and TEMPOL) derivatives, when incorporated into polymers or molecular gelators, are important components of organic batteries – pioneered by Nakahara et al. 170 and developed by Nishide and coworkers. 171-174

Although crystalline TEMPOL is an insulator with conductivity,  $\sigma_{RT} \approx 10^{-11} \text{ S cm}^{-1}$  at room temperature, in the molten state (neat liquid), its conductivity increases to  $\sigma \approx 5 \times 10^{-4} \text{ S cm}^{-1}$  at 380 K; it is not clear whether this increase is an intrinsic radical property or it occurs because of "doping" of the liquid with the products of partial decomposition of the radical at higher temperatures. We note that films of DPPH, which include some of the decomposition products, show significantly higher

conductivities, compared to single crystals.<sup>127</sup> A better defined system, such as **PTEO** – polymeric TEMPOL derivative (Figure 4), studied by Boudouris group, possesses  $\sigma_{RT} \approx 0.3$  S cm<sup>-1</sup> at room temperature – an achievement considering the nitroxides are not conjugated.<sup>176</sup>

Nitroxide radicals, including piperidine nitroxides, have important applications in biophysics as spin labels,  $^{177}$  especially for EPR distance measurements in biomolecules.  $^{178-180}$  The distance measurements, especially few-nm long, require spin labels with long electron spin coherence times  $T_{\rm m}$  of the order of a few  $\mu$ s,  $^{180}$  preferably at temperatures above 80 K. In typical *gem*-dimethyl nitroxides, onset of rotation of methyl groups on EPR time scale at T > 80 K, lowers  $T_{\rm m}$  significantly.  $^{181-183}$  To solve this problem, a number of "methyl-less" spin labels were prepared;  $^{184-188}$  for example, **Spiro-IA** enabled EPR distance measurements in immobilized proteins at room temperature  $^{187}$  and diazaadamantane derivative **IA-DZD** was used to demonstrate supramolecular approach to EPR distance measurement in proteins up to 150 K (Figure 4).  $^{188}$ 

Among pyrroline nitroxides, MTSL stands out as the most common spin label used for labeling of proteins (Figure 4).  $^{178,179,189}$  Bis-spirocyclic pyrroline nitroxides, **Spiro-Ox** and **-THF**, possess promising electron spin relaxation properties as indicated by the  $T_{\rm m}=0.71$  and  $0.50~\mu s$  (vs.  $0.34~\mu s$  for MTSL) measured at room temperature in 9:1 trehalose/sucrose matrix.  $^{190}$  Other pyrroline nitroxides, such as gem-DiCarboxy, in which the methyl groups bear a tiny fraction of spin density, show more modest values of  $T_{\rm m}$  at room temperature.  $^{190,191}$  In vitrified glycerol- $d_8$ /H<sub>2</sub>O/D<sub>2</sub>O ("DNP-juice"), a mixture of gem-DiCarboxy with triarylmethyl Ox-063 (Figure 1) led to the discovery of a truncated cross-effect (tCE) in DNP NMR.  $^{192}$  This unusual DNP effect, is very likely associated with aggregation of gem-DiCarboxy in DNP juice and/or association with Ox-063. Aggregation (and/or association) leads to very low electron spin  $T_1$  (and  $T_{\rm m}$ ) observed for 15 mM gem-DiCarboxy in DNP juice, which is more than 2 orders of magnitude lower, compared to Ox-063 in DNP juice or to 0.1 mM gem-DiCarboxy in trehalose/sucrose at similar temperature.  $^{191,192}$  Because of their electron withdrawing

groups, *gem*-DiCarboxy and a related derivative are readily reduced, including rapid reduction by ascorbate; <sup>193</sup> this is in contrast to tetraethyl pyrroline (TEP) nitroxides, which are among the most difficult to reduce nitroxide radicals. <sup>193,194</sup> Consequently, a derivative of TEP, such as **sTEO-TEP**, provided rapid and specific spin-labeling of tetrazine-amino-acid-containing proteins both *in vitro* and in live cells. Resistance of TEP to reduction enabled EPR distance measurements on native (sub-micromolar) concentrations of labeled proteins in live eukaryotic cells. <sup>195</sup>

Numerous compact profluorescent probes were designed and studied, based on covalent linking of tetramethyl isoindoline nitroxides (**TMII**) with various chromophores (Figure 4). <sup>196</sup> The stability of nitroxide and the presence of benzene ring has facilitated functionalization radicals via Pd-catalyzed and click reactions. <sup>197,198</sup> In 2000, Rassat group showed that tetraethyl isoindoline nitroxides (**TEII**) possess greatly increased resistance to reduction of radical, compared to **TMII** – the first case for the unusual effect of the *gem*-diethyl substitution. <sup>199</sup> **TEII** linked to fluorescein was an excellent agent for imaging of oxidative stress in live cells by two-photon fluorescence microscopy. <sup>200</sup> Recent studies indicated lower stability of **TEII** derivative in the presence of rat liver microsomes, compared to that for tetraethyl-derivatives of pyrrolidine (**Carboxy-TEP**) and analogous pyrroline nitroxides. <sup>201</sup>

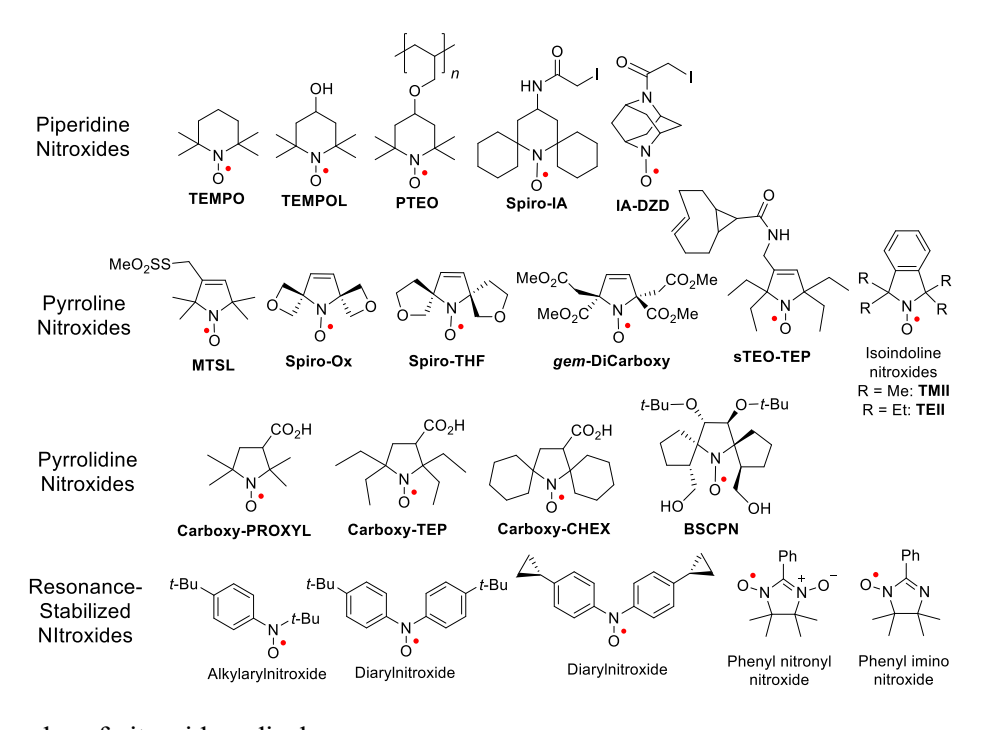


Figure 4. Examples of nitroxide radicals.

Pyrrolidine nitroxides, such as Carboxy-PROXYL and in particular tetraethyl-derivatives, are among the most difficult to reduce organic radicals.<sup>202-205</sup> For example, Carboxy-TEP (Figure 4) is slightly more resistant to reduction than C-centered radical such as Finland trityl (FT in Figure 1).<sup>205</sup> Derivatives of Carboxy-CHEX incorporated into various polymers provided organic radical contrast agents (ORCA) for MRI, with superior resistance to reduction and outstanding <sup>1</sup>H water relaxivities.<sup>206-210</sup> Although BSCPN has somewhat inferior resistance to reduction, compared to Carboxy-TEP, it provides an interesting example of a chiral, non-racemic nitroxide with bis-spirocyclic structure.<sup>211</sup>

Alkylaryl- and diarylnitroxides, together with phenyl nitronyl nitroxides and phenyl imino nitroxides (Figure 4),<sup>212,213</sup> were used as building blocks to design various high-spin di- and triradicals (Section 4.3). As di- and polyradicals, they have been also employed as model compounds to study exchange coupling and electron-spin relaxation.<sup>214-219</sup>

Interestingly, half-lives of 2 months and 1 month in benzene at room temperature for bis-cyclopropyl- and bis-*tert*-butyl-substituted diarylnitroxide were determined, respectively. Greater persistence of cyclopropyl derivative may be associated with delocalization of spin density onto the cyclopropane moiety; that spin density is likely small enough not to trigger the potential radical clock reaction.<sup>220,221</sup>

Galvinoxyl radical (Figure 5) is also a well-known stable radical that is inert to oxygen, and is representative of the phenoxyl family of radicals.<sup>222</sup>\_Galvinoxyl radicals attached as pendants to a polystyrene backbone served as the n-type redox material in memory devices<sup>223</sup> and as cathode in allorganic batteries.<sup>224</sup>

Dioxyphenalene and trioxytriangulene (Figure 5) represent more recent additions to the phenoxyl family of radicals. Dioxyphenalenes, R = H and t-Bu, were stable in the absence of air at room temperature as solids and in toluene solution. X-ray structures of  $\pi$ -dimers of dioxyphenalenes, R = t-Bu, p-BrC<sub>6</sub>H<sub>4</sub>, and p-IC<sub>6</sub>H<sub>4</sub>, show intradimer plane-to-plane distances of 3.49 – 3.55, 3.38 – 3.51,

and 3.36 – 3.43 Å, respectively. These distances are considerably longer than 3.20 – 3.32 Å in  $\pi$ -dimer of 2,5,8-tri-*tert*-butylphenalenyl (Figure 1); consequently,  $\Delta E_{\rm ST} = -0.77$  kcal mol<sup>-1</sup> for R = p-BrC<sub>6</sub>H<sub>4</sub> corresponds to considerably weaker antiferromagnetic interaction than  $\Delta E_{\rm ST} = -4$  kcal mol<sup>-1</sup> found in 2,5,8-tri-*tert*-butylphenalenyl (Section 2.1).<sup>226</sup>

Precursors to 4,8,12-trioxytriangulene radical (**TOT**) (Figure 5), may be traced to the corresponding phenol (R = H) in the classic work by  $Clar^{227}$  and to the pioneering work by Bushby in 1990's on the corresponding monoanion and triplet ground state diradical trianion (R = t-Bu). <sup>228,229</sup> In 2011, Takui group reported first derivatives of **TOT** (R = t-Bu and Br) radical and demonstrated their promising applications as electrode active materials in organic batteries; <sup>230</sup> this promise was based on outstanding stability of **TOT** derivatives (see: below) and their ability to undergo reversible 4-electron reductions (to tetraanions), providing materials with good electrical conductivity (see: below). <sup>230</sup>

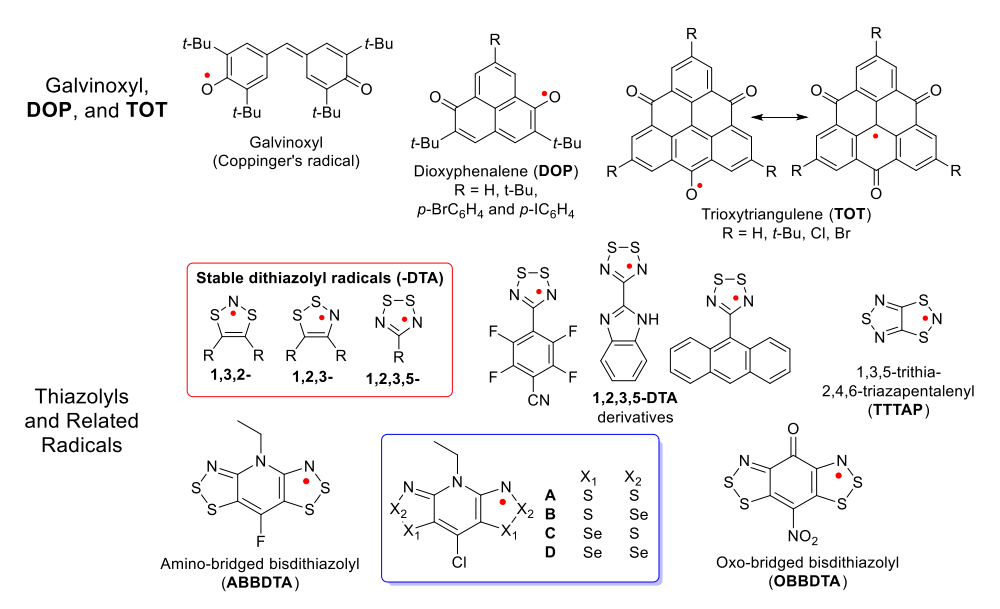


**Figure 5.** Examples of phenoxyls, thiazyls, and related radicals.

Single crystal of **TOT** (R = Br) measured along the stacking direction had  $\sigma_{RT} = 1.8 \times 10^{-3} \text{ S cm}^{-1}$  with  $E_a = 0.31 \text{ eV}$ ; this good electrical conductivity, coincided with the presence of equidistant TOT moieties (3.43 Å) within the slipped  $\pi$ -stack. The highest conductivity,  $\sigma_{RT} = 125 \text{ S cm}^{-1}$  with  $E_a = 12 \text{ meV}$ , was obtained in the combination of **TOT** (R = Cl) radical and monoanion with Li<sup>+</sup> as counterion. The crystal of this compound contained 1-D  $\pi$ -stacks with the equidistant stacking distance

In addition to various substituted TOTs,  $^{232,233}$  TOT (R = H),  $^{234}$  as well as dicyanomethylenesubstituted triangulene derivative (R = t-Bu),  $^{235}$  were prepared. For **TOT** (R = H), the onset of thermal decomposition (TGA), defined as 1% mass loss, is perhaps at about 100–150 °C, compared to >300  $^{\circ}$ C for **TOT** (R = t-Bu); similar findings were obtained by UV-vis spectral follow-up in solution saturated with air with half-lives of the radicals being ca. 18 and 56 days, respectively. 234 Moderately thick films (100 - 1000 nm) of **TOT** (R = H) were prepared by evaporation under vacuum, however, no evidence for intact radicals in the films was provided. 236 At high evaporation rates (ca. 1 nm/s), an edge-on-oriented films, in which the 1-dimensional  $\pi$ -stacks of **TOT** are parallel to the SiO<sub>2</sub>/Si or ITO glass substrates. The films showed anisotropic conductivities,  $\sigma_{RT} = 0.025$  and  $2 \times 10^{-5}$  S cm<sup>-1</sup> parallel and perpendicular to the glass substrate. Notably, single crystal sample of TOT (R = H) gave an excellent  $\sigma_{RT} = 0.32 \text{ S cm}^{-1}$  with  $E_a = 90 \text{ meV}.^{236}$  Films grown on graphite substrates provided a faceon orientation independent of deposition rate.<sup>236</sup> Such films were found to yield slightly more durable cathode materials in lithium batteries, compared to edge-on films on ITO glass.<sup>237,238</sup> More recently, electrochemical growth of conducting films of **TOT** was explored.<sup>239</sup> **TOT** (R = t-Bu) was also used as a building block for triplet ground state diradical.<sup>240</sup>

Stable dithiazolyl (**DTA**) radicals occur in three major classes,<sup>241,242</sup> as outlined in Figure 5. In particular, 1,2,3,5-**DTA** (or dithiadiazolyl) derivatives, which generally show strong propensity for dimerization,<sup>241,242</sup> provided both organic radical with the highest ordering temperature and interesting cases of magnetic bistability;.<sup>243-246</sup> that is, 4-cycanoterafluorophenyl derivative is a weak ferromagnet (canted antiferromagnet) with ordering temperature of 36 K.<sup>243,244,247,248,249</sup> At high pressure, his material reaches ordering temperature of 70 K but with the trade-off of decreased spontaneous magnetization (decreased canting).<sup>244</sup>

Another interesting stable DTA-radical is TTTAP (Figure 4), originally reported by

Wolmershäuser and Johann in 1989.<sup>250</sup> Ten years later, magnetic properties of this radical were studied by Awaga who discovered a first-order magnetic phase transition with an unusually wide thermal hysteresis loop in the 230–305 K range.<sup>251</sup> The same compound was thoroughly studied by Rawson and Palacio groups giving hysteresis loop in the 234 – 317 K range.<sup>252</sup> As it is typical for this type of transitions, the high- and low-temperature phases are paramagnetic and diamagnetic, respectively; paramagnetic phase is modelled by 1D  $S = \frac{1}{2}$  Heisenberg chain with antiferromagnetic J/k = -320 K, with relatively strong interchain couplings, and diamagnetic phase corresponds to formation of dimers with strong intermolecular antiferromagnetic coupling ( $\Delta E_{ST} < -4$  kcal mol<sup>-1</sup>).<sup>252,253</sup>

Interestingly, one of the crystalline polymorphs of amino-bridged bis(1,2,3-**DTA**), **ABBDTA** (Figure 5), forms essentially diamagnetic  $\sigma$ -dimer, containing hypervalent S-S bond, up to 380 K. Above this temperature there is a sharp increase in  $\chi T$  leading to paramagnetic phase with S-S bonds broken. Upon cooling, the  $\sigma$ -dimers are reformed at 375 K, thus providing a narrow thermal hysteresis loop but at high temperature.<sup>254</sup>

The selenium-based radicals ( $\mathbf{B} - \mathbf{D}$ , Figure 5) also displayed strong exchange interactions, which gave rise to ferromagnetically ordered phases with relatively high ordering temperatures (up to 17 K for  $\mathbf{D}$ ) and coercive fields (up to 1400 Oe for  $\mathbf{D}$ ). Although for  $\mathbf{A} - \mathbf{D}$ ,  $\sigma_{RT} < 0.001$  S cm<sup>-1</sup>,  $\sigma_{RT}$  shows an increase by 2 orders of magnitude together with  $E_a$  decrease with increasing selenium content from  $E_a = 0.43$  eV in  $\mathbf{A}$  to 0.19 eV in  $\mathbf{D}$ .

Finally, oxo-bridged bis(1,2,3-**DTA**), **OBBDTA** (Figure 4), may be viewed as a recent culmination of research on neutral **DTA**-radical-based single component conductors, with  $\sigma_{RT}$  near 0.04 S cm<sup>-1</sup> and  $E_a = 0.05$  eV.<sup>257</sup> This radical also exhibits Pauli-like temperature independent paramagnetic behavior, with  $\chi_{TIP} = 6 \times 10^{-4}$  emu mol<sup>-1</sup>. At the pressure of 6 – 8 GPa,  $\sigma_{RT} \approx 10$  S cm<sup>-1</sup> and  $E_a < 0.257$  For comparison, both  $\sigma_{RT}$  and  $\sigma_{383K}$  for **ABBDTA** are only ~10<sup>-4</sup> S cm<sup>-1</sup> (at pressure of 0.5 GPa).<sup>254</sup>

## 3. Radicals and Radical Ions with SOMO-HOMO Inversion (SHI)

## 3.1. General overview.

There are now quite a few organic radicals with an electronic energy structure, defined as SOMO-HOMO level inversion, which then formally violates the Aufbau principle, that is, the energy level of singly occupied molecular orbital (SOMO) is below the level of the highest occupied molecular orbital (HOMO). The topic of SOMO-HOMO inversion (SHI) was the subject of three recent reviews. 259-261

In our review, we define SHI by the difference in energy of electrons in HOMO (average of  $\alpha$ -MO and  $\beta$ -MO) vs. SOMO ( $\alpha$ -MO); i.e., SHI > 0 implies that the energy of SOMO is below the energy of HOMO on the per electron basis (Eq. 1). Alternatively, SHI < 0 implies that the energy of SOMO is above that of the HOMO on the per electron basis, i.e., orbital electron energies follow the usual Aufbau principle.

Our definition encompasses, the more restrictive, commonly used criterion for SHI in terms of  $\alpha$ -MO's, that is, SHI > 0 means that the energy of  $\alpha$ -SOMO is below  $\alpha$ -HOMO (Eq. 2).

SHI = 
$$[(\alpha - HOMO + \beta - HOMO)/2] - \alpha - SOMO$$
 (1)

$$\alpha SHI = \alpha - HOMO - \alpha - SOMO \tag{2}$$

The initial hint for possibility of SHI > 0 came from unrestricted INDO computation on galvinoxyl radical (Figure 5, Section 2.3), which showed the energy of  $\alpha$ -SOMO in between  $\alpha$ -HOMO and  $\beta$ -HOMO, with apparent SHI <  $0.^{262}$  The first organic radical with SHI > 0 was reported for **TEMPO-TTF** in 1993 by Sugimoto et al. (Figure 6). Significance of SHI > 0 was first recognized by Sugawara and coworkers in a series of '1990 – '2000 publications, <sup>264-268</sup> describing an effort to develop

purely organic ferromagnetic metals, which was beautifully summarized in their '2011 review article.<sup>269</sup> Their radicals largely consist of nitronyl nitroxide connected via C2 to an electron-rich  $\pi$ -systems (Figure 6); upon 1-electron oxidation of the  $\pi$ -system S=1 ground state diradical cation is typically obtained, as discussed in Section 4.3. The SHI > 0 in such radicals may be rationalized<sup>270</sup> by higher electronegativity of oxygens and nitrogens, associated with nitronyl nitroxide, at which SOMO orbital is primarily localized; HOMO is primarily localized on the  $\pi$ -system.

Figure 6. Examples of Sugimoto (1993), Sugawara (1994 – 2009), and Coote (2013) radicals with SHI > 0.

The '2013 landmark publication by Coote and co-workers demonstrated both computationally and experimentally that distonic radicals (spin and charge localized on separate atoms), such as **4-Carboxy-TEMPO** (Figure 6), are stabilized by SHI > 0 in the gas phase, as shown by smaller NO-H bond dissociation energies associated with the SHI > 0 radical.<sup>271</sup> However, later they showed that the effect is diminishing in polar solvents, and especially in water, where SHI < 0 is obtained.<sup>272</sup> Luccarini et al. confirmed experimentally the absence of extra stabilization in polar solvents for the radicals such as **4-Carboxy-TEMPO**.<sup>273</sup>

While organic radicals in general serve as efficient fluorescence quenchers,  $^{196,274}$  certain radicals with donor acceptor structures (D–A•), where A• is an electron withdrawing radical unit, may be luminescent. Is In such radicals, the ground state and excited state are both doublet (S = 1/2) states, facilitating spin-allowed radiative transitions, which is especially important for organic light emitting diodes (OLEDs). Discovery of photoluminescence in tris(2,4,6-trichlorophenyl)methyl (TTM) radical substituted with electron-rich  $\pi$ -systems based on carbazoles dates to 2006/2007, though the reported quantum yields of fluorescence were rather low,  $\Phi_f < 0.6\%$ . Analogous perchlorotriarylmethyl (PTM) radicals, with SHI > 0, showed outstanding photostability, e.g., PTM-3NCz (Figure 7). The analogous of  $\Phi_f$  (Figure 7). When  $\Phi_f = 0.6\%$  are found to possess very high values of  $\Phi_f = 0.2\%$ . Such radical-based non-alternant  $\Phi_f = 0.2\%$ . Such radical-based red-colored OLEDs could be refined to give a very good maximum external quantum efficiency (EOE<sub>max</sub>) of up to 27% (Figure 7). Such Proposed in the colored of the provide of the proposed in the colored of the provide of the prov

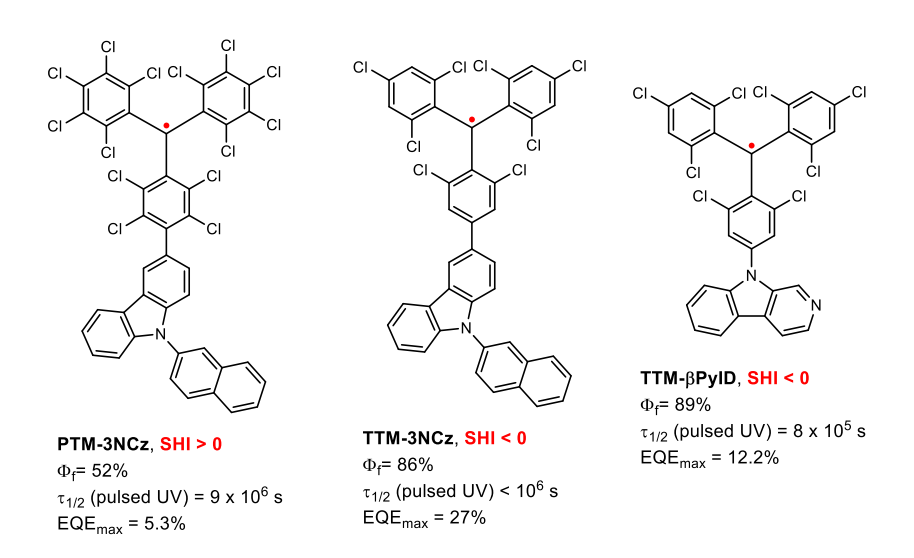


**Figure 7.** Examples of luminescent chlorinated triarylmethyl radicals.

## 3.2. Radicals and radical ions embedded in helical $\pi$ -systems.

[n]Helicenes and corresponding double helical structures are fascinating compounds with some of strongest molecular chiroptical properties. Paramagnetism, associated with an  $S = \frac{1}{2}$  radical

conjugated within helical or double helical  $\pi$ -system, may render unique properties due to the combination of chirality and delocalized electronic spin that could facilitate discovery of new organic magneto-optic materials and devices. There are relatively few open-shell helical molecules with such a distinctive combination of properties, and they are mostly represented by radicals or radical ions of short helical structures. In Figure 8, we show recent examples helical radicals, for which the sign of SHI was not reported.  $^{295-298}$ 

**Figure 8.** Examples of helical  $S = \frac{1}{2}$  radicals.

Notably, monolayer of diamagnetic [4]helicene quinacridinyl cation (derived from the radical in Figure 8) on highly oriented pyrolytic graphite (HOPG) provides efficient spin filtering with ca. 50% spin polarization at room temperature, as measured with magnetic conductive probe atomic force microscopy; also, the same cation gives an unusual temperature independent (1.6 – 300 K), antisymmetric magnetoresistance, MR = 2%, with the enantiomer-dependent sign. <sup>290</sup> Considering that achiral organic  $S = \frac{1}{2}$  radicals were computed to provide significant spin polarizations, depending on the radical type and substitution, <sup>294</sup> chiral helical and double helical radicals have a significant potential in development of organic spin filters.

Since SHI > 0 becomes commonly associated with improved stability of the radical, it is important to compare different radicals vs. their SHI status (Figure 9). For example, among hetero[7]helicene radical cations<sup>299,300</sup> and aminyl radical,<sup>300</sup> SHI > 0 may be associated with longer  $\tau_{1/2}$  in solution at room temperature, e.g., for relatively sterically unencumbered aminyl radical **AT7HA**  $\tau_{1/2} = 8$  h in

dichloromethane/acetonitrile (DCM/MeCN) at room temperature was determined in 2016 (Figure 9).<sup>300</sup> Conjoined double helical radical cation **CD5H** shows SHI > 0 according to Eq. 1 (Figure 9), though as reported in 2019 its  $\alpha$ SHI is less than 0 ("near degenerate  $\alpha$ -SOMO and  $\alpha$ -HOMO").<sup>301</sup> The persistence of the radical cation, which could be isolated and handled on air with near perfect spin concentration, was not studied rigorously. However, the corresponding S = 1 ground state diradical dication, which is most likely more reactive than the radical cation, possessed  $\tau_{1/2} = 16$  d in air-saturated dibutyl-phthalate in the presence of excess of oxidant ([NO][SbF6]).<sup>301</sup>

In 2020, Favereau and coworkers were able to isolate, resolve, and characterize two radical cations with SHI > 0: axially chiral **DCb** and helical **DCb7H**.<sup>302</sup> The greater persistence of **DCb**, compared to **DCB7H**, may possibly be associated with the stronger SHI (Figure 9).<sup>259</sup>

Racemic radical cations of thiophene double helix, with high spin concentrations, were studied in solution in 2021.<sup>303</sup> Interestingly, spin density was delocalized just over the carbon atoms (*g*-values of 2.0012 and 2.0017) in the single  $\alpha$ ,β-cyclooctatetrathiophene ( $\alpha$ ,β-COTh) moiety, highlighted in yellow color for **TDH**-TMS<sub>8</sub> and **TDH**-TMS<sub>12</sub> (Figure 9). Consequently, reduction potentials for both radical cations were similar (ca. +1.33 V vs SCE). It should be noted that while  $D_2$ -symmetric radical cation **TDH**-TMS<sub>8</sub> consists of a single central  $\alpha$ ,β-COTh moiety, which is flanked by the two  $\beta$ ,β-COTh moieties,  $C_2$ -symmetric radical cation **TDH**-TMS<sub>12</sub> consists of three  $\alpha$ ,β-COTh moieties, flanking the two  $\beta$ ,β-COTh moieties. Notably, **TDH**-TMS<sub>8</sub> with SHI < 0 was considerably more persistent ( $\tau_{1/2} > 12$  h in degassed DCM at rt), compared to **TDH**-TMS<sub>12</sub> ( $\tau_{1/2} \approx 5$  min in degassed DCM at rt). This is an unusual case where SHI does not control the persistence of radicals. The greater persistence of **TDH**-TMS<sub>8</sub> was associated with steric shielding of all carbons bearing significant spin density within  $\alpha$ ,β-COTh moiety by the two adjacent  $\beta$ ,β-COTh moieties (and TMS groups). <sup>303</sup>

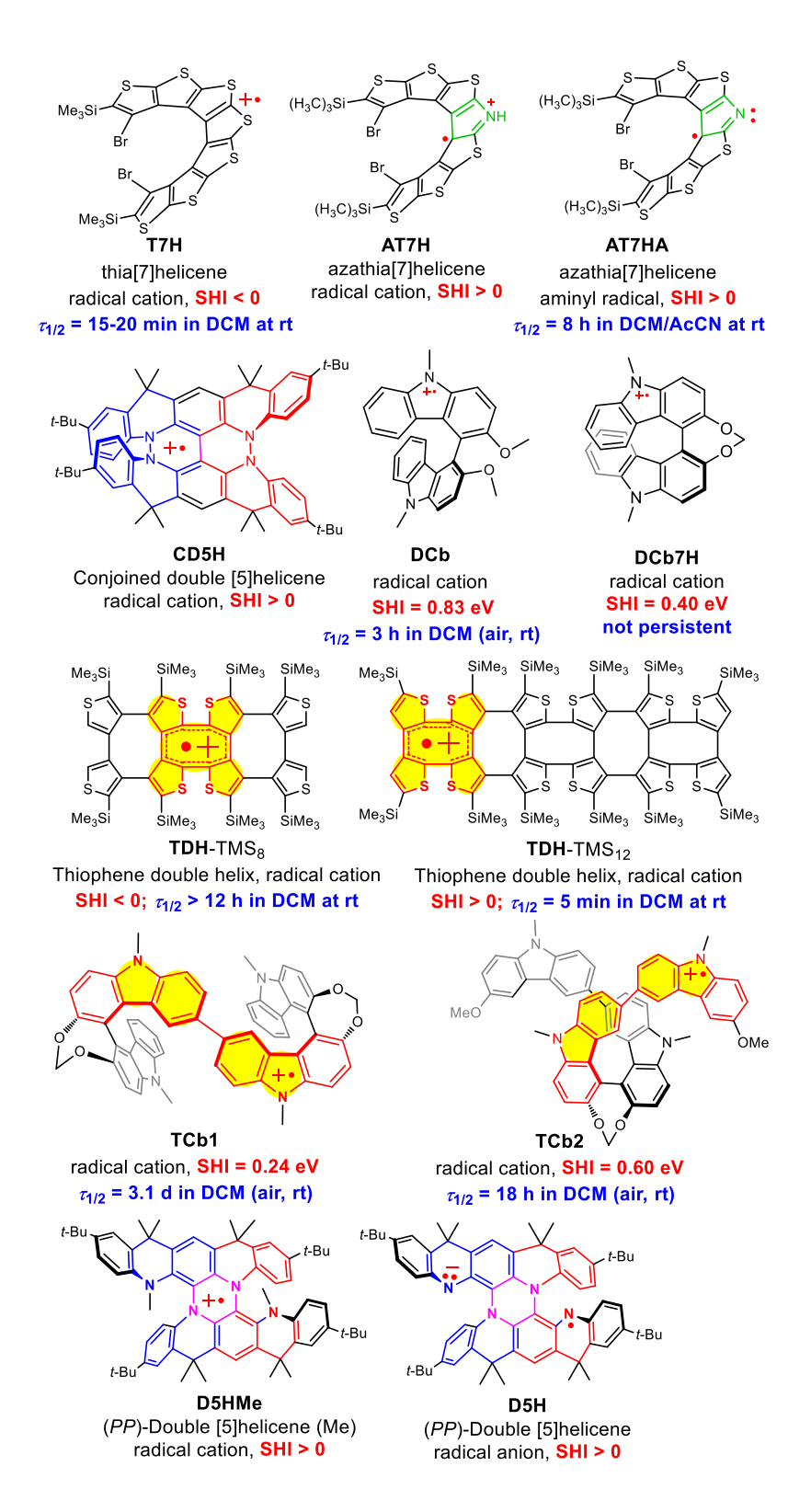


**Figure 9.** Examples of helical and double helical  $S = \frac{1}{2}$  radicals for which SHI (eq. 1) was determined.

In 2022, Favereau and coworkers were able to synthesize, resolve, and study tetra-carbazole radical cations (and the corresponding diradical dications) **TCb1** and **TCb2**, both with SHI > 0, derived from previously prepared **DCb7H** (Figure 9).<sup>304</sup> In these radical cations, spin density is localized primarily on the 6,6'-dicarbazole (6,6'-DiCb) moiety as highlighted in yellow for **TCb1**. In analogy

to the thiophene double helices discussed above, **TCb1** consists of a single central 6,6'-DiCb moiety, flanked by two carbazoles, **TCb2** consists of two terminal 6,6'-DiCb moieties. Based on the discussion in the preceding paragraph, it is not surprising that **TCb2** is less persistent (vs. **TCb1**), in spite of having stronger SHI > 0 and being "protected" by the methoxy groups. We note that enantiomerically enriched tetra-carbazole radical cations provided surprisingly weak chiroptical properties, e.g.,  $\Delta\varepsilon$  of the order of 5 L mol<sup>-1</sup> cm<sup>-1</sup>.<sup>304</sup>

We conclude this section with a note concerning the ground states of the single electron oxidized species corresponding to compounds in Figure 9, to be discussed in a more general fashion in the following Section 3.3. While the radical cation derived from relatively persistent aminyl radical **AT7HA** was predicted computationally to possess S = 1 ground state (Section 3.3),<sup>300</sup> we were not able to confirm it experimentally. Diradical dication of **CD5H** in dibutyl-phthalate possesses S = 1 ground state with experimentally determined  $\Delta E_{ST} \approx 0.3$  kcal mol<sup>-1</sup> (Section 4.4).<sup>301</sup> Favereau's diradical dications and those derived from thiophene double helices are either singlet ground states or possess near degenerate singlet and triplet states.<sup>303,304</sup> Diradical dication of **D5HMe** and aminyl diradical of **D5H** are predicted by DFT computations to be triplet ground states (Section 3.3).

# 3.3. Is there a relation between the SOMO-HOMO electron energy difference (SHI) in monoradicals (ions) and singlet triplet energy gap ( $\Delta E_{ST}$ ) in diradicals (ions)?

Sugawara in his '2011 review noted that when some of the nitronyl nitroxide radicals with SHI > 0 are oxidized to the corresponding radical cations, triplet ground state species are obtained, with some exceptions. Here we seek a more quantitative relationship between SHI in  $S = \frac{1}{2}$  monoradicals, defined by Eq. 1, and  $\Delta E_{ST}$  in the corresponding diradicals. Since SHI is derived from DFT computations, we explore a relationship between DFT-determined  $\Delta E_{ST}$  and SHI in the gas phase. In Figure 10, we summarize the structures of  $S = \frac{1}{2}$  monoradicals with their SHI values, which provide

an excellent linear regression with  $\Delta E_{ST}$  in the corresponding diradicals (Figure 11). Structures of the

three outliers, not included in the regression, are shown in Figure 12.

TATHP: Tetrazatetrahydropyrene AT7HA: Azathia[7]helicene aminyl, C1 UB3LYP/6-31G(d) gas ph. CD5H: Conjoined double [5]helicene, D2 UB3LYP/6-31G(d,p) gas ph. Radical cation,  $D_2$ ,  ${}^2B_2$ , SHI = 5.35 (0.49) UB3LYP/6-31G(d) gas ph. Aminyl monoradical: SHI = 3.03 (2.38) Diradical dication,  $D_{2h}$ ,  $\Delta E_{ST} = 4.02$ Radical cation,  ${}^{2}B_{3}$ , SHI = 1.38 (-3.06) Diradical cation:  $\Delta E_{ST} = 1.53$ Diradical dication:  $\Delta E_{ST} = 0.59$ MWS1: McMasters-Wirz-Snyder 1 UB3LYP/6-31+G(d,p) gas ph. Radical anion,  $C_s/C_{2v}$ , SHI = -1.35 (-6.67) Diradical,  $C_{2v}$ ,  ${}^3B_2$ ,  $\Delta E_{ST} = 0.44$ D5HMe: (PP)-Double [5]helicene (Me), C2 MWS2: McMasters-Wirz-Snyder 2 UB3LYP/6-31G(d) gas ph. UB3LYP/6-31+G(d,p) gas ph. TMM: Trimethylenemethane Radical cation,  ${}^{2}A$ , SHI = 6.94 (5.68) Radical anion,  $C_{s}/C_{2v}$ , SHI = 4.08 (-1.15) UB3LYP/6-311+G(d,p) gas ph. Diradical dication:  $\Delta E_{ST} = 3.90$ Diradical,  $C_{2v}$ ,  ${}^{3}B_{2}$ ,  $\Delta E_{ST} = 3.55$ Radical anion,  $C_{2v}$ ,  ${}^{2}A_{2}$ ; SHI = 31.06 (24.97) Diradical,  $D_{3h}$ ,  ${}^{3}A_{1}$ ,  $\Delta E_{ST} = 18.52$ MX: m-Xylylene UB3LYP/6-311+G(d,p) gas ph. Radical anion,  $C_{\rm S}/C_{\rm 2v}$ ,  $^{2}{\rm B}_{\rm 1}$  SHI = 23.30 (16.77) Diradical,  $C_{2v}$ ,  ${}^{3}B_{2}$ ,  $\Delta E_{ST} = 11.98$ **DATHP**: Diazatetrahydropentacene, C<sub>2v</sub> UB3LYP/6-31+G(d,p) gas ph. Radical anion,  ${}^{2}A_{2}$ , SHI = 12.21 (6.20) Diradical,  $\Delta E_{ST} = 7.25$ PTAM: Planarized triarylmethyl, C2 Clar triangulene DAMX: Diaza-m-xylylene UB3LYP/6-31+G(d,p) gas ph. UB3LYP/6-311+G(d,p) gas ph. UB3LYP/6-31+G(d,p) gas ph. Radical anion,  $C_{2v}$ ,  ${}^{2}B_{1}$ , SHI = 18.64 (15.26) Radical anion,  ${}^{2}A$ , SHI = 9.82 (3.54)

Figure 10. Structures and spin density maps (isodensity level of 0.002 electron/Bohr) used for linear regression of singlet-triplet energy gaps,  $\Delta E_{\rm ST}$  (kcal mol<sup>-1</sup>) vs. SHI (kcal mol<sup>-1</sup>); see: the following Figure 11.  $\Delta E_{\rm ST}$  values are for diradicals and SHI values are for one-electron reduced species; e.g., radical anions for neutral diradicals. Except for double helical **D5HMe**, all diradicals were studied before; also, spin density maps for **AT7H**, **CD5H**, and TATHP may be found in refs 300 and 301. SHI values are from eq. 1 and the values in parentheses are in terms of  $\alpha$ -MO's (eq. 2). Values of  $\Delta E_{ST}$  were typically computed at the UB3LYP/6-31G(d,p)+ZPVE (or UB3LYP/6-311+G(d,p)+ZPVE) level of theory (gas phase) and were corrected for spin contamination; geometries for both triplet and BS singlet (checked for stability) were optimized.

Diradical,  $D_{3h}$ ,  ${}^{3}B_{2}$ ,  $\Delta E_{ST} = 10.43$  (Figure 45)

Diradical,  ${}^{3}B$ ,  $\Delta E_{ST} = 6.39$ 

Radical anion,  $C_1/C_{2v}$ , SHI = 28.82 (23.12)

Diradical,  $C_{2v}$ ,  ${}^{3}B_{2}$ ,  $\Delta E_{ST} = 15.77$ 

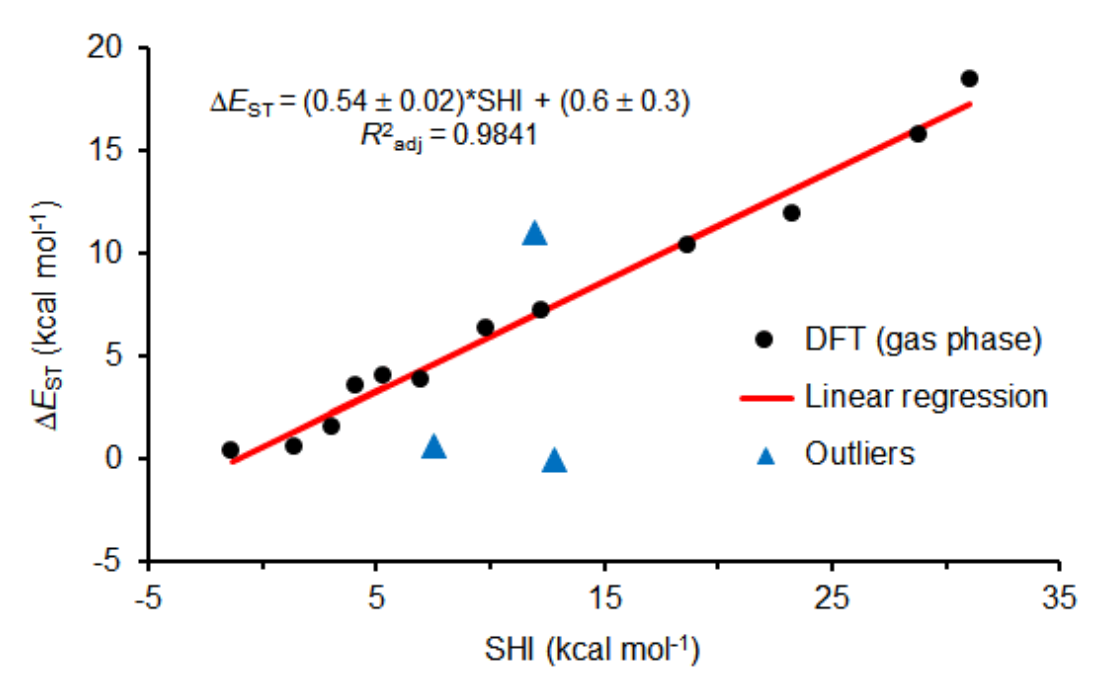


**Figure 11.** Linear regression between DFT-computed  $\Delta E_{\rm ST}$  and SHI (Eq. 1) for twelve C- and N-centered diradicals. The value of  $P = 1.55 \times 10^{-10}$  for slope indicates that the value of 0.54 is reliably determined, however, P = 0.099 > 0.05 for intercept indicates that the value of 0.6 is not statistically significant. All  $\Delta E_{\rm ST}$  and SHI values are computed in the gas phase (see: preceding Figure 10), typically, at the UB3LYP/6-31G(d,p)+ZPVE and UB3LYP/6-31+G(d,p)+ZPVE levels of theory, respectively. Outliers are not included in the linear regression (see: following Figure 12).

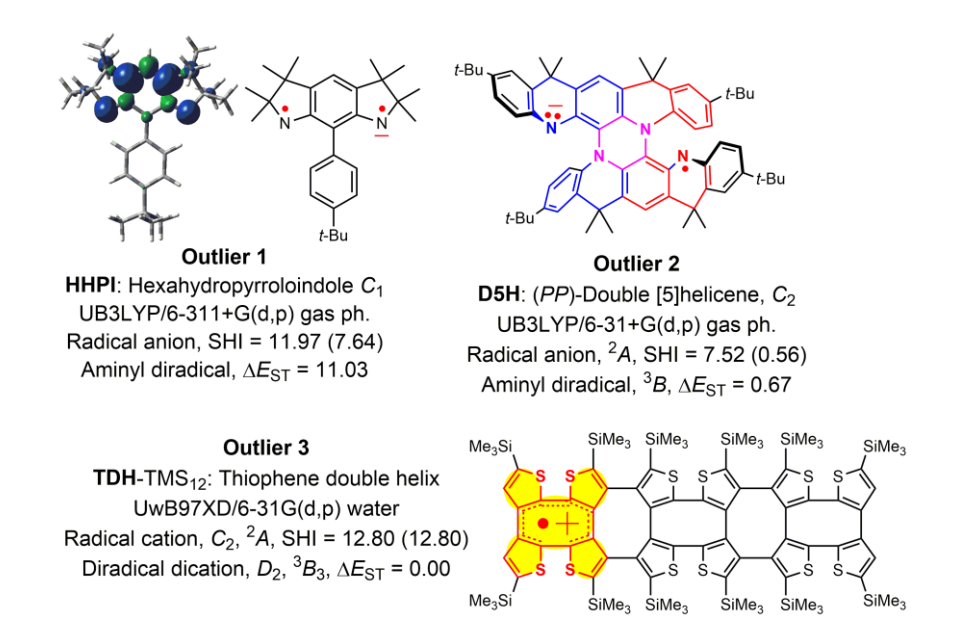


**Figure 12.** Structures for outliers in the linear regression of singlet-triplet energy gaps,  $\Delta E_{\rm ST}$  (kcal mol<sup>-1</sup>) vs. SHI (kcal mol<sup>-1</sup>); see: the preceding Figure 11.  $\Delta E_{\rm ST}$  values are for diradicals, and SHI values are one-electron reduced species, e.g., radical anions derived from neutral diradicals. Aminyl diradical (corresponding to Outlier 1)<sup>112,114</sup> and radical cation (Outlier 3)<sup>303</sup> were studied both experimentally and computationally. Radical anion **D5HMe** and corresponding aminyl diradical were not previously studied. SHI values in parentheses are in terms of α-MO's. Values of  $\Delta E_{\rm ST}$  were typically computed at the UB3LYP/6-31G(d,p)+ZPVE (or UB3LYP/6-311+G(d,p)+ZPVE) level of theory (gas phase) and were corrected for spin contamination.

values of  $\alpha$ SHI (as defined by Eq. 2) is significantly worse, as indicated by the values of statistically adjusted coefficients of determination, i.e.,  $R_{adj}^2 = 0.935$  vs 0.984 (Figure 11).

One of the weaknesses of the present approach is the use of the UB3LYP functional in the gas phase, which provides symmetric structures for radical anions, especially for m-phenylene-based structures. Already in 1991, it was established experimentally that in tetrahydrofuran or 2-methyltetrahydrofuran (THF or 2-MeTHF) in the non-planarized m-phenylene-based triarylmethyl radical anions (for a "planarized" version, i.e., **PTAM**, see: Figure 10), spin density is localized on one of the triarylmethyl moieties on the EPR spectroscopic time scale. This distortion was rationalized in terms of second order Jahn-Teller effect. <sup>305</sup> Consequently, for radical anion of m-xylylene, **MX** (Figure 10), we find that while using UB3LYP  $C_{2v}$ -symmetric structure is obtained, but when employing UwB97XD functional in THF PCM solvent model,  $C_s$ -symmetric structure, with spin density confined to one phenylmethyl moiety, is found to be the global minimum. Analogous results were found for **TDH-TMS**<sub>12</sub> (and related radical cations) <sup>303</sup> and radical anions **DAMX** (Figure 10), as well as **PTAM**.

Next, we investigated nitronyl nitroxide based radical anions derived from S = 1 ground state diradicals, spanning a wide range of DFT-computed  $\Delta E_{\rm ST}$  from 1.4 to 9.8 kcal mol<sup>-1</sup> (Figure 13). The first three radical anions in Figure 13 are derived from thoroughly studied experimentally S = 1 ground state diradicals (Section 4.3). The other three radical anions or diradicals are not explored experimentally yet. We were somewhat surprised by the bad linear regression between  $\Delta E_{\rm ST}$  and SHI (Figure 14), despite structural similarity between all six diradicals. In particular, P-values of >>0.05 for slope and intercept, 0.60 and 0.38, indicate that they are not statistically significant.

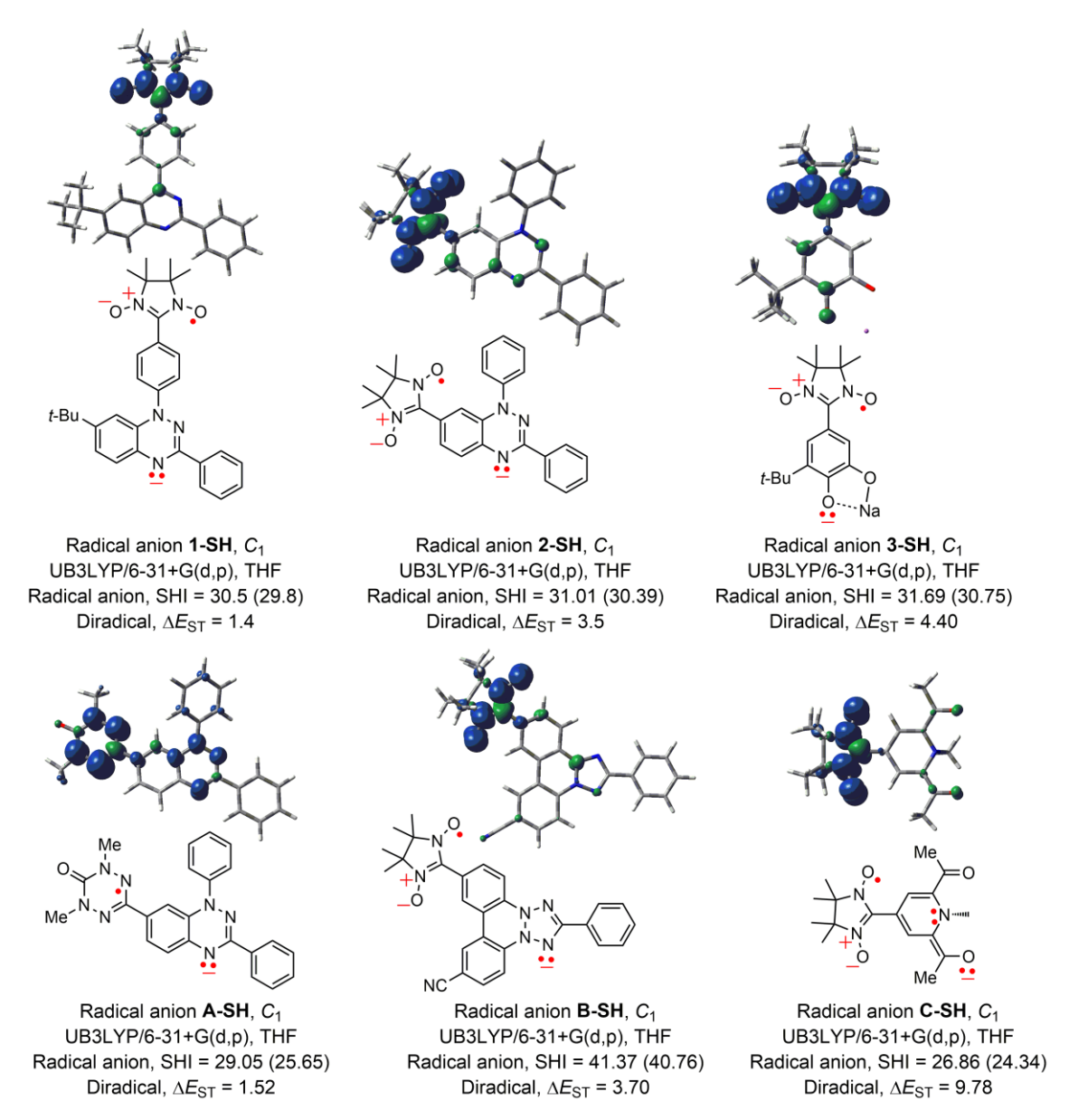


**Figure 13.** Structures and spin density maps ((isodensity level of 0.002 electron/Bohr) of radical anions with strong SHI (kcal mol<sup>-1</sup>), which fail to provide linear regression with corresponding diradicals singlet-triplet energy gaps,  $\Delta E_{\rm ST}$  (kcal mol<sup>-1</sup>); see: following Figure 14. Radical anions **1-SH** – **3-SH** are derived from previously synthesized diradicals; radical anions **A-SH** – **C-SH** and corresponding diradicals were not previously studied. SHI in parenthesis is in terms of α-MO's. Values of  $\Delta E_{\rm ST}$  were typically computed at the UB3LYP/6-31G(d,p)+ZPVE (gas phase) level of theory and were corrected for spin contamination.

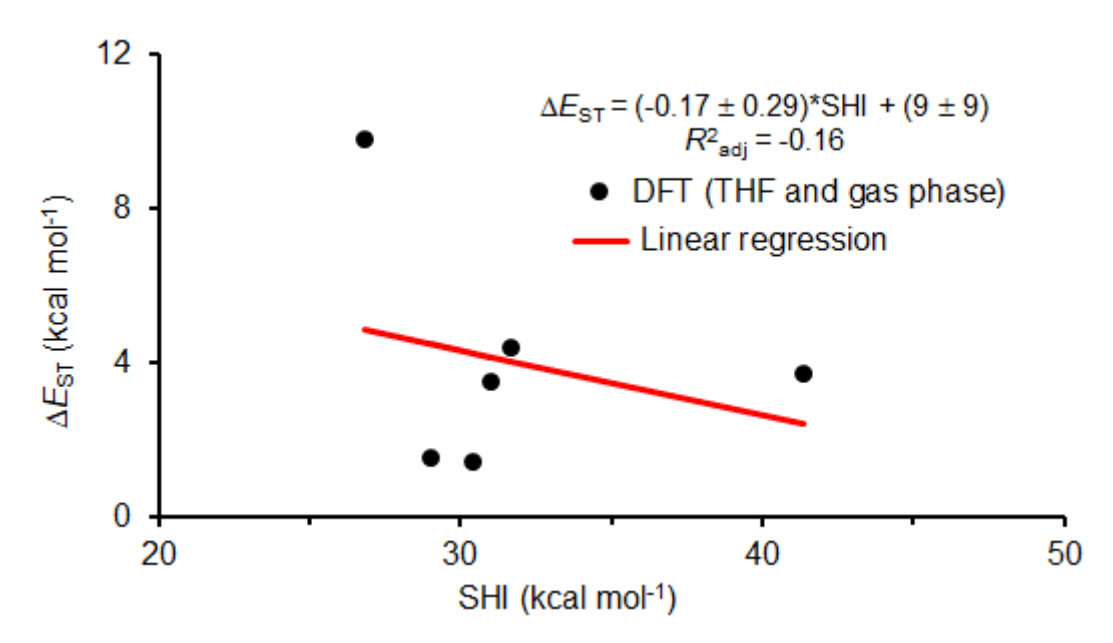


**Figure 14.** Failed linear regression between DFT-computed  $\Delta E_{ST}$  (gas phase) and SHI (THF) for nitronyl nitroxide (and oxo-verdazyl) based high-spin diradicals and corresponding radical anions; see: preceding Figure 13.

We associate this failed linear regression (Figure 14) to dominance of electronegativity as the major factor controlling the value of SHI in nitronyl nitroxide based radical anions. Also, some of the structures show significant distortions from planarity.

## 4. High-Spin Di- and Tri-Radicals.

## 4.1. Design rules for high-spin di- and polyradicals.

Stable high spin organic radicals ( $S \ge 1$ ) are attractive targets for organic materials for potential applications such as organic magnets,  $^{32,306,307}$  spintronics,  $^{7,308}$  spin filters,  $^{308-310}$  and memory devices.  $^{311,312}$  Compared to many existing stable  $S = \frac{1}{2}$  monoradicals, only relatively few of stable and even fewer thermally robust high-spin organic radicals were reported. Developing new high-spin molecules is challenging, and this part of the review will focus on recent work from ours and other groups.

Organic monoradicals, containing one unpaired electron, can be considered as the fundamental spin-bearing units or centers  $(S = \frac{1}{2})$ . In a di- or triradical, in which multiple radical  $S = \frac{1}{2}$  centers are

conjugated, exchange coupling between  $S = \frac{1}{2}$  spin centers may lead to either high- or low-spin ground state. The main objective in the molecular design of high-spin di- and triradicals is to obtain ferromagnetic coupling between  $S = \frac{1}{2}$  centers, leading to a high-spin  $(S \ge 1)$  ground state. This ferromagnetic interaction should ideally be strong, leading to a large separation in energy between the high-spin ground state and low-spin excited states.

Design of high-spin di- and triradicals for practical applications requires that the following two minimal conditions are satisfied.<sup>313,14</sup>

- (1) The high-spin ground state should be at least a couple of kcal mol<sup>-1</sup> (>> RT = 0.6 kcal mol<sup>-1</sup>  $\approx$  thermal energy at room temperature) below the lowest excited state,
- (2) The radicals should be stable, or at least persistent, at room temperature to be easily handled without special precautions.

In a diradical, exchange coupling between two  $S = \frac{1}{2}$  spin centers  $S_1$  and  $S_2$  could be described by the effective Heisenberg Hamiltonian:  $\frac{314,315}{2}$ 

$$H = -2/S_1 \bullet S_2 \tag{3}$$

where the factor of "-2" is traditionally used in chemistry literature. Parameter J is the exchange coupling constants, usually given in Kelvins (K) as J/k (k is the Boltzmann constant), or alternatively, singlet triplet energy gap,  $2J = \Delta E_{\rm ST}$ , usually reported in kcal mol<sup>-1</sup>. Negative J value requires the lowest energy state to have antiparallel spins, leading to antiferromagnetic interaction, i.e., the case of low-spin ground state. Positive J value means the lowest energy states have parallel spins and ferromagnetic interaction occurs, i.e., the case of high-spin ground state. The energy gap between singlet and triplet states ( $\Delta E_{\rm ST}$ ) therefore is given by 2J. In other words, the ground state type, high-spin or low-spin, and the corresponding energy gap are decided by the sign and magnitude of J value.  $^{313,14}$ 

In planar  $\pi$ -conjugated diradicals, corresponding to alternant  $\pi$ -systems, ferromagnetic vs.

antiferromagnetic exchange coupling between S = 1/2 spin centers is governed by the  $\pi$ -connectivity and can be qualitatively predicted using Ovchinnikov parity models.<sup>316</sup> It is also assumed that the through-bond exchange interactions between  $S = \frac{1}{2}$  spin centers are dominant in  $\pi$ -conjugated radicals.<sup>313,14</sup> In the models, each adjacent spin in the  $\pi$ -system is assumed to possess the opposite spin of its nearest neighbor. The difference between the spin-up count vs the spin-down count decides the ground state, e.g., if difference equals to two, then the S = 1 triplet ground state is predicted (Figure 15).<sup>316</sup>

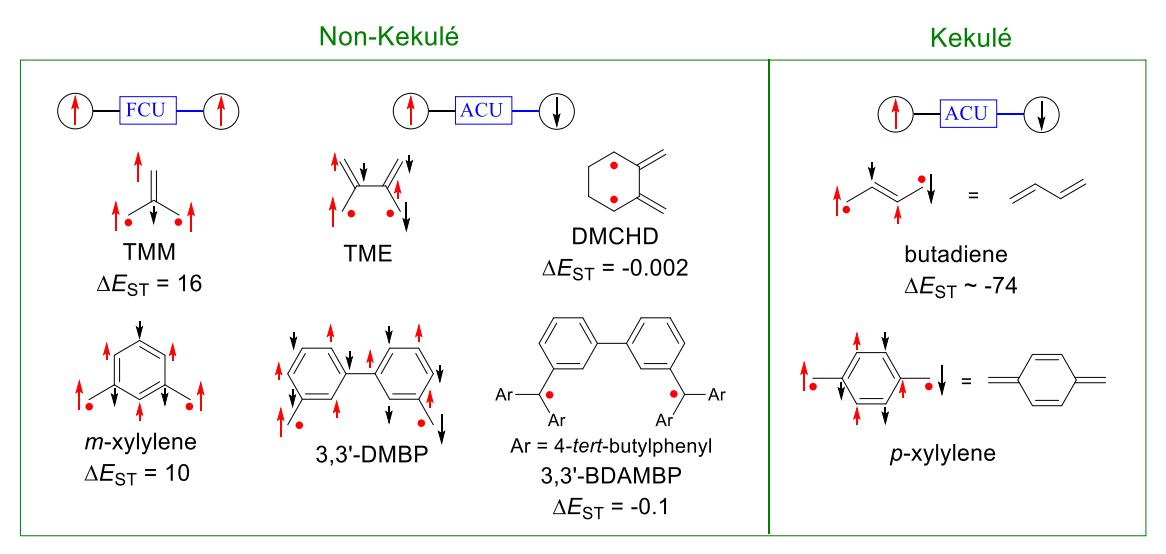


**Figure 15.** Ferromagnetic and antiferromagnetic exchange coupling predicted using Ovchinnikov parity models. Values of  $\Delta E_{ST}$  are in kcal mol<sup>-1</sup>. Reproduced from ref 314. Copyright 2015 American Chemical Society.

Using methyl radicals as  $S = \frac{1}{2}$  spin centers and ethylene as a coupling unit, we can see that the 1,1-connection at ethylene leads to non- Kekulé TMM, a triplet ground state molecule and 1,2-connection provides Kekulé butadiene, a closed shell molecule with a singlet ground state. While TMM and butadiene possess large  $\Delta E_{\rm ST}$ ,  $^{317-319}$  another non- Kekulé molecule such as TME, obtained by 1,1-connection of two ethylenes with two methyl radicals, is a singlet ground state with a very small  $\Delta E_{\rm ST}$ . Analogous results are obtained for *m*-xylylene, *p*- and *o*-xylylene and 3,3'-dimethylenebiphenyl (3,3'-DMBP) (Figure 15).  $^{322,323}$ 

Coupling units that lead to ferromagnetic coupling between  $S = \frac{1}{2}$  spin centers (e.g., 1,1-ethylene,

*m*-phenylene) are termed ferromagnetic coupling units (FCU's), and those that lead to antiferromagnetic coupling (e.g., 3,3'-biphenyl) are termed antiferromagnetic coupling units (ACU's) (Figure 15).<sup>313,324</sup>

Although it was believed for a long time that the presence of Kekulé resonance form implied a singlet ground state, the exceptions to this rule will be discussed in Section 4.4.

Ovchinnikov parity models are simple and convincing tools for predicting the ground state of  $\pi$ conjugated diradicals. However, the strength of exchange interaction is unclear from the parity models.

What causes the huge difference in  $|\Delta E_{ST}|$  between TMM and TME? To understand this problem, the
singly occupied molecular orbitals (SOMOs) are considered in the diradicals. Borden and Davidson
classified the SOMOs can be non-disjoint (spatially coinciding at some atoms) and disjoint (not
spatially coinciding at any atoms). Exchange interaction is weak for disjoint SOMOs such as in
TME, while exchange interaction is strong and ferromagnetic for non-disjoint SOMOs in TMM
(Figure 16). TMM, when two unpaired electrons align parallel, a node is introduced in the
spatial part of the wave function and, as a result, the Coulombic repulsion is reduced effectively in the
spatially coinciding area. Analogous conclusions are reached for m-xylylene and 3,3'-DNBP (Figure

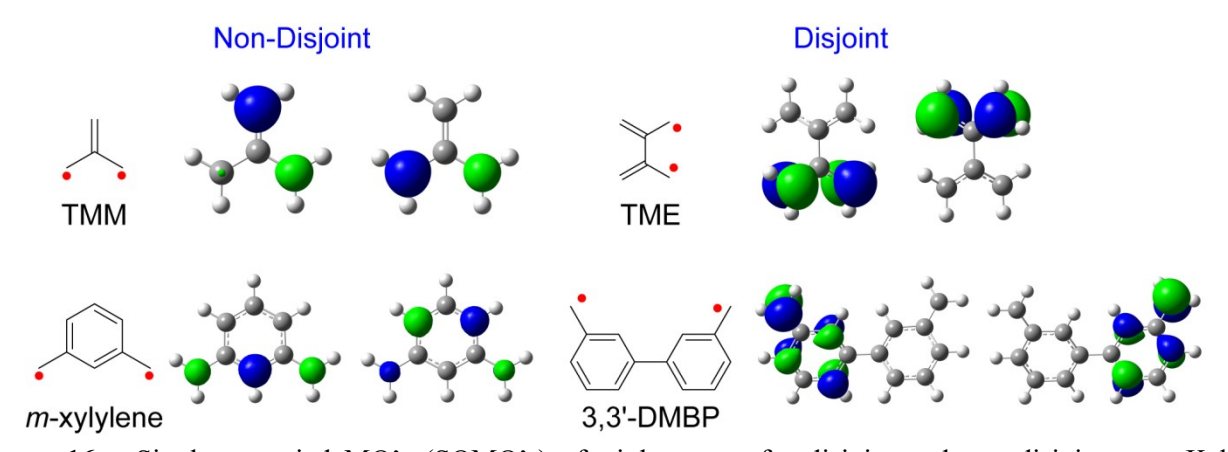


**Figure 16.** Singly occupied MO's (SOMO's) of triplet states for disjoint and non-disjoint non-Kekulé diradicals at the UB3LYP/6-311G(d,p) level. Reproduced from ref 314. Copyright 2015 American Chemical Society.

# 4.2. Magnetic characterization of diradicals and triradicals.

Electron paramagnetic resonance (EPR) spectroscopy and superconducting quantum interference device (SQUID) magnetometry are two dominant tools for studying magnetic properties of high-spin radicals. There is also a role for NMR spectroscopy. Most important objectives are determination of ground state and of energy gaps between low- and high-spin states,  $\Delta E_{LS-HS}$ .

## 4.2.1. EPR spectroscopy.

Continuous wave (CW) EPR spectroscopy is widely utilized to measure the high-spin state spectra of radicals ( $S \ge 1$ ), for which g-tensor and zero-field splitting (ZFS) parameters D and E, and in favorable cases, large components of nuclear hyperfine coupling tensors A, are obtained. Because the ZFS parameters are inherently anisotropic, the samples are measured in frozen glassy matrices, with typical radical concentration of <1 mM, to minimize the intermolecular interactions. Specifically in organic radicals, composed of light elements, ZFS parameters largely originate in purely anisotropic magnetic dipole – dipole interactions, thus D-value in diradicals provides approximate measure interspin distance.  $^{326,327}$ 

For  $S \ge 1$  states with significant (D/v)-values, where v is microwave frequency, characteristic half-field, formally forbidden transitions ( $|\Delta m_S| = 2$ ) may be detected; in the absence of resolvable nuclear hyperfine couplings,  $|\Delta m_S| = 2$  transition corresponds to a single peak for S = 1 state, while more complex pattern is observed for  $S \ge 3/2$  states. <sup>24,328,329</sup> In favorable cases,  $|\Delta m_S| = 3$  transition (third-field) may be detected for triradicals at low temperature using commonly available X-band instruments (v = 9 GHz). <sup>24,328,329</sup>

Detection of EPR spectra for high-spin state only shows that the high-spin state is significantly populated at the temperature of measurement, and it does not establish the ground state. This is especially true for diradicals because the low-spin state (S = 0) is typically EPR silent. The same

statements are valid for more sophisticated pulse EPR nutation spectra, where the frequencies characteristic for S = 1/2, 1, 3/2... states may be observed. Note that that even if only nutation frequencies corresponding to S > 1 state are observed, this does not mean that this state is the ground state, because the low-spin  $S \ge 1/2$  states may possess unfavorable electron spin relaxation times to be efficiently observed in the nutation experiment.

The traditional way to obtain a better insight to the nature of the ground state was to study the double integrated intensity (I) of EPR spectrum vs. temperature (T). When a curved plot of IT vs. T or I vs. 1/T is obtained then the ground state may be unequivocally established, when the precautions against microwave saturation are taken (see: below). That is, if the plots are curved upwards at lower T, which implies increased population of high-spin state, and this, in turn, implies high-spin ground state. Downward curvatures at lower T imply low-spin ground state. Energy gaps between the low- and high-spin state,  $\Delta E_{LS-HS}$ , may be obtained by numerical fitting to equations obtained by solutions of Heisenberg Hamiltonian (eq. 4),

$$\boldsymbol{H} = -2\Sigma J_{ki} \boldsymbol{S}_{k} \bullet \boldsymbol{S}_{i} \tag{4}$$

where the nearest neighbor spins are typically considered,  $J_{kj}$  is the pairwise exchange coupling constant, and the summation is done over all nearest neighbors for k, j from 1 to n (n = total number of  $S = \frac{1}{2}$  sites). To a diradical, singlet triplet energy gap,  $\Delta E_{ST} = 2J_{kj}$ ; more complex, connectivity dependent formulas are found for doublet quartet energy gap  $\Delta E_{DQ}$  in triradicals.

However, the most common occurrence is a flat plot of IT vs. T or linear plot of I vs. 1/T, which indicates the temperature independent ratio of the high- to low-spin states; consequently, this implies either high-spin ground state (case 1) or near degenerate high- and low-spin states (case 2). Specifically, in the second case, the energy gap between the low- and high-spin state,  $|\Delta E_{LS-HS}| < 0.5RT_{lowest}$ , where  $T_{lowest}$  is the lowest temperature at which the I is measured; in the first case of the high-spin ground state, this means approximately  $\Delta E_{LS-HS} > 2RT_{highest}$ , where  $T_{highest}$  is the highest

temperature of the *I*-measurement. For example, if  $T_{lowest} = 5$  K and  $T_{highest} = 150$  K, then the following limiting values may be obtained:  $|\Delta E_{LS-HS}| < 0.005$  kcal mol<sup>-1</sup> or  $\Delta E_{LS-HS} > 0.6$  kcal mol<sup>-1</sup> for the second and first case, respectively. It is important to avoid microwave saturation, especially at low temperatures, by either obtaining rigorous microwave saturation plots (*I* vs.  $P^{1/2}$ ) at near  $T_{lowest}$ , where *P* is microwave power in the range of at least two orders of magnitude, or by acquiring the *I* vs *T* data at significantly different microwave powers. <sup>323,329,331</sup> Typically, *I* of  $|\Delta ms| = 2$  transition is studied, because this partially forbidden transition is much more difficult to saturate <sup>332</sup> and it may be well separated from the impurity peaks. In addition, when claiming purity of S = 1 diradical, one has to make sure that the spectrum is obtained under the conditions, in which the  $S = \frac{1}{2}$  monoradical is not partially saturated.

More recently, our group introduced quantitative variable temperature EPR spectroscopy for studies of di- and triradicals.  $^{147,149,150,301,333}$  Instead of IT vs. T plots,  $\chi T$  vs. T are plotted, where  $\chi$  is paramagnetic susceptibility of the sample, determined with  $S = \frac{1}{2}$  reference. The  $\chi T$  vs. T plots are advantageous when trying to extract more than one J-value<sup>150</sup> because, if the radical is pure and its weight is known accurately, 150 then there are no additional parameters, beyond the J-values, to fit, thus avoiding over parametrization – a common problem when fitting EPR intensity or magnetic data. Notably, in selected not-too-polar solvents and matrices, such as dibutyl phthalate, toluene/chloroform, etc., reliable values of  $\chi T$  can be obtained at near and above room temperature in a fluid solvent.  $^{147,150,301}$  It is important that the  $S = \frac{1}{2}$  reference (e.g., TEMPONE) is dissolved in the identical solvent as the sample and its spectra are obtained with comparable parameters. Now there is no ambiguity concerning the ground state because, if only high-spin ground state is predominantly populated, then, assuming  $g \approx 2$ ,  $\gamma T = S(S+1)/2$  emu K mol<sup>-1</sup>, e.g.,  $\gamma T = 1.00$  emu K mol<sup>-1</sup> for S = 1ground state diradical. In contrast, when low- and high-spin states are near degenerate, which essentially means a mixture of  $S = \frac{1}{2}$  radicals, for polyradical with  $n S = \frac{1}{2}$  sites,  $\chi T = n*0.5(0.5+1)/2$  emu K mol<sup>-1</sup>, e.g.,  $\gamma T = 0.75$  emu K mol<sup>-1</sup> for a diradical with near degenerate singlet and triplet states.

For some di-, tri-, and tetraradicals, the  $\chi T$  vs. T plots are not feasible up to near room temperature because of limited stability and/or preparation conditions for radical, requiring use of relatively polar ethereal solvents such as 2-MeTHF. In those cases,  $\chi T$ -values are measured at low temperatures (T < 130 K), near or below the glass transition of the solvent. <sup>114,115</sup> In special cases, such as S = 3/2 aminyl triradicals AT1 and AT2 (Figure 17), where the EPR spectra for S = 3/2 ground state and  $S = \frac{1}{2}$ \* excited state (as well as for other admixed species) are significantly different, then the doublet-quartet energy gap  $\Delta E_{DQ} \approx 1$  kcal mol<sup>-1</sup> may be obtained from direct spectral simulation by finding the ratio of  $S = \frac{1}{2}$ \* to S = 3/2 state. <sup>115</sup> The obtained values of  $\Delta E_{DQ}$  are in excellent agreement with those obtained from the SQUID data (see: below) but they require spectral simulations of multiple samples.

**Figure 17.** Aminyl triradicals with S = 3/2 ground states.

EPR spectroscopy is also a useful tool to investigate the persistence of radicals. When well-resolved spectra are available, monitoring of I vs. time is equivalent to obtaining concentration vs. time curve. When overlapped spectra are present, this approach provides depressed rate constants for the original high-spin radical, leading to overestimated half-lives, e.g., for S = 3/2 triradicals **AT1** and

**AT2** (Figure 17). To obtain correct concentration (or molar fraction) vs. time curves, the spectra of decayed mixture of radicals must be simulated and corrected for the presence of diamagnetic species by the measurement of  $\chi T$  at each time point. This allows to unravel complex consecutive kinetics, such as for **AT1** and **AT2**. This allows to unravel complex consecutive kinetics,

#### 4.2.2. SQUID magnetometry.

Determination of the ground state value of total spin S and the energy gap  $\Delta E_{LS-HS}$  by SQUID magnetometry is based on thermal population of either  $m_S$ -substates or low- vs. high-spin electronic (spin) states.

Magnetic measurements are traditionally carried out on polycrystalline solids. Because most organic radicals exhibit weak-to-moderate intermolecular antiferromagnetic interactions, this prevents implementation of the most powerful Brillouin function-based method for determination of the ground state for high-spin radical. This method is fundamentally based on detection of thermal population of  $m_{\rm S}$ -substates in the presence of external magnetic field. To weaken the intermolecular interactions, SQUID measurements may be performed on dilute, 5 - 20 mM, samples in matrices. While various high- $T_g$  polymer matrices were used for this purpose, our group have developed and perfected over the years solution/matrix sample containers that allow sample preparation at low temperature and minimize diamagnetic background.  $^{31,111,115}$  Using 5 – 20 mM radical samples, magnetization (M) is measured vs. external magnetic field (H) at low temperatures (usually 1.8, 2, 3, and 5 K). The saturated magnetization  $M_{sat}$  and the total spin S are obtained by fitting the plots of normalized magnetization  $M/M_{\rm sat}$  vs.  $H/(T-\theta)$  to the Brillouin function, where  $\theta$  corresponds to the mean-field correction for residual intermolecular interactions (typically,  $\theta < 0.1$  K). Because the values of S are based upon the curvature of the  $M/M_{\rm sat}$  vs.  $H/(T-\theta)$  plots, they are independent of sample concentration. The values of  $M_{\rm sat}$  (in  $\mu_{\rm B}$  = Bohr magnetons) are concentration dependent and they provide spin concentration,

i.e., fraction of unpaired electron per radical site, e.g.,  $M_{\rm sat} = 1.0~\mu_{\rm B}$  implies perfect, 100% spin concentration per radical site. <sup>110-113,115,148</sup>

For pure polycrystalline radicals, measurement of M vs. T at fixed values of H (e.g., 3, 0.5, and 0.05 Tesla) in both warming and cooling modes allows for routinely obtaining reliable  $\chi T$  vs. T plots in the wide temperature range (1.8–400 K). With the oven option for SQUID instrument, an extended temperature range of up to 800 K is available (Figure 18).

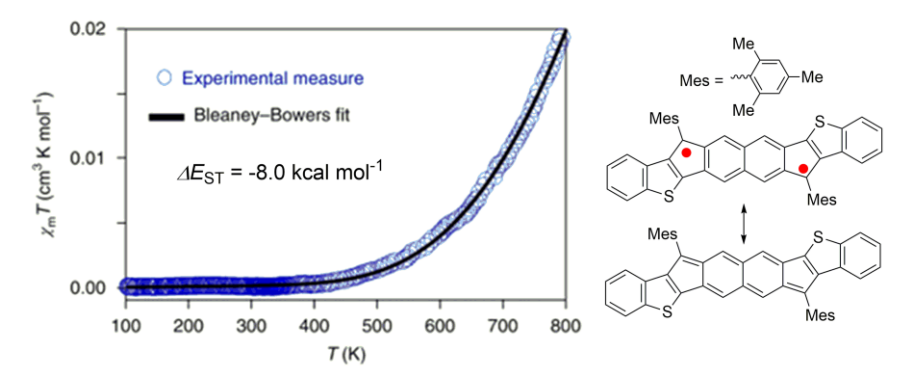


**Figure 18.** Example of SQUID magnetometry in the temperature range of 100 - 800 K, with fit to  $\chi T$  vs. T data giving  $\Delta E_{\rm ST} \approx -8.0$  kcal mol<sup>-1</sup>. <sup>334</sup> Reproduced with permission from ref 334. Copyright 2018 Springer Nature.

To obtain reliable values of  $\chi$ , especially at high T (near or above the room temperature) two critical conditions must be met.

(1) The sample must be perfectly free of magnetic impurities (e.g., rust or other magnetic metal contaminants); i.e., as a minimum,  $\chi T$  vs. T plots must be coinciding at widely different values of H, (2) A reliable correction for diamagnetism should be performed; as Pascal constant-based correction usually overestimates amount of diamagnetism, and thus leads to overestimated values of  $\Delta E_{\rm ST}$  – a common problem in the literature. A better approach is to do point-by-point correction with the diamagnetic precursor to the radical.

For a dilute radical in solution/matrix, obtaining a reliable  $\chi T$  vs. T plot is much more challenging. First, the positive  $M_{\rm rad} > 0$  with  $M_{\rm rad} \sim 1/T$  from radical will be superposed on a large negative  $M_{\rm matrix}$ < 0 that is constant (i.e., independent of temperature); therefore, it is expected that for the measured M=  $M_{\rm rad} + M_{\rm matrix}$ , diamagnetic M < 0 values at high T and paramagnetic M > 0 at low T will be obtained. Consequently, at some intermediate temperature range where  $M \approx 0$ , the value of M could not be measured reliably. Second, correction for diamagnetism is much more demanding; for solution samples, complete point-by-point correction is practical for radicals with limited persistence,<sup>31</sup> and for polymer matrix samples, point-by-point correction can be carried out in order to at least offset the diamagnetism of the matrix and the sample holder.<sup>148,150</sup> Third, while for thermally robust di- and triradicals in polystyrene matrix ( $T_g = 373$  K), in custom-made quartz tubes, practical temperature range of 1.8 - 370 K is available.<sup>148,149</sup> For radicals in organic solvents (e.g., THF and 2-MeTHF), a more limited range of 1.8 - 150 K is typical.<sup>110-113,115</sup> (For a relatively concentrated, 20 mM tetraradical in 2-MeTHF, the  $\gamma T$  vs. T data in the 1.8 - 200 K in the cooling mode could be obtained.)<sup>214</sup>

Once a reliable  $\chi T$  vs. T plot is obtained, and assuming that no strong intermolecular exchange interactions are present, the ground state may be determined as outlined in the EPR spectroscopy Section 4.2.1. Because the SQUID data are typically obtained with less scatter, compared to  $\chi T$ -values in quantitative EPR spectra, the more reliable values of  $\Delta E_{\text{LS-HS}}$  may be extracted from fits to the  $\chi T$  vs. T (or  $\chi$  vs. T) data; in the case, of a flat  $\chi T$  vs. T plot, significantly more robust limiting values for  $\Delta E_{\text{LS-HS}}$  (or  $|\Delta E_{\text{LS-HS}}|$ ) are available from SQUID measurements.

As shown in the Figure 19 (below), determination of ground state and  $\Delta E_{ST}$  for a diradical faces the following challenges:

- (1) for very low values of  $\Delta E_{ST} \sim \pm 2$  K the sample must consist of magnetically isolated diradicals, that is, laborious SQUID studies on progressively more dilute samples are needed and
- (2) for very high values  $\Delta E_{\rm ST} > 1000$  K, correction for diamagnetism has to be perfect and the sample should be perfectly pure, especially without traces of magnetic impurities; for example, when the highest temperature of measurement is typical 300 K, the relative difference in  $\chi T$  is only of the order of 1.1%, when comparing diradicals with  $\Delta E_{\rm ST} = 1000$  K and  $\Delta E_{\rm ST} = 2000$  K; when comparing  $\Delta E_{\rm ST} = 2000$  K and  $\Delta E_{\rm ST} = 4000$  K, the difference becomes a negligible 0.04%.

The plots in Figure 19, also illustrate why diradicals with  $\Delta E_{\rm ST} >> 0.6$  kcal mol<sup>-1</sup> are important. That is for a diradical with  $\Delta E_{\rm ST} > 2.0$  kcal mol<sup>-1</sup>, occupancy of the triplet state is greater than ~99% at room temperature. It should be noted that, for a diradical, value of  $\chi T$  (in emu K mol<sup>-1</sup> and g = 2) is equal to a molar fraction of triplet state.

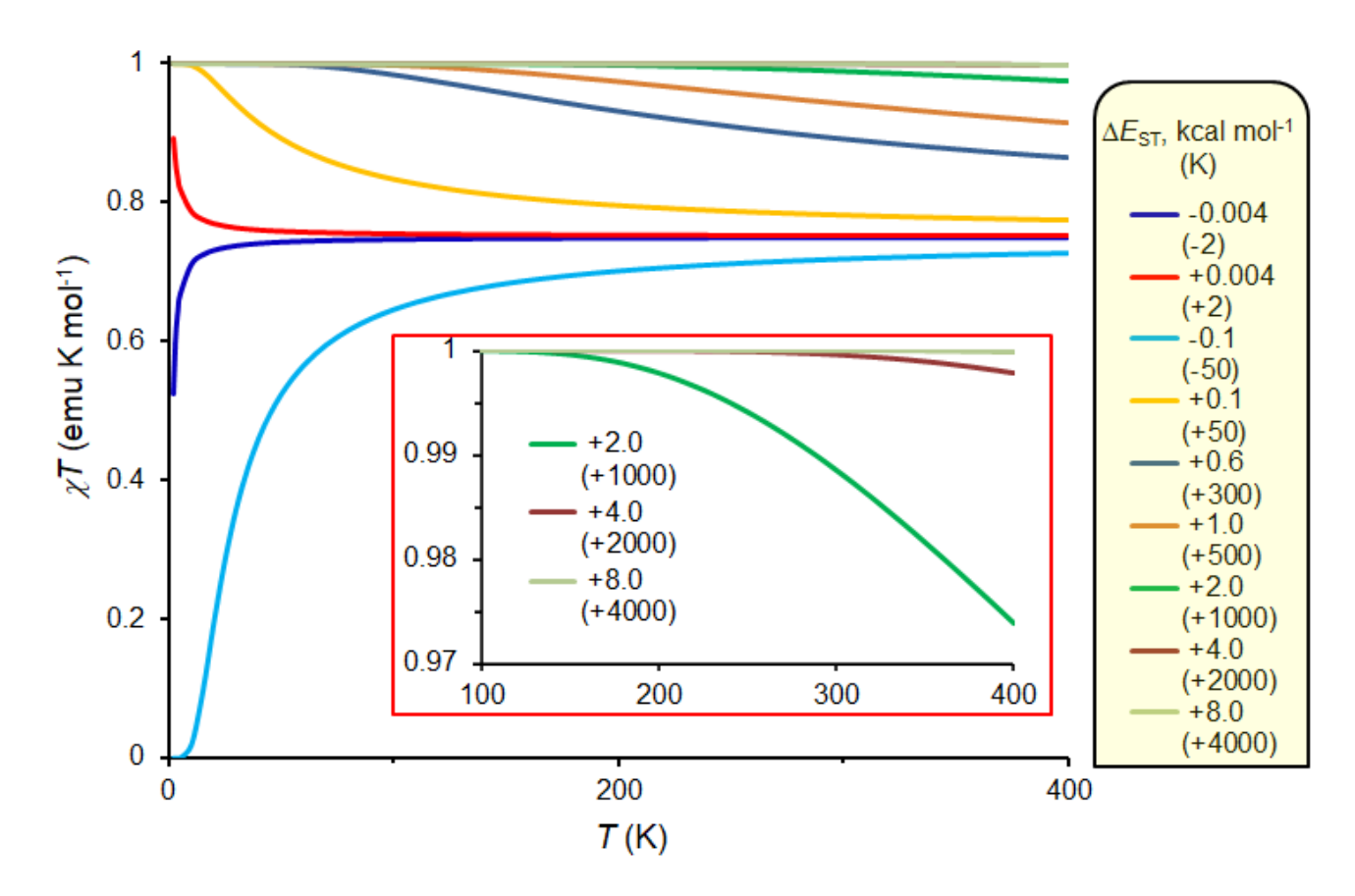


**Figure 19.** Plots of  $\chi T$  vs. T, with T=2-400 K, for diradicals with various values of  $\Delta E_{\rm ST}$ . Note that value of  $\chi T$  (as plotted in emu K mol<sup>-1</sup> and g=2) is equal to a molar fraction of triplet state; alternatively,  $\chi T^*100\%$  is equivalent to a percent occupancy of triplet state. Inset plot: expanded plot for diradicals with  $\Delta E_{\rm ST}=2.0-8.0$  kcal mol<sup>-1</sup> (1000 – 4000 K) illustrating challenge of determination large values of  $\Delta E_{\rm ST}>2.0$  kcal mol<sup>-1</sup>.

We also note the feasibility of determining relatively small  $\Delta E_{\rm LS-HS}$  (and especially negative) based on fitting the plots of normalized magnetization  $M/M_{\rm sat}$  vs. H/T at low temperatures, e.g.,  $\Delta E_{\rm ST} \sim -1$  K, H=0-5 Tesla, T=1.8-3 K. In this approach, the thermal population of  $m_{\rm S}$ -substates is perturbed by the presence of nearby low-spin state.  $^{214,321,323}$ 

Although rarely used, the variable temperature NMR-based paramagnetic shift method may be used to assess  $\Delta E_{\rm ST} \approx RT$ ,  $^{313,335}$  analogously to the IT vs T data, where I corresponds to the EPR

intensity, in variable temperature EPR spectroscopy. In addition, <sup>1</sup>H NMR Evans method<sup>336,337</sup> is occasionally used to determine values of  $\chi T$ , especially at room temperature – this is a useful tool to confirm purity of radicals.<sup>214,217</sup>

### 4.3. High-spin di- and triradicals based on nitronyl nitroxide (NN)

According to Ovchinnikov parity models, trimethylenenemethane (TMM) is a high-spin diradical possessing a triplet ground state with  $\Delta E_{\rm ST} \approx 16$  kcal mol<sup>-1</sup> (Figure 15).  $^{318,319}$  TMM is a great prototype for designing high-spin radicals.  $^{35,124}$  Moreover, nitronyl nitroxide can be regarded as a potential TMM-type radical if the C2 position, possessing negative spin density, is connected to other radical center with positive spin density at the atom X, forming C2-X bond; consequently, a diradical with high-spin ground state is obtained (Figure 20). Alternatively, when the spin density at atom X is negative (e.g., a node in the SOMO at atom X), then the singlet ground state diradical, with connectivity analogous to TME (Figure 15), is obtained (Figure 20).

**Figure 20.** The structures of trimethylenenemethane (TMM) and tetramethyleneethane (TME), and C2-substituted nitronyl nitroxides.

In general, radical stability could be improved when radical center is well shielded by bulky groups, or its spin density delocalized via resonance. Among many types of radicals, nitroxides play pivotal

role in radical families. Most of nitroxides are stabilized by tertiary alkyl groups at  $\alpha$ -carbon position to prevent dimerization or hydrogen abstraction. In addition, spin delocalization over two nitrogen and two oxygen atoms provides good thermodynamic and chemical stability. In summary, the nitronyl nitroxides possess excellent stability, enabling wide range of applications.  $^{253,338}$ 

#### 4.3.1. Synthetic routes to high-spin nitronyl nitroxide-based radicals

In 1968, Osiecki and Ullman first reported a new stable nitroxide radical called nitronyl nitroxide,  $^{212}$  which was prepared by condensation of aldehydes with 2,3-bis(hydroxyamino)-2,3-dimethylbutane followed by oxidation reaction with NaIO<sub>4</sub> (Scheme 1).  $^{339}$  It is worth noticing that for nitronyl nitroxide with R = H (Scheme 1), the pK<sub>a</sub> of the C2-H (C2 is the carbon atom between two nitrogen atoms) is 21.9,  $^{340}$  allowing many further modifications after deprotonation, including reactions with electrophilic reagents.  $^{341,342}$  Since seminal derivative R= Au-PPh<sub>3</sub> (NN-Au) reported by Okada group,  $^{343,344}$  a series of organometallic derivatives R = M-L have been prepared and investigated,  $^{342-347}$  such as, R = Li from Tretyakov group  $^{342}$  and R = ZnCl from Suzuki group.  $^{346}$  Those NN derivatives dramatically promote the discovery of high-spin radicals though direct coupling compared to the condensation reactions.

The NN-based high-spin di- or tri-radicals are generally prepared through condensation or coupling method. In the condensation reaction, the nitronyl nitroxide is synthesized through reaction of aldehydes (R-CHO) and 2,3-bis(hydroxyamino)-2,3-dimethylbutane and followed by oxidation reaction. If the R group in aldehydes is either a stable radical or it can be converted to radical fragment, the final NN-based high-spin di- and triradicals are possible (*vide infra*). However, this approach requires multistep reactions to construct final high-spin molecules, and the yield sometimes is far from satisfying.

An alternative approach is based on the low pK<sub>a</sub> of C2-H, which was mentioned in the preceding

paragraph. This allows for C2-functionalization of nitronyl nitroxide by deprotonation with NaOH or LHMDS, and then reacting with electrophilic reagents, such as nitrones,<sup>349</sup> or cross-coupling with aryl iodide.<sup>344-346</sup> One of the recent advances involve the use of electron rich sterically encumbered phosphines as ligands in NN-Au or in Pd-catalysts, which enables cross-couplings with aryl bromides or electron-rich open-shell aryl iodides.<sup>149,350</sup> This direct coupling method also can install skeletons of high-spin NN radicals, providing a powerful and flexible way to synthesize and increase the diversity of high-spin NN radicals. Based on these two approaches, high-spin radicals have been synthesized (Scheme 1).

**Scheme 1.** Synthetic approaches to nitronyl nitroxide-based high-spin radicals.

### 4.3.2. High-spin nitronyl nitroxide-based neutral di- and triradicals

The simplest stable TMM-analogues are based on the connection of the NN (or imino nitroxide) moiety with alkyl or aryl nitroxide fragments (Figure 20); the short through-bond pathway between two spin centers leads to strong ferromagnetic exchange interactions in diradicals  $\mathbf{1} - \mathbf{4}$  (Figure

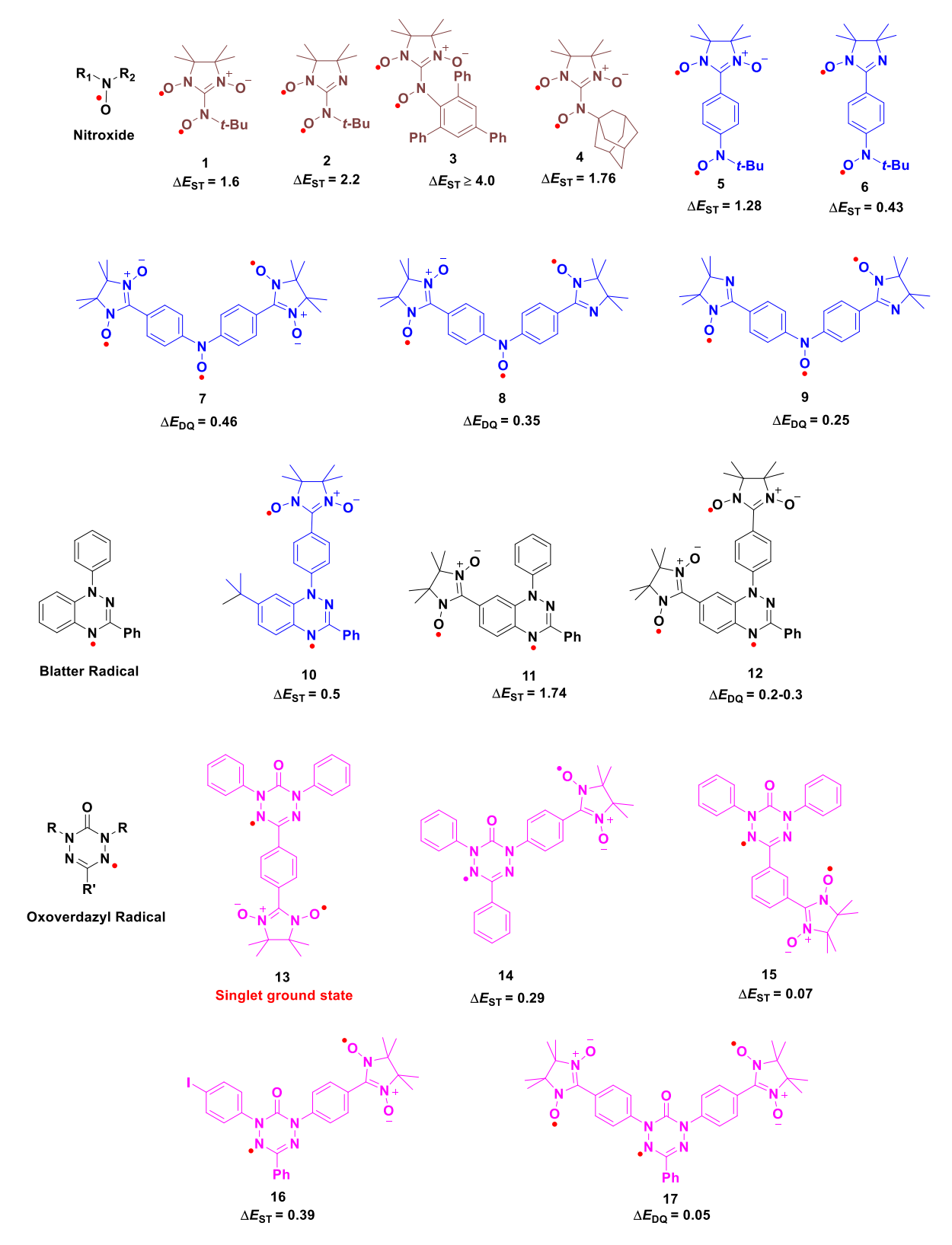


**Figure 21.** Structures of stable, neutral high-spin di- and tri-radicals based on the nitronyl nitroxide.  $\Delta E_{\rm ST}$  and  $\Delta E_{\rm DQ}$  (doublet quartet energy gap) are in kcal mol<sup>-1</sup>.

In 2010, Okada and co-workers prepared nitronyl nitroxide **1** and imino nitroxide **2**.<sup>349</sup> Diradical **1** was assembled by nucleophilic addition of the 2-lithio(nitronyl nitroxide) with *tert*-butyl nitrone

followed by oxidation with lead (VI) dioxide. Deoxygenation of nitronyl nitroxide 1 by nitrous acid provided imino nitroxide 2. Using analogous nucleophilic addition strategy, the same group synthesized diradical 3 in 2022,<sup>351</sup> and very recently, Tretyakov group synthesized diradical 4.<sup>352</sup>

These diradicals are stable under ambient conditions and possess strong ferromagnetic interactions: reported values of  $\Delta E_{\rm ST}$  are 1.56, 2.2, >4.0, and 1.76 kcal mol<sup>-1</sup> for 1, 2, 3, and 4 respectively. Furthermore, 1 and 2 can be sublimed at 55 – 70 °C without decomposition under reduced pressure. The dihedral angles between the nitronyl nitroxide and C, N, O unit of the *tert*-butylnitroxide group in 1 and 2 are 73° and 40°, which may explain the larger  $\Delta E_{\rm ST}$  in 2 since an enhanced intramolecular exchange interaction with less torsional angle. Analogous dihedral angles in 3 and 4 are 18 and 64°. We note that diradicals 1 and 2 are analogous to diradicals 5 and 6, and the stronger intramolecular exchange interactions stem from the shorter exchange coupling pathway between two spin centers.

The EPR spectra of **1** and **2** in glassy diethylphthalate matrix exhibit  $|\Delta m_S| = 1$  and partially forbidden  $|\Delta m_S| = 2$  transitions, characteristic for triplet state of a diradical (Figure 22). Stronger  $|\Delta m_S| = 2$  transition of **2** agrees with larger spectral width (higher |D| value) of the  $|\Delta m_S| = 1$  transitions. Diradical **1** and **2** possess strong intramolecular interactions and weak intermolecular interactions based on SQUID results. When decreasing temperature from 300 to 150 K, the  $\chi T$  vs T plots of diradical **1** increase from 0.983 emu K mol<sup>-1</sup> to 1.000 emu K mol<sup>-1</sup>. Compared to diradical **1**, the  $\chi T$  vs T plots of radical **2** is slightly increased from 0.990 emu K mol<sup>-1</sup> to 0.995 emu K mol<sup>-1</sup> for broader temperature range of 300 to 100 K. When lowering temperature from 150 to  $\sim$ 2 K,  $\chi T$  values of diradical **1** and **2** decrease dramatically due to the intermolecular antiferromagnetic interaction. The plots of  $\chi T$  vs T are fitted to the modified Bleaney-Brower equation (eq. 5) for diradical ( $H = -2JS_1 \cdot S_2$ ).

$$\chi T = \frac{2N_A \mu_B^2 g^2 T}{k_B (T - \theta) [3 + \exp\left(-\frac{2J}{k_B T}\right)]}$$
 (5)

Where  $N_A$  is the Avogardo constant,  $\mu_B$  is Bohr magneton and  $k_B$  is Boltzmann constant. Mean-field

parameter  $\theta$  (in K) is used to characterize the strength of intermolecular interaction.<sup>7</sup> When the  $\theta$  is positive value, it suggests ferromagnetic interaction between molecules. Otherwise, negative  $\theta$  value means antiferromagnetic interaction between molecules. Diradical 1 and 2 have moderate antiferromagnetic interactions with  $\theta$  value of -1.5 and -2.7 K, respectively. The key parameters for magnetic characterization of diradicals 1 – 4 are listed in Table 4.3.2.

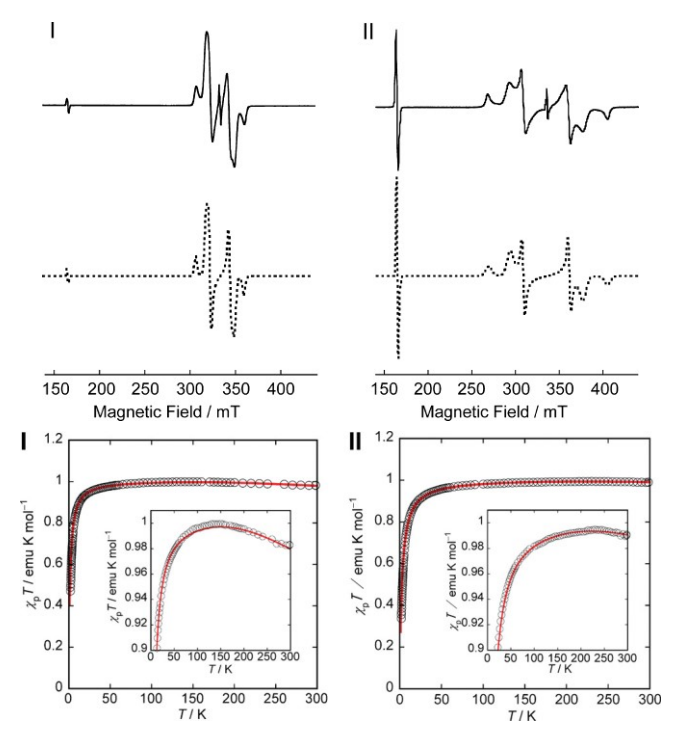


**Figure 22.** Top: EPR spectrum of **1** (I) and of **2** (II) measured in frozen diethylphthalate matrix at 200 K with v = 9.416402 GHz (for **1**) and v = 9.425181 GHz (for **2**). Bottom: Variable temperature  $\chi T$  vs T for **1** (I) and **2** (II). The red solid lines are the simulation lines based on a modified Bleaney-Bowers model. Reproduced from ref. 349. Copyright 2010 American Chemical Society

Table 4.3.2. Magnetic properties of diradicals 1, 2, 3, and 4.

Radical		D	E	J/k	
		(MHz)	(MHz)	(K)	
1	EPR/SQUID	758	48	390	
2	EPR/SQUID	1916	150	550	
3	EPR/SQUID	561	38	>1000	
4	EPR/SQUID	845	60	440	

oxyamino)phenyl]-4,4,5,5-tetramethyl-4,5-dihydroimidazol-3-oxide-l-oxy and analogous iminonitroxide diradical **6** (Figure 21).<sup>348</sup> The diradical **5** was prepared by condensation method and isolated as violet needles. X-ray crystal structure of **5** shows the three moieties, nitronyl nitroxide, *para*phenylene ring and C, N, O unit of the *tert*-butylnitroxide group, are twisted (the dihedrals are 27° and  $22^{\circ}$ , respectively). The moderate dihedrals facilitate the delocalization of spin densities, producing large intramolecular exchange interaction. Polycrystalline diradical **5** and **6** form chain structure with the contacts between the NO groups as the intermolecular antiferromagnetic interactions. Subsequently,  $\Delta E_{ST}$  is determined to 1.28 kcal mol<sup>-1</sup> for diradical **5** and 0.43 kcal mol<sup>-1</sup> for imino-nitroxide diradical **6** by spin-1/2 Heisenberg ferromagnetic-antiferromagnetic alternating chain model (HFAA chain model).<sup>353</sup>

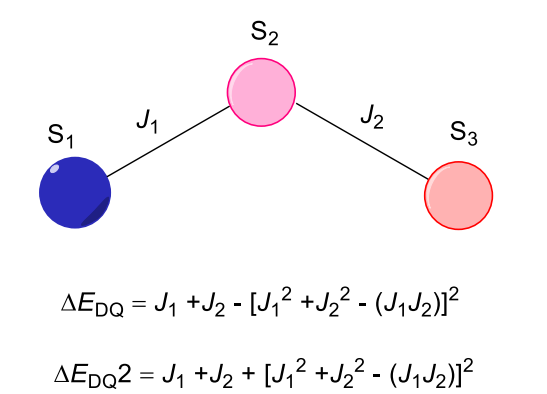
Subsequently, Iwamura group synthesized triradical 7,354 using condensation method, as they utilized in preparation of diradical 5. By deoxygenation of 7, imino-nitroxide (IN) triradicals 8 and 9 were obtained.<sup>354</sup> These triradicals are stable and isolated as powders. X-ray crystal structure of 8 shows the NN moiety has resonance contribution of quinonoid form, while IN moiety does not contribute to such resonance form. Specifically, two short C-C bond distances are 1.370 Å and four long C-C bond distances are 1.401 – 1.431 Å in para-phenylene ring linked to the NN moiety, leading to the change from a regular hexagon structure towards a bond-alternating quinonoid structure. However, the C-C bond distances in para-phenylene linked to the IN moiety are more uniform (1.380 - 1.411 Å) and the ring maintains the regular hexagon structure. The quinonoid form enhances the exchange interaction between center nitroxide and nitronyl nitroxide (Figure 23); therefore, the exchange coupling  $J_1/k$  and  $J_2/k$  in 8 are expected to be different. This phenomenon was not obvious in diradical 5: the crystal structure analysis shows the bond distances in para-phenylene ring is changed by 0.01 - 0.02 Å (two short C-C bond distances: 1.365 and 1.373 Å, four long C-C bond distances: 1.387 – 1.393 Å).348 The quinonoid form enhances the exchange interaction between nitroxide and nitronyl nitroxide; therefore, the exchange coupling  $J_1/k$  in 5 vs. 8 are expected to be somewhat different (Figure 24).

Figure 23. The resonance structures of 5 and 8, and selected bond distances (Å).

EPR spectra of triradicals 7 - 9 in glassy 2-methyltetrahydrofuran at 7 - 12 K show an intense center peak for all triradicals. All the  $\chi T$  vs T plots of triradicals show the magnetic susceptibilities increase from 300 K to roughly 60 K then decrease dramatically to 2 K. The former increase is due to the greater population of molecules in the quartet ground state when temperature is decreasing. The latter decrease comes from the intermolecular antiferromagnetic interaction at lower temperature. The intramolecular coupling constants are determined by the asymmetric linear triradical model (eq. 6).

$$\mathbf{H} = -2(J_1\mathbf{S}_1 \cdot \mathbf{S}_2 + J_2\mathbf{S}_2 \cdot \mathbf{S}_3) \tag{6}$$

Where  $J_1$  ( $J_2$ ) is the exchange coupling constant between  $S_1$  and  $S_2$  ( $S_2$  and  $S_3$ ); eq. 6 corresponds to specific case for a more general eq. 4. Intramolecular coupling constant  $J_{13}$  between two terminal radicals is ignored because it is much smaller than  $J_1$  and  $J_2$ . Here  $J_{13}$  is assumed to be 2 orders of magnitude smaller than  $J_1$  and  $J_2$ , according to study the properties of one-dimensional nonclassical polymers (NCP).<sup>355</sup> In triradicals 7 - 9, coupling constants are in a good agreement with the intramolecular coupling constants of diradicals 5 and 6 (Figure 24).



Radical		$J_1/k$ (K)	J <sub>2</sub> /k (K)
5	SQUID	319	-
6	SQUID	108	-
7	SQUID	231	231
8	SQUID	349	130
9	SQUID	127	127

Figure 24. Model for exchange coupling in triradicals 7 - 9 (linear triradical model, it is asymmetric when  $J_1 \neq J_2$ ) and doublet-quartet energy gap  $\Delta E_{DQ}$  for the lowest S = 1/2 excited state,  $\Delta E_{DQ2}$  for the second lowest S = 1/2 excited state.<sup>354</sup> The table summarizes exchange coupling constants J/k of diradicals 5, 6 and triradicals 7 - 9.

Annulated hydrazyls such as 1,2,4-benzotriazinyl radical (Blatter radical) and oxoverdazyl radical possess excellent stability. Their stability originates from excellent spin delocalization optimized by  $\pi$ -orbital overlap between the atoms in the 6-membered ring structure, making them great radical fragments for constructing stable high-spin radicals.<sup>3</sup> In addition, Okada and co-workers recently discovered the Pd(0)-catalyzed cross-coupling reaction between gold(I)-nitronyl nitroxide(NN-Au) complex and aryl iodides,<sup>344</sup> inducing the development of cross-coupling reaction between gold(I)-nitronyl nitroxide complex and derivatives of Blatter radical and oxoverdazyl radical.<sup>149,153,154</sup>

In 2016 – 2021, our group had designed and synthesized high-spin diradicals 10,  $^{147}$  11,  $^{148,149}$  and triradical  $12^{149}$  based on NN and Blatter radical (Figure 21). These NN-Blatter diradicals and triradical possess robust thermal stability and good magnetic properties, which have been applied to form thin films via evaporation under controlled conditions.  $^{148,149}$  Diradicals 10 and 11 are originally synthesized by the condensation of corresponding formyl-benzotriazinyl (formyl-Blatter) radical and 2,3-bis(hydroxyamino)-2,3-dimethylbutane followed by oxidation reaction, with isolated yields of 4-12 % and 18-29 % in the multistep syntheses. The overall yield of a similar procedure for triradical 12 is rather low,  $\leq 1\%$ .

In contrast to the disappointing yield under condensation conditions, direct cross-coupling reaction of di-iodo-Blatter radical with **NN-Au** (Scheme 1), using the highly reactive Pd(0)-catalyst, Pd[(*t*-Bu)<sub>3</sub>P]<sub>2</sub>, gives significantly higher 19 – 42 % yield, in a shorter, more convergent synthesis. Similarly, diradical **11** is generated in 30 – 44 % yield when mono-iodo-Blatter radical is cross-coupled with **NN-Au**.<sup>149</sup>

We discuss X-ray crystal structures of **10**, **11**, and **12** (Figure 25) to better understand the structure-property relationships regarding magnetic properties.

In diradical 10, two dihedral angles between the NN moiety and Blatter radical  $\pi$ -system are ~30° and 49°, respectively. Two nonequivalent molecules, A and B, are observed in diradical 11. In molecule A, the NN moiety is nearly coplanar with the Blatter radical  $\pi$ -system with the corresponding torsional angle in the (-13) – (-15)° range, while in molecule B, there is considerably greater out-of-plane twisting with the corresponding torsions of 28 – 30°. In the crystal, molecules A and B pack in an alternating fashion into one-dimensional chains along crystallographic *a*-axis with close intermolecular N···N and O···N contacts.

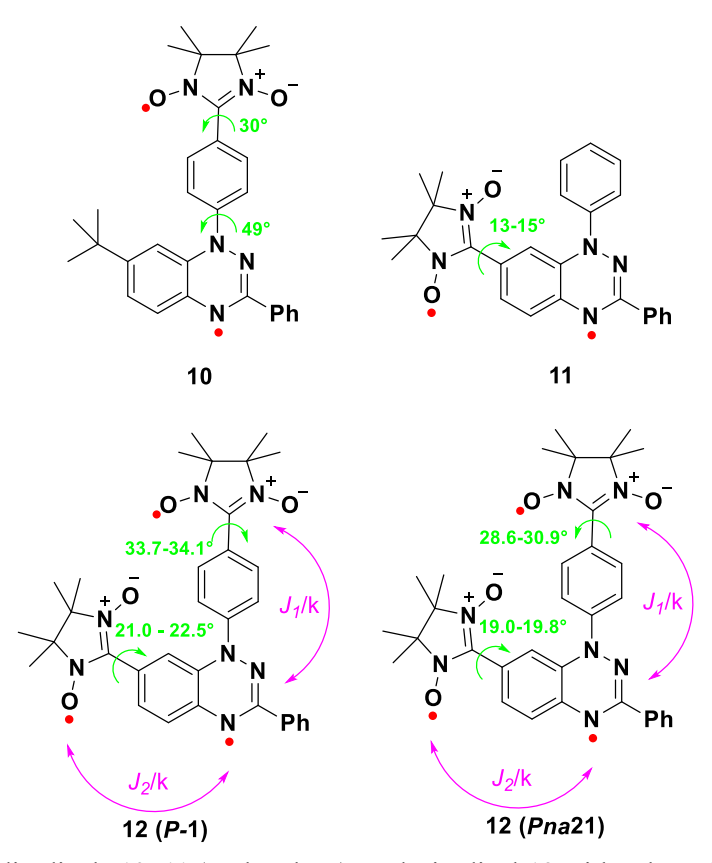


Figure 25. Structures of diradicals 10, 11 (molecule A), and triradical 12 with selected torsional angles. For 12, two pseudo polymorphs are shown.

For triradical 12, two single crystal X-ray structures were obtained: triclinic (centrosymmetric P-1) and orthorhombic (Pna21). The orthorhombic structure contains one molecule of chloroform, which is a solvent polymorph. The two pseudo polymorphs have significantly different crystal packing. The triclinic structure consists of  $C_i$ -symmetric dimers of triradical molecules, while the orthorhombic structure contains one-dimensional  $\pi$ -stacks of triradical molecules. For triclinic structure, both NN moieties are nearly coplanar with the Blatter radical  $\pi$ -system with torsional angles of 21.0 - 22.5° and 33.7 - 34.1°. Similar torsional angles between NN moieties and Blatter radical  $\pi$ -system are found in the orthorhombic structure, i.e., 19.0 - 19.8° and 28.6 - 30.9°. We note that the exchange coupling pathways between NN moiety and Blatter radical  $\pi$ -system are different. Therefore, the exchange couplings constants,  $J_1/k$  and  $J_2/k$ , are expected to be significantly different in 12 (Figure 25).

Furthermore, quantitative EPR spectroscopy and SQUID magnetometry of radicals in various glassy matrices and/or polycrystalline powders give  $\Delta E_{\rm ST} = 0.5$  kcal mol<sup>-1</sup> for **10**,  $\Delta E_{\rm ST} \ge 1.7$  for **11** and  $\Delta E_{\rm DQ} \approx 0.2 - 0.3$  kcal mol<sup>-1</sup>,  $\Delta E_{\rm DQ2} \approx 1.2 - 1.8$  kcal mol<sup>-1</sup> for triradical **12**. Triplet ground states are

established unequivocally by magnetization data. Low-temperature EPR spectra of diradical 10 and 11 show triplet state (S=1) and diradical 10 has a much smaller ZFS parameter |D|, compared to that for 11. For polycrystalline 10 and 11, strong intermolecular antiferromagnetic interactions are observed in SQUID magnetometry. The plots of  $\chi T$  vs. T are fitted to the modified Bleaney-Brower equation for diradical requiring relatively large absolute value of negative mean-field parameters,  $\theta \approx -6$  K and -14 K, respectively. Notably, fitting both  $\chi T$  vs. T and  $\chi$  vs. T data at low temperatures of polycrystalline 11 satisfies 1-D antiferromagnetic S=1 chain model, with relatively large intrachain J'/k=-14 K, which is consistent with its crystal packing.

Low-temperature EPR spectra of triradical 12 show a quartet state (S=3/2) in 2-MeTHF or toluene/chloroform (3:1) glassy matrices. Only a weak  $|\Delta m_S|=2$  transition can be detected and no  $|\Delta m_S|=3$  transition is observed. The spectral width for S=3/2 triradical 12 in toluene/chloroform glass is  $4D\approx 320$  MHz, which is intermediate between  $2D\approx 140$  MHz for S=1 diradical 10 and  $2D\approx 480$  MHz for 11. This reflects the intermediate strength of magnetic dipole-dipole interactions in 12 that dominate the EPR spectra in glassy matrices. Energy gaps  $\Delta E_{DQ}\approx 0.2$  kcal mol<sup>-1</sup> and  $\Delta E_{DQ2}\approx 1.2$  kcal mol<sup>-1</sup> are obtained by variable temperature quantitative EPR spectroscopy on triradical 12 in toluene/chloroform glass/solution. When the triradical 12 is prepared in polystyrene glass and measured by SQUID magnetometry, the quartet ground state is unequivocally confirmed by magnetization data, as well as  $\Delta E_{DQ}\approx 0.30$  kcal mol<sup>-1</sup> and  $\Delta E_{DQ2}\approx 1.83$  kcal mol<sup>-1</sup> are obtained from  $\chi T$  vs T plots. We speculate that different values for doublet quartet energy gaps might be associated with slightly different conformations (dihedral angles) for 12 in different glassy matrices/solutions. Both EPR and SQUID data of triradical 12 are fitted to the asymmetric linear triradical model (Figure 24).

Both diradicals and triradical are very stable and they can be purified by silica gel column chromatography under ambient conditions. It is worth noticing that diradicals 10, 11 and triradical 12

may be viewed as thermally robust; they show onsets of decomposition in thermal gravimetry analysis (TGA) at 175 °C, 160 °C and 160 °C, respectively. Diradical 10 can be sublimed without decomposition at 140 °C under vacuum ( $p \approx 6 \times 10^{-6}$  mbar). Such excellent thermal stable di- and triradicals paved avenue for further pure organic high-spin materials designs and applications. The diradical 11 and triradical 12 were evaporated under ultra-high vacuum (UHV) conditions to form thin films (ca. 1 nm nominal thickness) on SiO<sub>2</sub>/Si (111) wafers by using organic molecular beam deposition (OMBD) at room temperature. The films were investigated by X-ray photoelectron spectroscopy (XPS), which can report on the chemical environment of C 1s core and N 1s core. Specifically, the C 1s core level line and the N 1s core level line of diradical 11 and triradical 12 are similar since they are both from NN moieties and Blatter radical  $\pi$ -system and have similar chemical environment. Specifically, the spectra show 3 types of carbon and 4 types of nitrogen with different ratios, e.g., the high bonding energy peak (~402 eV) in N 1s core level spectrum of triradical 12 is more intense than that of diradical 11 owing to the contribution of two NN moieties. While the films are stable under UHV, they show signs of decomposition in XPS after few hours at ambient conditions. 148,149 Notably, drop-cast films of 12, with thickness of the order of hundreds nm, show much slower decay at ambient conditions, with XPS spectra showing saturation (plateau) behavior after a few days. 149

Recently, a series of high-spin radicals 14 – 17 have been designed and synthesized in good yields via the cross-coupling reaction of iodo-oxoverdazyl radicals and NN-Au by Tretyakov and coworkers. 153,154 The design is similar relying on connection of two stable radicals to provide TMM topology, which generates a spin exchange coupling through the connecting C-C bond. However, the degree of spin delocalization onto the phenyl groups in oxoverdazyl radical is smaller than that in Blatter radical, leading to lower spin density at the carbon, which is bonded to carbon C2 of the NN moiety. Consequently, significantly weaker exchange couplings between oxoverdazyl radical and

nitronyl nitroxide are found. Thus, these diradicals and triradicals possess rather small  $\Delta E_{\rm ST}$  and  $\Delta E_{\rm DO}$ . 153,154

All these radicals are very stable, and they can be purified by silica gel column chromatography under ambient condition as well. In addition, diradicals **13**, **14** and **15** show an apparent onset of decomposition in TGA at 217 °C, 192 °C and 183 °C, respectively. No TGA data of diradical **16** and triradical **17** was reported.<sup>154</sup>

In these radicals, different torsional angles  $(9-36^{\circ} \text{ in } 13-15, 28.3-51.3^{\circ} \text{ in } 16 \text{ and } 17)$  are found between the NN moieties and respective phenyl rings, and between the phenyl rings and oxoverdazyl moieties  $(13-47^{\circ} \text{ in } 13-15, 6.9-53.2^{\circ} \text{ in } 16 \text{ and } 17)$ .

Singlet ground state for diradical 13 is confirmed by SQUID magnetometry and characterization of 13 will not be discussed here. Low-temperature EPR spectra of diradical 14 and 15 are recorded. Simulation of low-temperature EPR spectra of diradical 14 and 15 show axial symmetry (E = 0). Larger |D| for diradical 15 is consistent with stronger  $|\Delta m_S| = 2$  transition. The simulation of room temperature EPR spectra of 14 and 15 corresponds to 6 nitrogen hyperfine interaction (2 from NN moiety and 4 from verdazyl moiety). For diradical 16 and triradical 17, only room temperature EPR spectra are reported. Simulations of EPR spectra for 16 and 17 indicate that the hyperfine couplings originate from 6 and 8 nitrogens ( $^{14}$ N), respectively.

Polycrystalline samples of diradicals 14-16 and triradical 17 are investigated by SQUID magnetometry. The  $\chi T$  vs T data for diradical 14 and 15 show the value of  $\chi T$  is close to 0.75 K·emu·mol<sup>-1</sup> at 300 K, which is close to the theoretical value of two magnetically independent  $S = \frac{1}{2}$  spins. Relatively small singlet-triplet energy gaps,  $\Delta E_{\rm ST} \approx 0.29$  kcal mol<sup>-1</sup> for 14,  $\Delta E_{\rm ST} \approx 0.07$  kcal mol<sup>-1</sup> for 15 are reported. High-spin diradical 16 and triradical 17 have moderate low-spin high-spin energy gaps,  $\Delta E_{\rm ST} \approx 0.39$  kcal mol<sup>-1</sup> for 16, and  $\Delta E_{\rm DQ} \approx 0.05$  kcal mol<sup>-1</sup>, and  $\Delta E_{\rm DQ2} \approx 0.43$  kcal mol<sup>-1</sup> for 17, obtained by fitting to the modified Bleaney-Bowers equation of diradical and the asymmetric linear

triradical model (Figure 24), respectively.

## 4.3.3. High-spin nitronyl nitroxide-based diradical anions

The radical metal complexes are significant in the design of single-molecule magnet (SMM) because the paramagnetic spin centers can be bridges between metal centers and enhance the spin exchange interaction between metal centers and radicals. Among these radicals, both semiquinone radical anion and nitronyl nitroxide radical are widely used as paramagnetic ligands in SMMs.

In 2000 and 2003, Shultz and co-workers reported semiquinone-nitronyl nitroxide diradical anion Zn complexes 18 and 19 (Figure 26). 357,358 The complexes 18 and 19 were prepared by the condensation method (Scheme 1), starting with catechol-aldehyde synthetic intermediate, and then reacted with metal complexes and oxidized on air. Magnetic susceptibilities of polycrystalline complexes 18 and 19 are measured by SQUID magnetometry. Notably, strong intramolecular ferromagnetic coupling constant J in 18 is estimated as the lower limit >0.89 kcal mol<sup>-1</sup> (>310 cm<sup>-1</sup>) by the absence of curvature in the plot of  $\chi T$  vs T of polycrystalline sample. Intramolecular coupling constant J in 19 is determined to 0.28 kcal mol<sup>-1</sup> (100 cm<sup>-1</sup>) by fitting to the Bleaney-Brower equation without intermolecular interaction.

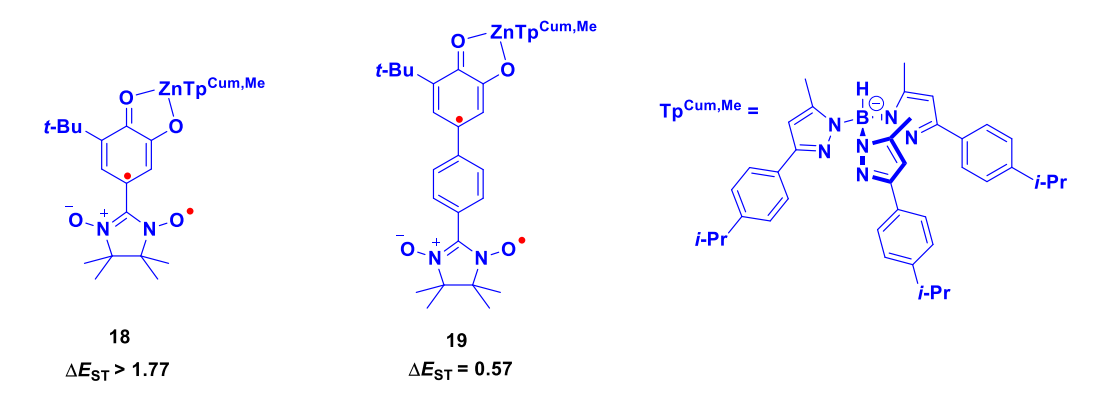


**Figure 26.** Structures of Shultz semiquinone – nitronyl nitroxide high-spin diradicals (diradical anions). Values of  $\Delta E_{ST}$  are in kcal mol<sup>-1</sup>.

## 4.3.4. High-spin nitronyl nitroxide-based di- and triradical cations.

Stable organic radical cations provide another attractive feature in the design of high-spin di- and triradicals. The important prerequisite for the design of stable radical-substituted radical cation systems is that the 1<sup>st</sup> oxidation potential ( $E_1^{\circ}$ ) for the radical is significantly more positive, compared to the 1<sup>st</sup> oxidation potential of the neutral precursor to the radical cation. Because heteroatom substituted extended  $\pi$ -systems have typically  $E_1^{\circ}$  of the order of +0.5 V (vs. SCE), nitronyl nitroxide with  $E_1^{\circ} \approx$  +0.9 V<sup>311</sup> for nitronyl nitroxide or even oxoverdazyl  $E_1^{\circ} \approx$  +0.6 V (vs. SCE)<sup>359</sup> are good choices. We note that Blatter radical ( $E_1^{\circ} = +0.10 \text{ V}$ )<sup>360</sup> and phototetrazolinyl radical **DiCN-PHT** ( $E_1^{\circ} = -0.14 \text{ V}$ ) (Figure 3)<sup>161</sup> are too easy to oxidize, and thus they are not suitable.

In 2000, thianthrene linked nitronyl nitroxide radicals 20, 21, and 22 were synthesized by Sugawara and co-workers (Figure 27). High-spin states in diradical cation and triradical cations are detected by pulsed EPR nutation spectroscopy at low temperatures. However, the energy gaps,  $\Delta E_{\rm ST}$  and  $\Delta E_{\rm DQ}$  were not measured. We note that the 1st oxidation potential for thianthrene,  $E_1^{\circ} = +1.26$  V (vs. SCE), though comparable to  $E_1^{\circ} \approx +0.9$  V for nitronyl nitroxide, implies that a significant fraction of nitronyl nitroxide radical will get oxidized to diamagnetic cation, giving complex mixtures of radicals.

More recently, Okada and his co-workers have rationally designed and synthesized high-spin stable NN-linked electron donors di- and triradical cations, based on diphenyldihydrophenazine (DPP<sup>-+</sup>-NN, **23** – **25**),<sup>361,362</sup> trioxytriphenylamine (TOT<sup>-+</sup>-NN, **26** and DOTT<sup>+</sup>-NN, **27**),<sup>363,364</sup> and phenothiazine (PTZ<sup>-+</sup>-NN, **28**).<sup>365</sup> These high-spin di- and triradical cations **23**, **25** – **28** have good stability and large intramolecular exchange couplings between electron-donor moiety and nitronyl nitroxide (Figure 27).

In 2004, Okada and co-workers synthesized high-spin diradical cation **23** based on diphenyldihydrophenazine (DPP<sup>·+</sup>-NN).<sup>361</sup> The diradical cation salt can be isolated as perchlorate (ClO<sub>4</sub><sup>-</sup>) salt and is stable at ambient conditions. X-ray crystallography of **23** shows formation of a

dimer (Figure 28). Intramolecular interaction in polycrystalline 23 is determined from  $\chi T$  vs. T data using SQUID magnetometry. Lower limit for singlet triplet energy gap,  $\Delta E_{\rm ST} \geq 2.8$  kcal mol<sup>-1</sup>, is obtained by fitting dimer model ( $H = -2J_1(\mathbf{S}_{\rm NN1} \cdot \mathbf{S}_{\rm DPhz1} + \mathbf{S}_{\rm NN2} \cdot \mathbf{S}_{\rm DPhz2}) - J_2\mathbf{S}_{\rm DPhz1} \cdot \mathbf{S}_{\rm DPhz2})$ . This result is apparently only reproducible at T > 100 K. However, we doubt the reliability of the finding of such large  $\Delta E_{\rm ST} \geq 2.8$  kcal mol<sup>-1</sup> (or pairwise  $J/k \geq 800$  K) in 23 (*vide infra*). In addition, when tetrabromoferrate (FeBr<sub>4</sub><sup>-</sup>) is used as a counter anion for diradical cation 23, a three-dimensional, long-range ferrimagnet is observed with ordering at  $T_c = 6.7$  K, based upon measurements of dc and ac magnetic susceptibilities and heat capacity.<sup>366</sup>

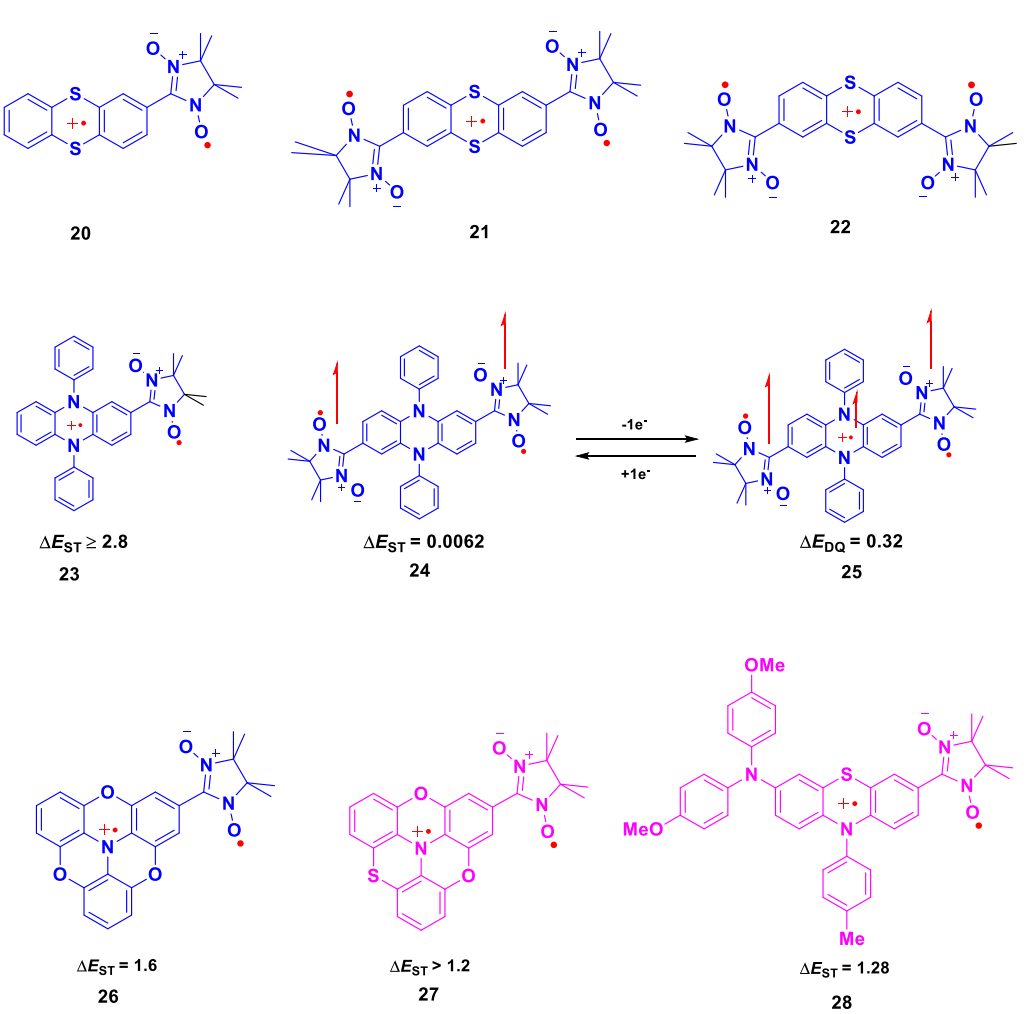


**Figure 27.** Structures of stable high-spin diradicals and triradical cations based on nitronyl nitroxide. Values of  $\Delta E_{\text{ST}}$  and  $\Delta E_{\text{DQ}}$  are in kcal mol<sup>-1</sup>.

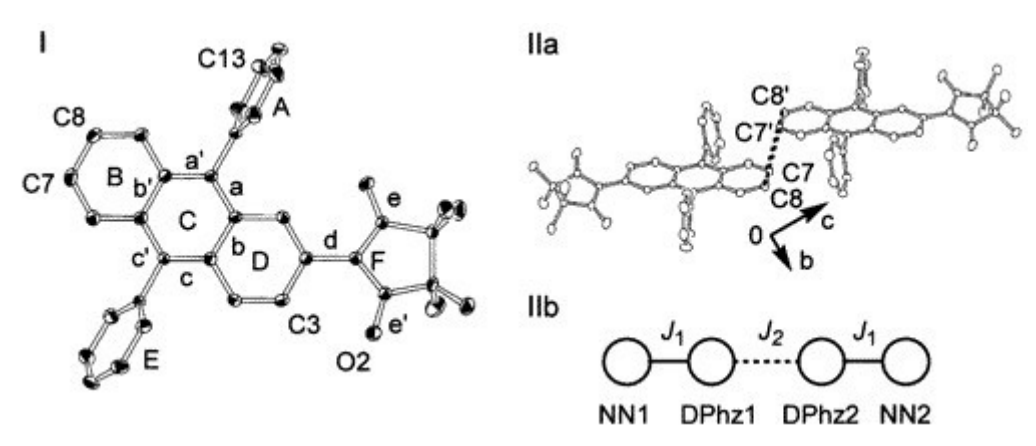


**Figure 28.** Molecular structure (I), a dimer structure in the crystal packing (IIa), and a schematic diagram of magnetic interaction (IIb) for diradical cation **23**. (I) Drawn at 50% ellipsoids level; hydrogen atoms, the counter anion, and the solvent are eliminated for clarity. Reproduced from ref. 361. Copyright 2004 American Chemical Society

In 2020, Okada group reported another high-spin diradical/triradical system based on NN-DPP-NN 24, which can be switched by redox-induced modulation. 362 Triradical cation NN-DPP +-NN 25 is generated by one-electron oxidation of diradical 24. Both neutral diradical and triradical cation are stable and can be isolated as solids. For diradical 24, very weak intramolecular exchange coupling between two nitronyl nitroxide is observed due to the long through-bond, cross-conjugated pathway between two spin centers. In contrast, NN-DPP<sup>-+</sup>-NN 25 has stronger intramolecular exchange interaction because of the shorter exchange coupling pathways and smaller dihedral angles between the dihydrophenazine plane and the NN moieties. EPR spectrum of diradical 24 at room temperature shows a well-resolved nine-line spectrum, which corresponds to four equivalent <sup>14</sup>N nuclei (Figure 29a). EPR spectrum of triradical cation 25 at 200 K show a strong center single peak and two small side peaks. Forbidden  $|\Delta m_S| = 2$  transitions are observed and their intensities are increased when the temperature is decreasing, which suggests the quartet ground state of 25. Intramolecular interactions of polycrystalline 24 and 25 are determined by  $\chi T$  vs T from SQUID magnetometry. High-spin diradical 24 and triradical cation 25 have small singlet-triplet energy gap,  $\Delta E_{\rm ST} = 0.0062$  kcal mol<sup>-1</sup> for 24, and moderate doublet quartet energy gap,  $\Delta E_{DQ} = 0.32 \text{ kcal mol}^{-1} (J/k = 160 \text{ K})$  for 25 by fitting to the modified Bleaney-Brower equation of diradical and symmetric linear triradical model (Figure 24), respectively.

We note that for  $\Delta E_{\rm DQ} \approx 0.3$  kcal  $\rm mol^{-1}$ , there will be a significant population of the lowest  $S = \frac{1}{2}*$  excited state at 200 K; presumably, large part of the difference between the experimental and simulated intensity for the center peak of **25** might be assigned to the  $S = \frac{1}{2}*$  state, in addition to incidental  $S = \frac{1}{2}*$  impurities (Figure 29b). This suggests that the pairwise J/k = 160 is correct, at least concerning order of magnitude; this would imply that pairwise  $J/k \geq 800$  K (and  $\Delta E_{\rm ST} \geq 2.8$  kcal  $\rm mol^{-1}$ ) in diradical cation **23** are badly overestimated (see: further discussion in Section 4.3.5). We add that the pairwise J/k values in the classic Iwamura's nitroxide di- and symmetric triradicals are similar: 319 K (**5**) vs. 231 K (**7**) and 108 K (**6**) vs 127 K (**9**) as illustrated in Figure 24.

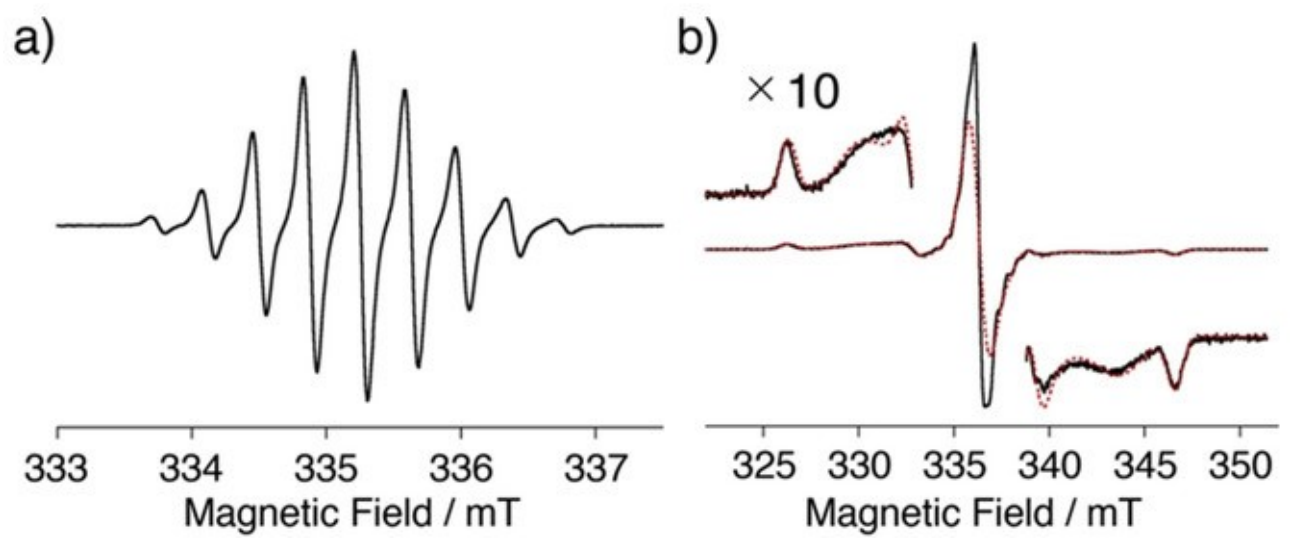


**Figure 29.** EPR spectra of a) **24** in toluene at 293 K (9.41575 GHz,  $g_{iso}$ =2.0067) and b) **25**. For b), black solid and red broken lines showed the observed spectrum of the allowed transition in a glassy diethyl phthalate matrix at 200 K (9.438855 GHz) and simulated spectrum of the quartet species by using  $g_{xx}$ =2.0080,  $g_{yy}$ =2.0040,  $g_{zz}$ =2.0030,  $g_{av}$ =2.0055, |D/hc| =0.00473 cm<sup>-1</sup>, and |E/hc| =0.00057 cm<sup>-1</sup>, respectively. Reproduced with permission from ref. 362. Copyright 2020 Wiley.

Subsequently, Okada and coworkers reported the diradical cations **26** (NN-TOT<sup>+</sup>) and **27** (NN-DOTT<sup>+</sup>) (Figure 27).<sup>363,364</sup> NN-TOT was synthesized by condensation of TOT-formyl derivative with 2,3-bis(hydroxyamino)-2,3-dimethylbutane and followed by oxidation reaction. NN-DOTT was assembled by Pd(0) cross-coupling reaction of iodo-DOTT and NN-Au. X-ray structures show moderate dihedral angles between radical cation plane and NN moiety (28° for **26** and 33° for **27**, respectively), which is helpful in generating large spin exchange intramolecular interaction.

The  $\chi T$  vs T of polycrystalline **26**-GaCl<sub>4</sub><sup>-</sup> and **27**-SbF<sub>6</sub><sup>-</sup> are investigated by SQUID magnetometry. The  $\chi T$  value of **26**-GaCl<sub>4</sub><sup>-</sup> is 0.964 emu K mol<sup>-1</sup> at 300 K and increases to 0.992 emu K mol<sup>-1</sup> at 200 K. This value is so close to 1.000 (pure S=1 spin with g=2.000), which implies there is a strong intramolecular exchange coupling, J/k > 300 K, between the NN moisty and TOT<sup>+</sup> radical cation. Simulation of the  $\chi$  vs T data in the T=3-300 K range, using modified "S=1" Fisher chain model provided intramolecular feromagnetic exchange coupling J/k=400 K and intra-chain (inter molecular) antiferromagnetic exchange coupling J/k=1.85 K; this corresponds to  $\Delta E_{ST}=1.6$  kcal mol<sup>-1</sup> (2J/k=1.85 K).

For 27-SbF<sub>6</sub>,  $\chi T$  value is 0.884 emu K mol<sup>-1</sup> at 300 K and slightly decreases to ~ 0.8 emu K mol<sup>-1</sup> at 100 K. The intramolecular exchange coupling between the NN moiety and DOTT<sup>+</sup> radical cation is assumed to be larger than thermal energy, J/k > 300 K (*vide infra*), and S = 1 (NN-DOTT<sup>+</sup>) spin is applied to  $\chi$  vs T data when simulating the intermolecular antiferromagnetic interactions, using modified Fisher S = 1 chain model. A weak intra-chain interaction, J'/k = -7.4 K, and a comparable inter-chain interaction, zJ''/k = 2.5 K are found. While the fit of  $\chi T$  vs T data with the modified Fisher chain model is satisfactory at low temperatures, near the room temperature, the fit is not as good. Most likely, the interaction between NN moiety and DOTT<sup>+</sup> is not strong enough to regard as a S = 1 spin near the room temperature. We note that the value of  $\chi T = 0.884$  emu K mol<sup>-1</sup> at 300 K is close to 0.89 emu K mol<sup>-1</sup> for a diradical with singlet triplet gap, 2J/k = 300 K (Section 4b2, Figure 19).

In addition, diradical cation 27 shows a magnetic phase transition from the antiferromagnetic state to the weak ferromagnetic state at  $T_N$ = 2.65 K based on susceptibility and heat capacity measurements. For the FeBr<sub>4</sub> salts of 27 magnetic phase transition into a weak ferromagnet at 7 K is suggested.

Recently, Okada also reported a diradical cation **28** (DAA-PTZ-NN<sup>+</sup>) (Figure 27), which was synthesized by Pd(0) cross-coupling reaction of iodophenothiazine DAA-PTZ-I with **NN-Au** (Scheme 1) followed by oxidation reaction of the PTZ moiety to corresponding radical cation. Here, both GaBr<sub>4</sub><sup>-</sup>

(S=0) and FeBr<sub>4</sub><sup>-</sup> (S=5/2) are used as counter anions.<sup>365</sup> The EPR spectrum is relatively narrow with |D|=60 MHz and a weak  $|\Delta m_S|=2$  transition is found for **28**-GaBr<sub>4</sub> in butyronitrile glass at 100 K. The  $\chi T$  vs T plot for polycrystalline **28**-GaBr<sub>4</sub><sup>-</sup> is obtained using SQUID magnetometry. Specifically, the  $\chi T$  value of **28**-GaBr<sub>4</sub><sup>-</sup> is 0.96 emu K mol<sup>-1</sup> at 300 K and the value is approaching 0.99 emu K mol<sup>-1</sup> at 100 K, then the  $\chi T$  value decreases rapidly when temperature is lowered to about 0.5 emu K mol<sup>-1</sup> at 2 K. This indicates a strong intramolecular and weak intermolecular exchange coupling in polycrystalline **28**-GaBr<sub>4</sub><sup>-</sup>. Value of  $\Delta E_{\rm ST}=1.28$  kcal mol<sup>-1</sup> (J/k=320 K) for **28**-GaBr<sub>4</sub><sup>-</sup> is determined. It should be mentioned that diradical cation of NN-PTZ without diarylamine substituent could not be isolated – presumably due to its lack of sufficient persistence.<sup>346</sup>

# 4.3.5. The relation between the hyperfine coupling constant in monoradicals and pairwise exchange coupling constant J/k in NN-based diradicals and triradicals.

Large spatial "coincidence" of spin density at the two adjacent radical fragments, one with  $\alpha$  and one with  $\beta$  spin at the connecting atoms, are necessary for strong ferromagnetic exchange interaction in the resultant TMM-like, NN-based high-spin di- or triradical (Figure 20). Spin density delocalization into the ferromagnetic coupling unit (FCU) can then affect the pairwise exchange coupling constant J/k in the high-spin di- or triradical, with the greater spin density within the FCU, corresponds to the greater J/k.<sup>313</sup> The magnitude of spin density within the FCUs of these high-spin di- and triradicals, and thus the magnitude of pairwise J/k will be governed by two factors: spin density at the atom X within the C2-X bond and average torsion angle  $\theta$  (Figure 30). Since spin density at atom X is directly related to absolute value of hyperfine coupling constant,  $|A(^1H)|$ , for  $^1H$  within the X-H bond in the corresponding monoradical, we should be able to correlate J/k with  $|A(^1H)|$  and  $\theta$  (Figure 30).

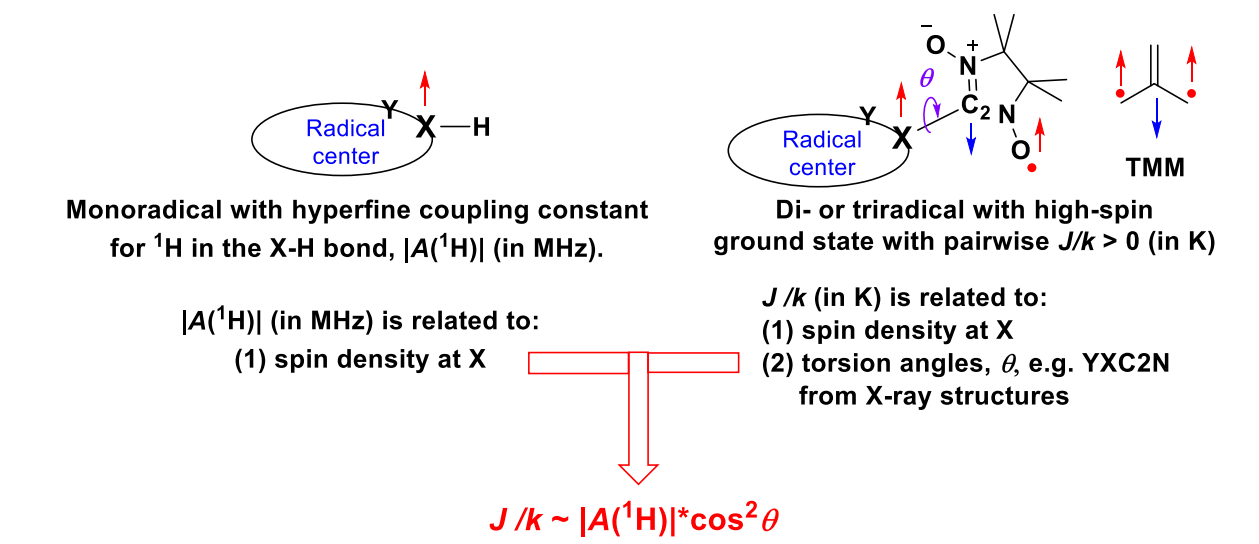


**Figure 30.** Conceptual relationship between pairwise J/k in NN-based high spin di- and triradicals, and  $|A({}^{1}\mathrm{H})|$  in monoradicals.

McConnell's relationship<sup>367</sup> estimates of the spin density at sp<sup>2</sup>-hybridized carbon atom in organic radicals as:

$$A(^{1}\mathrm{H}) = Q_{\mathrm{CH}} * \rho_{\mathrm{C}} \tag{7}$$

where  $A(^{1}\text{H})$  (in MHz) is hyperfine coupling constant for  $^{1}\text{H}$  within the C-H bond and  $\rho_{C}$  is the spin density at carbon. Value of the "constant"  $Q_{CH}$  generally depends on the type of monoradical, as its value decreases with negative and increases with positive charge. Typical values of  $Q_{CH}$  (in MHz or Gauss) fall into the following ranges:

- (1) radical anions, -56 (-76) MHz or -20 (-27) Gauss
- (2) neutral radicals, -64 (-84) MHz or -23 (-30) Gauss
- (3) radical cations, -73 (-90) MHz or -26 (-32) Gauss

A relationship analogous to that in eq. 7 can be applied to sp<sup>2</sup>-hybridized nitrogens: <sup>368,370</sup>

$$A(^{1}\mathrm{H})_{\mathrm{N}} = Q_{\mathrm{NH}} * \rho_{\mathrm{N}} \tag{8}$$

where  $A(^{1}\text{H})_{N}$  is hyperfine coupling constant for  $^{1}\text{H}$  within the N-H bond and  $\rho_{N}$  is the spin density at nitrogen. We will use unambiguously determined value  $Q_{NH} = A(^{1}\text{H})_{N} = -72.5$  MHz ( $A_{NH} = -25.9$  Gauss) in NH<sub>3</sub> radical cation.<sup>371</sup> Because in isoelectronic methyl radical,  $Q_{CH} = A(^{1}\text{H}) = -64.5$  MHz ( $A_{CH} = -23.0$  Gauss), <sup>369</sup> we will use a factor of  $Q_{CH}/Q_{NH}$  to convert experimentally determined values

of  $A(^{1}H)_{N}$  (or  $A_{NH}$ ) to "adjusted  $|A(^{1}H)|$ " (or "adjusted  $A_{CH}$ ").

Values of experimental  $|A_{\text{CH}}|$  (or "adjusted  $|A_{\text{CH}}|$ ") in Gauss for the following monoradicals are converted to  $|A(^{1}\text{H})|$  in MHz, using experimental g-values, as summarized in Figure 31 and Table 4.3.5: methyl nitroxide (its "adjusted  $|A(^{1}\text{H})|$ " is used for tert-butyl nitroxide),  $^{372,373}$  phenyl nitroxide,  $^{374,375}$  tert-butylphenyl nitroxide,  $^{376}$  diphenyl nitroxide,  $^{377}$  Blatter radical,  $^{378}$  oxoverdazyl radical,  $^{379}$  3,5-di-tert-butyl-semiquinone,  $^{380}$  3-tert-butyl-5-phenylsemiquinone,  $^{358}$  dihydro-phenazine radical cation,  $^{381}$  trioxytriphenylamine radical cation,  $^{382}$  and phenothiazine radical cation.  $^{383}$ 

Linear regression of J/k vs.  $|A(^{1}\text{H})|$  is reasonable,  $^{313,358}$  only when diradical cation 23 and diradicals 1, 3, and 4 are excluded as outliers (Figure 32). The reasons for exclusion of 23 were discussed in the preceding paragraphs - 23 is a clear-cut outlier. Diradicals 1 and 4 must be excluded because of large torsion angles  $\theta$  and 3 is excluded because of large error in its large value of J/k reported as the lower limit. For other 16 values of J/k, good correlation with  $|A(^{1}\text{H})|$  is obtained, with statistically adjusted  $R^{2} = 0.8777$ , because in the corresponding di- and triradicals the torsion angles  $\theta$  are low to moderate (Table 4.3.5). In addition, this may suggest that differences in McConnell constants ( $Q_{\text{CH}}$ , Eq. 8) between neutral radicals and radical ions are either not significant in our set of monoradicals (Figure 31) or these differences are built-in to J/k. In the second case, this would mean that, with identical spin densities at atom X, values J/k are in the following order: radical cations > neutral radicals > radical anions.

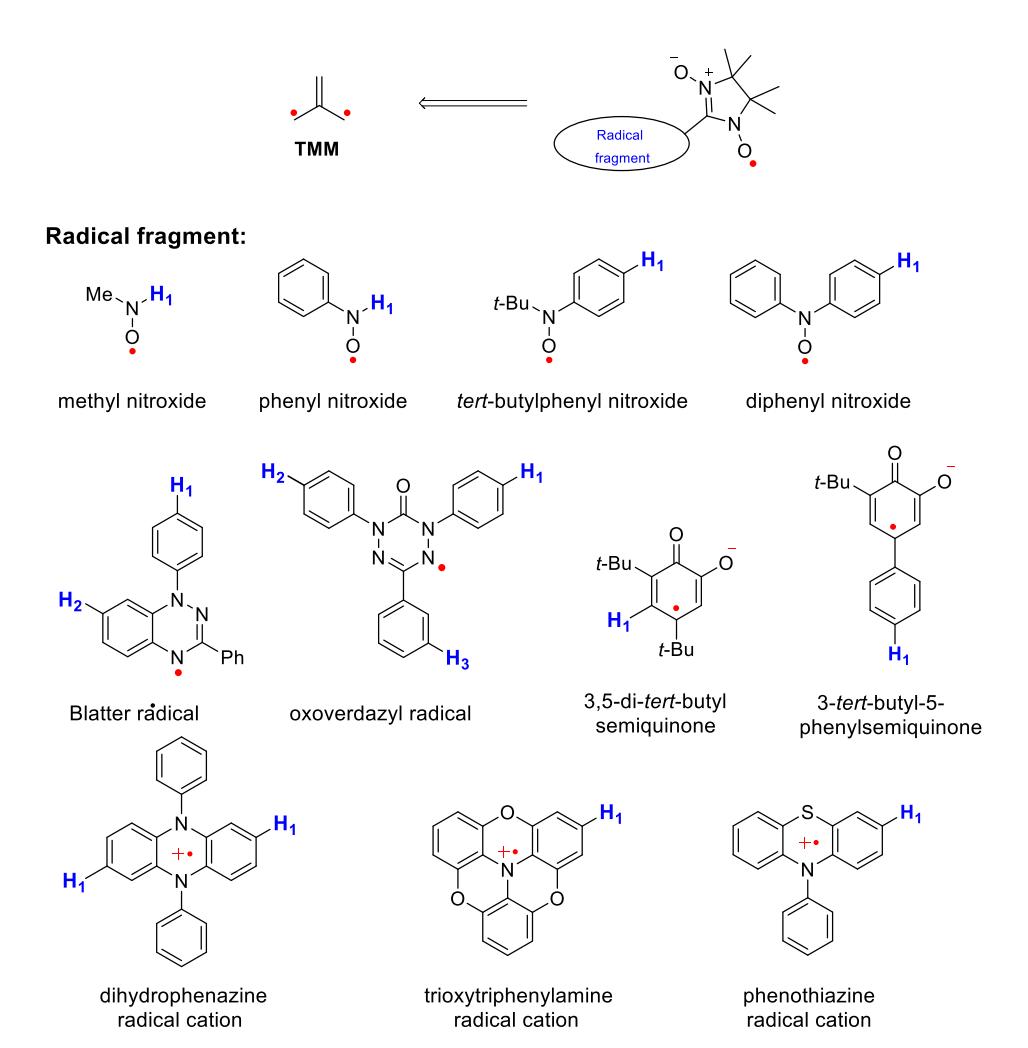


**Figure 31.** Structures of monoradical centers – fragments of NN-based di- and triradicals. Hydrogen atoms (protons), for which values of  $A_{CH}$  and  $|A(^{1}H)|$  are listed in Table 2, are highlighted in blue color. For 3,5-di-*tert*-butyl semiquinone, it is assumed that the spin densities at C4 and C5 are very similar.<sup>380</sup>

**Table 4.3.5.** Experimental J/k for selected high-spin di- and triradicals (Figures 21, 26, and 27) and hyperfine coupling constants ( $|A(^{1}H)|$ ) for the corresponding monoradicals (Figure 31).

Di- or	Corresponding	$^{a}g$	$ A_{\mathrm{CH}} $	<sup>b</sup>  A( <sup>1</sup> H)	$^c heta_{ m avg}$	$ A(^{1}\mathrm{H}) *\cos^{2}\underline{\theta}$	$^{d}J/k$	Monoradical
triradical	monoradical		(Gauss)	(MHz)	(°)	(MHz)	(K)	reference
1	alkyl nitroxide	2.0055	<sup>e</sup> 12.3	34.49	72.7	3.05	390	372/373
3	phenyl nitroxide	2.0055	e11.3	35.75	17.6	28.85	>1000	374/375
4	alkyl nitroxide	2.0055	e12.3	34.49	64.1	6.58	440	372/373
5	tert-butylphenyl nitroxide	2.0060	1.9	5.33	27.4	4.62	319	376
7	diphenyl nitroxide	2.0056	1.83	5.14	<sup>f</sup> 26.5	4.11	231	377
8	diphenyl nitroxide	2.0056	1.83	5.14	25.5	4.18	349	377
10	Blatter radical	g2.0033	0.61	1.71	28.6	1.32	121.5	36
11	Blatter radical	g2.0033	1.84	5.16	<sup>i</sup> 21.5	4.46	438	37
12	Blatter radical	g2.0033	0.61	1.71	31.8	1.23	94	38
			1.84	5.16	20.6	4.52	352	38
14	oxoverdazyl radical	2.0037	0.65	1.82	35.7	1.20	72	39
15	oxoverdazyl radical	2.0037	0.18	0.50	21.5	0.44	17.8	39
17	oxoverdazyl radical	2.0037	0.65	1.83	51.2	0.72	17	40
17			0.65	1.83	28.1	1.42	105	40
18	3,5-di- <i>tert</i> -butyl- semiquinone	<sup>h</sup> 2.0047	3.33	9.33	1.0	9.33	446	380
19	3-t <i>ert</i> -butyl-5- phenylsemiquinone	<sup>h</sup> 2.0047	0.61	1.71	<sup>i</sup> 10.5	1.65	144	358
23	dihydrophenazine radical cation	2.0029	1.75	4.90	20.4	4.31	700	381
25	dihydrophenazine radical cation	2.0029	1.75	4.91	10.1	4.75	160	381
26	trioxytriphenylamine radical cation	2.0031	2.60	7.28	29.8	5.48	400	382
28	phenothiazine radical cation	2.0052	2.15	6.03	13.1	5.72	320	383

 $^a$ g is the isotropic g-value of monoradicals.  $^b$ Δ $v = ΔB(gμ_B/h)$ , conversion from Gauss to MHz, where h is the Plank's constant, g is the isotropic g and  $μ_B$  is the Bohr magnetron.  $^c$ The  $\theta$  is the average of torsional angles between NN moieties and corresponding monoradical-fragments in di- and triradicals; all data are from the crystallographic files.  $^d$ The J/k is from SQUID, while the values of J/k for 10 and 12 are the averages from SQUID and quantitative EPR spectroscopy.  $^e$  The "adjusted  $|A_{\rm CH}|$ " of alkyl nitroxides is derived from that of methyl nitroxide,  $|A_{\rm NH}| = 13.8$  G, and for 1,3,5-triphenylphenyl nitroxide from that of phenyl nitroxide,  $|A_{\rm NH}| = 12.75$  G; these values are converted to the corresponding "adjusted  $|A_{\rm CH}|$ " by correcting for the different values of McConnell's Q constants for nitrogen vs carbon; e.g., for alkyl nitroxides "adjusted  $|A_{\rm CH}|$ " = 13.8/(-25.9)\*(-23.0) G = 12.3 G.  $^f$ The single crystal structure of 7 is not obtained, thus for this triradical  $\theta$  is assumed to be the average  $\theta$  for 5 and 8.  $^g$ The g-value is from SI of ref 384.  $^h$ The g-value is from ref 385.  $^i$ The structures of diradical 11 and diradical anion 19 contain two different molecules, their  $\theta$  is the average value of two molecules. When it is assumed that in DCM-free polycrystalline material of 11, used for SQUID magnetometry, only molecules A are present, with  $|\theta_{\rm avg}| \approx 14$  °, then  $|A(^1{\rm H})|^*\cos^2\theta = 4.86$ .

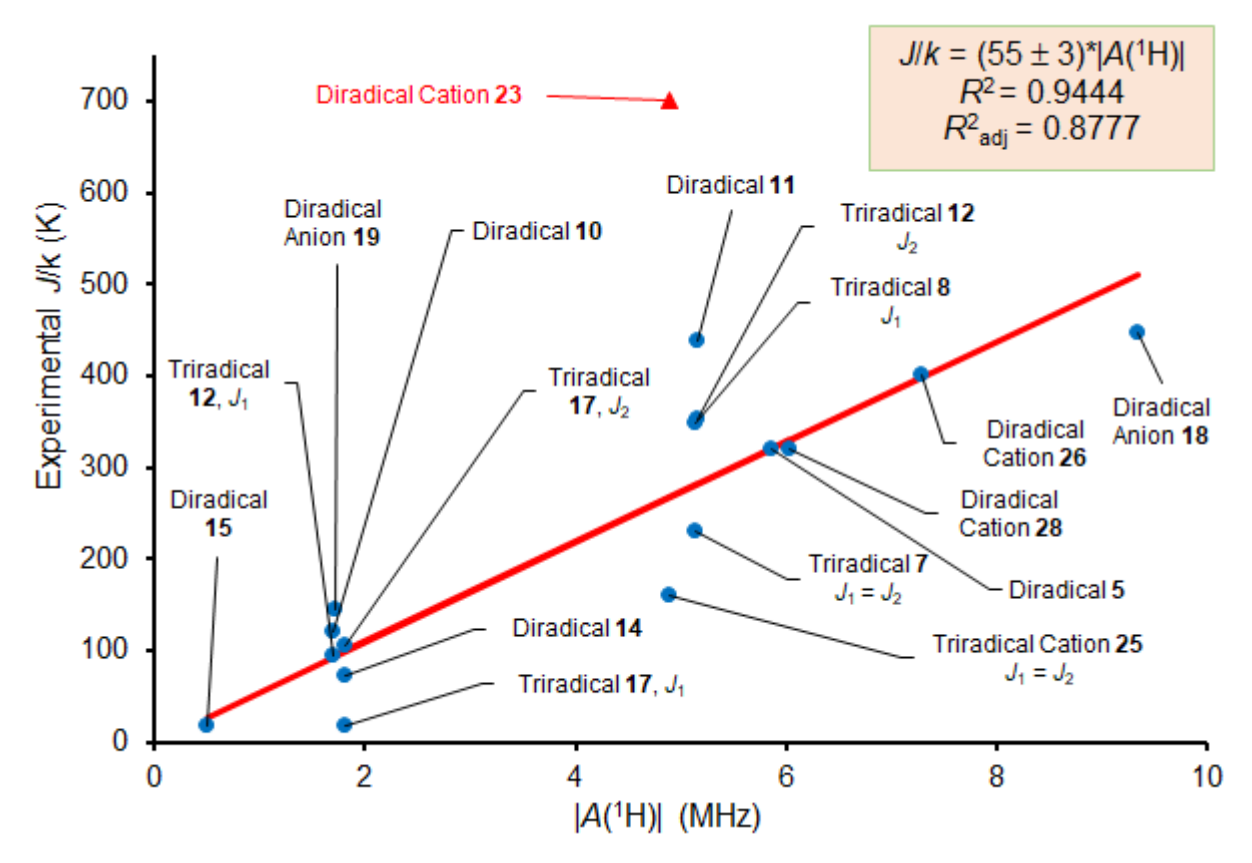


**Figure 32.** Plot of experimental J/k vs.  $|A(^{1}H)|$  and linear regression. Outliers, such as diradical cation 23, diradical 1, diradical 3, and diradical 4 are not included in the linear regression; diradical cation 23 is shown in red color and diradicals 1, 3, and 4 are out of range of the plot and are not shown. Based on linear regression, predicted values of J/k for 23 and 3 are 268 and 1700 K, respectively.

In 2003, in ground-breaking contributions, Shultz and coworkers<sup>386,387</sup> established the Karplus-Conroy-type<sup>388</sup> relation between pairwise exchange coupling constant J (cm<sup>-1</sup>) and torsional angles  $\theta$  between radical center (fragments) and ferromagnetic coupling unit, such as 1,2-connected ethene (Figure 33, Eq 9):

$$J = A\cos^2(\theta) - B \tag{9}$$

where A is the constant for ferromagnetic term and B is the constant for antiferromagnetic term.

Two series of TMM-based diradicals, bis(semiquinone) and bis(nitroxide), are studied (Figure 33). For bis(semiquinone) diradicals, A = 213 and B = 44 cm<sup>-1</sup> and for bis(nitroxide) diradicals, A = 44 and B = 17 cm<sup>-1</sup> are determined. Smaller values of A and B for bis(nitroxides) reflect smaller spin densities at the connecting atom of monoradical nitroxide fragment. Thus, when the torsional angle is smaller than  $\sim 50^{\circ}$  for bis(semiquinone) diradicals and less than  $\sim 60^{\circ}$  for bis(nitroxide) diradicals, they possess

ferromagnetic intramolecular exchange interactions. Otherwise, they possess antiferromagnetic intramolecular exchange interactions. It should be noted that in these diradicals, the larger  $\theta$  leads to increased antiferromagnetic through-space exchange coupling between the monoradicals, thus leading to relatively large values of B.

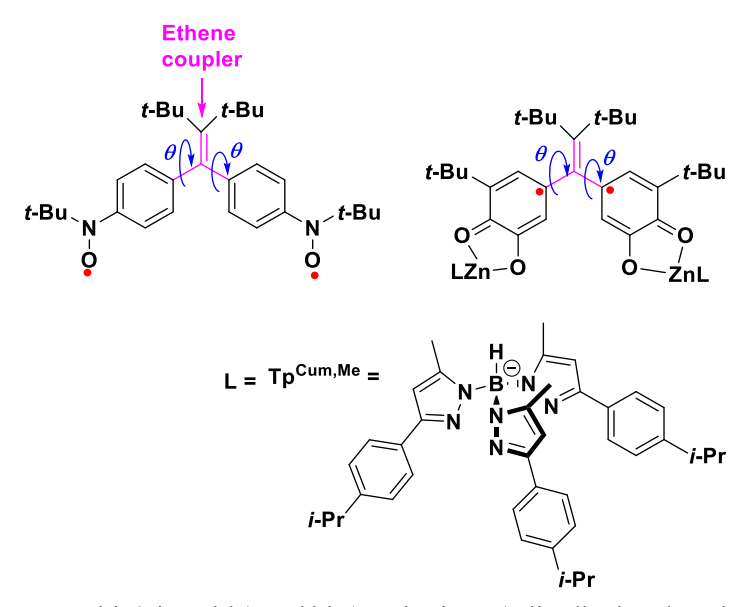


**Figure 33.** Selected TMM-type bis(nitroxide) and bis(semiquinone) diradicals. The ethene coupler and torsional angle  $\theta$  are shown.

In addition to Shultz's relation (eq. 9), we should consider Heller-McConnell relation<sup>389,390</sup> for hyperfine coupling constant for  $\beta$  protons (eq. 10):

$$A(^{1}\mathrm{H})_{\beta} = \mathrm{Q_{CH}}^{\beta*} \rho_{\mathrm{C}} * \cos^{2}(\theta) \tag{10}$$

where  $A(^{1}\text{H})_{\beta}$  (in MHz) is the hyperfine coupling constant for  $\beta$  proton (H $\beta$ ),  $\rho_{C}$  is the spin density at  $\alpha$  carbon (C $\alpha$ ),  $Q_{CH}{}^{\beta}$  is the constant (in MHz). Dihedral (torsion) angle  $\theta$  is defined by the H $\beta$ -C $\beta$ -C $\alpha$  plane and the axis of  $2p_{\pi}$  orbital with unpaired electron at C $\alpha$  (Figure 34).

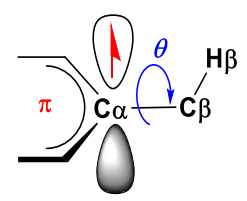


**Figure 34.** Hyperfine coupling to  $\beta$  protons.

Based on the above discussion, the torsional angle between NN moiety and bonding radical fragment in the NN-based high-spin radicals may need to be considered in the intramolecular exchange

interaction. We note that in Shultz's relations, A < B, and, for each pairwise J/k, two average torsion (or dihedral) angles  $\theta$  are involved. However, in our system only a single average torsion angle between NN moiety and the bonded radical fragment is involved (Figure 30), and thus much larger  $\theta$  (~90°) might be required for crossover to antiferromagnetic J/k. In view of the above discussion and Heller-McConnell relation, we propose the relation between the following experimental variables: pairwise J/k in NN-based high-spin di- and triradicals (neutral and ions) and torsion corrected  $|A(^1H)|$  in related monoradicals:

$$J/k = A^*|A(^{1}H)|^*\cos^2(\theta)$$
 (11)

where A is the constant (slope in a linear regression). After exclusion of diradicals 1, 3, and 23 from linear regression, statistically adjusted  $R^2 = 0.8721$  for the set of 17 values of J/k is obtained, indicating a reliable correlation. Based on the regression (Figure 35), we predict for 1, 3, and 23, "correct" values of J/k = 190, 1800, and 268 K, compared to experimental values 390, >1000, and >800 K, respectively. The experimental value of  $\Delta E_{ST}$  for 1 was likely overestimated while for 23, as discussed in the prior sections, it was incorrect. For diradical 3, we confirm very large value of  $\Delta E_{ST} \approx 7.2$  kcal mol<sup>-1</sup>, which would be challenging to be determined by the experiment, based on the detection of thermal population of the lowest singlet excited state (Figure 19).

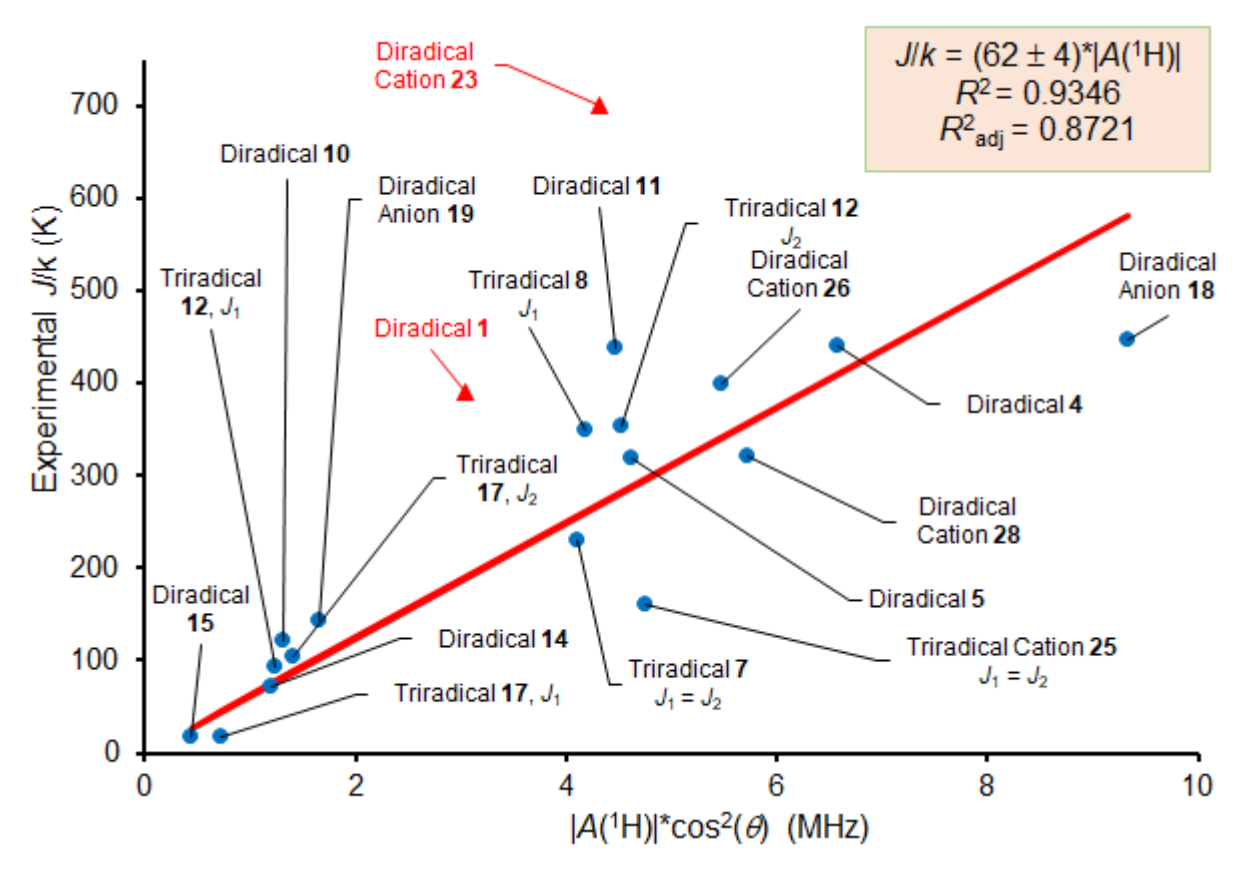


**Figure 35.** Plot of experimental J/k vs.  $|A(^{1}H)|^{*}\cos^{2}(\theta)$  and linear regression. Outliers, such as diradical cation **23**, diradical **1**, and diradical **3** (not shown) are not included in the linear regression; data points for **23** and **1** are shown in red color. Based on the linear regression, predicted values of J/k for **23**, **1**, and **3** are 268, 190, and 1800 K, respectively.

In addition, the average torsional angles  $\varepsilon$  of the phenyl groups (connected to N or C) in Blatter and oxoverdazyl radical are considered (Figure 36). Because the change of  $\varepsilon$  angles can affect the overlap of  $2p_{\pi}$ -orbitals and then alter the spin delocalization. For instance, the average  $\varepsilon$  in Blatter radical is  $54.2^{\circ}$ .<sup>391</sup> These angles decrease to  $45.4^{\circ}$  in 10,<sup>147</sup>  $41.1^{\circ}$  in 11,<sup>148</sup> and  $45.1^{\circ}$  or  $49.8^{\circ}$  in 12 (12 has two pseudo polymorphs).<sup>149</sup> The smaller  $\varepsilon$  angle can increase the effective  $|A(^{1}H)|$  in the Blatter radical moiety. Thus, the effective  $|A(^{1}H)|$  in diradical 10 is larger than that of parent Blatter, thus 10 lies above the regression line (Figure 35).

Two  $\varepsilon$  angles in 1,3,5-triphenyl-6-oxoverdazyl radical are 38.2°.<sup>379</sup> However, the  $\varepsilon$  angles in 17 are different, 25.3° and 46.6°.<sup>154</sup> As a result, two different  $\varepsilon$  angles in triradical 17 enhance the difference between  $J_1/k$  and  $J_2/k$ , due to two different  $\theta$  angles (Table 4.3.5).

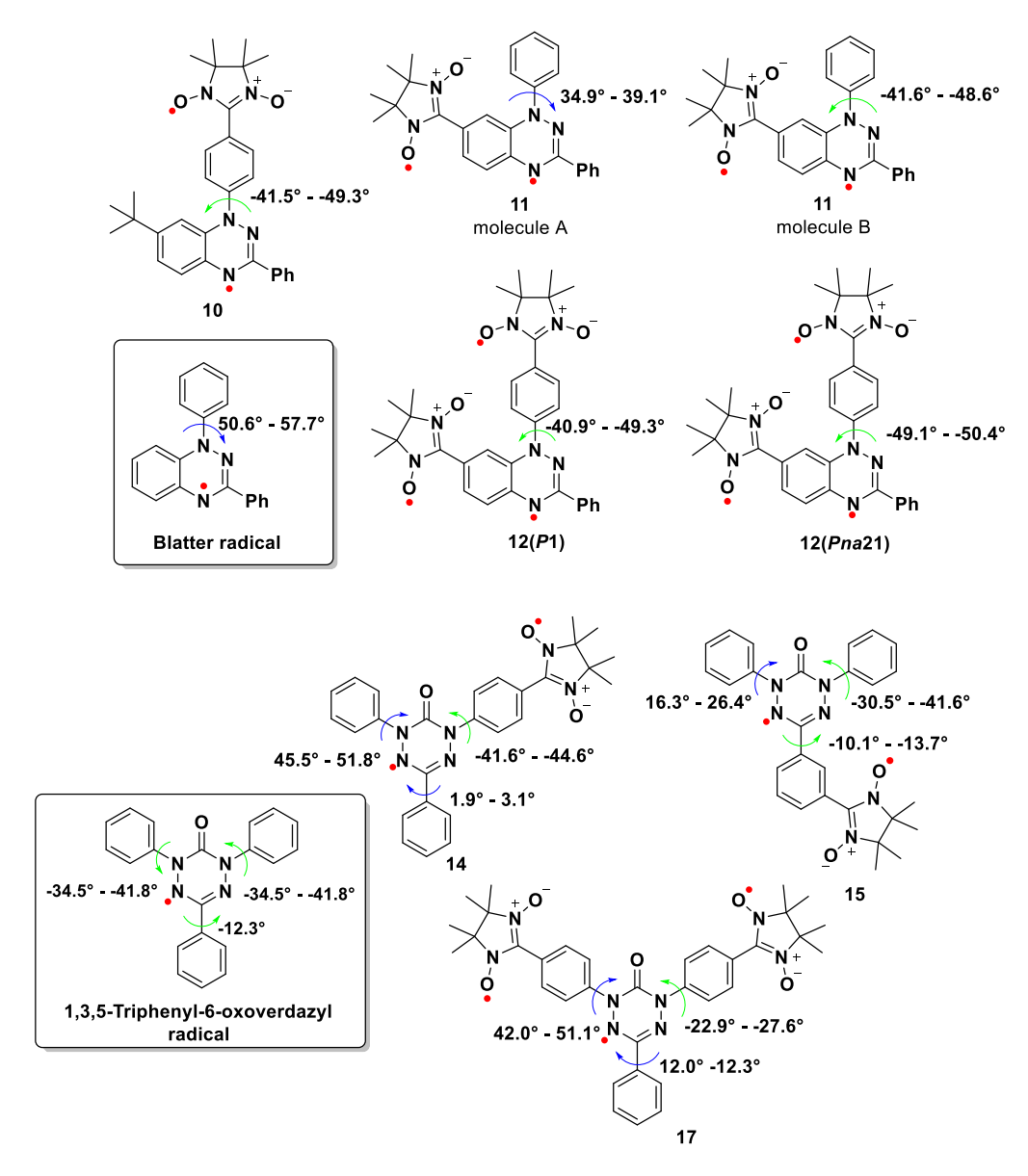


**Figure 36.** Structures of Blatter radical, oxoverdazyl radical, corresponding di- and tri-radicals and definition of torsional angles  $\varepsilon$ . All the angles are from the X-ray crystal structures. <sup>147-149, 153, 154, 391</sup>

# 4.4. High-spin diradicals with Kekulé resonance forms – rule breakers?

In this section, we discuss exceptional high-spin diradicals, which possess Kekulé resonance forms. There is a significant classic work done, both experimental and computational, on antiaromatic diradicals, such as pentadienyl cation<sup>392-395</sup> and benzene dication.<sup>396--398</sup> In 2021, definitive work on triplet ground state of benzene dianion have appeared.<sup>399</sup> We will focus our discussion on recent examples where the significant effort was done to determine the ground state, starting with odd alternant  $\pi$ -systems and ending with even-alternant chiral  $\pi$ -systems.

1,8-Perinaphthyldiyl is a well-known non-Kekulé,  $C_{2v}$ -symmetric molecule<sup>400</sup> with planar, alternant  $\pi$ -system (Figure 37), possessing connectivity corresponding to triplet ground state (Figures 15 and 16). Recent computations by Borden et al at the (12/12)CASPT2/aug-cc-PVDZ+ZPVE level predict triplet ground state with  $\Delta E_{ST} = 4.4$  kcal mol<sup>-1</sup>.<sup>401</sup> (We should note that at the same level of theory, analogous 1,8-naphthoquinodimethane is predicted to be singlet ground state with  $\Delta E_{ST} = -2.1$  kcal mol<sup>-1</sup>.<sup>401</sup>) Wirz et al studied R = H and R = Me derivatives of 1,8-perinaphthyldiyl and also concluded that both molecules are triplet ground state. This conclusion was largely based on the absence of temperature dependence in UV-vis absorption, excitation, and fluorescence spectra, and their agreement with the computed spectra for triplet state; experimental absorption spectra showed absence of NIR bands, which were computed for the spectra of singlet state. Unfortunately, EPR I vs. 1/T plots showed some downward curvature at low temperatures (e.g., for R = Me,  $\Delta E_{ST} \approx -0.006$  kcal mol<sup>-1</sup>), which were tentatively associated with either inadequate temperature control or microwave saturation (Section 4b1).<sup>402,403</sup> In summary, we conclude that 1,8-perinaphthyldiyls are triplet ground states with substantial  $\Delta E_{ST}$ .

In 1997, McMasters, Wirz, and Snyder reported on two 1,8-perinaphthyldiyl derivatives, with nonalternant  $\pi$ -systems, that also possess Kekulé resonance forms, i.e., 2,2-dimethyl-2H-benzo[cd]fluoranthene (29) and 2,2-dimethyl-2Hdibenzo[cd,k]fluoranthene (30) (Figure 37).  $^{404,405}$  These molecules compensate the formal loss of a double bond in the diradical non-Kekulé resonance form with the aromatic resonance energy of fluoranthene and benzo[k]fluoranthene, respectively. Ground states for both diradicals are established based on the UV-vis-NIR absorption spectra; that is, for 29, well-resolved NIR bands extending to ca. 1300 nm are found, while for 30, the spectrum extends to just 665 nm, where a very sharp band is observed. These distinct spectral features for singlet vs. triplet states are reproduced by the Pariser-Pople-Parr (PPP) semiempirical type of computations.  $^{405}$ 

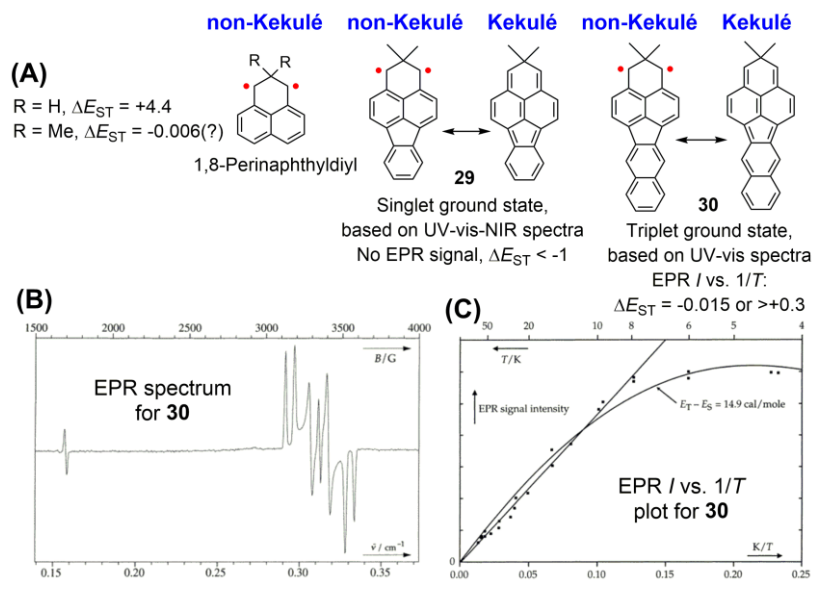


**Figure 37.** (A) McMaster, Wirz, and Snyder diradicals **29** and **30**. Values of  $\Delta E_{ST}$  are in kcal mol<sup>-1</sup>. (B) and (C) EPR spectroscopy of diradical **30**. Parts (B) and (C) of the figure are reproduced from ref. 405. Copyright 2001 American Chemical Society

Singlet ground state for **29** is also supported by the absence of EPR signal for triplet state at temperatures up to 170 K, thus providing a rough upper limit estimate,  $\Delta E_{\rm ST} < -1$  kcal mol<sup>-1</sup>. In contrast to **29**, a strong EPR spectrum corresponding to paramagnetically pure triplet state of **30** is detected in 2-MeTHF at 90 K; that is, the center peak at 3340 Gauss was assigned to double quantum transition in the triplet state (Figure 37). While plot of I vs 1/T is approximately linear in the 50 - 8 K (and 75 - 8 K) temperature range, when data points at 6 and 4 K are included, a curved plot, corresponding to  $\Delta E_{\rm ST} < -0.015$  kcal mol<sup>-1</sup>, is obtained. Analogously to the authors' studies of 1,8-perinaphthyldiyl (see above),  $^{402,403}$  the downward curvature of the I vs. 1/T plot is tentatively associated with inadequate temperature control or microwave saturation (Section 4b1).  $^{405}$  In summary, we conclude that diradical **30** is the triplet ground state with estimated lower limit of  $\Delta E_{\rm ST} > +0.3$  kcal mol<sup>-1</sup>.

In 2022, Yasuda, Konishi, Kishi, and coworkers have succeeded in preparation of the 7<sup>th</sup> (final) nonalternant isomer of pyrene **31** (Figure 38A).<sup>406</sup> Diradicals **31a** and **31b** are sensitive to air, with  $\tau_{1/2} = 19$  and 73 h. Both diradicals possess singlet ground state, and not surprisingly **31b** possesses larger  $|\Delta E_{\rm ST}|$ , suggesting better stabilization of zwitterionic singlet state by the electron withdrawing

group (Dcp). However, the magnitude of this effect  $(3 - 4 \text{ kcal mol}^{-1})$  is rather surprising (Figure 38A).

**Figure 38.** (A) Final nonalternant isomer of pyrene (azulene-based): singlet ground state with substituent dependent  $\Delta E_{ST}$ . (B) Nonalternant diradical **32**: most likely, triplet ground state with large  $\Delta E_{ST}$ . Values of  $\Delta E_{ST}$  are in kcal mol<sup>-1</sup>.

In 2022, Shintani, Sato, Shimizu and coworkers were successful in synthesis, isolation, and crystallographic characterization of air-sensitive ( $\tau_{1/2} \ll 15$  min on air) diradical  $32^{.407}$  The diradical resonance form is clearly much better stabilized, compared to the Kekulé resonance form, which also comprises of antiaromatic  $32 \pi$ -electron perimeter (Figure 38B). This is unlike in diradical 31, where the Kekulé form has an aromatic  $14 \pi$ -electron perimeter and zwitterionic form (with two benzenoid rings) is a significant contributor (Figure 38A). Consequently broken-symmetry DFT computations predict triplet ground state with large  $\Delta E_{ST} = 6.3$  kcal mol<sup>-1</sup>, which is comparable to  $\Delta E_{ST} = 6.4$  kcal mol<sup>-1</sup> computed at the similar level of theory (UB3LYP/6-31G(d)+ZPVE) for the planarized triarylmethyl diradical (see: the corresponding radical anion PTAM in Figure 10). This is reasonable because the DFT-computed spin density distributions in the triplet states of 32 and diradical PTAM are similar (Figure 39). Because the EPR spectrum of 32 shows a significant contamination ( $\geq 50\%$ ) with unknown  $S = \frac{1}{2}$  impurities (Figure 39ab,f), the authors are able to obtain only I vs. 1/T plot for  $|\Delta m_s| = 2$  transition.<sup>407</sup> (Authors fail to display full scale spectrum showing the center peak for  $S = \frac{1}{2}$  impurities and to demonstrate whether the spectrum was obtained under the conditions, in which  $S = \frac{1}{2}$ 

 $\frac{1}{2}$  species are not partially saturated; this makes our estimate of amount of  $S = \frac{1}{2}$  impurities very approximate.) An approximate linearity of this plot in the 4.7 - 68 K temperature range suggests either near-degenerate singlet and triplet states with  $|\Delta E_{ST}| < 0.02$  kcal mol<sup>-1</sup> or triplet ground state with  $\Delta E_{ST} > 0.3$  kcal mol<sup>-1</sup>. We note that in the work done more than 30 years ago,<sup>34</sup> air-sensitive diradical **PTAM** could be isolated as a reasonably pure polycrystalline solid, with a clean triplet EPR spectrum in glassy 2-MeTHF and SQUID data on the polycrystalline sample provided clear-cut evidence of the triplet ground state. We conclude that diradical **32** is most likely triplet ground state.

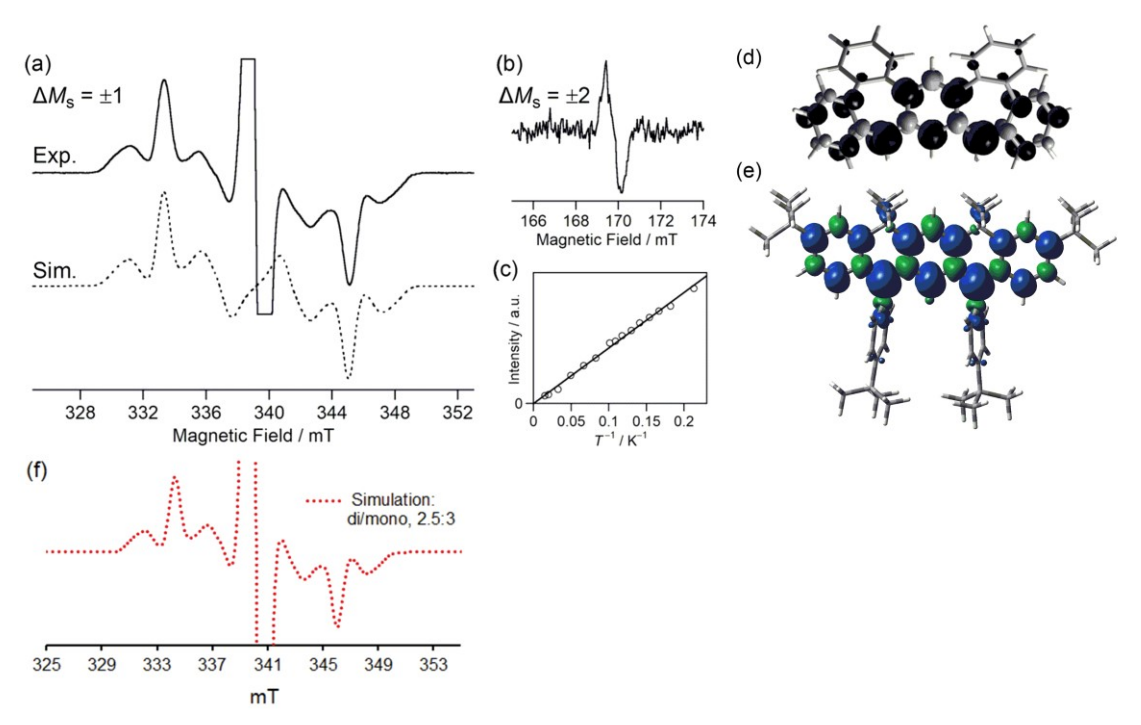


**Figure 39.** EPR spectra of diradical **32** in toluene at 69 K (solid line: experiment, dashed line: simulation), (a)  $|\Delta m_s| = 1$  and (b)  $|\Delta m_s| = 2$ . (c) Plot of the temperature dependence of the triplet signal intensity *I* versus 1/T from 68 to 4.7 K. (d) and (e) Spin density maps for triplet states of diradicals: simplified **32** ((d)) and **PTAM** ((e), isodensity level of 0.002 electron/Bohr); darker and blue colors correspond to positive spin densities. (f) Simulation of the spectrum in (a) with monoradical-to-S = 1 diradicals molar ratio of 3:2.5; for both monoradical and two conformers of diradical (1.5:1), the parameters listed in ref 407 (Fig. S9, SI) are employed. Parts (a) – (d) of the figure are reproduced with permission from ref. 407. Copyright 2022 Wiley.

In 2019, our group reported an air-stable diradical dication 33 of chiral  $D_2$ -symmetric conjoined bis[5]diazahelicene with a high-spin (S = 1) ground state and  $\Delta E_{ST} \approx 0.3$  kcal mol<sup>-1</sup> (Figure 40).<sup>301</sup> (For a structure of analogous  $S = \frac{1}{2}$  radical cation, see Figure 10.) This diradical dication possesses closed-shell (Kekulé) resonance forms with Hückel antiaromatic 16  $\pi$ -electron perimeters, as shown for a simplified structures of 33a in Figure 40.

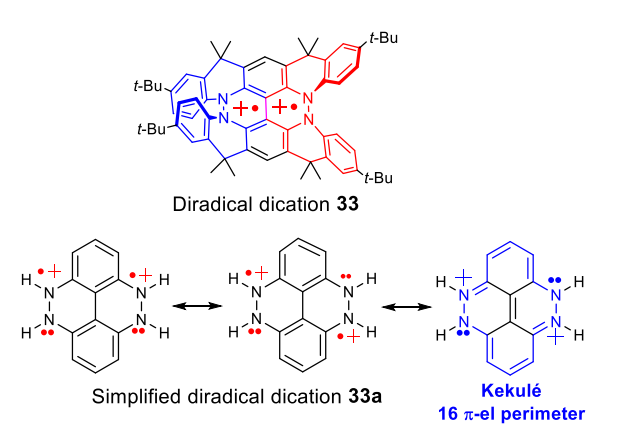


**Figure 40.** Structure drawing of diradical dication **33** and the representative resonance forms for simplified structure **33a**. Reproduced from ref. 301. Copyright 2019 American Chemical Society.

We note that the non-Kekulé resonance forms of 33a possess Hückel antiaromatic  $16 \pi$ -electron perimeters, but these are well offset by two benzenoid rings, thus leading to relative stabilization of open-shell forms.

The diradical dication is monomeric in dibutyl phthalate (DBP) solution/matrix and its EPR spectra are paramagnetically pure (Figure 41). Quantitative EPR spectroscopy is used to determine the ground state and  $\Delta E_{\rm ST}$  by the by measurements of  $\chi T$  in the T=105-330 K range (Figure 41). The following standard procedure is employed: "Values of  $\chi T$  are obtained by spin counting using a standard such as TEMPONE in DBP (in triplicate, n=3) and then are fit to the Bleaney–Bowers equation (e.g., eq. 5 with  $\theta=0$ ) to provide a singlet–triplet energy gap  $2J/k=145\pm4$  K (mean  $\pm$  SE), i.e.,  $\Delta E_{\rm ST}\approx0.3$  kcal mol<sup>-1</sup>."<sup>301</sup>

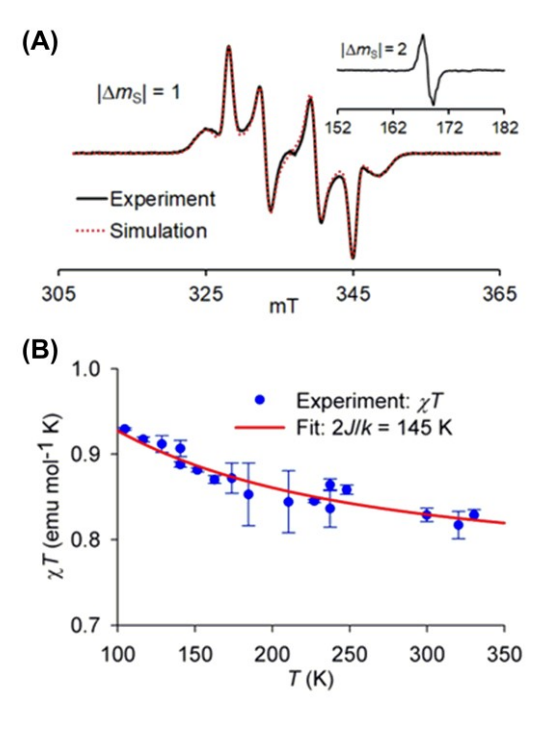


**Figure 41.** EPR spectroscopy of 0.82 mM diradical dication **33** in DBP: (A) spectra at 117 K; (B) plot of  $\chi T$  vs. T, obtained by quantitative EPR spectroscopy. Reproduced from ref. 301. Copyright 2019 American Chemical Society.

In a different experiment, quantitative EPR spectroscopy with 14 time points in the 0–48 h range and with accurate measurements (n = 3) of  $\chi T$  at 117 K, provides  $\tau_{1/2} > 2$  weeks at ambient conditions (on air) in the presence of excess oxidant (NO<sup>+</sup>SbF<sub>6</sub><sup>-</sup>).

Partially enantiomerically enriched samples of **33** show good chiroptical properties with  $\Delta \varepsilon_{\text{max}} \approx 30 \text{ L mol}^{-1} \text{ cm}^{-1}$  and anisotropy factor  $|g| = |\Delta \varepsilon|/\varepsilon \approx 0.005;^{301}$  this value will be re-measured, as recently, we are able to isolate enantiomerically and paramagnetically pure **33**, and to obtain its X-ray structure. The reported value of |g| for **33** is comparable to |g| = 0.004 for the Osuka's air-stable porphyrin-based S = 1/2 radical (Figure 8)<sup>298</sup> and to those of [6]helicene (|g| = 0.007)<sup>408</sup> and neutral carbon–sulfur [7]helicene (|g| = 0.004)<sup>409</sup> but smaller than the |g| = 0.039 for neutral carbon–sulfur double helix.<sup>410</sup>

In summary, the first triplet ground state diradical (dication), in which the spin density is delocalized over double helical (or helical)  $\pi$ -system. Notably, *triplet ground state was found despite* the presence of Kekule resonance form with alternant  $\pi$ -system. Although its chiroptical properties

appear promising, the  $\Delta E_{\rm ST} \approx 0.3$  kcal mol<sup>-1</sup> is still a bit too low and counterions are likely to affect the properties in the single crystals and thin films. We were able to identify two new triplet ground state diradicals, with double helical  $\pi$ -systems, one neutral and another dicationic but with higher  $\Delta E_{\rm ST}$  (Figures 10 and 12).

## 4.5. High-spin Blatter-based diradical as electrical conductor – rule breaker?

This Section is focused on high-spin diradical **34** (Figure 42), which also possesses good electrical conductivity,  $\sigma_{RT} = 0.044 \pm 0.012$  S cm<sup>-1</sup> (mean  $\pm$  SE), at room temperature. These measurements were carried out on 15 randomly selected single crystals, with the best single crystal device possessing  $\sigma_{RT} = 0.13$  S cm<sup>-1</sup>. The discovery of good electrical conductivity in **34** is unusual because its cross-conjugated  $\pi$ -system does not promote electron delocalization of conductance. For example as mentioned in Section 3, in triarylmethyl-based radical anion, which formally derived by 1-electron reduction of high-spin ground state m-phenylene diradical, has the spin density localized on one of the two triarylmethyl moieties, based on EPR spectra (also, see: spin density maps for radical anion **MX** in Figure 10);  $^{305,313}$  similar localization of spin density is observed in high-spin diradical anions and diradical dianions formally derived from the corresponding high-spin tri- and tetraradicals. Significantly lower single molecule conductance observed for cross-conjugated  $\pi$ -systems  $^{412,413}$  may be associated with quantum interference.

We will start with an overview of electrical conductivity in stable organic radicals, which were discussed throughout Section 2. Typical neutral  $\pi$ -radicals are insulators with  $\sigma_{RT} < 10^{-10}$  S cm<sup>-1</sup>, e.g., DPPH (Figure 3),<sup>127,128</sup> galvinoxyl (Figure 5),<sup>128</sup> and TEMPOL (Figure 4).<sup>175</sup> Even recently prepared radicals forming  $\pi$ -dimers or equidistant  $\pi$ -stacks such as **OR1**,<sup>81</sup> **BR1**,<sup>82</sup> and Kubo's phenalenyl<sup>79</sup> with R = perfluorophenyl (Figure 1) possess very low conductivity  $\sigma_{RT} < 3 \times 10^{-9}$  S cm<sup>-1</sup>. We note that equidistant  $\pi$ -stacks for **BR1** and Kubo's phenalenyl has plane-to-plane distances of 3.565 and

3.503 Å, respectively. In comparison Haddon's zwitterionic spiro-bis(phenalenyl) (R = benzyl) (Figure 1), forming a uniform one-dimensional  $S = \frac{1}{2}$  antiferromagnetic Heisenberg chain (J/k = -75 K) and possessing closest C---C contacts of 3.47 and 3.58 Å along the stacking direction, has  $\sigma_{RT} = 1.4 \times 10^{-3}$  S cm<sup>-1</sup> with  $E_a = 200$  meV.<sup>85</sup> Similarly, single crystal **TOT** (R = Br) (Figure 5), which forms slipped  $\pi$ -stack with equidistant TOT moieties (3.43 Å), has  $\sigma_{RT} = 1.8 \times 10^{-3}$  S cm<sup>-1</sup> with  $E_a = 0.310$  meV.<sup>231</sup> Single crystal **TOT** (R = H) (Figure 5) possesses is reported to possess even higher  $\sigma_{RT} = 0.32$  S cm<sup>-1</sup> with  $E_a = 90$  meV.<sup>236</sup> This conductivity is similar to that in Boudouris' thin films of **PTEO** (Figure 4)<sup>176</sup> with  $\sigma_{RT} \approx 0.3$  S cm<sup>-1</sup> and Haddon's zwitterionic spiro-bis(phenalenyl) (R = n-hexyl) (Figure 1) with  $\sigma_{RT} \approx 0.3$  S cm<sup>-1</sup> and  $E_a = 50$  meV.<sup>84</sup> Oakley's best optimized neutral radical, oxo-bridged bisthiazolyl, **OBBDTA** (Figure 5), attains  $\sigma_{RT} \approx 0.04$  S cm<sup>-1</sup> with  $E_a = 50$  meV;<sup>257</sup> at high pressure, this radical exhibits metal-like behavior with  $\sigma_{RT} \approx 0.04$  S cm<sup>-1</sup> and  $E_a < 0.257$ 

Examination of the spin density in Blatter radical reveals large positive and negative spin densities at C7 and C3. Therefore, application of parity rules (Figure 15) indicates to us that a connection between the C7 and C3 positions would provide a di-Blatter high-spin diradical (Figure 42).

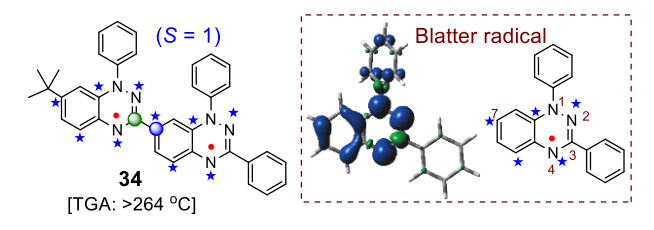


**Figure 42.** Structure drawing of diradical **34** and the design leading to high-spin ground state. An asterisk corresponds to spin-up in Figure 15; spin up at N2 spans both N1 and N2. TGA onset of decomposition  $\approx 1\%$  mass loss. Blatter radical and its spin density map at the UB3LYP/6-31G(d,p) level of theory; positive (blue) and negative (green) spin densities are shown at the isodensity level of 0.002 electron/Bohr. Reproduced from ref. 150. Copyright 2022 American Chemical Society.

Diradical **34** may be viewed as thermally ultra-robust, based on the high onset temperature (1% mass loss) in TGA (Figure 42). In the crystal, two fused-ring Blatter radical moieties are nearly

coplanar, thus providing the conformation of 34 in the crystal that is near optimum for attaining both strong ferromagnetic coupling and electrical conductivity (Figure 43). The latter is promoted by the formation of 1D  $\pi$ -stacks along the

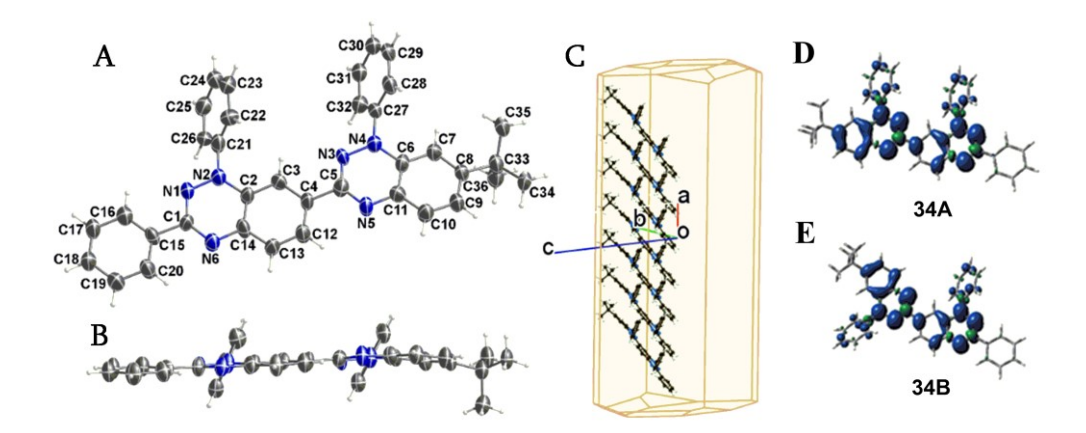


**Figure 43.** Single-crystal X-ray structure of diradical **34** at 100 K, with carbon and nitrogen atoms depicted using thermal ellipsoids set at the 50% probability level (A, B); the Bravais, Friedel, Donnay, and Harker (BFDH) crystal morphology of **34** (C), confirmed by the experimental face index; needle and stacking direction are along the *a*-axis. (D, E) Spin density maps for triplet states of two conformations **34A** and **34B** (at the UB3LYP/6-31G(d,p)+ZPVE level). Reproduced from ref. 150. Copyright 2022 American Chemical Society.

crystallographic a-axis, which coincides with the longest dimension of the single-crystal needle (Figure 43C), with an average plane-to-plane distance of 3.482 Å (planes defined by the N1–N6 and C1–C20 atoms). Because of multiple intermolecular C···C and N···C contacts within the sum of van der Waals radii plus 0.1 Å distances, in addition to a short C10···C12 = 3.381 Å contact (within the 1D  $\pi$ -stack), involving predominantly atoms with significant (and same sign) spin densities, strong intermolecular antiferromagnetic interactions are anticipated in crystalline diradical **34**.

DFT computations at the UB3LYP/6-31G(d,p)+ZPVE level reveal that conformer **34A**, corresponding to that found in crystalline **34** (Figure 43), is a global minimum with  $\Delta E_{\rm ST} \approx 1.37$  kcal mol<sup>-1</sup>, compared  $\Delta E_{\rm ST} \approx 0.34$  kcal mol<sup>-1</sup> for **34B**. Because the  $\Delta E_{\rm ST} > 0$  is overestimated at this level of theory, conformer **34B** may be a singlet ground state ( $\Delta E_{\rm ST} < 0$ ). Indeed, the  $\chi T$  vs. T data, obtained by quantitative EPR spectroscopy for the diradical in toluene/chloroform soft glass/fluid in the T = 110-331 K range, are best fit to a model of two conformations, one with  $\Delta E_{\rm ST} > 0$  (ca. +0.4

kcal mol<sup>-1</sup>) and the other, a minor one, with  $\Delta E_{\rm ST} < 0.^{150}$  Major conformation may be trapped in a rigid polystyrene glass as confirmed by quantitative EPR spectroscopy, giving  $2J/k = 275 \pm 36$  K, i.e.,  $\Delta E_{\rm ST} \approx +0.5$  kcal mol<sup>-1</sup>. The  $M/M_{\rm sat}$  vs H/T data at T=1.8,3, and 5 K for 34 in polystyrene matrix approximately coincide with the S=1 Brillouin curve, thus providing unequivocal evidence for the triplet ground state. Thus, we may conclude that 34A found in the crystal is the triplet ground state with  $\Delta E_{\rm ST}$  of the order of 0.5 kcal mol<sup>-1</sup>. 150

We are surprised to obtain unusual linear plots of conductivity,  $\sigma$  vs. T (Figure 44A, inset plot). Such plots may be interpreted in terms of temperature dependent effective  $E_a$ , which is ca. 12 meV and 0.03 meV in the high and low temperature ranges, respectively. To illustrate the smallness of  $E_a$ , it is perhaps better to express it as  $E_a/k$ ; in the high and low temperature ranges we have  $E_a/k = 140$  and 0.06 K, respectively. Therefore,  $E_a/k \ll T$ , especially in the low temperature range, where carrier—phonon interactions are lowered, implies band-like transport. 176

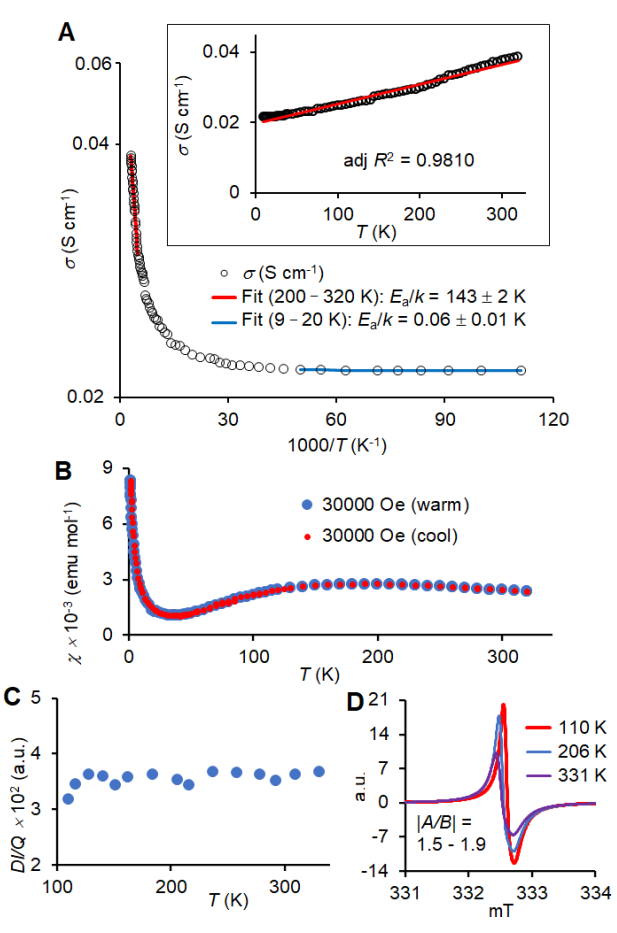


**Figure 44.** Solid state characterization of diradical **34.** A, main plot: single crystal conductivity,  $\sigma$ , of diradical **34** (plotted on a logarithmic scale) as a function of the reciprocal temperature (1000/T), with the fits

in the high- and low-temperature ranges, showing effective activation energies ( $E_a/k$ ). Inset plot: single crystal  $\sigma$  vs. T, showing near-linear relationship. **B**, SQUID magnetometry of polycrystalline **34**: magnetic susceptibility,  $\chi$  vs. T for T = 1.8 - 320 K. **C** and **D**, EPR spectroscopy of polycrystalline **34** with particle size of <75  $\mu$ m:  $DI/Q \sim \chi$  vs. T and representative EPR spectra, showing Dysonian line-shape, where DI is a double integrated intensity and Q is a microwave cavity quality factor. Reproduced from ref. 150. Copyright 2022 American Chemical Society.

Magnetic studies on polycrystalline **34** confirm this "near-metal-like" behavior. <sup>150</sup> The plot of static of  $\chi$  vs. T is nearly temperature-independent in the range from 20 to 320 K, and the value of  $\chi \approx 2-3 \times 10^{-3}$  emu mol<sup>-1</sup> is consistent with Pauli paramagnetism (Figure 44B). This value of  $\chi$  is greater than  $\chi \approx 5-6 \times 10^{-4}$  emu mol<sup>-1</sup> observed in spiro-bis(phenalenyl) (R = n-hexyl) (Figure 1) and oxobridged bisthiazolyl, **OBBDTA** (Figure 5) monoradicals. <sup>84,257</sup> Also, we note that the residual paramagnetism from some crystals in the polycrystalline sample appears as a shallow broad maximum at about 200 K due to one-dimensional S=1 antiferromagnetic chains with a large  $J^*/k \sim -150$  K.

The EPR spectroscopy on polycrystalline **34**, with particle sizes <75  $\mu$ m, confirms the temperature-independent  $\chi$  in the T=110–331 K range (Figure 44C). In addition, a Dysonian line shape (A/B > 1) (Figure 44D) confirms good electrical conductivity of polycrystalline **34**.

Notably, this diradical can be evaporated under UHV to obtain thin films (nominal thickness of ca. 1 nm) on silicon substrates, which remain unchanged after exposure to air for at least 18 h - a testament to its thermal ultra-robustness.  $^{150,414}$ 

## 4.6 High-spin triangulene diradicals.

As we discussed in Section 2.3, trioxytriangulenes have a long history dating to the classic contributions by Clar (35)<sup>227</sup> and to the pioneering report by Bushby in 1993 of the triplet ground state diradical trianion 36 (Figure 45).<sup>228</sup> Also, in 1925, Weiß and Korczyn synthesized derivatives of 35 and recognized them as "trimethylene-triarylmethanes".<sup>415</sup>

Clar's attempts to obtain diradical 35 (Figure 45) by de-hydrogenation of various multihydro-

triangulenes, using Pd-catalyst, apparently resulted in polymers/oligomers, which could not be characterized at that time.<sup>227</sup> In 2019, Richardson and coworkers developed a simplified synthesis of various dihydro-triangulenes and related compounds.<sup>416</sup> Oxidation of one of the dihydro-triangulenes with *p*-chloranil resulted in a solid product, which according to laser desorption ionization mass spectrometry (LDI-MS) analysis showed peaks up to m/z = 1400 – likely corresponding to oligomers of 35.<sup>416</sup> It should be noted that Mou and Kertesz predicted by DFT the dimerization energy of –23 kcal mol<sup>-1</sup> for singly  $\sigma$ -bonded dimer of 35,<sup>417</sup> thus, suggesting that oligomerization of 35 will be quite exothermic.

In 2017, Gross and coworkers prepared **35** on surface and characterized it by scanning tunneling and atomic force microscopy. Surface synthesis of aza-triangulene diradical cation **40** (Figure 46) was reported in 2022. Assignment of triplet state for **35** and **40** is based on weaker intensity of Kondo resonance, compared to  $S = \frac{1}{2}$  radical, however, no clear-cut evidence about  $\Delta E_{ST}$  is available.

**Figure 45.** Triangulene diradicals. Abbreviation: Mes = 2.4.6-Me<sub>3</sub>C<sub>6</sub>H<sub>2</sub>.

Bushby and coworkers<sup>228</sup> were able to prepare three-fold symmetric S = 1 diradical **36** (|D| = 192 MHz and |E| = 0), with a modest admixture of the corresponding  $S = \frac{1}{2}$  radical dianion. Although  $|\Delta m_S| = 2$  is observed at 13 K, it is rather weak and not suitable for obtaining I vs 1/T plot. In the EPR spectrum, height of the center peak, assigned to  $S = \frac{1}{2}$  radical, is only twice, compared to the S = 1

side peaks – a remarkable feat because the diradical was prepared by the challenging 2-electron reduction of the corresponding diamagnetic anion ( $E^{1-/2-} = -2.07 \text{ V}$  and  $E^{2-/3-} = -2.37 \text{ V}$  vs AgNO<sub>3</sub>/Ag), using Na/K in dimethylformamide (DMF). Relatively low content of  $S = \frac{1}{2}$  impurity allows to obtain accurately fraction of S = 1 state intensity (I) by spectral simulation. Linear plot of I vs 1/T in the 13 - 37 K range is consistent with either near-degenerate singlet and triplet states with  $|\Delta E_{\rm ST}| < 0.01$  kcal mol<sup>-1</sup> or triplet ground state with  $\Delta E_{\rm ST} > 0.15$  kcal mol<sup>-1</sup>. Based on what we know about triangulene system, this result suggests triplet ground state for **36**.

The authors<sup>228</sup> report that a solution of **36** in DMF does not lose its EPR intensity, when stored for up to 5 months at room temperature, however, upon exposure to air, **36** is rapidly oxidized to the precursor diamagnetic anion.

In 2001, Nakatsuji and coworkers,  $^{421}$  when attempting to prepare triangulene 37 (Figure 45), were able to obtain an EPR spectrum in toluene at 123 K, which they assigned to an  $S = \frac{1}{2}$  impurity (huge center peak of unknown height) and S = 1 state of 37. The S = 1 spectrum consisted of four symmetrically disposed side peaks, corresponding to D = 219 MHz and E = 0. Half-field transition,  $|\Delta m_S| = 2$ , was referred to as "extremely weak",  $^{421}$  and therefore, not suitable to obtain I vs 1/T plot. Nevertheless, the authors show linear I vs 1/T plot in the 3.7 - 16 K temperature range, where I is claimed to be triplet intensity.  $^{421}$  Assuming that I is associated with S = 1 state, then this linear plot would imply either near-degenerate singlet and triplet states with  $|\Delta E_{ST}| < 0.004$  kcal mol<sup>-1</sup> or triplet ground state with  $\Delta E_{ST} > 0.06$  kcal mol<sup>-1</sup>. However, if I is obtained from the  $|\Delta m_S| = 1$  spectrum, dominated by the  $S = \frac{1}{2}$  impurity, it is likely to be heavily weighted by the  $S = \frac{1}{2}$  intensity, which will always lead to the linear plot, when measured properly. In summary, the triplet ground state for 37 is not firmly established by the described experiments.

In 2022, Juríček and coworkers, have reported synthesis of triangulene 38, <sup>422</sup> using similar methodology to that for 37. Corresponding triangulene  $S = \frac{1}{2}$  radical was isolated and characterized

by X-ray crystallography. Although diradical **37** is claimed to be persistent at room temperature for up to 3 weeks, there is no magnetic characterization by SQUID magnetometry or by quantitative EPR spectroscopy; authors' EPR spectroscopic measurements does not even establish the triplet ground state.

Nakatsuji's '2001 communication, describing trinagulene 37, concluded with the following sentence: "Further stabilization of triangulene by additional substitutions is under way to isolate genuine non-Kekule' PNBs in the crystalline state." Some 20 years later, in 2021, Shimizu and coworkers have finally realized that vision, by reporting synthesis, isolation, and characterization of 39.<sup>423</sup> Triangulene diradical is prepared by the reduction of the precursor diol with SnCl<sub>2</sub> in the presence of trifluoroacetic acid anhydride – most likely, via two one-electron reductions of the corresponding carbocations. Diradical 39 is isolated and characterized by the first X-ray structure for a triangulene diradical. Triplet ground state is established by SQUID magnetometry, giving a flat  $\gamma T$ vs. T plot in the 20 – 300 K temperature range, with the value of  $\gamma T > 0.75$  emu K mol<sup>-1</sup>. This value is assigned to 82% S=1 diradical and 18%  $S=\frac{1}{2}$  radical; the same  $S=\frac{1}{S}=\frac{1}{2}$  ratio gives a reasonable fit to the M vs H/T Brillouin curve at 1.9 K.<sup>423</sup> These data provide unequivocal confirmation of triplet ground state for triangulene diradical and suggest  $\Delta E_{\rm ST} >> 1.2~{\rm kcal~mol^{-1}}$ . Further evidence for triplet ground state is obtained from heat capacity measurements under magnetic fields. 423 Notably, the CW EPR spectra in rigid matrices showed surprisingly small value of "apparent |D|" and, consequently, extremely weak  $|\Delta m_S| = 2$  transition (vide infra).

In 2022, Wu and coworkers<sup>424</sup> attempted preparation of aza-triangulene diradical cation 41. It is not clear whether the diradical cation was actually synthesized because its EPR spectrum at room temperature does not match the simulated spectrum (see: red arrows in Figure 46B),<sup>424</sup> as noticed by the authors in ref 424. In addition, because DFT-computed spin density distributions in triangulenes and aza-triangulenes are similar, the reported  $\Delta E_{\rm ST} \approx 0.8$  kcal mol<sup>-1</sup> is way too small (Figure 46C).

While there may be many reasons for this result, it is plausible that this is an artefact due to Q-value of the cavity increasing at low temperatures. We should mention that for triangulene 35,  $\Delta E_{\rm ST} \approx 10$  kcal mol<sup>-1</sup> is computed at the UB3LYP/6-31G(d)+ZPVE level of theory, with both triplet and broken-symmetry (BS) singlet geometries optimized (Figure 10), and Shimizu reports experimental value of  $\Delta E_{\rm ST} >> 1.2$  kcal mol<sup>-1</sup> for triangulene 39.<sup>423</sup> In addition for aza-triangulene 42,  $\Delta E_{\rm ST} > 2$  kcal mol<sup>-1</sup> is measured by SQUID magnetometry (*vide infra*). We note that the X-ray structure of 41 is refined with a large number of constraints, leading to a relatively small reflections/(parameters + restraints) ratio; also there is a large residual electron density of ca. 1.5 electrons, possibly associated with SbCl<sub>6</sub><sup>-</sup> counterion.

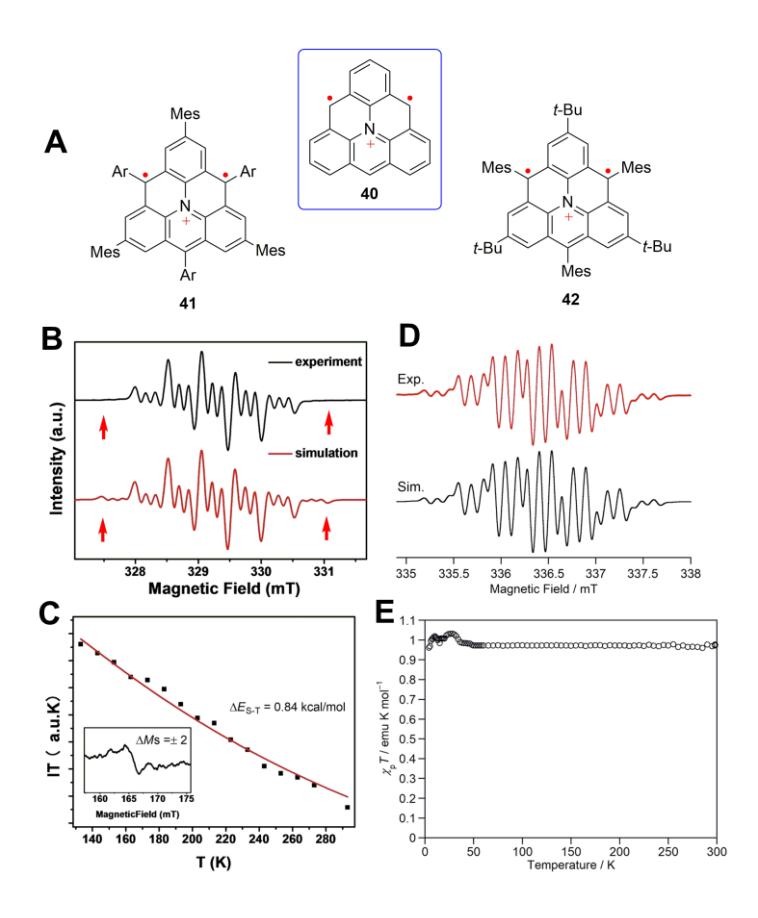


**Figure 46. A**: Aza-triangulene diradical cations **40**, **41**, and **42**. Abbreviations: Mes = 2,4,6-Me<sub>3</sub>C<sub>6</sub>H<sub>2</sub> and Ar = 2,4,6-Cl<sub>3</sub>C<sub>6</sub>H<sub>2</sub>. **B** and **C**: EPR spectroscopy of **41**. **D** and **E**: EPR spectroscopy and SQUID magnetometry of **42**. Parts B, C, D, and E were reproduced form refs 424 and 425. Copyright 2022 and 2023 Wiley.

In 2023, Shintani and coworkers<sup>425</sup> synthesized and isolated aza-triangulene diradical cation **42**. Its EPR spectrum at room temperature perfectly matches the simulated spectrum (Figure 46D). Magnetic studies of polycrystalline **42** by SQUID magnetometry provide a flat  $\chi T$  vs. T plot in the 50 – 300 K temperature range, corresponding to near perfect  $\chi T \approx 0.95 - 0.98$  emu K mol<sup>-1</sup>. These data provide unequivocal confirmation of triplet ground state for aza-triangulene diradical and, based on authors' analysis of correction for diamagnetism, suggest  $\Delta E_{\rm ST} > 2$  kcal mol<sup>-1</sup>. <sup>425</sup> X-ray structure of **42** is refined with adequate reflections/parameters ratio and small residual electron-and-hole densities.

Notably, aza-triangulene **42**, with nearly exclusively thermally populated triplet state at room temperature, shows a significant fluorescence at room temperature with quantum yield of about 1%. <sup>425</sup>

Somewhat surprisingly, CW EPR spectra in triangulenes 38, 39, 41, and 42 in rigid matrices give only relatively narrow center peaks without any discernible side peaks and very weak  $|\Delta m_S| = 2$  transitions. Even for 42 dispersed in diamagnetic matrix, consisting of precursor diol of triangulene 39, a similar EPR spectrum, but with a relatively broader center peak, is obtained, which can be simulated with "apparent  $|D| \approx 37$  MHz". The question arises what is the possible origin of very low values of "apparent |D|" found in triangulenes 38, 39, 41, and 42?

It was noted by the authors in ref 425, that three-fold symmetric conformations (E = 0) of triradicals **AT1** and **AT2** (Figure 17) also have rather low values of |D| = 36 - 37 MHz;<sup>115</sup> however, the inter-spin distances in the triradicals are significantly longer than in **42** and other triangulenes. For analogous S = 1 diradicals **AD-a-b** (Figure 47A), with similar inter-spin distances to **AT1** and **AT2**, experimental |D| = 61 - 71 MHz<sup>115</sup> are comparable to |D| = 75 MHz, reported for the analogous 3,4'-biphenyl-based triarylmethyl diradical.<sup>323</sup>

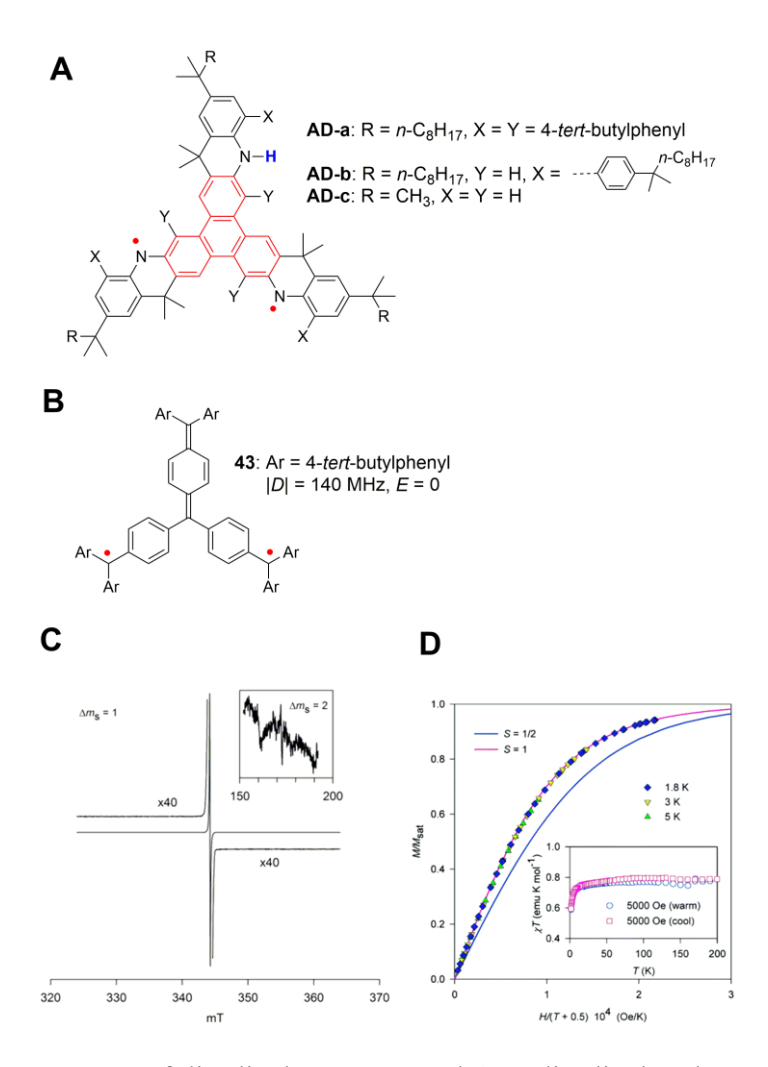


**Figure 47. A** and **B**: Structures of diradicals **AD-a-c** and **43** – diradicals relevant to the apparent small value of |D| in triangulene diradicals. **C** and **D**: EPR spectra at 140 K and SQUID magnetometry for the identical sample of 20 mM diradical **43** in THF- $d_8$ , following annealing at room temperature for 1 h. After annealing at room temperature for additional 2 days, practically identical data are obtained, indicating that **43** is long-term persistent. Parts C and D are reproduced from ref 35. Copyright 2005 American Chemical Society.

We then turn to ORCA-computations of zero-field splitting (parameters D and E), <sup>426</sup> that are carried out at the B3LYP/EPR-II (UNO) level of theory, using dipolar spin-spin approximation (DSS) and neglecting spin-orbit contributions. <sup>427</sup> For triangulene **35**, we compute E = 0 and D = +492 MHz. We note that for analogous diradicals, with the same D-tensor orientations (D > 0), values of D are overestimated by a factor of about 2 at the same level of theory. <sup>112,114</sup> For diradicals

**AD-a-c** (Figure 47A) with D < 0, this overestimate is by a factor of about 2.5 - 3. This would suggest that the experimental |D| for triangulenes **38**, **39**, **41**, and **42** should be in the 200 - 250 MHz range, which is in good agreement with Nakatsuji's |D| = 219 MHz for **37**. Along Notably, Bushby obtained a smaller |D| = 192 MHz because in **36** effective inter-spin distances may be somewhat longer due to a small fraction of spin density residing at the oxygens.

We postulate that the very low values of "apparent |D|" found in triangulenes **38**, **39**, **41**, and **42** are due to exchange narrowing in aggregated samples that are relatively concentrated in poorly matched solvents/matrices. As early as 2005, we demonstrated this phenomenon in long-term persistent S = 1 ground state diradical **43** (Figure 47B).<sup>35</sup> In a dilute frozen solution of ca. 2 mM **43** in 2-MeTHF/THF at 100 K, EPR spectrum consists of a sharp center line (peak-to-peak line width of 0.09 mT) with relative peak height of 100 and four symmetrically distributed well-resolved side-peaks with relative peak height of one, corresponding to the triplet state with E = 0 and  $|D| \approx 140$  MHz. The center peak does mostly correspond to an exchange narrowed diradical **43** because of the following findings.

In more concentrated frozen solutions of ca. 20 mM **43** in THF- $d_8$ , EPR spectrum at 140 K consists of narrow center peak with a line width of 0.08 mT, and  $|\Delta m_S| = 2$  transition is practically not detectable (Figure 47C). SQUID magnetometry on the identical sample is clearly showing almost pure S = 1 ground state diradical, based on magnetization data; the value of  $\chi T < 1.00$  emu K mol<sup>-1</sup> is found because of difficulty in attaining quantitative mass transfers during the low-temperature preparation of **43** (Figure 47D).<sup>35</sup> The indirect evidence for exchange narrowing due to aggregation of 20 mM **43** in THF- $d_8$  is from correlation between mean-field parameter  $\theta = -0.05 - (-0.5)$  K, a measure of intermolecular antiferromagnetic exchange couplings, derived from  $M/M_{\rm sat}$  vs  $H/(T - \theta)$  magnetization data (as well as  $\chi T$  vs T plots at low temperatures) and the line-widths in the EPR spectra; that is, the narrower EPR spectra correspond to the greater value of  $|\theta|$ .<sup>35</sup>

## Conclusion

Over 120 years after Gomberg's discovery of triarylmethyl radicals, research on stable radicals continues to surprise us by the multitude discoveries of new properties and applications in diverse fields of science and technology. More recently, stable, and thermally robust high-spin di- and triradicals, with nearly planar  $\pi$ -systems, have emerged as the new frontier in organic radicals. When properly designed, such radicals possess large energy gaps (vs. thermal energy) separating the high-spin ground state and low-spin excited state. Thus, these radicals may possess relatively large populations of their high-spin ground state at room temperature, and their properties related to paramagnetism, scale with the factor of S(S+1), where the total spin quantum number S corresponds to the high-spin ground state. This implies scaling with approximately  $n^2$ , where n is the number of "unpaired" electrons, for many properties, including relaxivity of MRI contrast agents, dynamic nuclear polarization (DNP), etc., assuming that other controlling factors can be optimized too.

Thermal robustness enables preparation of interesting thin films via evaporation, thus facilitating their potential applications in electronics and spintronics. One example of such high–spin diradical, so far, is a good electrical conductor – contrary to expectations.

Two relations are established:

- (1) between DFT computed singlet triplet energy gap ( $\Delta E_{ST}$ ) in a subset of 12 diradicals and SHI, which is the difference in energy of electrons in HOMO vs. SOMO in the corresponding one electron reduced  $S = \frac{1}{2}$  species (mostly radical anions),
- (2) between 17 experimental pairwise exchange coupling constants J/k (e.g., equal to the half of the  $\Delta E_{\rm ST}$  in a diradical) in nitronyl nitroxide based high-spin di- or triradicals vs. hyperfine coupling constants in the corresponding monoradicals.

Both relations may allow us to identify outliers, which may correspond to radicals where J/k is not measured or computed with sufficient accuracy, e.g., because of the large magnitude of

experimental J/k.

Double helical (or helical) high-spin di- and polyradicals, in which spin density is delocalized

over the chiral  $\pi$ -system, have been barely explored. Notably, the sole example of such high-spin

diradical possesses alternant  $\pi$ -system with Kekulé resonance form. Finally, derivatives of

triangulene diradical provide stable high-spin diradicals with singlet triplet energy gaps, estimated as

a few kcal mol<sup>-1</sup>, which are comparable to the previously reported persistent but air sensitive planar

aminyl diradicals.

We hope this review provides critical analyses that may contribute to the development of new

magnetically and thermally ultra-robust high-spin radicals, which may contribute to ever emerging

applications.

**AUTHOR INFORMATION** 

\* Corresponding Authors

Andrzej Rajca: e-mail, arajca1@unl.edu

**Notes** 

The authors declare no competing financial interests.

**ACKNOWLEDGMENTS** 

We thank all the former Rajca group students and postdoctoral associates who contributed to the

research on high-spin molecules, and whose names appear in the references. We thank Dr. Maren

Pink (Indiana University) for quarter-of-century-long collaboration and her re-refinement of X-ray

structure of diradical 32. We would like to thank the NSF Chemistry Division and the National

Institutes of Health for the support of our research on stable radicals under the following grant numbers: CHE-1665256, CHE-1955349, CHE-2247170, NIGMS R01GM124310-01, and NIBIB R01EB019950-01A1.

- † Present address: Toyota Research Institute of North America, 1555 Woodridge Ave, Ann Arbor, MI 48105, USA.
- <sup>⊥</sup> Present address: Element Biosciences Inc., 10055 Barnes Canyon Rd, Suite 100, San Diego, CA 92121, USA.

## References

- 1. Gomberg, M. An Instance of Trivalent Carbon: Triphenylmethyl. *J. Am. Chem. Soc.* **1900**, *22*, 757–771. DOI: <a href="https://doi.org/10.1021/ja02049a006">https://doi.org/10.1021/ja02049a006</a>
- 2. Gomberg, M. Triphenylmethyl, ein Fall von dreiwerthigem Kohlenstoff. *Ber. Dtsch. Chem. Ges.* **1900**, *33*, 3150–3163. DOI: <a href="https://doi.org/10.1002/cber.19000330369">https://doi.org/10.1002/cber.19000330369</a>
- 3. Hicks, R., Ed., *Stable Radicals: Fundamentals and Applied Aspects of Odd-Electron Compounds*; Wiley: Chichester, **2011**; pp 1–606. DOI:10.1002/9780470666975
- 4. Gerson, F.; Huber, W. *Electron Spin Resonance Spectroscopy of Organic Radicals*. Wiley-VCH: Weinheim, **2003**; pp 1–464. DOI: 10.1002/3527601627
- 5. Forrester, A. R.; Hay, J. M.; Thomson, R. H. *Organic Chemistry of Stable Free Radicals*; Academic Press: New York, **1968**.
- 6. Eberson, L. Gomberg and the Nobel Price. *Adv. Phys. Org. Chem.* **2001**, *36*, 59–84. DOI: https://doi.org/10.1016/S0065-3160(01)36003-3
- 7. Tan, Y.; Hsu, S.-N.; Tahir, H.; Dou, L.; Savoie, B. M.; Boudouris, B. W. Electronic and Spintronic Open-Shell Macromolecules, Quo Vadis? *J. Am. Chem. Soc.* **2022**, *144*, 626–647 (Perspective). DOI: <a href="https://doi.org/10.1021/jacs.1c09815">https://doi.org/10.1021/jacs.1c09815</a>
- 8. Murto, P.; Bronstein, H. Electro-optical π-radicals: design advances, applications and future perspectives. *J. Mater. Chem. C* **2022**, *10*, 7368–7403. DOI: https://doi.org/10.1039/D1TC05268C
- 9. Ahmed, J.; Mandal, S. K. Phenalenyl Radical: Smallest Polycyclic Odd Alternant Hydrocarbon Present in the Graphene Sheet. *Chem. Rev.* **2022**, *122*, 11369–11431. DOI: <a href="https://doi.org/10.1021/acs.chemrev.1c00963">https://doi.org/10.1021/acs.chemrev.1c00963</a>

- 10. Chen, Z. X.; Li, Y.; Huang, F. Persistent and Stable Organic Radicals: Design, Synthesis, and Applications. *Chem* **2021**, *7*, 288–332. DOI: https://doi.org/10.1016/j.chempr.2020.09.024
- 11. Yuan, D.; Liu, W.; Zhu, X. Design and Applications of Single-Component Radical Conductors. *Chem* **2021**, *7*, 333–357. DOI: https://doi.org/10.1016/j.chempr.2020.10.001
- 12. Stuyver, T.; Chen, B.; Zeng, T.; Geerlings, P.; de Proft, F.; Hoffmann, R. Do Diradicals Behave Like Radicals? *Chem. Rev.* **2019**, *119*, 11291–11351. DOI: https://doi.org/10.1021/acs.chemrev.9b00260
- 13. Wingate, A. J.; Boudouris, B. W. Recent advances in the syntheses of radical-containing macromolecules. *J. Polym. Sci., Part A: Polym. Chem.* **2016**, *54*, 1875–1894. DOI: <a href="https://doi.org/10.1002/pola.28088">https://doi.org/10.1002/pola.28088</a>
- 14. Gallagher, N.; Olankitwanit, A.; Rajca, A. High-Spin Organic Molecules. *J. Org. Chem.* **2015**, 80, 1291–1298. DOI: https://doi.org/10.1021/jo502505r
- 15. Winkler, M.; Sander, W. Triradicals. *Acc. Chem. Res.* **2014**, *47*, 31–44. DOI: <a href="https://doi.org/10.1021/ar4000218">https://doi.org/10.1021/ar4000218</a>
- 16. Abe, M. Diradicals. *Chem. Rev.* **2013**, *113*, 7011–7088. DOI: <a href="https://doi.org/10.1021/cr400056a">https://doi.org/10.1021/cr400056a</a>
- 17. Griller, D.; Ingold, K. U. Persistent Carbon-Centered Radicals. *Acc. Chem. Res.* **1976**, *9*, 13–19. DOI: <a href="https://doi.org/10.1021/ar50097a003">https://doi.org/10.1021/ar50097a003</a>
- 18. Colle, K. S.; Glaspie, P. S.; Lewis, E. S. Equilibrium Dissociation of Triphenylmethyl Dimer. *Chem. Comm.* **1975**, 266–267. DOI: <a href="https://doi.org/10.1039/C39750000266">https://doi.org/10.1039/C39750000266</a>
- 19. Jacobson, P. Zur "Triphenylmethyl"-Frage. *Ber. Dtsch. Chem. Ges.* **1905**, *38*, 196–199. DOI: <a href="https://doi.org/10.1002/cber.19050380138">https://doi.org/10.1002/cber.19050380138</a>
- 20. Lankamp, H.; Nauta, W. T.; MacLean, C. New Interpretation of the Monomer-Dimer Equilibrium of Triphenylmethyl- and Alkylsubstituted-Diphenyl Methyl-Radicals in Solution. *Tetrahedron Lett.* **1968**, 249–254. DOI: <a href="https://doi.org/10.1016/S0040-4039(00)75598-5">https://doi.org/10.1016/S0040-4039(00)75598-5</a>
- 21. McBride, J. M. The Hexaphenylane Riddle. *Tetrahedron* **1974**, *30*, 2009–2022. DOI: <a href="https://doi.org/10.1016/S0040-4020(01)97332-6">https://doi.org/10.1016/S0040-4020(01)97332-6</a>
- 22. Duennebacke, D.; Neumann, W. P.; Penenory, A; Ulrich, S. Über sterisch gehinderte freie Radikale, XIX. Stabile 4,4',4"-trisubstituierte Triphenylmethyl-Radikale. *Chem. Ber.* **1989**, *122*, 533–535. DOI: <a href="https://doi.org/10.1002/cber.19891220322">https://doi.org/10.1002/cber.19891220322</a>
- 23. Rajca, A. A Polyarylmethyl Quintet Tetraradical. *J. Am. Chem. Soc.* **1990**, *112*, 5890–5892. DOI: <a href="https://doi.org/10.1021/ja00171a045">https://doi.org/10.1021/ja00171a045</a>
- 24. Rajca, A.; Utamapanya, S. Polyarylmethyl Quartet Triradicals and Quintet Tetraradicals. *J. Am. Chem. Soc.* **1993**, *115*, 2396–2401. DOI: <a href="https://doi.org/10.1021/ja00059a039">https://doi.org/10.1021/ja00059a039</a>
- 25. Rajca, A.; Lu, K.; Rajca, S. High-spin polyarylmethyl polyradical: Fragment of a macrocyclic 2-strand based upon calix[4]arene rings. *J. Am. Chem. Soc.* **1997**, *119*, 10335–10345. DOI: https://doi.org/10.1021/ja971493j

- 26. Rajca, A.; Wongsriratanakul, J.; Rajca, S. High-Spin Organic Polyradicals as Spin Clusters: Ferromagnetic Spin Coupling through Biphenyl Unit in Polyarylmethyl Tri-, Penta-, Hepta-, and Hexadecaradicals. *J. Am. Chem. Soc.* **1997**, *119*, 11674–11686. DOI: https://doi.org/10.1021/ja972378b
- 27. Rajca, A.; Rajca, S.; Wongsriratanakul, J. Very High-Spin Organic Polymer: π-Conjugated Hydrocarbon Network with Average Spin of *S* ≥ 40. *J. Am. Chem. Soc.* **1999**, *121*, 6308–6309. DOI: <a href="https://doi.org/10.1021/ja990881d">https://doi.org/10.1021/ja990881d</a>
- 28. Rajca, S.; Rajca, A.; Wongsriratanakul, J.; Butler, P.; Choi, S. Organic Spin Clusters. Dendritic-Macrocyclic Polyarylmethyl Polyradical with Very High-Spin of *S* = 10 and its Derivatives: Synthesis, Magnetic Studies, and Small Angle Neutron Scattering. *J. Am. Chem. Soc.* **2004**, *126*, 6972–6986. DOI: <a href="https://doi.org/10.1021/ja031548j">https://doi.org/10.1021/ja031548j</a>
- 29. Rajca, A.; Wongsriratanakul, J.; Rajca, S.; Cerny, R. L. Organic Spin Clusters: Annelated Macrocyclic Polyarylmethyl Polyradicals and Polymer with Very High-Spin *S* = 6–18. *Chem. Eur. J.* **2004**, *10*, 3144–3157. DOI: <a href="https://doi.org/10.1002/chem.200306036">https://doi.org/10.1002/chem.200306036</a>
- 30. Rajca, A.; Wongsriratanakul, J.; Rajca, S. Organic Spin Clusters: Macrocyclic-Macrocyclic Polyarylmethyl Polyradicals with Very High-Spin S = 5–13. *J. Am. Chem. Soc.* **2004**, *126*, 6608–6626. DOI: https://doi.org/10.1021/ja031549b
- 31. Rajca, A. The Physical Organic Chemistry of Very High-Spin Polyradicals. *Adv. Phys. Org. Chem.* **2005**, *40*, 153–199. DOI: <a href="https://doi.org/10.1016/S0065-3160(05)40004-0">https://doi.org/10.1016/S0065-3160(05)40004-0</a>
- 32. Rajca, A.; Wongsriratanakul, J.; Rajca, S. Magnetic ordering in an organic polymer. *Science* **2001**, *294*, 1503–1505. DOI: <a href="https://doi.org/10.1126/science.1065477">https://doi.org/10.1126/science.1065477</a>
- 33. Rajca, A.; Utamapanya, S.; Xu, J. Control of Magnetic Interactions in Polyarylmethyl Triplet Diradicals Using Steric Hindrance. *J. Am. Chem. Soc.* **1991**, *113*, 9235–9241. DOI: <a href="https://doi.org/10.1021/ja00024a032">https://doi.org/10.1021/ja00024a032</a>
- 34. Rajca, A.; Utamapanya, S. π-Conjugated Systems with Unique Electronic Structure: A Case of "Planarized" 1,3-Connected Polyarylmethyl Carbodianion and Stable Triplet Hydrocarbon Diradical. *J. Org. Chem.* **1992**, *57*, 1760–1767. DOI: https://doi.org/10.1021/jo00032a030
- 35. Rajca, A.; Shiraishi, K.; Vale, M.; Han, H.; Rajca, S. Stable Hydrocarbon Diradical, an Analogue of Trimethylenemethane. *J. Am. Chem. Soc.* **2005**, *127*, 9014–9020. DOI: <a href="https://doi.org/10.1021/ja052002v">https://doi.org/10.1021/ja052002v</a>
- 36. Ballester, M.; Riera, J.; Castaner, J.; Badía, C.; Monsó, J. M. Inert Carbon Free Radicals. I. Perchlorodiphenylmethyl and Perchlorotriphenylmethyl Radical Series. *J. Am. Chem. Soc.* **1971**, 93, 2215–2225. DOI: <a href="https://doi.org/10.1021/ja00738a021">https://doi.org/10.1021/ja00738a021</a>
- 37. Falle, H. R.; Luckhurst, G. R.; Horsfield, A.; Ballester. M. Electron Resonance Studies of Perchlorodiphenylmethyl and Perchlorotriphenylmethyl Free Radicals. *J. Chem. Phys.* **1969**, *50*, 258–264. DOI: https://doi.org/10.1063/1.1670787
- 38. Ballester, M. Inert free radicals (IFR): a unique trivalent carbon species. *Acc. Chem. Res.* **1985**, *18*, 380-387. DOI: https://doi.org/10.1021/ar00120a004

- 39. Ballester, M. Perchloro-organic chemistry: structure, spectroscopy and reaction pathways. *Adv. Phys. Org. Chem.* **1989**, *25*, 267–445. DOI: https://doi.org/10.1016/S0065-3160(08)60020-9
- 40. Ratera, I.; Vidal-Gancedo, J.; Maspoch, D.; Bromley, S. T.; Crivillers, N.; Mas-Torrent, M. Perspectives for polychlorinated trityl radicals. *J. Mater. Chem. C* **2021**, *9*, 10610–10623. DOI: <a href="https://doi.org/10.1039/D1TC02196F">https://doi.org/10.1039/D1TC02196F</a>
- 41. Armet, O.; Veciana, J.; Rovira, C.; Riera, J.; Castaner, J.; Molins, E.; Rius, J.; Miravitlles, C.; Olivella, S.; Brichfeus, J. Inert Carbon Free Radicals. 8. Polychlorotriphenylmethyl Radicals: Synthesis, Structure, and Spin-Density Distribution. *J. Phys. Chem.* **1987**, *91*, 5608–5616. DOI: <a href="https://doi.org/10.1021/j100306a023">https://doi.org/10.1021/j100306a023</a>
- 42. Hayes, K.; Nagumo, M.; Blount, J. F.; Mislow, K. Structure, optical resolution, and conformational stability of perchlorotriphenylamine. *J. Am. Chem. Soc.* **1980**, *102*, 2773–2776. DOI: <a href="https://doi.org/10.1021/ja00528a043">https://doi.org/10.1021/ja00528a043</a>
- 43. Veciana, J.; Rovira, C.; Crespo, M. I.; Armet, O.; Domingo, V. M.; Palacio, F. Stable polyradicals with high-spin ground state. 1. Synthesis, separation, and magnetic characterization of the stereoisomers of 2,4,5,6-tetrachloro-. alpha.,. alpha.,. alpha.'.alpha.'-tetrakis(pentachlorophenyl)-m-xylene biradical. *J. Am. Chem. Soc.* **1991**, *113*, 2552–2561. DOI: <a href="https://doi.org/10.1021/ja00007a033">https://doi.org/10.1021/ja00007a033</a>
- 44. Veciana, J.; Rovira, C.; Ventosa, N.; Crespo, M. I.; Palacio, F. Stable polyradicals with high-spin ground states. 2. Synthesis and characterization of a complete series of polyradicals derived from 2,4,6-trichloro-.alpha.,.alpha.,.alpha.',.alpha.',.alpha.",.alpha."-hexakis(pentachlorophenyl)mesitylene with *S* = 1/2, 1, and 3/2 ground states. *J. Am. Chem. Soc.* **1993**, *115*, 57–64. DOI: https://doi.org/10.1021/ja00054a008
- 45. Gaudenzi, R.; Burzuri, E.; Reta, D.; Moreira, I. d. P. R.; Bromley, S. T.; Rovira, C.; Veciana, J.; van der Zant, H. S. J. Exchange Coupling Inversion in a High-Spin Organic Triradical Molecule. *Nano Lett.* **2016**, *16*, 2066–2071. DOI: <a href="https://doi.org/10.1021/acs.nanolett.6b00102">https://doi.org/10.1021/acs.nanolett.6b00102</a>
- 46. Joergensen, M.; Rise, F.; Andersson, S.; Almen, T.; Aabye, A.; Wistrand, L. G.; Wikstroem, H.; Golman, K.; Servin, R.; Michelsen, P. Triarylmethyl Radicals and The Use of Inert Carbon Free Radicals in MRI. PCT Int. Appl. wo/9112024, **1991**.
- 47. Reddy, T. J.; Iwama, T.; Halpern, H. J.; Rawal, V. H. General Synthesis of Persistent Trityl Radicals for EPR Imaging of Biological Systems. *J. Org. Chem.* **2002**, *67*, 4635–4639. DOI: <a href="https://doi.org/10.1021/jo011068f">https://doi.org/10.1021/jo011068f</a>
- 48. Poncelet, M.; Huffman, J. L.; Khramtsov, V. V.; Dhimitruka, I.; Driesschaert, B. Synthesis of hydroxyethyl tetrathiatriarylmethyl radicals OX063 and OX071. *RSC Adv.* **2019**, *9*, 35073–35076. DOI: https://doi.org/10.1039/C9RA08633A
- 49. Poncelet, M.; Ngendahimana, T; Gluth, T. D.; Hoblitzell, E.H.; Eubank, T.D.; Eaton, G.R.; Eaton, S.S.; Driesschaert, B. Synthesis and characterization of a biocompatible <sup>13</sup>C1 isotopologue of trityl radical OX071 for *in vivo* EPR viscometry. *Analyst* **2022**, *147*, 5643–5648. DOI: <a href="https://doi.org/10.1039/D2AN01527G">https://doi.org/10.1039/D2AN01527G</a>

- 50. Owenius, R.; Eaton, G. R.; Eaton, S. S. Frequency (250 MHz to 9.2 GHz) and viscosity dependence of electron spin relaxation of triarylmethyl radicals at room temperature. *J. Magn. Reson.* **2005**, *172*, 168–175. DOI: <a href="https://doi.org/10.1016/j.jmr.2004.10.007">https://doi.org/10.1016/j.jmr.2004.10.007</a>
- 51. Hu, K.-N.; Bajaj, V. S.; Rosay, M.; Griffin, R. G. High-frequency dynamic nuclear polarization using mixtures of TEMPO and trityl radicals. *J. Chem. Phys.* **2007**, *126*, 044512. https://doi.org/10.1063/1.2429658
- 52. Mathies, G.; Caporini, M. A.; Michaelis, V. K.; Liu, Y.; Hu, K.-N.; Mance, D.; Zweier, J. L.; Rosay, M.; Baldus, M.; Griffin, R. G. Efficient Dynamic Nuclear Polarization at 800 MHz/527 GHz with Trityl-Nitroxide Biradicals. *Angew. Chem. Int. Ed.* **2015**, *54*, 11770–11774. DOI: <a href="https://doi.org/10.1002/anie.201504292">https://doi.org/10.1002/anie.201504292</a>
- 53. Zhai, W.; Feng, Y.; Liu, H.; Rockenbauer, A.; Mance, D.; Li, S.; Song, Y.; Baldus, M.; Liu, Y. Diastereoisomers of L-proline-linked tritylnitroxide biradicals: synthesis and effect of chiral configurations on exchange interactions. *Chem. Sci.* **2018**, *9*, 4381–4391. DOI: <a href="https://doi.org/10.1039/C8SC00969D">https://doi.org/10.1039/C8SC00969D</a>
- 54. Palani, R. S.; Mardini, M.; Quan, Y.; Griffin, R. G. Dynamic nuclear polarization with trityl radicals. *J. Magn. Reson.* **2023**, *349*, 107411. DOI: <a href="https://doi.org/10.1016/j.jmr.2023.107411">https://doi.org/10.1016/j.jmr.2023.107411</a>
- 55. Dhimitruka, I.; Bobko, A. A.; Eubank, T. D.; Komarov, D. A.; Khramtsov, V. V. Phosphonated trityl probes for concurrent in vivo tissue oxygen and pH monitoring using electron paramagnetic resonance-based techniques. *J. Am. Chem. Soc.* **2013**, *135*, 5904–5910. DOI: <a href="https://doi.org/10.1021/ja401572r">https://doi.org/10.1021/ja401572r</a>
- 56. Yang, Z.; Liu, Y.; Borbat, P.; Zweier, J. L.; Freed, J. H.; Hubbell, W. L. Pulsed ESR dipolar spectroscopy for distance measurements in immobilized spin labeled proteins in liquid solution. *J. Am. Chem. Soc.* **2012**, *134*, 9950–9952. DOI: <a href="https://doi.org/10.1021/ja303791p">https://doi.org/10.1021/ja303791p</a>
- 57. Shevelev, G. Y.; Krumkacheva, O. A.; Lomzov, A. A.; Kuzhelev, A. A.; Rogozhnikova, O. Y.; Trukhin, D. V.; Troitskaya, T. I.; Tormyshev, V. M.; Fedin, M. V.; Pyshnyi, D. V.; et al. Physiological-temperature distance measurement in nucleic acid using triarylmethyl-based spin labels and pulsed dipolar EPR spectroscopy. *J. Am. Chem. Soc.* **2014**, *136*, 9874–9877. DOI: <a href="https://doi.org/10.1021/ja505122n">https://doi.org/10.1021/ja505122n</a>
- 58. Yang, Z.; Bridges, M.D.; López, C.J.; Rogozhnikova, O.Y.; Trukhin, D.V.; Brooks, E.K.; Tormyshev, V.; Halpern, H. J.; Hubbell, W. L. A triarylmethyl spin label for long-range distance measurement at physiological temperatures using T<sub>1</sub> relaxation enhancement. *J. Magn. Reson.* **2016**, *269*, 50–54. DOI: https://doi.org/10.1016/j.jmr.2016.05.006
- 59. Jassoy, J. J.; Berndhäuser, A.; Duthie, F.; Kühn, S. P.; Hagelueken, G.; Schiemann, O. Versatile Trityl Spin Labels for Nanometer Distance Measurements on Biomolecules In Vitro and within Cells. *Angew. Chem. Int. Ed.* **2017**, *56*, 177–181. DOI: <a href="https://doi.org/10.1002/anie.201609085">https://doi.org/10.1002/anie.201609085</a>
- 60. Yang, Y.; Pan, B.-B.; Tan, X.; Yang, F.; Liu, Y.; Su, X.-C.; Goldfarb, D. In-Cell Trityl-Trityl distance measurements on proteins. *J. Phys. Chem. Lett.* **2020**, *11*, 1141–1147. DOI: https://doi.org/10.1021/acs.jpclett.9b03208

- 61. Hasanbasri, Z.; Singewald, K.; Gluth, T. D.; Driesschaert, B.; Saxena, S. Cleavage-Resistant Protein Labeling with Hydrophilic Trityl Enables Distance Measurements In-Cell. *J. Phys. Chem. B* **2021**, *125*, 5265–5274. DOI: <a href="https://doi.org/10.1021/acs.jpcb.1c02371">https://doi.org/10.1021/acs.jpcb.1c02371</a>
- 62. Hasanbasri, Z.; Poncelet, M.; Hunter, H.; Driesschaert, B.; Saxena, S. A new 13C trityl-based spin label enables the use of DEER for distance measurements. *J. Magn. Reson.* **2023**, *347*, 107363-1-8. DOI: https://doi.org/10.1016/j.jmr.2022.107363
- 63. Poncelet, M.; Driesschaert, B. A <sup>13</sup>C-Labeled triarylmethyl radical as an EPR spin probe highly sensitive to molecular tumbling. *Angew. Chem. Int. Ed.* **2020**, *59*, 16451–16454. DOI: <a href="https://doi.org/10.1002/anie.202006591">https://doi.org/10.1002/anie.202006591</a>
- 64. Koelsch, C. F. Syntheses with Triarylvinylmagnesium Bromides. α,γ-Bisdiphenylene-β-phenylallyl, a Stable Free Radical. *J. Am. Chem. Soc.* **1957**, *79*, 4439–4441. DOI: <a href="https://doi.org/10.1021/ja01573a053">https://doi.org/10.1021/ja01573a053</a>
- 65. Mandal, S.; Sigurdsson, S. Th. On the Limited Stability of BDPA Radicals. *Chem. Eur. J.* **2020**, *26*, 7486–7491. DOI: https://doi.org/10.1002/chem.202001084
- 66. Haze, O.; Corzilius, B.; Smith, A. A.; Griffin, R. G.; Swager, T. M. Water-Soluble Narrow-Line Radicals for Dynamic Nuclear Polarization. *J. Am. Chem. Soc.* **2012**, *134*, 14287–14290. DOI: <a href="https://doi.org/10.1021/ja304918g">https://doi.org/10.1021/ja304918g</a>
- 67. Michaelis, V. K.; Smith, A. A.; Corzilius, B.; Haze, O.; Swager, T. M.; Griffin, R. G. High-Field <sup>13</sup>C Dynamic Nuclear Polarization with a Radical Mixture. *J. Am. Chem. Soc.* **2013**, *135*, 2935–2938. DOI: <a href="https://doi.org/10.1021/ja312265x">https://doi.org/10.1021/ja312265x</a>
- 68. Palani, R. S.; Mardini, M.; Delage-Laurin, L.; Banks, D.; Ouyang, Y.; Bryerton, E.; Kempf, J. G.; Swager, T. M.; Griffin, R. G. Amplified Overhauser DNP with Selective Deuteration: Attenuation of Double-Quantum Cross-Relaxation. *J. Phys. Chem. Lett.* **2023**, *14*, 95–100. DOI: <a href="https://doi.org/10.1021/acs.jpclett.2c03087">https://doi.org/10.1021/acs.jpclett.2c03087</a>
- 69. Li, Y.; Equbal, A.; Tabassum, T.; Han, S. <sup>1</sup>H Thermal Mixing Dynamic Nuclear Polarization with BDPA as Polarizing Agents. *J. Phys. Chem. Lett.* **2020**, *11*, 9195–9202. DOI: <a href="https://doi.org/10.1021/acs.jpclett.0c01721">https://doi.org/10.1021/acs.jpclett.0c01721</a>
- 70. Biedenbänder, T.; Aladin, V.; Saeidpour, S.; Corzilius, B. Dynamic Nuclear Polarization for Sensitivity Enhancement in Biomolecular Solid-State NMR. *Chem. Rev.* **2022**, *122*, 9738–9794. DOI: <a href="https://doi.org/10.1021/acs.chemrev.1c00776">https://doi.org/10.1021/acs.chemrev.1c00776</a>
- 71. Mandal, S.; Sigurdsson, S. T. Water-Soluble BDPA Radicals with Improved Persistence. *Chem. Commun.* **2020**, *56*, 13121–13124. DOI: <a href="https://doi.org/10.1039/D0CC04920D">https://doi.org/10.1039/D0CC04920D</a>
- 72. Kuzhelev, A. A.; Denysenkov, V.; Ahmad, I. M.; Rogozhnikova, O. Y.; Trukhin, D. V.; Bagryanskaya, E. G.; Tormyshev, V. M.; Sigurdsson, S. T.; Prisner, T. F. Solid-Effect Dynamic Nuclear Polarization in Viscous Liquids at 9.4 T Using Narrow-Line Polarizing Agents. *J. Am. Chem. Soc.* **2023**, *145*, 10268–10274. DOI: <a href="https://doi.org/10.1021/jacs.3c01358">https://doi.org/10.1021/jacs.3c01358</a>
- 73. Morita, Y.; Suzuki, S.; Sato, K.; Takui, T. Synthetic organic spin chemistry for structurally well-defined open-shell graphene fragments. *Nat. Chem.* **2011**, *3*, 197–204. DOI: <a href="https://doi.org/10.1038/nchem.985">https://doi.org/10.1038/nchem.985</a>

- 74. Goto, K.; Kubo, T.; Yamamoto, K.; Nakasuji, K.; Sato, K.; Shiomi, D.; Takui, T.; Kubota, M.; Kobayashi, T.; Yakusi, K.; et al. A Stable Neutral Hydrocarbon Radical: Synthesis, Crystal Structure, and Physical Properties of 2,5,8-Tri-*tert*-butyl-phenalenyl. *J. Am. Chem. Soc.* **1999**, *121*, 1619–1620. DOI: https://doi.org/10.1021/ja9836242
- 75. Small, D.; Zaitsev, V.; Jung, Y.; Rosokha, S. V.; Head-Gordon, M.; Kochi, J. K. Intermolecular π-to-π bonding between stacked aromatic dyads. *J. Am. Chem. Soc.* **2004**, *126*, 13850–13858. DOI: https://doi.org/10.1021/ja046770i
- 76. Zaitsev, V.; Rosokha, S. V.; Head-Gordon, M.; Kochi, J. K. Steric modulations in the reversible dimerizations of phenalenyl radicals via unusually weak carbon-centered π- and σ-bonds. *J. Org. Chem.* **2006**, *71*, 520–526. DOI: https://doi.org/10.1021/jo051612a
- 77. Uchida, K.; Mou, Z.; Kertesz, M.; Kubo, T. Fluxional σ-Bonds of the 2,5,8-Trimethylphenalenyl Dimer: Direct Observation of the Sixfold σ-Bond Shift via a π-Dimer. *J. Am. Chem. Soc.* **2016**, *138*, 4665–4672. DOI: https://doi.org/10.1021/jacs.6b01791
- 78. Kubo, T. Synthesis, Physical Properties, and Reactivity of Stable, π-Conjugated, Carbon-Centered Radicals. *Molecules* **2019**, *24*, 665. DOI: https://doi.org/10.3390/molecules24040665
- 79. Uchida, K.; Hirao, Y.; Kurata, H.; Kubo, T.; Hatano, S.; Inoue, K. Dual Association Modes of the 2,5,8-Tris(pentafluorophenyl)phenalenyl Radical. *Chem. Asian J.* **2014**, *9*, 1823–1829.
- 80. Mou, Z.; Uchida, K.; Kubo, T.; Kertesz, M. Evidence of σ- and π-Dimerization in a Series of Phenalenyls. *J. Am. Chem. Soc.* **2014**, *136*, 18009–18022. DOI: <a href="https://doi.org/10.1021/ja509243p">https://doi.org/10.1021/ja509243p</a>
- 81. Xiang, Q.; Guo, J.; Xu, J.; Ding, S.; Li, Z.; Li, G.; Phan, H.; Gu, Y.; Dang, Y.; Xu, Z; et al. Stable Olympicenyl Radicals and Their π-Dimers. *J. Am. Chem. Soc.* **2020**, *142*, 11022–11031. DOI: <a href="https://doi.org/10.1021/jacs.0c02287">https://doi.org/10.1021/jacs.0c02287</a>
- 82. Guo, Y.; Ding, S.; Zhang, N.; Xu, Z.; Wu, S.; Hu, J.; Xiang, Q.; Li, Z.-Y.; Chen, X.; Sato, S.; et al. π-Extended Doublet Open-Shell Graphene Fragments Exhibiting One-Dimensional Chain Stacking. *J. Am. Chem. Soc.* **2022**, *144*, 2095–2100. DOI: <a href="https://doi.org/10.1021/jacs.1c12854">https://doi.org/10.1021/jacs.1c12854</a>
- 83. Chi, X.; Itkis, M. E.; Patrick, B. O.; Barclay, T. M.; Reed, R. W.; Oakley, R. T.; Cordes, A. W.; Haddon, R. C. The First Phenalenyl-Based Neutral Radical Molecular Conductor. *J. Am. Chem. Soc.* **1999**, *121*, 10395–10402. DOI: <a href="https://doi.org/10.1021/ja992040c">https://doi.org/10.1021/ja992040c</a>
- 84. Pal, S. K.; Itkis, M. E.; Tham, F. S.; Reed, R. W.; Oakley, R. T.; Haddon, R. C. Resonating valence-bond ground state in a phenalenyl-based neutral radical conductor. *Science* **2005**, *309*, 281–284. DOI: 10.1126/science.1112446
- 85. Pal, S. K.; Itkis, M. E.; Reed, R. W.; Oakley, R. T.; Cordes, A. W.; Tham, F. S.; Siegrist, T.; Haddon, R. C. Synthesis, Structure and Physical Properties of the First One-Dimensional Phenalenyl-Based Neutral Radical Molecular Conductor. *J. Am. Chem. Soc.* **2004**, *126*, 1478–1484. DOI: <a href="https://doi.org/10.1021/ja037864f">https://doi.org/10.1021/ja037864f</a>
- 86. Bag, P.; Itkis, M. E.; Pal, S. K.; Donnadieu, B.; Tham, F. S.; Park, H.; Schlueter, J. A.; Siegrist, T.; Haddon, R. C. Resonating Valence Bond and σ-Charge Density Wave Phases in a

- Benzannulated Phenalenyl Radical. *J. Am. Chem. Soc.* **2010**, *132*, 2684–2694. DOI: https://doi.org/10.1021/ja908768a
- 87. Hartzler, H. D. Polycyano Radicals. *J. Org. Chem.* **1966**, *31*, 2654–2658. DOI: https://doi.org/10.1021/jo01346a047
- 88. de Jongh, H. A. P.; de Jonge, C. R. H. I.; Sinnige, H. J. M.; de Klein, W. J.; Huysmans, W. G. B.; Mijs, W. J.; van den Hoek, W. J.; Smidt, J. Oxidation carbon-carbon coupling. II. Effect of ring substituents on the oxidative carbon-carbon coupling of arylmalonic esters, arylmalodinitriles, and arylcyanoacetic esters. *J. Org. Chem.* **1972**, *37*, 1960–1966. DOI: <a href="https://doi.org/10.1021/jo00977a021">https://doi.org/10.1021/jo00977a021</a>
- 89. Kobashi, T.; Sakamaki, D.; Seki, S. *N*-Substituted Dicyanomethylphenyl Radicals: Dynamic Covalent Properties and Formation of Stimuli-Responsive Cyclophanes by Self-Assembly. *Angew. Chem., Int. Ed.* **2016**, *55*, 8634–8638. DOI: https://doi.org/10.1002/anie.201603409
- 90. Wang, D.; Capel Ferrón, C.; Li, J.; Gámez-Valenzuela, S.; Ponce Ortiz, R.; López Navarrete, J. T.; Hernández Jolín, V.; Yang, X.; Peña Álvarez, M.; García Baonza, V.; et al. New Multiresponsive Chromic Soft Materials: Dynamic Interconversion of Short 2,7-Dicyanomethylenecarbazole-Based Biradicaloid and the Corresponding Cyclophane Tetramer. *Chem. Eur. J.* **2017**, *23*, 13776–13783. https://doi.org/DOI: 10.1002/chem.201702659
- 91. Peterson, J. P.; Geraskina, M. R.; Zhang, R.; Winter, A. H. Effect of Substituents on the Bond Strength of Air-Stable Dicyanomethyl Radical Thermochromes. *J. Org. Chem.* **2017**, *82*, 6497–6501. DOI: <a href="https://doi.org/10.1021/acs.joc.7b01188">https://doi.org/10.1021/acs.joc.7b01188</a>
- 92. Okino, K.; Hira, S.; Inoue, Y.; Sakamaki, D.; Seki, S. The Divergent Dimerization Behavior of *N*-Substituted Dicyanomethyl Radicals: Dynamically Stabilized versus Stable Radicals. *Angew. Chem. Int. Ed.* **2017**, *56*, 16597–16601. DOI: <a href="https://doi.org/10.1002/ange.201710354">https://doi.org/10.1002/ange.201710354</a>
- 93. Peterson, J. P.; Winter, A. H. Solvent Effects on the Stability and Delocalization of Aryl Dicyanomethyl Radicals: The Captodative Effect Revisited. *J. Am. Chem. Soc.* **2019**, *141*, 12901–12906. DOI: <a href="https://doi.org/10.1021/jacs.9b06576">https://doi.org/10.1021/jacs.9b06576</a>
- 94. Peterson, J. P.; Winter, A. H. Solvent-Responsive Radical Dimers. *Org. Lett.* **2020**, *22*, 6072–6076. DOI: <a href="https://doi.org/10.1021/acs.orglett.0c02152">https://doi.org/10.1021/acs.orglett.0c02152</a>
- 95. Peterson, j. P.; Ellern, A.; Winter, A. H. Spin Delocalization, Polarization, and London Dispersion Forces Govern the Formation of Diradical Pimers. *J. Am. Chem. Soc.* **2020**, *142*, 5304–5313. DOI: <a href="https://doi.org/10.1021/jacs.0c00190">https://doi.org/10.1021/jacs.0c00190</a>
- 96. Zhang, R.; Ellern, A.; Winter, A. H. Steric Hindrance Favors σ Dimerization over π Dimerization for Julolidine Dicyanomethyl Radicals. *J. Org. Chem.* **2022**, 87, 1507–1511. DOI: <a href="https://doi.org/10.1021/acs.joc.1c02246">https://doi.org/10.1021/acs.joc.1c02246</a>
- 97. Okino, K.; Sakamaki, D.; Seki, S. Dicyanomethyl Radical-Based Near-Infrared Thermochromic Dyes with High Transparency in the Visible Region. *ACS Mater. Lett.* **2019**, *1*, 25–29. DOI: <a href="https://doi.org/10.1021/acsmaterialslett.9b00049">https://doi.org/10.1021/acsmaterialslett.9b00049</a>

- 98. Zhang, R.; Ellern, A.; Winter, A. H. Anti-Aromaticity Relief as an Approach to Stabilize Free Radicals. *Angew. Chem. Int. Ed.* **2021**, *60*, 25082–25088. DOI: <a href="https://doi.org/10.1002/anie.202110870">https://doi.org/10.1002/anie.202110870</a>
- 99. Adinarayana, B.; Shimizu, D.; Osuka, A. Stable (B<sup>III</sup>-Subporphyrin-5-yl)dicyanomethyl Radicals. *Chem. Eur. J.* **2019**, *25*, 1706–1710. DOI: <a href="https://doi.org/10.1002/chem.201805601">https://doi.org/10.1002/chem.201805601</a>
- 100. Ishimoto, M.; Sakamaki, D.; Fujiwara, H. A dicyanomethyl radical stabilized by ferrocene: a new building block for radical-based dynamic covalent chemistry with redox activity. *Chem. Commun.* **2022**, *58*, 3553–3556. DOI: <a href="https://doi.org/10.1039/D1CC07253F">https://doi.org/10.1039/D1CC07253F</a>
- 101. Albrecht, A.; Rupf, S. M.; Sellin, M.; Schlögl, J.; Riedel, S.; Malischewski, M. Increasing the oxidation power of TCNQ by coordination of B(C<sub>6</sub>F<sub>5</sub>)<sub>3</sub>. *Chem. Commun.* **2022**, *58*, 4958–4961. DOI: <a href="https://doi.org/10.1039/D2CC00314G">https://doi.org/10.1039/D2CC00314G</a>
- 102. Liu, M.; Yang, X.; Sun, Q.; Wang, T.; Pei, R.; Yang, X.; Zhao, Y.; Zhao, L.; Frenking, G.; Wang, X. Lewis Acid-Mediated Radical Stabilization and Dynamic Covalent Bonding: Tunable, Reversible and Photocontrollable. *Angew. Chem. Int. Ed.* 2023, 62, e202300068. DOI: <a href="https://doi.org/10.1002/anie.202300068">https://doi.org/10.1002/anie.202300068</a>
- 103. Haider, K.; Soundararajan, N.; Shaffer, M.; Platz, M. S. EPR spectroscopy of a diaza derivative of meta-xylylene. *Tetrahedron Lett.* **1989**, *30*, 1225–1228. DOI: <a href="https://doi.org/10.1016/S0040-4039(00)72721-3">https://doi.org/10.1016/S0040-4039(00)72721-3</a>
- 104. Quast, H.; Nüdling, W.; Klemm, G.; Kirschfeld, A.; Neuhaus, P.; Sander, W.; Hrovat, D. A.; Borden, W. T. A Perimidine-Derived Non-Kekulé Triplet Diradical. *J. Org. Chem.* **2008**, *73*, 4956–4961. DOI: <a href="https://doi.org/10.1021/jo800589y">https://doi.org/10.1021/jo800589y</a>
- 105. Pratley, C.; Fenner, S.; Murphy, J. A. Nitrogen-Centered Radicals in Functionalization of sp2 Systems: Generation, Reactivity, and Applications in Synthesis. *Chem. Rev.* **2022**, *122*, 8181–8260. DOI: https://doi.org/10.1021/acs.chemrev.1c00831
- 106. Chen, N.; Xu, H. C. Electrochemical generation of nitrogen-centered radicals for organic synthesis. *Green Synth. Catal.* **2021**, *2*, 165–178. DOI: https://doi.org/10.1016/j.gresc.2021.03.002
- 107. Pang, H.; Walker, L. M.; Silakov, A.; Zhang, P.; Yang, W.; Elliott, S. J.; Yokoyama, K. Mechanism of Reduction of an Aminyl Radical Intermediate in the Radical SAM GTP 3',8-Cyclase MoaA. *J. Am. Chem. Soc.* **2021**, *143*, 13835–13844. DOI: <a href="https://doi.org/10.1021/jacs.1c06268">https://doi.org/10.1021/jacs.1c06268</a>
- 108. Neugebauer, F. A.; Fischer, H.; Bamberger, S.; Smith, H. O. Aminyle, 6. tert.-Butyl-substituierte 9-Carbazolyl-Radikale, Carbazol-Radikalkationen und Carbazol-9-oxyl-Radikale. *Chem. Ber.* **1972**, *105*, 2694–2713. DOI: <a href="https://doi.org/10.1002/cber.19721050830">https://doi.org/10.1002/cber.19721050830</a>
- 109. Ballester, N.; Castaner, J.; Olivella, S. Syntheses and isolation of the perchlodiphenylaminyl, an exceptionally stable radical. *Tetrahedron Lett.* **1974**, *15*, 615–616. DOI: <a href="https://doi.org/10.1016/S0040-4039(01)82286-3">https://doi.org/10.1016/S0040-4039(01)82286-3</a>
- 110. Rajca, A.; Shiraishi, K.; Pink, M.; Rajca, S. Triplet (*S* = 1) Ground State Aminyl Diradical. *J. Am. Chem. Soc.* **2007**, *129*, 7232–7233. DOI: <a href="https://doi.org/10.1021/ja071881d">https://doi.org/10.1021/ja071881d</a>

- 111. Boratyński, P.; Pink, M.; Rajca, S.; Rajca, A. Isolation of the Triplet Ground State Aminyl Diradical. *Angew. Chem. Int. Ed.* **2010**, *49*, 5459–5462. DOI: <a href="https://doi.org/10.1002/anie.201002811">https://doi.org/10.1002/anie.201002811</a>
- 112. Rajca, A.; Olankitwanit, A.; Rajca, S. Triplet Ground State Derivative of Aza-*m*-Xylylene Diradical with Large Singlet–Triplet Energy Gap. *J. Am. Chem. Soc.* **2011**, *133*, 4750–4753. DOI: <a href="https://doi.org/10.1021/ja200708b">https://doi.org/10.1021/ja200708b</a>
- 113. Rajca, A.; Olankitwanit, A.; Wang, Y.; Boratynski, P. J.; Pink, M.; Rajca, S. High-Spin *S* = 2 Ground State Aminyl Tetraradicals. *J. Am. Chem. Soc.* **2013**, *135*, 18205–18215. DOI: <a href="https://doi.org/10.1021/ja409472f">https://doi.org/10.1021/ja409472f</a>
- 114. Olankitwanit, A.; Pink, M.; Rajca, S.; Rajca, A. Synthesis of Aza-*m*-Xylylene Diradicals with Large Singlet-Triplet Energy Gap and Statistical Analyses of their EPR Spectra. *J. Am. Chem. Soc.* **2014**, *136*, 14277–14288. DOI: <a href="https://doi.org/10.1021/ja508119d">https://doi.org/10.1021/ja508119d</a>
- 115. Zhang, H.; Pink, M.; Wang, Y.; Rajca, S.; Rajca, A. High-Spin S = 3/2 Ground-State Aminyl Triradicals: Toward High-Spin Oligo-Aza Nanographenes. *J. Am. Chem. Soc.* **2022**, *144*, 19576–19591. DOI: <a href="https://doi.org/10.1021/jacs.2c09241">https://doi.org/10.1021/jacs.2c09241</a>
- 116. Shimizu, D.; Osuka, A. A Benzene-1,3,5-Triaminyl Radical Fused with Zn-II-Porphyrins: Remarkable Stability and a High-Spin Quartet Ground State. *Angew. Chem. Int. Ed.* **2018**, *57*, 3733–3736. DOI: https://doi.org/10.1002/anie.201801080
- 117. Skórka, Ł.; Maurel, V.; Gosk, J. B.; Puźniak, R.; Mouesca, J. -M.; Kulszewicz-Bajer, I. Highly Efficient Tuning of Ferromagnetic Spin Interactions in High-Spin Arylamine Structures by Incorporation of Spin Bearing Carbazole Units. *J. Phys. Chem. B* 2018, 122, 9584–9591. DOI: <a href="https://doi.org/10.1021/acs.jpcb.8b07496">https://doi.org/10.1021/acs.jpcb.8b07496</a>
- 118. Wang, Y.; Olankitwanit, A.; Rajca, S.; Rajca, A. Intramolecular Hydrogen Atom Transfer in Aminyl Radical at Room Temperature with Large Kinetic Isotope Effect. *J. Am. Chem. Soc.* **2017**, *139*, 7144–7147. DOI: <a href="https://doi.org/10.1021/jacs.7b02692">https://doi.org/10.1021/jacs.7b02692</a>
- 119. Wang, Y.; Rajca, S.; Rajca, A. PEGylated, Water-Soluble, Stable Aminyl Radical. *J. Org. Chem.* **2017**, *82*, 7512–7518. DOI: <a href="https://doi.org/10.1021/acs.joc.7b01212">https://doi.org/10.1021/acs.joc.7b01212</a>
- 120. Kosower, E. M.; Poziomek, E. J. Isolation and Distillation of 1-Ethyl-4-carbomethoxypyridinyl. *J. Am. Chem. Soc.* **1963**, *85*, 2035–2036. DOI: <a href="https://doi.org/10.1021/ja00896a043">https://doi.org/10.1021/ja00896a043</a>
- 121. Kosower, E. M.; Poziomek, E. J. Stable Free Radicals. I. Isolation and Distillation of 1-Ethyl-4-carbomethoxypyridinyl. *J. Am. Chem. Soc.* **1964**, *86*, 5515–5523. DOI: <a href="https://doi.org/10.1021/ja01078a025">https://doi.org/10.1021/ja01078a025</a>
- 122. Hermolin, J.; Levin, M.; Ikegami, Y.; Sawayanagi, M.; Kosower, E. M. 1-Alkyl-2-(carbomethoxy)pyridinyl radicals: monomers and dimers defined through chemical and photochemical properties and electron paramagnetic resonance. *J. Am. Chem. Soc.* **1981**, *103*, 4795–4800. DOI: <a href="https://doi.org/10.1021/ja00406a021">https://doi.org/10.1021/ja00406a021</a>
- 123. Okada, K.; Matsumoto, K.; Oda, M.; Murai, H.; Akiyama, K.; Ikegami, Y. Preparations and spin-spin interactions of 4,4'-(*m*-phenylene)-bis-(1-methyl-2,6-diphenylpyridinyl) and its

- analogue. *Tetrahedron Lett.* **1995**, 36, 6689–6692. DOI: <a href="https://doi.org/10.1016/00404-0399(50)1261-F">https://doi.org/10.1016/00404-0399(50)1261-F</a>
- 124. Matsumoto, K.; Inokuchi, D.; Hirao, Y.; Kurata, H.; Sato, K.; Takui, T.; Kubo, T. Synthesis and Identification of a Trimethylenemethane Derivative π-Extended with Three Pyridinyl Radicals. *Org. Lett.* **2010**, *12*, 836–839. DOI: <a href="https://doi.org/10.1021/ol902937k">https://doi.org/10.1021/ol902937k</a>
- 125. Goldschmidt, S.; Renn, K. Zweiwertiger stickstoff: Über das α,α-diphenyl-β-trinitrophenyl hydrazyl. *Ber. Dtsch. Chem. Ges. B* **1922**, *B55*, 628–643. DOI: <a href="https://doi.org/10.1002/cber.19220550308">https://doi.org/10.1002/cber.19220550308</a>
- 126. Proll, P. J.; Sutcliffe, L. H. Kinetics of the decomposition of DPPH in some non-aqueous solvents. Trans. Faraday. Soc. **1963**, 59, 2090–2098. DOI: <a href="https://doi.org/10.1039/TF9635902090">https://doi.org/10.1039/TF9635902090</a>
- 127. Inokuchi, H., Harada, Y. & Maruyama, Y. Electric properties of the single-crystal and thin film of α,α'-diphenyl-β-picrylhydrazyl. *Bull. Chem. Soc. Jpn.* **1962**, *35*, 1559–1561. DOI: <a href="https://doi.org/10.1246/bcsj.35.1559">https://doi.org/10.1246/bcsj.35.1559</a>
- 128. Eley, D. D.; Jones, K. W.; Littler, J. G. F. & Willis, M. R. Semiconductivity of organic substances. Part 10. Electrical properties of galvinoxyl, *α*,*α*-diphenyl-*β*-picryl hydrazyl and related solid free radicals. *Trans. Faraday Soc.***1966**, *62*, 3192–3200. DOI: https://doi.org/10.1039/TF9666203192
- 129. Blatter, H. M.; Lukaszewski, H. A new stable free radical. *Tetrahedron Lett.* **1968**, *9*, 2701–2705. DOI: <a href="https://doi.org/10.1016/S0040-4039(00)89678-1">https://doi.org/10.1016/S0040-4039(00)89678-1</a>
- 130. Constantinides, C. P.; Koutentis, P. A.; Krassos, J.; Rawson, J. M.; Tasiopoulos, J. Characterization and Magnetic Properties of a "Super Stable" Radical 1,3-Diphenyl-7-trifluoromethyl-1,4-dihydro-1,2,4-benzotriazin-4-yl. *J. Org. Chem.* **2011**, *76*, 2798–2806. DOI: <a href="https://doi.org/10.1021/jo200210s">https://doi.org/10.1021/jo200210s</a>
- 131. Constantinides, C. P.; Koutentis, P. A. Stable N- and N/S-Rich Heterocyclic Radicals: Synthesis and Applications. *Adv. Heterocycl. Chem.* **2016**, *119*, 173–207. DOI: https://doi.org/10.1016/bs.aihch.2016.03.001
- 132. Rogers, F. J. M.; Norcott, P. L.; Coote, M. L. Recent advances in the chemistry of benzo[*e*][1,2,4]triazinyl radicals. *Org. Biomol. Chem.* **2020**, *18*, 8255–8277. DOI: <a href="https://doi.org/10.1039/D0OB01394C">https://doi.org/10.1039/D0OB01394C</a>
- 133. Ji, Y.; Long, L.; Zheng, Y. Recent advances of stable Blatter radicals: Synthesis, properties and applications. *Mater. Chem. Front.* **2020**, *4*, 3433–3443. DOI: <a href="https://doi.org/10.1039/D0QM00122H">https://doi.org/10.1039/D0QM00122H</a>
- 134. Obijalska, E.; Pietrzak, A.; Constantinides, C. P.; Sommer, R. D.; Kaszyński, P. "Super stable" Blatter radicals through ArLi addition: surprising chemistry of 7- (trifluoromethyl)benzo[e][1,2,4]triazine. *Chem. Commun.* **2023**, 59, 4008-4011. DOI: <a href="https://doi.org/10.1039/D3CC00832K">https://doi.org/10.1039/D3CC00832K</a>
- 135. Constantinides, C. P.; Berezin, A. A.; Zissimou, G. A.; Manoli, M.; Leitus, G. M.; Bendikov, M.; Probert, M. R.; Rawson, J. M.; Koutentis, P. A. A Magnetostructural Investigation of an

- Abrupt Spin Transition for 1-Phenyl-3-trifluoromethyl-1,4-dihydrobenzo[e][1,2,4]triazin-4-yl. *J. Am. Chem. Soc.* **2014**, *136*, 11906–11909. DOI: <a href="https://doi.org/10.1021/ja5063746">https://doi.org/10.1021/ja5063746</a>
- 136. Perras, F. A.; Flesariu, D. F.; Southern, S. A.; Nicolaides, C.; Bazak, J. D.; Washton, N. M.; Trypiniotis, T.; Constantinides, C. P.; Koutentis, P. A. Methyl-Driven Overhauser Dynamic Nuclear Polarization. *J. Phys. Chem. Lett.* 2022, *13*, 4000–4006. DOI: <a href="https://doi.org/10.1021/acs.jpclett.2c00748">https://doi.org/10.1021/acs.jpclett.2c00748</a>
- 137. Ciccullo, F.; Gallagher, N. M.; Geladari, O.; Chasse, T.; Rajca, A.; Casu, M. D. A Derivative of the Blatter Radical as a Potential Metal-Free Magnet for Stable Thin Films and Interfaces. *ACS Appl. Mater. Interfaces* **2016**, *8*, 1805–1812. DOI: <a href="https://doi.org/10.1021/acsami.5b09693">https://doi.org/10.1021/acsami.5b09693</a>
- 138. Zheng, Y.; Miao, M.-S.; Kemei, M. C.; Seshadri, R.; Wudl, F. The Pyreno-Triazinyl Radical Magnetic and Sensor Properties. *Isr. J. Chem.* **2014**, *54*, 774–778. DOI: <a href="https://doi.org/10.1002/ijch.201400034">https://doi.org/10.1002/ijch.201400034</a>
- 139. Casu, M. B. Nanoscale studies of organic radicals: surface, interface, and spinterface. *Acc. Chem. Res.* **2018**, *51*, 753–760. DOI: https://doi.org/10.1021/acs.accounts.7b00612
- 140. Junghoefer, T.; Calzolari, A.; Baev, I.; Glaser, M.; Ciccullo, F.; Giangrisostomi, E.; Ovsyannikov, R.; Kielgast, F.; Nissen, M.; Schwarz, J.; et al. Magnetic behavior in metal-free radical thin films. *Chem.* **2022**, *8*, P801–814. DOI: <a href="https://doi.org/10.1016/j.chempr.2021.11.021">https://doi.org/10.1016/j.chempr.2021.11.021</a>
- 141. Low, J. Z.; Kladnik, G.; Patera, L. L.; Sokolov, S.; Lovat, G.; Kumarasamy, E.; Repp, J.; Campos, L. M.; Cvetko, D.; Morgante, A.; et al. The Environment-Dependent Behavior of the Blatter Radical at the Metal–Molecule Interface. *Nano Lett.* **2019**, *19*, 2543–2548. DOI: <a href="https://doi.org/10.1021/acs.nanolett.9b00275">https://doi.org/10.1021/acs.nanolett.9b00275</a>
- 142. Cigl, M.; Pociecha, D.; Jakubowski, R.; Kapuściński, S.; Kaszyński, P. Paramagnetic Liquid Crystals With Close π–π Packing: The Effect of Blatter Radical Planarization on Behavior of Bent-Core Mesogens. *Chem. Eur. J.* 2023, 29, e202203288. DOI: <a href="https://doi.org/10.1002/chem.202203288">https://doi.org/10.1002/chem.202203288</a>
- 143. Jasiński, M.; Szczytko, J.; Pociecha, D.; Monobe, H.; Kaszyński, P. Substituent-dependent magnetic behavior of discotic benzo[*e*][1,2,4]triazinyls. *J. Am. Chem. Soc.* **2016**, *138*, 9421–9424. DOI: https://doi.org/10.1021/jacs.6b06444
- 144. Steen, J. S.; Nuismer, J. L.; Eiva, V.; Wiglema, A. E. T.; Daub, N.; Hjelm, J.; Otten, E. Blatter Radicals as Bipolar Materials for Symmetrical Redox-Flow Batteries. *J. Am. Chem. Soc.* **2022**, *144*, 5051–5058. DOI: <a href="https://doi.org/10.1021/jacs.1c13543">https://doi.org/10.1021/jacs.1c13543</a>
- 145. Ciccullo, F.; Calzolari, A.; Bader, K.; Neugebauer, P.; Gallagher, N. M.; Rajca, A.; van Slageren, J.; Casu, M. B. Interfacing a Potential Purely Organic Molecular Quantum Bit with a Real-Life Surface. *ACS Appl. Mater. Interfaces* **2019**, *11*, 1571–1578. DOI: https://doi.org/10.1021/acsami.8b16061
- 146. Poryvaev, A. S.; Gjuzi, E.; Polyukhov, D. M.; Hoffmann, F.; Frçba, M.; Fedin, M. V. Blatter-Radical-Grafted Mesoporous Silica as Prospective Nanoplatform for Spin Manipulation at Ambient Conditions. *Angew. Chem. Int. Ed.* 2021, 60, 8683–8688. DOI: <a href="https://doi.org/10.1002/anie.202015058">https://doi.org/10.1002/anie.202015058</a>

- 147. Gallagher, N. M.; Bauer, J. J.; Pink, M.; Rajca, S.; Rajca, A. High-Spin Organic Diradical with Robust Stability. *J. Am. Chem. Soc.* **2016**, *138*, 9377–9380. DOI: <a href="https://doi.org/10.1021/jacs.6b05080">https://doi.org/10.1021/jacs.6b05080</a>
- 148. Gallagher, N.; Zhang, H.; Junghoefer, T.; Giangrisostomi, E.; Ovsyannikov, R.; Pink, M.; Rajca, S.; Casu, M. B.; Rajca, A. Thermally and Magnetically Robust Triplet Ground State Diradical. *J. Am. Chem. Soc.* **2019**, *141*, 4764–4774. DOI: <a href="https://doi.org/10.1021/jacs.9b00558">https://doi.org/10.1021/jacs.9b00558</a>
- 149. Shu, C.; Pink, M.; Junghoefer, T.; Nadler, E.; Rajca, S.; Casu, M. B.; Rajca, A. Synthesis and Thin Films of Thermally Robust Quartet (*S* = 3/2) Ground State Triradical. *J. Am. Chem. Soc.* **2021**, *143*, 5508–5518. DOI: <a href="https://doi.org/10.1021/jacs.1c01305">https://doi.org/10.1021/jacs.1c01305</a>
- 150. Zhang, S.; Pink, M.; Junghoefer, T.; Zhao, W.; Hsu, S.-N.; Rajca, S.; Calzolari, A.; Boudouris, B. W.; Casu, M. B.; Rajca, A. High-Spin (*S* = 1) Blatter-Based Diradical with Robust Stability and Electrical Conductivity. *J. Am. Chem. Soc.* **2022**, *144*, 6059–6070. DOI: https://doi.org/10.1021/jacs.2c01141
- 151. Neugebauer, F. A. Hydrazidinyl Radicals: 1,2,4,5-Tetraazapentenyls, Verdazyls, and Tetrazolinyls. *Angew. Chem. Int. Ed.* **1973**, *12*, 455–464. DOI: <a href="https://doi.org/10.1002/anie.197304551">https://doi.org/10.1002/anie.197304551</a>
- 152. Gao, S.; Ding, J.; Yua, S.; Li, F. Stable nitrogen-centered radicals with anti-Kasha emission. *J. Mater. Chem. C*, **2023**, *11*, 6400–6406. DOI: <a href="https://doi.org/10.1039/D2TC05471J">https://doi.org/10.1039/D2TC05471J</a>
- 153. Tretyakov, E. V.; Zhivetyeva, S. I.; Petunin, P. V.; Gorbunov, D. E.; Gritsan, N. P.; Bagryanskaya, I. Y.; Bogomyakov, A. S.; Postnikov, P. S.; Kazantsev, M. S.; Trusova, M. E.; et al. Ferromagnetically Coupled *S* = 1 Chains in Crystals of Verdazyl-Nitronyl Nitroxide Diradicals. *Angew. Chem., Int. Ed.* **2020**, *59*, 20704–20710. DOI: <a href="https://doi.org/10.1002/anie.202010041">https://doi.org/10.1002/anie.202010041</a>
- 154. Tretyakov, E. V.; Petunin, P. V.; Zhivetyeva, S. I.; Gorbunov, D. E.; Gritsan, N. P.; Fedin, M. V.; Stass, D. V.; Samoilova, R. I.; Bagryanskaya, I. Y.; Shundrina, I. K.; et al. Platform for High-Spin Molecules: A Verdazyl-Nitronyl Nitroxide Triradical with Quartet Ground State. *J. Am. Chem. Soc.* **2021**, *143*, 8164–8176. DOI: https://doi.org/10.1021/jacs.1c02938
- 155. Neugebauer, F.A. Crystalline tetrazolinyl radical. *Angew. Chem. Int. Ed.* **1969**, *8*, 520–521. DOI: <a href="https://doi.org/10.1002/anie.196905201">https://doi.org/10.1002/anie.196905201</a>
- 156. Kuhn R.; Jerchel, D. Kristallisiertes 2,3-Diphenylen-5-phenyl-tetrazolium-Radikal. *Liebigs Ann. Chem* **1952**, *578*, 1–5. DOI: <a href="https://doi.org/10.1002/jlac.19525780102">https://doi.org/10.1002/jlac.19525780102</a>
- 157. Jerchel, D.; Fischer, H. 2,3-Diphenylen-tetrazoliumsalze und daraus entstehende Radicale. *Liebigs Ann. Chem* **1954**, *590*, 216–231. DOI: https://doi.org/10.1002/jlac.19545900304
- 158. Neugebauer, F. A. Substituted 5-*t*-butyl tetrazolinyl and phototetrazolinyl radicals. *Tetrahedron* **1970**, *26*, 4843-4851. DOI: <a href="https://doi.org/10.1016/S0040-4020(01)93136-9">https://doi.org/10.1016/S0040-4020(01)93136-9</a>
- 159. Kanal, F.; Schleier, D.; Nuernberger, P. Ultrafast Photogeneration of a Tetrazolinyl Radical. *ChemPhysChem* **2015**, *16*, 3143–3146. DOI: <a href="https://doi.org/10.1002/cphc.201500628">https://doi.org/10.1002/cphc.201500628</a>

- 160. Bolze, T.; Were, J.-L.; Kanal, F.; Schleier, D.; Nuernberger, P. Ultrafast Dynamics of a Fluorescent Tetrazolium Compound in Solution. *ChemPhysChem* **2018**, *19*, 138–147. DOI: <a href="https://doi.org/10.1002/cphc.201700831">https://doi.org/10.1002/cphc.201700831</a>
- 161. Yang, Z.; Pink, M.; Nowik-Boltyk, E. M.; Lu, S.; Junghoefer, T.; Rajca, S.; Stoll, S.; Casu, M. B.; Rajca, A. Thermally Ultra-Robust  $S = \frac{1}{2}$  Tetrazolinyl Radicals: Synthesis, Electronic Structure, Magnetism, and Nanoneedle Assemblies on Silicon Surface. *J. Am. Chem. Soc.* **2023**, *145*, 13335–13346. DOI: <a href="https://doi.org/10.1021/jacs.3c03402">https://doi.org/10.1021/jacs.3c03402</a>
- 162. Rosantzev, E. G.; Neiman, M. B. Organic Radical Reactions Involving No Free Valence. *Tetrahedron* **1964**, *20*, 131–137. DOI: <a href="https://doi.org/10.1016/S0040-4020(01)98404-2">https://doi.org/10.1016/S0040-4020(01)98404-2</a>
- 163. Rozantsev, E. G. *Free Nitroxyl Radicals*; Plenum Press: New York and London, 1970. DOI: <a href="https://doi.org/10.1007/978-1-4757-0710-6">https://doi.org/10.1007/978-1-4757-0710-6</a>
- 164. Nutting, J. E.; Rafiee, M.; Stahl, S. S. Tetramethylpiperidine N-Oxyl (TEMPO), Phthalimide N-Oxyl (PINO), and Related N-Oxyl Species: Electrochemical Properties and Their Use in Electrocatalytic Reactions. *Chem. Rev.* 2018, 118, 4834–4885. DOI: <a href="https://doi.org/10.1021/acs.chemrev.7b00763">https://doi.org/10.1021/acs.chemrev.7b00763</a>
- 165. Tebben, L.; Studer, A. Nitroxides: Applications in Synthesis and in Polymer Chemistry. *Angew. Chem., Int. Ed.* **2011**, *50*, 5034–5068. DOI: <a href="https://doi.org/10.1002/anie.201002547">https://doi.org/10.1002/anie.201002547</a>
- 166. Zagdoun, A.; Casano, G.; Ouari, O.; Schwarzwalder, M.; Rossini, A. J.; Aussenac, F.; Yulikov, M.; Jeschke, G.; Coperet, C.; Lesage, A.; et al. Large Molecular Weight Nitroxide Biradicals Providing Efficient Dynamic Nuclear Polarization at Temperatures up to 200 K. J. Am. Chem. Soc. 2010, 135, 12790–12797. DOI: https://doi.org/10.1021/ja405813t
- 167. Dane, E. L.; Corzilius, B.; Rizzato, E.; Stocker, P.; Maly, T.; Smith, A. A.; Griffin, R. G.; Ouari, O.; Tordo, P.; Swager, T. M. Rigid Orthogonal Bis-TEMPO Biradicals with Improved Solubility for Dynamic Nuclear Polarization. *J. Org. Chem.* **2012**, *77*, 1789–1797. DOI: <a href="https://doi.org/10.1021/jo202349j">https://doi.org/10.1021/jo202349j</a>
- 168. Soule, B. P.; Hyodo, F.; Matsumoto, K.; Simone, N. L.; Cook, J. A.; Krishna, M. C.; Mitchell, J. B. Therapeutic and clinical applications of nitroxide compounds. *Antioxid. Redox Signal.* **2007**, *9*, 1731–1743. DOI: https://doi.org/10.1089/ars.2007.1722
- 169. Matsumoto, K.; Mitchell, J. B.; Krishna, M. C. Multimodal Functional Imaging for Cancer/Tumor Microenvironments Based on MRI, EPRI, and PET. *Molecules* **2021**, *26*, 1614 (1-27). DOI: <a href="https://doi.org/10.3390/molecules26061614">https://doi.org/10.3390/molecules26061614</a>
- 170. Nakahara, K.; Iwasa, S.; Satoh, M.; Morioka, Y.; Iriyama, J.; Suguro, M.; Hasegawa, E. Rechargeable batteries with organic radical cathodes. *Chem. Phys. Lett.* **2002**, *359*, 351–354. DOI: <a href="https://doi.org/10.1016/S0009-2614(02)00705-4">https://doi.org/10.1016/S0009-2614(02)00705-4</a>
- 171. Nishide, H.; Oyaizu, K. Toward Flexible Batteries. *Science* **2008**, *319*, 737–738. DOI: 10.1126/science.1151831
- 172. Nishide, H. Organic redox polymers as electrochemical energy materials. *Green Chem.* **2022**, 24, 4650–4679. DOI: https://doi.org/10.1039/D2GC00981A

- 173. Sato, K.; Ichinoi, R.; Mizukami, R.; Serikawa, T.; Sasaki, Y.; Lutkenhaus, J.; Nishide, H.; Oyaizu, K. Diffusion-Cooperative Model for Charge Transport by Redox-Active Nonconjugated Polymers. *J. Am. Chem. Soc.* **2018**, *140*, 1049–1056. DOI: <a href="https://doi.org/10.1021/jacs.7b11272">https://doi.org/10.1021/jacs.7b11272</a>
- 174. Hatakeyama-Sato, K.; Wakamatsu, H.; Katagiri, R.; Oyaizu, K.; Nishide, H. An Ultrahigh Output Rechargeable Electrode of a Hydrophilic Radical Polymer/Nanocarbon Hybrid with an Exceptionally Large Current Density beyond 1 A cm<sup>-2</sup>. *Adv. Mater.* **2018**, *30*, 1800900. DOI: <a href="https://doi.org/10.1002/adma.201800900">https://doi.org/10.1002/adma.201800900</a>
- 175. Yu, I.; Jo, Y.; Ko, J.; Kim, D.-Y.; Sohn, D.; Joo, Y. Making Nonconjugated Small-Molecule Organic Radicals Conduct. *Nano Lett.* **2020**, *20*, 5376–5382. DOI: <a href="https://doi.org/10.1021/acs.nanolett.0c01730">https://doi.org/10.1021/acs.nanolett.0c01730</a>
- 176. Joo, Y.; Agarkar, V.; Sung, S. H.; Savoie, B. M.; Boudouris, B. W. A nonconjugated radical polymer glass with high electrical conductivity. *Science* **2018**, *359*, 1391–1395. DOI: 10.1126/science.aao7287
- 177. Stone, T. J.; Buckman, T.; Nordio, P. L.; McConnell, H. M. Spin-labeled biomolecules. *Proc. Natl. Acad. Sci. U. S. A.* **1965**, *54*, 1010–1017. DOI: <a href="https://doi.org/10.1073/pnas.54.4.1010">https://doi.org/10.1073/pnas.54.4.1010</a>
- 178. Hubbell, W. L.; Lopez, C. J.; Altenbach, C.; Yang, Z. Technological Advances in Site-Directed Spin Labeling of Proteins. *Curr. Opin. Struct. Biol.* **2013**, *23*, 725–733. DOI: https://doi.org/10.1016/j.sbi.2013.06.008
- 179. Haugland, M. M.; Lovett, J. E.; Anderson, E. A. Advances in the Synthesis of Nitroxide Radicals for Use in Biomolecule Spin Labelling. *Chem. Soc. Rev.* **2018**, *47*, 668–680. DOI: https://doi.org/10.1039/C6CS00550K
- 180. Jeschke, G. DEER Distance Measurements on Proteins. *Annu. Rev. Phys. Chem.* **2012**, *63*, 419–446. DOI: <a href="https://doi.org/10.1146/annurev-physchem-032511-143716">https://doi.org/10.1146/annurev-physchem-032511-143716</a>
- 181. Dzuba, S. A.; Maryasov, A. G.; Salikhov, K. M.; Tsvetkov, Yu. D. Superslow rotations of nitroxide radicals studied by pulse EPR spectroscopy. *J. Magn. Reson.* **1984**, *58*, 95–117. DOI: https://doi.org/10.1016/0022-2364(84)90010-6
- 182. Zecevic, A.; Eaton, G. R.; Eaton, S. S.; Lindgren, M. Dephasing of electron spin echoes for nitroxyl radicals in glassy solvents by non-methyl and methyl protons. *Mol. Phys.* **1998**, *95*, 1255–1263. DOI: <a href="https://doi.org/10.1080/00268979809483256">https://doi.org/10.1080/00268979809483256</a>
- 183. Eggeling, A.; Soetbeer, J.; Fábregas-Ibáñez, L.; Klose, D.; Jeschke, G. Quantifying methyl tunneling induced (de)coherence of nitroxides in glassy *ortho*-terphenyl at low temperatures. *Phys. Chem. Chem. Phys.* **2023**, *25*, 11145–11157. DOI: <a href="https://doi.org/10.1039/D3CP01299A">https://doi.org/10.1039/D3CP01299A</a>
- 184. Zaytseva, E. V.; Mazhukin, D. G. Spirocyclic Nitroxides as Versatile Tools in Modern Natural Sciences: From Synthesis to Applications. Part I. Old and New Synthetic Approaches to Spirocyclic Nitroxyl Radicals. *Molecules* 2021, 26, 677-(1-60). DOI: <a href="https://doi.org/10.3390/molecules26030677">https://doi.org/10.3390/molecules26030677</a>
- 185. Rajca, A.; Kathirvelu, V.; Roy, S. K.; Pink, M.; Rajca, S.; Sarkar, S.; Eaton, S. S.; Eaton, G. R. A Spirocyclohexyl Nitroxide Amino Acid Spin Label for Pulsed EPR Spectroscopy Distance

- Measurements. *Chem. Eur. J.* **2010**, *16*, 5778–5782. DOI: <a href="https://doi.org/10.1002/chem.200903102">https://doi.org/10.1002/chem.200903102</a>
- 186. Kirilyuk, I. A.; Polienko, Y. F.; Krumkacheva, O. A.; Strizhakov, R. K.; Gatilov, Y. V.; Grigor'ev, I. A.; Bagryanskaya, E. G. Synthesis of 2,5-Bis(spirocyclohexane)-Substituted Nitroxides of Pyrroline and Pyrrolidine Series, Including Thiol-Specific Spin Label: An Analogue of MTSSL with Long Relaxation Time. *J. Org. Chem.* **2012**, *77*, 8016–8027. DOI: <a href="https://doi.org/10.1021/jo301235j">https://doi.org/10.1021/jo301235j</a>
- 187. Meyer, V.; Swanson, M. A.; Clouston, L. J.; Boratyński, P. J.; Stein, R. A.; Mchaourab, H. S.; Rajca, A.; Eaton, S. S.; Eaton, G. R. Room Temperature Distance Measurements of Immobilized Spin Labeled Protein by Double Electron–Electron Resonance Spectroscopy. *Biophys. J.* **2015**, *108*, 1213–1219. DOI: <a href="https://doi.org/10.1016/j.bpj.2015.01.015">https://doi.org/10.1016/j.bpj.2015.01.015</a>
- 188. Yang, Z.; Stein, R. A.; Ngendahimana, T.; Pink, M.; Rajca, S.; Jeschke, G.; Eaton, S. S.; Eaton, G. R.; Mchaourab, H. S.; Rajca, A. Supramolecular Approach to Electron Paramagnetic Resonance Distance Measurement of Spin-Labeled Proteins. *J. Phys. Chem. B*, **2020**, *124*, 3291–3299. DOI: <a href="https://doi.org/10.1021/acs.jpcb.0c00743">https://doi.org/10.1021/acs.jpcb.0c00743</a>
- 189. Berliner, L. J.; Grunwald, J.; Hankovszky, H. O.; Hideg, K. A Novel Reversible Thiol Specific Spin Label: Papain Active Site Labeling and Inhibition. *Anal. Biochem.* **1982**, *119*, 450–455. DOI: https://doi.org/10.1016/0003-2697(82)90612-1
- 190. Huang, S.; Pink, M.; Ngendahimana, T.; Rajca, S.; Eaton, G. R.; Eaton, S. S.; Rajca, A. Bis-Spiro-Oxetane and Bis-Spiro-Tetrahydrofuran Pyrroline Nitroxide Radicals: Synthesis and Electron Spin Relaxation Studies. *J. Org. Chem.* **2021**, *86*, 13636–13643. DOI: https://doi.org/10.1021/acs.joc.1c01670
- 191. Huang, S.; Paletta, J. T.; Elajaili, H.; Huber, K.; Pink, M.; Rajca, S.; Eaton, G. R.; Eaton, S. S.; Rajca, A. Synthesis and Electron Spin Relaxation of Tetracarboxylate Pyrroline Nitroxides. *J. Org. Chem.* **2017**, *82*, 1538–1544. DOI: <a href="https://doi.org/10.1021/acs.joc.6b02737">https://doi.org/10.1021/acs.joc.6b02737</a>
- 192. Equbal, A.; Li, Y.; Leavesley, A.; Huang, S.; Rajca, S.; Rajca, A.; Han, S. Truncated Cross Effect Dynamic Nuclear Polarization: An Overhauser Effect Doppelgänger. *J. Phys. Chem. Lett.* **2018**, *9*, 2175–2180. DOI: <a href="https://doi.org/10.1021/acs.jpclett.8b00751">https://doi.org/10.1021/acs.jpclett.8b00751</a>
- 193. Huang, S.; Zhang, H.; Paletta, J. T.; Rajca, S.; Rajca, A. Reduction kinetics and electrochemistry of tetracarboxylate nitroxides. *Free Radic. Res.* **2018**, *52*, 327–334. DOI: <a href="https://doi.org/10.1080/10715762.2018.1437268">https://doi.org/10.1080/10715762.2018.1437268</a>
- 194. Wang, Y.; Paletta, J. T.; Berg, K.; Reinhart, E.; Rajca, S.; Rajca, A. Synthesis of Unnatural Amino Acids Functionalized with Sterically Shielded Pyrroline Nitroxides. *Org. Lett.* **2014**, *16*, 5298–5300. DOI: <a href="https://doi.org/10.1021/ol502449r">https://doi.org/10.1021/ol502449r</a>
- 195. Jana, S.; Evans, E. G. B.; Jang, H. S.; Zhang, S.; Zhang, H.; Rajca, A.; Gordon, S. E.; Zagotta, W. N.; Stoll, S.; Mehl, R. A. Ultra-Fast Bioorthogonal Spin-Labeling and Distance Measurements in Mammalian Cells Using Small, Genetically Encoded Tetrazine Amino Acids. *J. Am. Chem. Soc.* 2023, 145, 14608–14620. DOI: <a href="https://doi.org/10.1021/jacs.3c00967">https://doi.org/10.1021/jacs.3c00967</a>

- 196. Blinco, J. P.; Fairfull-Smith, K. E.; Morrow, B. J.; Bottle, S. E. Profluorescent Nitroxides as Sensitive Probes of Oxidative Change and Free Radical Reactions. *Aust. J. Chem.* **2011**, *64*, 373–389. DOI: <a href="https://doi.org/10.1071/CH10442">https://doi.org/10.1071/CH10442</a>
- 197. Keddie, D. J.; Fairfull-Smith, K. E.; Bottle, S. E. The palladium-catalysed copper-free Sonogashira coupling of isoindoline nitroxides: a convenient route to robust profluorescent carbon–carbon frameworks. *Org. Biomol. Chem.* **2008**, *6*, 3135. DOI: <a href="https://doi.org/10.1039/b806963h">https://doi.org/10.1039/b806963h</a>
- 198. Jason C. Morris, John C. McMurtrie, Steven E. Bottle and Kathryn E. Fairfull-Smith Generation of Profluorescent Isoindoline Nitroxides Using Click Chemistry. *J. Org. Chem.* **2011**, 76, 4964–4972. DOI: <a href="https://doi.org/10.1021/jo200613r">https://doi.org/10.1021/jo200613r</a>
- 199. Marxa, L.; Chiarellia, R.; Guiberteaub, T.; Rassat, A. A comparative study of the reduction by ascorbate of 1,1,3,3-tetraethylisoindolin-2-yloxyl and of 1,1,3,3-tetramethylisoindolin-2-yloxyl. *J. Chem. Soc., Perkin Trans. 1* **2000**, 1181–1182. DOI: https://doi.org/10.1039/B001891K
- 200. Ahn, H.-Y.; Fairfull-Smith, K. E.; Morrow, B. J.; Lussini, V.; Kim, B.; Bondar, M. V.; Bottle, S. E.; Belfield, K. D. Two-photon fluorescence microscopy imaging of cellular oxidative stress using profluorescent nitroxides. *J. Am. Chem. Soc.* **2012**, *134*, 4721–4730, DOI: https://doi.org/10.1021/ja210315x
- 201. Rančić, A.; Babić, N.; Orio, M.; Peyrot, F. Structural Features Governing the Metabolic Stability of Tetraethyl-Substituted Nitroxides in Rat Liver Microsomes. *Antioxidants* **2023**, *12*, 402. DOI: <a href="https://doi.org/10.3390/antiox12020402">https://doi.org/10.3390/antiox12020402</a>
- 202. Vianello, F.; Momo, F.; Scarpa, M.; Rigo, A. Kinetics of nitroxide spin label removal in biological systems: An in vitro and in vivo ESR study. *Magn. Reson. Imaging* **1995**, *13*, 219–226. DOI: <a href="https://doi.org/10.1016/0730-725X(94)00121-I">https://doi.org/10.1016/0730-725X(94)00121-I</a>
- 203. Paletta, J. T.; Pink, M.; Foley, B.; Rajca, S.; Rajca, A. Synthesis and Reduction Kinetics of Sterically Shielded Pyrrolidine Nitroxides. *Org. Lett.* **2012**, *14*, 5322–5325. DOI: https://doi.org/10.1021/ol302506f
- 204. Dobrynin, S. A.; Glazachev, Y. I.; Gatilov, Y. V.; Chernyak, E. I.; Salnikov, G. E.; Kirilyuk, I. A. Synthesis of 3,4-Bis(Hydroxymethyl)–2,2,5,5-Tetraethylpyrrolidin-1-Oxyl via 1,3-Dipolar Cycloaddition of Azomethine Ylide to Activated Alkene. *J. Org. Chem.* **2018**, *83*, 5392–5397. DOI: https://doi.org/10.1021/acs.joc.8b00085
- 205. Jagtap, A. P.; Krstic, I.; Kunjir, N. C.; Hänsel, R.; Prisner, T. F.; Sigurdsson, S. Th. *Free Radic. Res.* **2015**, *49*, 78–85. DOI: <a href="https://doi.org/10.3109/10715762.2014.979409">https://doi.org/10.3109/10715762.2014.979409</a>
- 206. Rajca, A.; Wang, Y.; Boska, M.; Paletta, J. T.; Olankitwanit, A.; Swanson, M. A.; Mitchell, D. G.; Eaton, S. S.; Eaton, G. R.; Rajca, S. Organic Radical Contrast Agents for Magnetic Resonance Imaging. J. Am. Chem. Soc. 2012, 134, 15724–15727. DOI: <a href="http://dx.doi.org/10.1021/ja3079829">http://dx.doi.org/10.1021/ja3079829</a>
- 207. Sowers, M. A.; McCombs, J. R.; Wang, Y.; Paletta, J. T.; Morton, S. W.; Dreaden, E. C.; Boska, M. D.; Ottaviani, M. F.; Hammond, P. T.; Rajca, A.; et al. *Nat. Commun.* **2014**, *5*, 5460 DOI: <a href="http://dx.doi.org/10.1038/ncomms6460">http://dx.doi.org/10.1038/ncomms6460</a>

- 208. Nguyen, H. V. T.; Chen, Q.; Paletta, J. T.; Harvey, P.; Jiang, Y.; Zhang, H.; Boska, M. D.; Ottaviani, M. F.; Jasanoff, A.; Rajca, A.; et al. Nitroxide-based macromolecular contrast agents with unprecedented transverse relaxivity and stability for magnetic resonance imaging of tumors. *ACS Cent. Sci.* **2017**, *3*, 800–811. DOI: http://dx.doi.org/10.1021/acscentsci.7b00253
- 209. Nguyen, H. V. T.; Detappe, A.; Gallagher, N. M.; Zhang, H.; Harvey, P.; Yan, C.; Mathieu, C.; Golder, M. R.; Jiang, Y.; Ottaviani, M. F.; et al. Triply Loaded Nitroxide Brush-Arm Star Polymers Enable Metal-Free Millimetric Tumor Detection by Magnetic Resonance Imaging. *ACS Nano* 2018, *12*, 11343–11354. DOI: https://doi.org/10.1021/acsnano.8b06160
- 210. Nguyen, H. V. T.; Detappe, A.; Harvey, P.; Gallagher, N.; Mathieu, C.; Agius, M. P.; Zavidij, O.; Wang, W.; Jiang, Y.; Rajca, A.; et al. Pro-organic radical contrast agents ("pro-ORCAs") for real-time MRI of pro-drug activation in biological systems. *Polym. Chem.* **2020**, *11*, 4768–4779. DOI: <a href="https://doi.org/10.1039/D0PY00558D">https://doi.org/10.1039/D0PY00558D</a>
- 211. Morozov, D. A.; Kirilyuk, I. A.; Komarov, D. A.; Goti, A.; Bagryanskaya, I. Y.; Kuratieva, N. V.; Grigorev, I. A. Synthesis of a Chiral C<sub>2</sub>-Symmetric Sterically Hindered Pyrrolidine Nitroxide Radical via Combined Iterative Nucleophilic Additions and Intramolecular 1,3-Dipolar Cycloadditions to Cyclic Nitrones. *J. Org. Chem.* 2012, 77, 10688–10698. DOI: <a href="https://doi.org/10.1021/jo3019158">https://doi.org/10.1021/jo3019158</a>
- 212. Osiecki, J. H.; Ullman, E. F. Studies of Free Radicals. I. a-Nitronyl Nitroxides a New Class of Stable Radicals. *J. Am. Chem. Soc.* **1968**, *90*, 1078–1079. DOI: <a href="https://doi.org/10.1021/ja01006a053">https://doi.org/10.1021/ja01006a053</a>
- 213. Ullman, E. F.; Boocock, D. G. B. J. "Conjugated" nitronyl-nitroxide and imino-nitroxide biradicals. *Chem. Soc. Chem. Commun.* **1969**, 1161–1162. DOI: https://doi.org/10.1039/C29690001161
- 214. Rajca, A.; Mukherjee, S.; Pink, M.; Rajca, S. Exchange Coupling Mediated Through-Bonds and Through-Space in Conformationally-Constrained Polyradical Scaffolds: Calix[4]arene Nitroxide Tetraradicals and Diradical. *J. Am. Chem. Soc.* **2006**, *128*, 13497–13507. DOI: <a href="http://doi.org/10.1021/ja063567%2B">http://doi.org/10.1021/ja063567%2B</a>
- 215. Rajca, A.; Mukherjee, S.; Pink, M.; Rajca, S.; Das, K. 1,3-Alternate Calix[4]arene Nitronyl Nitroxide Tetraradical and Diradical: Synthesis, X-ray Crystallography, Paramagnetic NMR Spectroscopy, EPR Spectroscopy, and Magnetic Studies. *Tetrahedron* **2007**, *63*, 10731–10742. DOI: <a href="http://doi.org/10.1016/j.tet.2007.07.051">http://doi.org/10.1016/j.tet.2007.07.051</a>
- 216. Sato, H.; Kathirvelu, V.; Spagnol, G.; Rajca, S.; Rajca, A.; Eaton, S. S.; Eaton, G. R. Impact of electron-electron spin interaction on electron spin relaxation of nitroxide diradicals and tetraradical in glassy solvents between 10 and 300 K. *J. Phys. Chem. B* **2008**, *112*, 2818–2828. DOI: <a href="http://doi.org/10.1021/jp073600u">http://doi.org/10.1021/jp073600u</a>
- 217. Olankitwanit, A.; Kathirvelu, V.; Rajca, S.; Eaton, G. R.; Eaton, S. S.; Rajca, A. Calix[4]arene nitroxide tetraradical and octaradical. *Chem. Commun.* **2011**, *47*, 6443–6445. DOI: <a href="http://doi.org/10.1039/C1CC11172H">http://doi.org/10.1039/C1CC11172H</a>
- 218. Rajca, A.; Shiraishi, K.; Rajca, S. Stable diarylnitroxide diradical with triplet ground state. *Chem. Commun.* **2009**, 4372–4374. DOI: <a href="http://doi.org/10.1039/b909741d">http://doi.org/10.1039/b909741d</a>

- 219. Rajca, A.; Shiraishi, K.; Boratynski, P. J.; Pink, M.; Miyasaka, M.; Rajca, S. Oxidation of Annelated Diarylamines: Analysis of Reaction Pathways to Nitroxide Diradical and Spirocyclic Products. *J. Org. Chem.* **2011**, *76*, 8447–8457. DOI: <a href="http://doi.org/10.1021/jo2017923">http://doi.org/10.1021/jo2017923</a>
- 220. Dulov, D. A.; Levitskiy, O. A.; Bogdanov, A. V.; Magdesieva, T. V. Redox-Amphoteric 4,4'-Dicyclopropyldiphenylnitroxyl Radical: Unexpectedly High Stability. *Chem. Select* **2021**, *6*, 9653–9656. DOI: https://doi.org/10.1002/slct.202102626
- 221. Levitskiy, O. A.; Dulov, D. A.; Bogdanov, A. V.; Grishin, Y. K.; Nefedov, S. E.; Magdesieva, T. V. Chameleonic Behavior of the α-Methylcyclopropyl Group and Its Through-Space Interactions: A Route to Stabilized Three Redox States in Diarylnitroxides. *Chem. Eur. J.* 2020, 26, 6793–6804. DOI: <a href="https://doi.org/10.1002/chem.202000165">https://doi.org/10.1002/chem.202000165</a>
- 222. Coppinger, G. M. A stable phenoxy radical inert to oxygen. *J. Am. Chem. Soc.* **1957**, *79*, 501–502. DOI: <a href="https://doi.org/10.1021/ja01559a073">https://doi.org/10.1021/ja01559a073</a>
- 223. Yonekuta, Y.; Susuki, K.; Oyaizu, K.; Honda, K.; Nishide, H. Battery-Inspired, Nonvolatile, and Rewritable Memory Architecture: a Radical Polymer-Based Organic Device. *J. Am. Chem. Soc.* **2007**, *129*, 14128–14129. DOI: <a href="https://doi.org/10.1021/ja075553p">https://doi.org/10.1021/ja075553p</a>
- 224. Suga, T.; Ohshiro, H.; Sugita, S.; Oyaizu, K.; Nishide, H. Emerging N-type redox-active radical polymer for a totally organic polymer-based rechargeable battery. *Adv. Mater.* **2009**, *21*, 1627–1630. DOI: https://doi.org/10.1002/adma.200803073
- 225. Morita, Y.; Ohba, T.; Haneda, N.; Maki, S.; Kawai, J.; Hatanaka, K.; Sato, K.; Shiomi, D.; Takui, T.; Nakasuji, K. New persistent radicals: Synthesis and electronic spin structure of 2,5-di-tert-butyl-6-oxophenalenoxyl derivatives. *J. Am. Chem. Soc.* **2000**, *122*, 4825–4826. DOI: <a href="https://doi.org/10.1021/ja000298t">https://doi.org/10.1021/ja000298t</a>
- 226. Nishida, S.; Kawai, J.; Moriguchi, M.; Ohba, T.; Haneda, N.; Fukui, K.; Fuyuhiro, A.; Shiomi, D.; Sato, K.; Takui, T.; et al. Control of exchange interactions in π dimers of 6-oxophenalenoxyl neutral π radicals: Spin-density distributions and multicentered-two-electron bonding governed by topological symmetry and substitution at the 8-position. *Chem. Eur. J.* **2013**, *19*, 11904–11915. DOI: https://doi.org/10.1002/chem.201301783
- 227. Clar, E.; Stewart, D. G. Aromatic Hydrocarbons. LXV. Triangulene Derivatives. *J. Am. Chem. Soc.* **1953**, *75*, 2667–2673. DOI: <a href="https://doi.org/10.1021/ja01107a035">https://doi.org/10.1021/ja01107a035</a>
- 228. Allinson, G.; Bushby, R. J.; Paillaud, J.-L.; Oduwole, D.; Sales, K. ESR Spectrum of a Stable Triplet π Biradical: Trioxytriangulene. *J. Am. Chem. Soc.* **1993**, *115*, 2062–2064. DOI: <a href="https://doi.org/10.1021/ja00058a076">https://doi.org/10.1021/ja00058a076</a>
- 229. Allinson, G.; Bushby, R. J.; Paillaud, J.-L.; Thornton-Pett, M., Synthesis of a derivative of triangulene; the first non-kekulé polynuclear aromatic. *J. Chem. Soc., Perkin Trans. 1* **1995**, 385–390. DOI: <a href="https://doi.org/10.1039/P19950000385">https://doi.org/10.1039/P19950000385</a>
- 230. Morita, Y.; Nishida, S.; Murata, T.; Moriguchi, M.; Ueda, A.; Satoh, M.; Arifuku, K.; Sato, K.; Takui, T. Organic tailored batteries materials using stable open-shell molecules with degenerate frontier orbitals. *Nat. Mater.* **2011**, *10*, 947–951. DOI: <a href="https://doi.org/10.1038/nmat3142">https://doi.org/10.1038/nmat3142</a>

- 231. Murata, T.; Yamada, C.; Furukawa, K.; Morita, Y. Mixed valence salts based on carbon-centered neutral radical crystals. *Chem. Commun.* **2018**, *1*, Article no.: 47. DOI: https://doi.org/10.1038/s42004-018-0048-5
- 232. Murata, T.; Yamamoto, Y.; Ueda, A.; Ise, T.; Shiomi, D.; Sato, K.; Takui, T.; Morita, Y. Synthesis and Physical Properties of Trioxotriangulene Having Methoxy and Hydroxy Groups at α-Positions: Electronic and Steric Effects of Substituent Groups and Intramolecular Hydrogen Bonds. *J. Org. Chem.* **2021**, *86*, 10154–10165. DOI: <a href="https://doi.org/10.1021/acs.joc.1c00880">https://doi.org/10.1021/acs.joc.1c00880</a>
- 233. Murata, T.; Yokoyama, M.; Ueda, A.; Kanzaki, Y.; Shiomi, D.; Sato, S.; Takui, T.; Morita, Y. Synthesis of trioxotriangulene stable neutral π-radicals having alkyl substituent groups, and their effects on electronic-spin and π-stacking structures. *Chem. Lett.* **2020**, *49*, 95–98. DOI: https://doi.org/10.1246/cl.190761
- 234. Morita, Y.; Murata, T.; Ueda, A.; Yamada, C.; Kanzaki, Y.; Shiomi, D.; Sato, K.; Takui, T. Trioxotriangulene: air- and thermally stable organic carbon-centered neutral π-radical without steric protection. *Bull. Chem. Soc. Jpn.* **2018**, *91*, 922–931. DOI: <a href="https://doi.org/10.1246/bcsj.20180074">https://doi.org/10.1246/bcsj.20180074</a>
- 235. Ueda, A.; Wasa, H.; Nishida, S.; Kanzaki, Y.; Sato, K.; Shiomi, D.; Takui, T.; Morita, Y. An Extremely Redox-Active Air-Stable Neutral π Radical: Dicyanomethylene-Substituted Triangulene with a Threefold Symmetry. *Chem. Eur. J.* **2012**, *18*, 16272–16276. DOI: <a href="https://doi.org/10.1002/chem.201203755">https://doi.org/10.1002/chem.201203755</a>
- 236. Ito, H.; Murata, T.: Miyata, T.; Morita, M.; Tsuji, R.; Morita, Y. Air-Stable Thin Films with High and Anisotropic Electrical Conductivities Composed of a Carbon-Centered Neutral π-Radical. *ACS Omega* **2019**, *4*, 17569–17575. DOI: <a href="https://doi.org/10.1021/acsomega.9b02700">https://doi.org/10.1021/acsomega.9b02700</a>
- 237. Murata, T.; Nakanishi, S.; Nakayama, H.; Ito, H.; Morita, M.; Tsuji, R.; Morita, Y. Rechargeable Batteries With 100% Cathode Active Materials Conductive Vapor-Deposited Films of a Stable Organic Neutral Radical. *ACS Appl. Energy Mater.* **2022**, *5*, 1218–1225. DOI: https://doi.org/10.1021/acsaem.1c03574
- 238. Ito, H.; Murata, T.; Fujisaki, M.; Tsuji, R.; Morita, Y. High capacity and energy density organic lithium-ion battery based on buckypaper with stable π-radical. *ChemSusChem* **2021**, *14*, 1377–1387. DOI: <a href="https://doi.org/10.1002/cssc.202002851">https://doi.org/10.1002/cssc.202002851</a>
- 239. Kitano, S.; Tanabe, I.; Shioya, N.; Hasegawa, T.; Murata, T.; Morita, Y.; Tsuji, R.; Fukui, K. Voltammetric and In Situ Spectroscopic Investigations on the Redox Processes of Trioxotriangulene Neutral Radicals on Graphite Electrodes. *Langmuir* **2023**, *39*, 6846–6854. DOI: https://doi.org/10.1021/acs.langmuir.3c00438
- 240. Murata, T.; Asakura, N.; Ukai, S.; Ueda, A.; Kanzaki, Y.; Sato, K.; Takui, T.; Morita, Y. Intramolecular magnetic interaction of spin-delocalized neutral radicals through *m*-phenylene spacers. *ChemPlusChem* **2019**, *84*, 680–685. DOI: <a href="https://doi.org/10.1002/cplu.201800662">https://doi.org/10.1002/cplu.201800662</a>
- 241. Rawson, J. M.; Alberola, A.; Whalley, A. Thiazyl radicals: old materials for new molecular devices. *J. Mater. Chem.* **2006**, *16*, 2560–2575. DOI: <a href="https://doi.org/10.1039/B603199D">https://doi.org/10.1039/B603199D</a>

- 242. Nascimento, M. A.; Rawson, J. M. 1,2,3,5-Dithiadiazolyl Radicals. *Encyclopedia of Inorganic and Bioinorganic Chemistry*, Online, **2019** John Wiley & Sons, Ltd. DOI: <a href="https://doi.org/10.1002/9781119951438.eibc2640">https://doi.org/10.1002/9781119951438.eibc2640</a>
- 243. Banister, A. J.; Bricklebank, N.; Lavender, I.; Rawson, J. M.; Gregory, C. I.; Tanner, B. K.; Clegg, W.; Elsegood, M. R. J.; Palacio, F. Spontaneous Magnetization in a Sulfur–Nitrogen Radical at 36 K. *Angew. Chem. Int. Ed. Engl.* 1996, *35*, 2533–2535. DOI: <a href="https://doi.org/10.1002/anie.199625331">https://doi.org/10.1002/anie.199625331</a>
- 244. Thomson, R. I.; Pask, C. M.; Lloyd, G. O.; Mito, M.; Rawson, J. M. Pressure-Induced Enhancement of Magnetic-Ordering Temperature in an Organic Radical to 70 K: A Magnetostructural Correlation. *Chem. Eur. J.* **2012**, *18*, 8629–8633. DOI: https://doi.org/10.1002/chem.201200760
- 245. Mills, M. B.; Wohlhauser, T.; Stein, B.; Verduyn, W. R.; Song, E.; Dechambenoit, P.; Rouzières, M.; Clérac, R.; Preuss, K. E. Magnetic bistability in crystalline organic radicals: the interplay of H-bonding, pancake bonding, and electrostatics in 4-(2'-benzimidazolyl)-1,2,3,5-dithiadiazolyl. *J. Am. Chem. Soc.* **2018**, *140*, 16904–16908. DOI: <a href="https://doi.org/10.1021/jacs.8b10370">https://doi.org/10.1021/jacs.8b10370</a>
- 246. Beldjoudi, Y.; Arauzo, A.; Campo, J.; Gavey, E. L.; Pilkington, M.; Nascimento, M. A.; Rawson, J. M. Structural, magnetic, and optical studies of the polymorphic 9'-anthracenyl dithiadiazolyl radical. *J. Am. Chem. Soc.* **2019**, *141*, 6875–6889. DOI: <a href="https://doi.org/10.1021/jacs.8b11528">https://doi.org/10.1021/jacs.8b11528</a>
- 247. Tamura, M.; Nakazawa, Y.; Shiomi, D.; Nozawa, K.; Hosokoshi, Y.; Ishikawa, M.; Takahashi, M.; Kinoshita, M. Bulk ferromagnetism in the β-phase crystal of the p-nitrophenyl nitronyl nitroxide radical. *Chem. Phys. Lett.* **1991**, *186*, 401–404.

  DOI: https://www.sciencedirect.com/science/article/abs/pii/000926149190198I
- 248. Allemand, P. M.; Khemani, K. C.; Koch, A.; Wudl F.; Holczer K.; Donovan S.; Grüner G.; Thompson J. D. Organic molecular soft ferromagnetism in a fullerene C60. *Science* **1991**, *253*, 301–302. DOI: https://doi.org/10.1126/science.253.5017.301
- 249. Narymbetov, B.; Omerzu, A.; Kabanov, V. V.; Tokumoto, M.; Kobayashi, H.; Mihailovic, D. Origin of ferromagnetic exchange interactions in a fullerene-organic compound. *Nature* **2000**, 407, 883–885. DOI: https://doi.org/10.1038/35038032
- 250. Wolmershäuser, G.; Johann, R. 1,3,5-Trithia-2,4,6-triazapentalenyl a Stable Sulfur-Nitrogen Radical. *Angew. Chem. Int. Ed.* **1989**, *28*, 920–921. DOI: <a href="https://doi.org/10.1002/anie.198909201">https://doi.org/10.1002/anie.198909201</a>
- 251. Fujita, W.; Awaga, K. Room-temperature magnetic bistability in organic radical crystals. *Science* **1999**, *286*, 261–262. DOI: 10.1126/science.286.5438.261
- 252. McManus, G. D.; Rawson, J. M.; Feeder, N.; van Duijn, J.; McInnes, E. J. L.; Novoa, J. J.; Burriel, R.; Palacio, F.; Oliete, P. Synthesis, crystal structures, electronic structure and magnetic behaviour of the trithiatriazapentalenyl radical, C2S3N3. *J. Mater. Chem.* **2001**, *11*, 1992–2003. DOI: <a href="https://doi.org/10.1039/B103303B">https://doi.org/10.1039/B103303B</a>

- 253. Rajca, A. Magnetism of Nitroxides in *Nitroxides: Synthesis, Properties and Applications*. Eds. Ouari, O.; Gigmes, D. **2021**, Ch. *9*, pp 359–391. The Royal Society of Chemistry. DOI: https://doi.org/10.1039/9781788019651-00359
- 254. Lekin, K.; Winter, S. M.; Downie, L. E.; Bao, X.; Tse, J. S.; Desgreniers, S.; Secco, R. A.; Dube, P. A.; Oakley, R. T. Hysteretic Spin Crossover between a Bisdithiazolyl Radical and Its Hypervalent σ-Dimer. *J. Am. Chem. Soc.* **2010**, *132*, 16212–16224. DOI: <a href="https://doi.org/10.1021/ja106768z">https://doi.org/10.1021/ja106768z</a>
- 255. Robertson, C. M.; Leitch, A. A.; Cvrkalj, K.; Reed, R. W.; Myles, D. J. T.; Dube, P. A.; Oakley, R. T. Enhanced conductivity and magnetic ordering in isostructural heavy atom radicals. *J. Am. Chem. Soc.* **2008**, *130*, 8414–8425. DOI: <a href="https://doi.org/10.1021/ja801070d">https://doi.org/10.1021/ja801070d</a>
- 256. Winter, S. M.; Hill, S.; Oakley, R. T. Magnetic Ordering and Anisotropy in Heavy Atom Radicals. *J. Am. Chem. Soc.* **2015**, *137*, 3720–3730. DOI: <a href="https://doi.org/10.1021/jacs.5b00672">https://doi.org/10.1021/jacs.5b00672</a>
- 257. Mailman, A.; Wong, J. W. L.; Winter, S. M.; Claridge, R. C. M.; Robertson, C. M.; Assoud, A.; Yong, W.; Steven, E.; Dube, P. A.; Tse, J. S.; et al. Fine tuning the performance of multiorbital radical conductors by substituent effects. *J. Am. Chem. Soc.* **2017**, *139*, 1625–1635. DOI: https://doi.org/10.1021/jacs.6b11779
- 258. Bohr, N. Über die Anwendung der Quantentheorie auf den Atombau. I. Die Grundpostulate der Quantentheorie. Z. *Physik.* **1923**, *13*, 117–165. DOI: <a href="https://doi.org/10.1007/BF01328209">https://doi.org/10.1007/BF01328209</a>
- 259. Kasemthaveechok, S.; Abella, L.; Crassous, J.; Autschbach, J.; Favereau, L. Organic radicals with inversion of SOMO and HOMO energies and potential applications in optoelectronics. *Chem. Sci.* **2022**, *13*, 9833–9847. DOI: <a href="https://doi.org/10.1039/D2SC02480B">https://doi.org/10.1039/D2SC02480B</a>
- 260. Murata, R.; Wang, Z.; Abe, M. Singly Occupied Molecular Orbital–Highest Occupied Molecular Orbital (SOMO–HOMO) Conversion. *Aust. J. Chem.* **2021**, *74*, 827–837. DOI: https://doi.org/10.1071/CH21186
- 261. Gryn'ova, G.; Coote, M. L.; Corminboeuf, C. Theory and practice of uncommon molecular electronic configurations. *WIREs Comput. Mol. Sci.* **2015**, *5*, 440–459. DOI: https://doi.org/10.1002/wcms.1233
- 262. Awaga, K.; Sugano, T.; Kinoshita, M. Ferromagnetic intermolecular interaction in the galvinoxyl radical: Cooperation of spin polarization and charge-transfer interaction. *Chem. Phys. Lett.* **1987**, *141*, 540–544. DOI: <a href="https://doi.org/10.1016/0009-2614(87)85077-7">https://doi.org/10.1016/0009-2614(87)85077-7</a>
- 263. Sugimoto, T.; Yamaga, S.; Nakai, M.; Ohmori, K.; Tsujii, M.; Nakatsuji, H.; Fujita, H.; Yamauchi, J. Intramolecular Spin-Spin Exchange in Cation Radicals of Tetrathiafulvalene Derivatives Substituted with Imino Pyrolidine- and Piperidine-1-oxyls. *Chem. Lett.* **1993**, *22*, 1361–1364. DOI: <a href="https://doi.org/10.1246/cl.1993.1361">https://doi.org/10.1246/cl.1993.1361</a>
- 264. Kumai, R.; Matsushita, M. M.; Izuoka, A.; Sugawara, T. Intramolecular Exchange Interaction in a Novel Cross-Conjugated Spin System Composed of .pi.-Ion Radical and Nitronyl Nitroxide. *J. Am. Chem. Soc.* **1994**, *116*, 4523–4524. DOI: <a href="https://doi.org/10.1021/ja00089a070">https://doi.org/10.1021/ja00089a070</a>

- 265. Izuoka, A.; Hiraishi, M.; Abe, T.; Sugawara, T.; Sato, K.; Takui, T. Spin Alignment in Singly Oxidized Spin-Polarized Diradical Donor: Thianthrene Bis(nitronyl nitroxide). *J. Am. Chem. Soc.* **2000**, *122*, 3234–3235. DOI: <a href="https://doi.org/10.1021/ja9916759">https://doi.org/10.1021/ja9916759</a>
- 266. Nakazaki, J.; Chung, I.; Matsushita, M. M.; Sugawara, T.; Watanabe, R.; Izuoka, A.; Kawada, Y. Design and preparation of pyrrole-based spin-polarized donors. *J. Mater. Chem.* **2003**, *13*, 1011–1022. DOI: <a href="https://doi.org/10.1039/b211986b">https://doi.org/10.1039/b211986b</a>
- 267. Komatsu, H.; Mogi, R.; Matsushita, M. M.; Miyagi, T.; Kawada, Y.; Sugawara, T. Synthesis and properties of TSF-based spin-polarized donor. *Polyhedron* **2009**, *28*, 1996–2000. DOI: <a href="https://doi.org/10.1016/j.poly.2008.12.005">https://doi.org/10.1016/j.poly.2008.12.005</a>
- 268. Sugawara, T.; Matsushita, M. M. Spintronics in Organic π-Electronic Systems. *J. Mater. Chem.* **2009**, *19*, 1738–1753. DOI: <a href="https://doi.org/10.1039/b818851n">https://doi.org/10.1039/b818851n</a>
- 269. Sugawara, T.; Komatsu, H.; Suzuki, K. Interplay between magnetism and conductivity derived from spin-polarized donor radicals. *Chem. Soc. Rev.* **2011**, *40*, 3105–3118. DOI: https://doi.org/10.1039/C0CS00157K
- 270. Abella, L.; Crassous, J.; Favereau, L.; Autschbach, J. Why is the Energy of the Singly Occupied Orbital in Some Radicals below the Highest Occupied Orbital Energy?. *Chem. Mater.* **2021**, *33*, 3678–3691. DOI: https://doi.org/10.1021/acs.chemmater.1c00683
- 271. Gryn'ova, G.; Marshall, D. L.; Blanksby, S. J.; Coote, M. L. Switching radical stability by pH-induced orbital conversion. *Nat. Chem.* **2013**, *5*, 474–481. DOI: <a href="https://doi.org/10.1038/nchem.1625">https://doi.org/10.1038/nchem.1625</a>
- 272. Gryn'ova, G.; Coote, M. L. Origin and Scope of Long-Range Stabilizing Interactions and Associated SOMO–HOMO Conversion in Distonic Radical Anions. *J. Am. Chem. Soc.* **2013**, *135*, 15392–15403. DOI: https://doi.org/10.1021/ja404279f
- 273. Franchi, P.; Mezzina, E.; Lucarini, M. SOMO–HOMO Conversion in Distonic Radical Anions: An Experimental Test in Solution by EPR Radical Equilibration Technique. *J. Am. Chem. Soc.* **2014**, *136*, 1250–1252. DOI: <a href="https://doi.org/10.1021/ja411662a">https://doi.org/10.1021/ja411662a</a>
- 274. Exner, J.; Maisuls, I.; Massolle, A.; Klabunde, S.; Hansen, M. R.; Strassert, C. A.; Neugebauer, J.; Eckert, H.; Studer, A. Electronic effects in profluorescent benzotriazinyl radicals: a combined experimental and theoretical study. *Phys. Chem. Chem. Phys.* 2021, 23, 2999–3007. DOI: <a href="https://doi.org/10.1039/D0CP05732K">https://doi.org/10.1039/D0CP05732K</a>
- 275. Lu, C.; Cho, E.; Cui, Z.; Gao, Y.; Cao, W.; Brédas, J.-L.; Coropceanu, V.; Li, F. Towards Efficient and Stable Donor-Acceptor Luminescent Radicals. *Adv. Mater.* **2023**, *35*, 2208190. DOI: https://doi.org/10.1002/adma.202208190
- 276. Velasco, D.; Castellanos, S.; López, M.; López-Calahorra, F.; Brillas, E.; Juliá, L. Red organic light-emitting radical adducts of carbazole and tris(2,4,6-trichlorotriphenyl)methyl radical that exhibit high thermal stability and electrochemical amphotericity. *J. Org. Chem.* **2007**, *72*, 7523–7532. DOI: https://doi.org/10.1021/jo0708846
- 277. Guo, H.; Peng, Q.; Chen, X.-K.; Gu, Q.; Dong, S.; Evans, E. W.; Gillett, A. J.; Ai, X.; Zhang, M.; Credgington, D.; et al. High stability and luminescence efficiency in donor-acceptor neutral

- radicals not following the Aufbau principle. *Nat. Mater.* **2019**, *18*, 977–984. DOI: <a href="https://doi.org/10.1038/s41563-019-0433-1">https://doi.org/10.1038/s41563-019-0433-1</a>
- 278. Heckmann, A.; Dümmler, S.; Pauli, J.; Margraf, M.; Köhler, J.; Stich, D.; Lambert, C.; Fischer, I.; Resch-Genger, U. Highly fluorescent open-shell NIR dyes: the time-dependence of back electron transfer in triarylamine-perchlorotriphenylmethyl radicals. *J. Phys. Chem. C* **2009**, *113*, 20958–20966. DOI: <a href="https://doi.org/10.1021/jp908425w">https://doi.org/10.1021/jp908425w</a>
- 279. Cho, E.; Coropceanu, V.; Brédas, J.-L. Organic Neutral Radical Emitters: Impact of Chemical Substitution and Electronic-State Hybridization on the Luminescence Properties. *J. Am. Chem. Soc.* **2020**, *142*, 17782–17786. DOI: https://doi.org/10.1021/jacs.0c08997
- 280. Ai, X.; Evans, E. W.; Dong, S.; Gillett, A. J.; Guo, H.; Chen, Y.; Hele, T. J. H.; Friend, R. H.; Li, F. Efficient radical-based light-emitting diodes with doublet emission. *Nature* **2018**, *563*, 536–540. DOI: <a href="https://doi.org/10.1038/s41586-018-0695-9">https://doi.org/10.1038/s41586-018-0695-9</a>
- 281. Hattori, Y.; Kusamoto, T.; Nishihara, H. Luminescence, stability, and proton response of an open-shell (3,5-dichloro-4-pyridyl)bis(2,4,6-trichlorophenyl)methyl radical. *Angew. Chem. Int. Ed.* **2014**, *53*, 11845–11848. DOI: <a href="https://doi.org/10.1002/anie.201407362">https://doi.org/10.1002/anie.201407362</a>
- 282. Peng, Q.; Obolda, A.; Zhang, M.; Li, F. Organic light-emitting diodes using a neutral π radical as emitter: the emission from a doublet. *Angew. Chem. Int. Ed.* **2015**, *54*, 7091–7095. DOI: https://doi.org/10.1002/anie.201500242
- 283. Dong, S. Z.; Xu, W.; Guo, H. Q.; Yan, W. F.; Zhang, M.; Li, F. Effects of substituents on luminescent efficiency of stable triaryl methyl radicals. *Phys. Chem. Chem. Phys.* **2018**, *20*, 18657–18662. DOI: <a href="https://doi.org/10.1039/C8CP01492B">https://doi.org/10.1039/C8CP01492B</a>
- 284. Abdurahman, A.; Hele, T. J. H.; Gu, Q.; Zhang, J.; Peng, Q.; Zhang, M.; Friend, R. H.; Li, F.; Evans, E. W. Understanding the luminescent nature of organic radicals for efficient doublet emitters and pure-red light-emitting diodes. *Nature Mat.* **2020**, *19*, 1224–1229. DOI: <a href="https://doi.org/10.1038/s41563-020-0705-9">https://doi.org/10.1038/s41563-020-0705-9</a>
- 285. Shen, Y.; Chen, C.-F. Helicenes: synthesis and applications. *Chem. Rev.* **2012**, *112*, 1463–1535. DOI: <a href="https://doi.org/10.1021/cr200087r">https://doi.org/10.1021/cr200087r</a>
- 286. Rajca, A.; Miyasaka, M. Synthesis and Characterization of Novel Chiral Conjugated Materials. In *Functional Organic Materials-Syntheses and Strategies*; Mueller, T. J. J., Bunz, U. H. F., Eds.; Wiley-VCH: New York, **2007**; pp 543–577. DOI: <a href="https://doi.org/10.1002/9783527610266.ch15">https://doi.org/10.1002/9783527610266.ch15</a>
- 287. Rajca, A.; Rajca, S.; Pink, M.: Miyasaka, M. Annelated, Chiral π-Conjugated Systems: Tetraphenylenes and Helical β-Oligothiophenes. *SynLett* **2007**, 1799–1822. DOI: 10.1055/s-2007-984538
- 288. Evers, F.; Aharony, A.; Bar-Gill, N.; Entin-Wohlman, O.; Hedegård, P.; Hod, O.; Jelinek, P.; Kamieniarz, G.; Lemeshko, M.; Michaeli, K.; et al. Theory of chirality induced spin selectivity: progress and challenges. *Adv. Mater.* **2022**, *34*, 2106629. DOI: <a href="https://doi.org/10.1002/adma.202106629">https://doi.org/10.1002/adma.202106629</a>

- 289. Naaman, R.; Paltiel, Y.; Waldeck, D. H. Chiral molecules and the electron spin. *Nat. Rev. Chem.* **2019**, *3*, 250–260. DOI: https://doi.org/10.1038/s41570-019-0087-1
- 290. Kira, V.; Mathew, S. P.; Cohen, S. R.; Delgado, I. H.; Lacour, J.; Naaman, R. Helicenes—A New Class of Organic Spin Filter. *Adv. Mater.* **2016**, *28*, 1957–1962. DOI: <a href="https://doi.org/10.1002/adma.201504725">https://doi.org/10.1002/adma.201504725</a>
- 291. Miyamoto, Y.; Rubio, A.; Louie, S. G.; Cohen, M. L. Self-inductance of chiral conducting nanotubes. *Phys. Rev. B: Condens. Matter Mater. Phys.* **1999**, *60*, 13885–13889. DOI: https://doi.org/10.1103/PhysRevB.60.13885
- 292. Sessoli, R.; Boulon, M.-E.; Caneschi, A.; Mannini, M.; Poggini, L.; Wilhelm, F.; Rogalev, A. Strong magneto-chiral dichroism in a paramagnetic molecular helix observed by hard X-ray. *Nat. Phys.* **2015**, *11*, 69–74. DOI: <a href="https://doi.org/10.1038/nphys3152">https://doi.org/10.1038/nphys3152</a>
- 293. Xu, X.; Li, W.; Zhou, X.; Wang, Q.; Feng, J.; Tian, W. Q.; Jiang, Y. Theoretical study of electron tunneling through the spiral molecule junctions along spiral paths. *Phys. Chem. Chem. Phys.* **2016**, *18*, 3765–3771. DOI: https://doi.org/10.1039/C5CP06726J
- 294. Herrmann, C.; Solomon, G. C.; Ratner, M. A. Organic Radicals As Spin Filters. *J. Am. Chem. Soc.* **2010**, *132*, 3682–3684. DOI: https://doi.org/10.1021/ja910483b
- 295. Ueda, A.; Wasa, H.; Suzuki, S.; Okada, K.; Sato, K.; Takui, T.; Morita, Y. Chiral Stable Phenalenyl Radical: Synthesis, Electronic-Spin Structure, and Optical Properties of [4]Helicene-Structured Diazaphenalenyl. *Angew. Chem. Int. Ed.* **2012**, *51*, 6691–6695. DOI: <a href="https://doi.org/10.1002/anie.201202654">https://doi.org/10.1002/anie.201202654</a>
- 296. Sørensen, T. J.; Nielsen, M. F.; Laursen, B. W. Synthesis and Stability of *N*,*N*'-Dialkyl-1,13-dimethoxyquinacridinium (DMQA<sup>+</sup>): A [4]Helicene with Multiple Redox States. *ChemPlusChem* **2014**, *79*, 1030–1035. DOI: https://doi.org/10.1002/cplu.201402058
- 297. Ravat, P.; Ribar, P.; Rickhaus, M.; Häussinger, D.; Neuburger, M.; Juríček, M. Spin-Delocalization in a Helical Open-Shell Hydrocarbon. *J. Org. Chem.* **2016**, *81*, 12303–12317. DOI: https://doi.org/10.1021/acs.joc.6b02246
- 298. Kato, K.; Furukawa, K.; Mori, T.; Osuka, A. Porphyrin-Based Air-Stable Helical Radicals. *Chem. Eur. J.* **2018**, *24*, 572–575. DOI: https://doi.org/10.1002/chem.201705291
- 299. Zak, J. K.; Miyasaka, M.; Rajca, S.; Lapkowski, M.; Rajca, A. Radical Cation of Helical, Cross-Conjugated β-Oligothiophene. *J. Am. Chem. Soc.* **2010**, *132*, 3246–3247. DOI: <a href="https://doi.org/10.1021/ja910076n">https://doi.org/10.1021/ja910076n</a>
- 300. Wang, Y.; Zhang, H.; Pink, M.; Olankitwanit, A.; Rajca, S.; Rajca, A. Radical Cation and Neutral Radical of Aza-thia[7]helicene with SOMO–HOMO Energy Level Inversion. *J. Am. Chem. Soc.* **2016**, *138*, 7298–7304. DOI: https://doi.org/10.1021/jacs.6b01498
- 301. Shu, C.; Zhang, H.; Olankitwanit, A.; Rajca, S.; Rajca, A. High-Spin Diradical Dication of Chiral π-Conjugated Double Helical Molecule. *J. Am. Chem. Soc.* **2019**, *141*, 17287–17294. DOI: https://doi.org/10.1021/jacs.9b08711

- 302. Kasemthaveechok, S.; Abella, L.; Jean, M.; Cordier, M.; Roisnel, T.; Vanthuyne, N.; Guizouarn, T.; Cador, O.; Autschbach, J.; Crassous, J.; et al. Axially and Helically Chiral Cationic Radical Bicarbazoles: SOMO-HOMO Level Inversion and Chirality Impact on the Stability of Mono- and Diradical Cations. *J. Am. Chem. Soc.* **2020**, *142*, 20409–20418. DOI: <a href="https://doi.org/10.1021/jacs.0c08948">https://doi.org/10.1021/jacs.0c08948</a>
- 303. Rajca, A.; Shu, C.; Zhang, H.; Zhang, S.; Wang, H.; Rajca, S. Thiophene-Based Double Helices: Radical Cations with SOMO-HOMO Energy Level Inversion. *Photochem. Photobiol.* **2021**, *97*, 1376–1390. DOI: https://doi.org/10.1111/php.13475
- 304. Kasemthaveechok, S.; Abella, L.; Jean, M.; Cordier, M.; Vanthuyne, N.; Guizouarn, T.; Cador, O.; Autschbach, J.; Crassous, J.; Favereau, L. Carbazole Isomerism in Helical Radical Cations: Spin Delocalization and SOMO–HOMO Level Inversion in the Diradical State. *J. Am. Chem. Soc.* 2022, 144, 7253–7263. DOI: https://doi.org/10.1021/jacs.2c00331
- 305. Utamapanya, S.; Rajca, A. Topological Control of Electron Localization in π-Conjugated Polyarylmethyl Carbopolyanions and Radical Anions. *J. Am. Chem. Soc.* **1991**, *113*, 9242 –9241. DOI: https://doi.org/10.1021/ja00024a032
- 306. Rajca, A. From High-Spin Organic Molecules to Polymers with Magnetic Ordering. *Chem. Eur. J.* **2002**, 8, 4834–4841. DOI: <a href="https://doi.org/10.1002/1521-3765(20021104)8:21<4834::AID-CHEM4834>3.0.CO;2-E.">https://doi.org/10.1002/1521-3765(20021104)8:21<4834::AID-CHEM4834>3.0.CO;2-E.</a>
- 307. Ratera, I; Veciana, J. Playing with organic radicals as building blocks for functional molecular materials. *Chem. Soc. Rev.* **2012**, 41, 303–349. DOI: <a href="https://doi.org/10.1039/C1CS15165G">https://doi.org/10.1039/C1CS15165G</a>
- 308. Sanvito, S. Molecular spintronics. *Chem. Soc. Rev.* **2011**, 40, 3336–3355. DOI: <a href="https://doi.org/10.1039/C1CS15047B">https://doi.org/10.1039/C1CS15047B</a>
- 309. Shil, S.; Bhattacharya, D.; Misra, A.; Klein, D. J. A high-spin organic diradical as a spin filter. *Phys. Chem. Chem. Phys.* **2015**, *17*, 23378–23383. DOI: <a href="https://doi.org/10.1039/C5CP03193A">https://doi.org/10.1039/C5CP03193A</a>
- 310. Cho, D.; Lee, J. Y. Organic Stable Radical Oligomers as Spin Filters. *J. Phys. Chem. C* **2023**, *127*, 8256–82625. DOI: <a href="https://doi.org/10.1021/acs.jpcc.3c00179">https://doi.org/10.1021/acs.jpcc.3c00179</a>
- 311. Lee, J.; Lee, E.; Kim, S.; Bang, G. S.; Shultz, D. A.; Schmidt, R. D.; Forbes, M. D. E.; Lee, H. Nitronyl Nitroxide Radicals as Organic Memory Elements with Both n- and p-Type Properties. *Angew. Chem. Int. Ed.* **2011**, 50, 4414–4418. DOI: <a href="https://doi.org/10.1002/anie.201004899">https://doi.org/10.1002/anie.201004899</a>
- 312. Gaudenzi, R.; de Bruijckere, J.; Reta, D.; Moreira, I. de P. R.; Rovira, C.; Veciana, J.; van der Zant, H. S. J.; Burzurí, E. Redox-Induced Gating of the Exchange Interactions in a Single Organic Diradical. *ACS Nano* **2017**, 11, 5879–5883. DOI: <a href="https://doi.org/10.1021/acsnano.7b01578">https://doi.org/10.1021/acsnano.7b01578</a>
- 313. Rajca, A. Organic Diradicals and Polyradicals: From Spin Coupling to Magnetism? *Chem. Rev.* **1994**, 94, 871–893. DOI: <a href="https://doi.org/10.1021/cr00028a002">https://doi.org/10.1021/cr00028a002</a>
- 314. Merzbacher, E. Quantum Mechanics; Wiley: New York, 1970; p 528.

- 315. Ciofini, I.; Adamo, C.; Barone, V.; Berthier, G.; Rassat, A. Mapping the many-electron generalised spin-exchange Hamiltonian to accurate post-HF calculations. *Chem. Phys.* **2005**, *309*, 133–141. DOI: <a href="https://doi.org/10.1016/j.chemphys.2004.09.001">https://doi.org/10.1016/j.chemphys.2004.09.001</a>
- 316. Ovchinnikov, A. A. Multiplicity of the ground state of large alternant organic molecules with conjugated bonds. *Theor. Chim. Acta* **1978**, 47, 297–304. DOI: https://doi.org/10.1007/BF00549259
- 317. Wenthold, P. G.; Hu, J.; Squires, R. R.; Lineberger, W. C. Photoelectron Spectroscopy of the Trimethylene-methane Negative Ion. The Singlet-Triplet Splitting of Trimethylenemethane. *J. Am. Chem. Soc.* **1996**, *118*, 475–476. DOI: https://doi.org/10.1021/ja9532547
- 318. Wenthold, P. G.; Hu, J.; Squires, R. R.; Lineberger, W. C. Photoelectron spectroscopy of the trimethylenemethane negative ion. *J. Am. Soc. Mass. Spectrom.* **1999**, *10*, 800–809. DOI: https://doi.org/10.1016/S1044-0305(99)00043-4
- 319. Hudson, B. S.; Kohler, B. E.; Schulten, K. *Excited States*; Lim, E. C., Ed.; Academic Press: New York, 1982; Vol. 6, pp 54–55.
- 320. Berson, J. A. A New Class of Non-Kekulé Molecules with Tunable Singlet-Triplet Energy Spacings. *Acc. Chem. Res.* **1997**, *30*, 238–244. DOI: <a href="https://doi.org/10.1021/ar9700015">https://doi.org/10.1021/ar9700015</a>
- 321. Matsuda, K.; Iwamura, H. Demonstration of the degeneracy of the singlet and triplet states in 2,3-dimethylenecyclohexane-1,4-diyl by measurement of its magnetic properties. *J. Chem. Soc.*, *Perkin Trans.* 2 **1998**, 1023–1026. DOI: https://doi.org/10.1039/A706301F
- 322. Wenthold, P. G.; Kim, J. B.; Lineberger, W. C. Photoelectron Spectroscopy of *m*-Xylylene Anion. *J. Am. Chem. Soc.* **1997**, *119*, 1354–1359. DOI: <a href="https://doi.org/10.1021/ja9623830">https://doi.org/10.1021/ja9623830</a>
- 323. Rajca, A.; Rajca, S. Intramolecular Antiferromagnetic vs Ferromagnetic Spin Coupling through the Biphenyl Unit. *J. Am. Chem. Soc.* **1996**, *118*, 8121–8126. DOI: <a href="https://doi.org/10.1021/ja961045w">https://doi.org/10.1021/ja961045w</a>
- 324. Dougherty, D. A. Spin control in organic molecules. *Acc. Chem. Res.* **1991**, *24*, 88–94. DOI: <a href="https://doi.org/10.1021/ar00003a005">https://doi.org/10.1021/ar00003a005</a>
- 325. Borden, W. T.; Davidson, E. R. Effects of electron repulsion in conjugated hydrocarbon diradicals. *J. Am. Chem. Soc.* **1977**, *99*, 4587–4594. DOI: <a href="https://doi.org/10.1021/ja00456a010">https://doi.org/10.1021/ja00456a010</a>
- 326. Rohde, O.; Van, S. P.; Kester, W. R.; Griffith, O. H. Spin labels as molecular rulers. Conformational analysis of a model system. 1, 4-Didoxylcyclohexane oriented in a crystalline host. *J. Am. Chem. Soc.* **1974**, *96*, 5311–5318. DOI: https://pubs.acs.org/doi/pdf/10.1021/ja00824a003
- 327. Riplinger, C.; Kao, J. P.; Rosen, G. M.; Kathirvelu, V.; Eaton, G. R.; Eaton, S. S.; Kutateladze, A.; Neese, F. Interaction of radical pairs through-bond and through-space: scope and limitations of the point-dipole approximation in electron paramagnetic resonance spectroscopy. *J. Am. Chem. Soc.* **2009**, *131*, 10092–10106. DOI: 10.1021/Ja901150J

- 328. Rajca, A.; Rajca, S.; Desai, S. R. Macrocyclic π-Conjugated Carbopolyanions and Polyradicals Based upon Calix[4]arene and Calix[3]arene Rings. *J. Am. Chem. Soc.* **1995**, *117*, 806–816. DOI: <a href="https://doi.org/10.1021/ja00107a025">https://doi.org/10.1021/ja00107a025</a>
- 329. Rajca, S.; Rajca, A. Novel High-Spin Molecules: π-Conjugated Polyradical Polyanions. Ferromagnetic Spin Coupling and Electron Localization. *J. Am. Chem. Soc.* **1995**, *117*, 9172–9179. DOI: <a href="https://doi.org/10.1021/ja00141a008">https://doi.org/10.1021/ja00141a008</a>
- 330. Belorizky, E; Fries, P. Exact solutions for simple spin clusters with isotropic Heisenberg exchange interactions. *J. Chim. Phys. Phys.-Chim. Biol.* **1993**, *90*, 1077–1100. DOI: <a href="https://doi.org/10.1051/jcp/1993901077">https://doi.org/10.1051/jcp/1993901077</a>
- 331. Rajca, A.; Rajca, S. Alkyl-Substituted Schlenk Hydrocarbon Diradicals with Triplet and Singlet Ground States in Frozen Solutions. *J. Chem. Soc. Perkin 2*, **1998**, 1077–1082. DOI: <a href="https://doi.org/10.1039/a70637">https://doi.org/10.1039/a70637</a>
- 332. Eaton, S. S.; More, K. M.; Sawant, B. M.; Eaton, G. R. Use of the EPR half-field transition to determine the interspin distance and the orientation of the interspin vector in systems with two unpaired electrons. *J. Am. Chem. Soc.* **1983**, *105*, 6560–6567. DOI: <a href="https://doi.org/10.1021/ja00360a005">https://doi.org/10.1021/ja00360a005</a>
- 333. Eaton, G. R.; Eaton, S. S.; Barr, D. P.; Weber, R. T. *Quantitative EPR*. Springer-Verlag: Vienna 2010, pp. 1–185. DOI: <a href="https://doi.org/10.1007/978-3-211-92948-3">https://doi.org/10.1007/978-3-211-92948-3</a>
- 334. Dressler, J. J.; Teraoka, M.; Espejo, G. L.; Kishi, R.; Takamuku, S.; Gómez-García, C. J.; Zakharov, L. N.; Nakano, M.; Casado, J.; Haley, M. M. Thiophene and Its Sulfur Inhibit Indenoindenodibenzothiophene Diradicals from Low-energy Lying Thermal Triplets. *Nat. Chem.* **2018**, *10*, 1134–1140. DOI: https://doi.org/10.1038/s41557-018-0133-5
- 335. Kopf, P. W.; Krellick, R. W. Magnetic resonance studies of some phenoxy and nitroxide biradicals. *J. Am. Chem. Soc.* **1969**, *91*, 6569–6573. DOI: <a href="https://doi.org/10.1021/ja01052a005">https://doi.org/10.1021/ja01052a005</a>
- 336. Evans, D. F. The determination of the paramagnetic susceptibility of substances in solution by nuclear magnetic resonance. *J. Chem. Soc.* **1959**, 2003–2005. DOI: https://doi.org/10.1039/jr9590002003
- 337. Live, D. H.; Chan, S. I. Bulk susceptibility corrections in nuclear magnetic resonance experiments using superconducting solenoids. *Anal. Chem.* **1970**, *42*, 791–792. DOI: <a href="https://doi.org/10.1021/ac60289a028">https://doi.org/10.1021/ac60289a028</a>
- 338. Tretyakov, E.V; Ovcharenko, V. I. The chemistry of nitroxide radicals in the molecular design of magnets. *Russ. Chem. Rev.* **2009**, *78*, 971–1007. DOI: <a href="https://doi.org/10.1070/RC2009v078n11ABEH004093">https://doi.org/10.1070/RC2009v078n11ABEH004093</a>
- 339. Ullman, E. F.; Osiecki, J. H.; Bobcock, D. G. B.; Darcy. R. Stable free radicals. X. Nitronyl nitroxide monoradicals and biradicals as possible small molecule spin labels, *J. Am. Chem. Soc.* **1972**, *94*, 7049–7059. DOI: https://doi.org/10.1021/ja00775a031
- 340. Bobcock, D. G. B.; Darcy, R.; Ullman, E. F. Studies of free radicals. II. Chemical properties of nitronylnitroxides. A unique radical anion, *J. Am. Chem. Soc.* **1968**, *90*, 5945–5946. DOI: <a href="https://doi.org/10.1021/ja01023a078">https://doi.org/10.1021/ja01023a078</a>

- 341. Chupakhin, O. N.; Utepova, I. A.; Varaskin, M. V.; Tretyakov, E. V.; Romanenko, G. V.; Stass, D. V.; Ovcharenko, V. I. S<sub>N</sub><sup>H</sup> Approach in the Synthesis of Nitronyl Nitroxides. *J. Org. Chem.* **2009**, *74*, 2870–2872. DOI: <a href="https://doi.org/10.1021/jo900085s">https://doi.org/10.1021/jo900085s</a>
- 342. Tretyakov, E. V.; Utepova, I.A.; Varaskin, M. V.; Tolstikov, S. E.; Romanenko, G. V.; Bogomyakov, A. S.; Stass, D. V.; Ovcharenko, V. I.; Chupakhin, O. N. New approach to synthesis of nitronyl and imino nitroxides based on S<sub>N</sub><sup>H</sup> methodology. *ARKIVOC* **2011**(viii), 76–98. DOI: <a href="http://dx.doi.org/10.3998/ark.5550190.0012.806">http://dx.doi.org/10.3998/ark.5550190.0012.806</a>
- 343. Zhang, X.; Suzuki, S.; Kozaki, M.; Okada, K. NCN Pincer-Pt Complexes Coordinated by (Nitronyl Nitroxide)-2-ide Radical Anion, *J. Am. Chem. Soc.* **2012**, *134*, 17866–17868. DOI: <a href="https://doi.org/10.1021/ja308103g">https://doi.org/10.1021/ja308103g</a>
- 344. Tanimoto, R.; Suzuki, S.; Kozaki, M.; Okada K. Nitronyl Nitroxide as a Coupling Partner: Pd-Mediated Cross-coupling of (Nitronyl nitroxide-2-ido) (triphenylphosphine) gold(I) with Aryl Halides, *Chem. Lett.* **2014**, 43, 678–680. DOI: https://doi.org/10.1246/cl.131162
- 345. Yamada, K.; Zhang, X.; Tanimoto, R.; Suzuki, S.; Kozaki, M.; Tanaka, R.; Okada, K. Radical Metalloids with N-Heterocyclic Carbene and Phenanthroline Ligands: Synthesis, Properties, and Cross-Coupling Reaction of [(Nitronyl Nitroxide)-2-ido]metal Complexes with Aryl Halides, *Bull. Chem. Soc. Jpn.* **2018**, *91*, 1150–1157. DOI: <a href="https://doi.org/10.1246/bcsj.20180033">https://doi.org/10.1246/bcsj.20180033</a>
- 346. Suzuki, S.; Nakamura, F.; Naota, T. A direct synthetic method for (nitronyl nitroxide)-substituted π-electronic compounds *via* a palladium-catalyzed cross-coupling reaction with a zinc complex, *Mater. Chem. Front.* **2018**, *2*, 591–596. DOI: <a href="https://doi.org/10.1039/C7QM00565B">https://doi.org/10.1039/C7QM00565B</a>
- 347. Suzuki, S.; Nakamura, F.; Naota, T. Environmentally Benign Strategy for Arylation of Nitronyl Nitroxide Using a Non-Transition Metal Nucleophile. *Org. Lett.* **2020**, *22*, 1350–1354. DOI: <a href="https://doi.org/10.1021/acs.orglett.9b04655">https://doi.org/10.1021/acs.orglett.9b04655</a>
- 348. Inoue, K.; Iwamura, H. 2-[*p*(*N*-*tert*-butyl-N-oxyamino)phenyl]-4,4,5,5-tetramethyl-4,5-dihydroimidazol-3-oxide-1-oxyl, a Stable Diradical with a Triplet Ground State. *Angew. Chem. Int. Ed.* **1995**, *34*, 927– 928. DOI: <a href="https://doi.org/10.1002/anie.199509271">https://doi.org/10.1002/anie.199509271</a>
- 349. Suzuki, S.; Furui, T.; Kuratsu, M.; Kozaki, M.; Shiomi, D.; Sato, K.; Takui, T.; Okada, K. Nitroxide-Substituted Nitronyl Nitroxide and Iminonitroxide. *J. Am. Chem. Soc.* **2010**, *132*, 15908–15910. DOI: https://doi.org/10.1021/ja107769z
- 350. Zayakin, I.; Tretyakov, E.; Akyeva, A.; Syroeshkin, M.; Burykina, J.; Dmitrenok, A.; Korlyukov, A.; Nasyrova, D.; Bagryanskaya, I.; Stass, D.; et al. Overclocking Nitronyl Nitroxide Gold Derivatives in Cross-Coupling Reactions. *Chem. Eur. J.* **2023**, *29*, e202203118. DOI: <a href="https://doi.org/10.1002/chem.202203118">https://doi.org/10.1002/chem.202203118</a>
- 351. Kumagai, T.; Suzuki, S.; Kanzaki, Y.; Shiomi, D.; Sato, K.; Takui, T.; Tanaka, R.; Okada, K.; Kozaki, M. Heteroatom-incorporated Trimethylenemethane: Synthesis and Properties of Triphenylphenylnitroxide(Nitronyl Nitroxide) Dyad. *Chem. Lett.* **2022**, *51*, 458–460. DOI: https://doi.org/10.1246/cl.220021
- 352. Mikhailova, M. V.; Dudko, E. M.; Nasyrova, D. I.; Akyeva, A. Ya.; Syroeshkin, M. A.; Bogomyakov, A. S.; Artyukhova, N. A.; Fedin, M. V.; Gorbunov, D. E.; Gritsan, N. P.; et al.

- Adamantyl-Substituted Triplet Diradical: Synthesis, Structure, Redox and Magnetic Properties. *Dokl. Chem.* **2022**, *507*, 270–280. DOI: <a href="https://doi.org/10.1134/S0012500822700148">https://doi.org/10.1134/S0012500822700148</a>
- 353. Hosokoshi, Y.; Takizawa, K.; Nakano, H.; Goto, T.; Takahashi, M.; Inoue, K. Construction of spin-1/2 Heisenberg ferromagnetic-antiferromagnetic alternating chains with various exchange couplings. *J. Magn. Magn. Mater.* **1998**, *177–181*, 634–635. DOI: <a href="https://doi.org/10.1016/S0304-8853(97)00413-7">https://doi.org/10.1016/S0304-8853(97)00413-7</a>
- 354. Tanaka, M.; Matsuda, K.; Itoh, T.; Iwamura, H. Syntheses and Magnetic Properties of Stable Organic Triradicals with Quartet Ground States Consisting of Different Nitroxide Radicals. *J. Am. Chem. Soc.* **1998**, *120*, 7168–7173. DOI: <a href="https://doi.org/10.1021/ja980817g">https://doi.org/10.1021/ja980817g</a>
- 355. Tyutyulkov, N. N.; Karabunarliev, S. C. Structure and Properties of Nonclassical Polymers. III. Magnetic Characteristics at Finite Temperatures. *Int. J. Quantum Chem.* **1986**. *29*, 1325–1337. DOI: https://doi.org/10.1002/qua.560290528
- 356. Demir, S.; Jeon, I-R.; Long, J. R.; Harris, T. D. S. Radical ligand-containing single-molecule magnets. *Coord. Chem. Rev.* **2015**, *289–290*, 149–176. DOI: <a href="https://doi.org/10.1016/j.ccr.2014.10.012">https://doi.org/10.1016/j.ccr.2014.10.012</a>
- 357. Shultz, D. A.; Bodnar, S. H.; Vostrikova, K. E.; Kampf, J. W. Synthesis and Structure of a Complex Having a Quartet Ground State with Three Entirely Different Spin Carriers: Nitronyl Nitroxide, *o*-Semiquinone, and Cu<sup>II</sup>. *Inorg. Chem.* **2000**, *39*, 6091–6093. DOI: https://doi.org/10.1021/ic0009122
- 358. Shultz, D. A.; Vostrikova, K. E.; Bodnar, S. H.; Koo, H. J.; Whangbo, M. H.; Kirk, M. L.; Depperman, E. C.; Kampf, J. W. Trends in Metal-Biradical Exchange Interaction for First-Row M<sup>II</sup>(Nitronyl Nitroxide-Semiquinone) Complexes. *J. Am. Chem. Soc.* **2003**, *125*, 1607–1617. DOI: <a href="https://doi.org/10.1021/ja020715x">https://doi.org/10.1021/ja020715x</a>
- 359. Gilroy, J. B.; McKinnon, S. D. J.; Koivisto, B. D.; Hicks, R. G. Electrochemical Studies of Verdazyl Radicals. *Org. Lett.* **2007**, *9*, 4837–4840. DOI: <a href="https://doi.org/10.1021/o1702163a">https://doi.org/10.1021/o1702163a</a>
- 360. Connelly, N. G.; Geiger, W. E. Chemical Redox Agents for Organometallic Chemistry. *Chem. Rev.* **1996**, *96*, 877–910. DOI: <a href="https://doi.org/10.1021/cr940053x">https://doi.org/10.1021/cr940053x</a>
- 361. Hiraoka, S.; Okamoto, T.; Kozaki, M.; Shiomi, D.; Sato, K.; Takui, T.; Okada, K. A Stable Radical-Substituted Radical Cation with Strongly Ferromagnetic Interaction: Nitronyl Nitroxide-Substituted 5,10-Diphenyl-5,10-dihydrophenazine Radical Cation. *J. Am. Chem. Soc.* **2004**, *126*, 58–59. DOI: <a href="https://doi.org/10.1021/ja0367748">https://doi.org/10.1021/ja0367748</a>
- 362. Nagata, A.; Hiraoka, S.; Suzuki, S.; Kozaki, M.; Shiomi, D.; Sato, K.; Takui, T.; Tanaka, R.; Okada, K. Redox-Induced Modulation of Exchange Interaction in a High-Spin Ground-State Diradical/Triradical System. *Chem. Eur. J.* **2020**, *26*, 3166–3172. DOI: <a href="https://doi.org/10.1002/chem.201905465">https://doi.org/10.1002/chem.201905465</a>
- 363. Kuratsu, M.; Suzuki, S.; Kozaki, M.; Shiomi, D.; Sato, K.; Takui, T.; Kanzawa, T.; Hosokoshi, Y.; Lan, X.-Z.; Miyazaki, Y.; et al. (Nitronyl Nitroxide)-Substituted Trioxytriphenylamine Radical Cation Tetrachlorogallate Salt: A 2p-Electron-Based Weak Ferromagnet Composed of a

- Triplet Diradical Cation. *Chem. Asian J.* **2012**, *7*, 1604–1609. DOI: https://doi.org/10.1002/asia.201200084
- 364. Yokoyama, N.; Tanaka, N.; Fujimoto, N.; Tanaka, R.; Suzuki, S.; Shiomi, D.; Sato, K.; Takui, T.; Kozaki, M.; Okada. K. Syntheses and Properties of (Nitronyl nitroxide)-substituted Triphenylamine ortho-Bridged by Two Oxygen and Sulfur Atoms. *Chem Asian J.* **2021**, *16*, 72–79. DOI: <a href="https://doi.org/10.1002/asia.202001227">https://doi.org/10.1002/asia.202001227</a>
- 365. Tahara, T.; Suzuki, S.; Kozaki, M.; Shiomi, D.; Sugisaki, K.; Sato, K.; Takui, T.; Miyake, Y.; Hosokoshi, Y.; Nojiri, H.; et al. Triplet Diradical-Cation Salts Consisting of the Phenothiazine Radical Cation and a Nitronyl Nitroxide. *Chem. Eur. J.* **2019**, *25*, 7201–7209. DOI: <a href="https://doi.org/10.1002/chem.201900513">https://doi.org/10.1002/chem.201900513</a>
- 366. Masuda, Y.; Kuratsu, M.; Suzuki, S.; Kozaki, M.; Shiomi, D.; Sato, K.; Takui, T.; Hosokoshi, Y.; Lan, X.-Z.; Miyazaki, Y.; et al. A New Ferrimagnet Based on a Radical-Substituted Radical Cation Salt. *J. Am. Chem. Soc.* **2009**, *131*, 4670–4673. DOI: https://doi.org/10.1021/ja808093z
- 367. McConnell, H. M.; Chesnut, D. B. Theory of Isotropic Hyperfine Interactions in π-Electron Radicals. *J. Chem. Phys.* **1958**, *28*, 107–117. DOI: <a href="https://doi.org/10.1063/1.1744052">https://doi.org/10.1063/1.1744052</a>
- 368. Gerson, F.; Huber, W. *Electron Spin Resonance Spectroscopy of Organic Radicals*. Wiley-VCH: Weinheim, 2003, pp 49–64.
- 369. Howarth, O. W.; Fraenkel, G. K. Electron Spin Resonance Study of Mono- and Dimeric Cations of Aromatic Hydrocarbons. *J. Am. Chem. Soc.* **1966**, *88*, 4514–4515. DOI: https://doi.org/10.1021/ja00971a043
- 370. Barton, B. L.; Fraenkel, G. K. Electron Spin Resonance Spectra of Methyl-Substituted Dihydropyrazine Cations and Related Radicals. *J. Chem. Phys.* **1964**, *41*, 1455–1468. DOI: https://doi.org/10.1063/1.1726090
- 371. Cole, T. Paramagnetic Defects in Irradiated NH<sub>4</sub>ClO<sub>4</sub>. *J. Chem. Phys.* **1961**, *35*, 1169–1173. DOI: <a href="https://doi.org/10.1063/1.1732018">https://doi.org/10.1063/1.1732018</a>
- 372. Gerson, F.; Huber, W. *Electron Spin Resonance Spectroscopy of Organic Radicals*. Wiley-VCH: Weinheim, 2003, p. 201.
- 373. Adams, J. Q.; Niksic, S. W.; Thomas, J. R. Paramagnetic Resonance of Alkyl Nitroxides, *J. Chem. Phys.* **1966**, *45*, 654–661. DOI: <a href="https://doi.org/10.1063/1.1727625">https://doi.org/10.1063/1.1727625</a>
- 374. Gerson, F.; Huber, W. *Electron Spin Resonance Spectroscopy of Organic Radicals*. Wiley-VCH: Weinheim, 2003, p. 299.
- 375. Barbarella, G.; Rassat, A. Nitroxides. XXXIV. Substituted *tert*-butyl phenyl nitroxide derivatives electron paramagnetic resonance. Ultrafine deviations due to nitrogen. *Bull. Soc. Chim. Fr.* **1969**, 7, 2378–2385. Google Scholar:

  <a href="https://scholar.google.com/scholar\_lookup?journal=Bulletin+de+la+Societe+Chimique+de+France&title=Nitroxides.+XXXIV.+Substituted+tert-butyl+phenyl+nitroxide+derivatives+electron+paramagnetic+resonance.+Ultrafine+deviations+due+to+nitrogen&author=G+Barbarella&author=A+Rassat&volume=7&publication\_year=1969&pages=2378-2385&</a>

- 376. Kazuhiko, I.; Hiroshi, N.; Kazuo, M.; Masahiro, K.; Takamitsu, Y. The ENDOR Spectra of *t*-Butylphenylnitroxide. *Chem. Lett.* **1973**, *2*, 1261–1264. DOI: <a href="https://doi.org/10.1246/cl.1973.1261">https://doi.org/10.1246/cl.1973.1261</a>
- 377. Fischer, P. H. H.; Neugebauer, F. A. Elektronenspinresonanz p-substituierter Diarylstickstoffoxyde. *Z. für Naturforsch. A*, **1964**, *19*, 1514–1517. DOI: <a href="https://doi.org/10.1515/zna-1964-1314">https://doi.org/10.1515/zna-1964-1314</a>
- 378. Neugebauer, F. A.; Rimmler, G. ENDOR and Triple Resonance Studies of 1,4-Dihydro-1,2,4-Benzotriazinyl Radicals and 1,4-Dihydro-1,2,4-Benzotriazine Radical Cations. *Magn. Reson. Chem.* **1988**, *26*, 595–600. DOI: https://doi.org/10.1002/mrc.1260260712
- 379. Neugebauer, F. A.; Fischer, H.; Krieger, C. Verdazyls. Part 33. EPR and ENDOR studies of 6-oxo- and 6-thioxoverdazyls. X-Ray molecular structure of 1,3,5-triphenyl-6-oxoverdazyl and 3-tert-butyl-1,5-diphenyl-6-thioxoverdazyl. *J. Chem. Soc., Perkin Trans* 2, **1993**, 535–544. DOI: http://dx.doi.org/10.1039/P29930000535
- 380. Shultz, D. A.; Boal, A. K.; Campbell, N. P. Effect of Aliphatic Amine Bases on the Aggregation of Alkali Metal Salts of 3,5-Di-*tert*-butylsemiquinone (3,5-DBSQ). *Inorg. Chem.* **1998**, *37*, 1540–1543. DOI: https://doi.org/10.1021/ic971113v
- 381. Cauquis, G.; Delhomme, H.; Serve, D. Les caracteristiques des radicaux cations de quelques diaryl-5,10 dihydro-5,10 phenazines et des tetraarylhydrazines correspondantes. La degradation de ces dernieres par les acides. *Tetrahedron Lett.* **1971**, *12*, 4649–4652. DOI: <a href="https://doi.org/10.1016/S0040-4039(01)97553-7">https://doi.org/10.1016/S0040-4039(01)97553-7</a>
- 382. Kuratsu, M.; Kozaki, M.; Okada, K. 2,2':6',2'':6'',6-Trioxytriphenylamine: Synthesis and Properties of the Radical Cation and Neutral Species. *Angew. Chem. Int. Ed.* **2005**, *44*, 4056–4058. DOI: <a href="https://doi.org/10.1002/anie.200500397">https://doi.org/10.1002/anie.200500397</a>
- 383. Clarke, D.; Gilbert, B. C.; Hanson, P. Heterocyclic Free Radicals. Part V. An Electron Spin Resonance Investigation of the Cation-radicals of 10-Phenylphenoxazine and 10-Phenylphenothiazine. *J. Chem. Soc. Perkin Trams.* 2 **1975**, 1078–1082. DOI: https://doi.org/10.1039/P29750001078
- 384. Kaszyński, P.; Constantinides, C. P.; Young Jr., V. G. The Planar Blatter Radical: Structural Chemistry of 1,4-Dihydrobenzo[e][1,2,4]triazin-4-yls. *Angew. Chem. Int. Ed.* **2016**, *55*, 11149–11152. DOI: https://doi.org/10.1002/anie.201605612
- 385. Hales, B. J. Immobilized radicals. I. Principal electron spin resonance parameters of the benzosemiquinone radical. *J. Am. Chem. Soc.* **1975**, *97*, 5993–5997. DOI: https://doi.org/10.1021/ja00854a007
- 386. Shultz, D. A.; Fico, R. M.; Bodnar, S. H.; Kumar, R. K.; Vostrikova, K. E.; Kampf, J. W.; Boyle. P. D. Trends in Exchange Coupling for Trimethylenemethane-Type Bis(semiquinone) Biradicals and Correlation of Magnetic Exchange with Mixed Valency for Cross-Conjugated Systems. *J. Am. Chem. Soc.* **2003**, *125*, 11761–11771. DOI: https://doi.org/10.1021/ja0367849
- 387. Shultz, D. A.; Fico, R. M.; Lee, H.; Kampf, J. W.; Kirschbaum, K.; Pinkerton, A. A.; Boyle. P. D. Mechanisms of Exchange Modulation in Trimethylenemethane-type Biradicals: The Roles of

- Conformation and Spin Density. *J. Am. Chem. Soc.* **2003**, *125*, 15426–15432. DOI: <a href="https://doi.org/10.1021/ja0377870">https://doi.org/10.1021/ja0377870</a>
- 388. Karplus, M. Vicinal Proton Coupling in Nuclear Magnetic Resonance. *J. Am. Chem. Soc.* **1963**, 85, 2870–2871. DOI: https://doi.org/10.1021/ja00901a059
- 389. Heller, C.; McConnell, H. M. Radiation Damage in Organic Crystals. II. Electron Spin Resonance of (CO<sub>2</sub>H)CH<sub>2</sub>CH(CO<sub>2</sub>H) in β-Succinic Acid. *J. Chem. Phys.* **1960**, *32*, 1535–1539. DOI: <a href="https://doi.org/10.1063/1.1730955">https://doi.org/10.1063/1.1730955</a>
- 390. Fessenden, R. W.; Schuler, R. H. Electron Spin Resonance Studies of Transient Alkyl Radicals. *J. Chem. Phys.* **1963**, *39*, 2147–2195. DOI: <a href="https://doi.org/10.1063/1.1701415">https://doi.org/10.1063/1.1701415</a>
- 391. Gubaidullin, A. T.; Buzykin, B. I.; Litvinov, I. A.; Gazetdinova, N. G. Molecular and Crystal Structure of a Superstable Free Radical, 1,3-Diphenyl-1,4-dihydro-1,2,4-benzotriazin-4-yl. *Russ. J. Gen. Chem.* **2004**, *74*, 939–943. DOI: https://doi.org/10.1023/B:RUGC.0000042432.08612.2a
- 392. Saunders, M.; Berger, R.; Jaffe, A.; McBride, J. M.; O'Neill, J.; Breslow, R.; Hoffmann, J. M. Jr; Perchonock, C.; Wasserman, E.; Hutton, R. S.; et al. Unsubstituted Cyclopentadienyl Cation, a Ground-state Triplet. *J. Am. Chem. Soc.* **1973**, *95*, 3017–3018. DOI: <a href="https://doi.org/10.1021/ja00790a049">https://doi.org/10.1021/ja00790a049</a>
- 393. Borden, W. T.; Davidson, E. R. Potential Surfaces for the Planar Cyclopentadienyl Radical and Cation. *J. Am. Chem. Soc.* **1979**, *101*, 3771–3775. DOI: <a href="https://doi.org/10.1021/ja00508a012">https://doi.org/10.1021/ja00508a012</a>
- 394. Worner, H. J.; Merkt, F. Photoelectron Spectroscopic Study of the First Singlet and Triplet States of the Cyclopentadienyl. *Angew. Chem. Int. Ed.* **2006**, *45*, 293–296. DOI: <a href="https://doi.org/10.1002/anie.200503032">https://doi.org/10.1002/anie.200503032</a>
- 395. Costa, P.; Trosien, I.; Mieres-Perez, J.; Sander, W. Isolation of an Antiaromatic Singlet Cyclopentadienyl Zwitterion, *J. Am. Chem. Soc.* **2017**, *139*, 13024–13030. DOI: <a href="https://doi.org/10.1021/jacs.7b05807">https://doi.org/10.1021/jacs.7b05807</a>
- 396. Wasserman, E.; Hutton, R. S.; Kuck, V. J.; Chandross, E. A. Dipositive ion of hexachlorobenzene. Ground-state triplet. *J. Am. Chem. Soc.* **1974**, *96*, 1965–1966. DOI: <a href="https://doi.org/10.1021/ja00813a068">https://doi.org/10.1021/ja00813a068</a>
- 397. Miller, J. S.; Dixon, D. A.; Calabrese, J. C. Crystal Structure of Hexaazaoctadecahydrocoronene Dication [HAOC]<sup>2+</sup>, a Singlet Benzene Dication. *Science* **1988**, 240, 1185–1188. DOI: https://doi.org/10.1126/science.240.4856.1185
- 398. Breslow, R.  $4n \pi$ -Electron Triplet Species and Their Potential Use in Organic Ferromagnets. *Mol. Cryst. Liq. Cryst.* **1989**, *176*, 199–210. DOI: <a href="https://doi.org/10.1080/00268948908037480">https://doi.org/10.1080/00268948908037480</a>
- 399. Gould, C. A.; Marbey, J.; Vieru, V.; Marchiori, D. A.; Britt, R. D.; Chibotaru, L. F.; Hill, S.; Long, J. R. Isolation of a Triplet Benzene Dianion. *Nat. Chem.* **2021**, *13*, 1001–1005. DOI: <a href="https://doi.org/10.1038/s41557-021-00737-8">https://doi.org/10.1038/s41557-021-00737-8</a>
- 400. Cation Fisher, J. J.; Penn, H.; Dohnert, D.; Michl, J. Polarized IR spectroscopy of a triplet 1,3-biradical: the structure of a methylene-bridged 1,8-naphthoquinodimethane. *J. Am. Chem. Soc.* **1986**, *108*, 1715–1716. DOI: https://doi.org/10.1021/ja00267a066

- 401. Hrovat, D. A.; Wang, X.-B.; Borden, W. T. Calculations on 1,8-naphthoquinone predict that the ground state of this diradical is a singlet. *J. Comput. Chem.* **2019**, *40*, 119–126. DOI: <a href="https://doi.org/10.1002/jec.25551">https://doi.org/10.1002/jec.25551</a>
- 402. Gisin, M.; Rommel, E.; Wirz, J.; Burnett, M. N.; Pagni, R. M. Biradicaloid intermediates in photochemistry: spectroscopic and kinetic study of 1,4-perinaphthadiyl and related 1,8-naphthoquinodimethans. *J. Am. Chem. Soc.* **1979**, *101*, 2216–2218. DOI: https://doi.org/10.1021/ja00502a055
- 403. Hasler, E.; Gassmann, E.; Wirz, J. Conjugated Biradical Intermediates: Spectroscopic, Kinetic, and Trapping Studies of 2,2-Dimethyl-1,3-perinaphthadiyl. *Helv. Chim. Acta* **1985**, *68*, 777–788. DOI: <a href="https://doi.org/10.1002/hlca.19850680328">https://doi.org/10.1002/hlca.19850680328</a>
- 404. McMasters, D. R.; Wirz, J.; Snyder, G. J. 2,2-Dimethyl-2H-dibenzo[cd,k]fluoranthene, the First Kekulé Hydrocarbon with a Triplet Ground State. *J. Am. Chem. Soc.* **1997**, *119*, 8568–8569. DOI: https://doi.org/10.1021/ja971635+
- 405. McMasters, D. R.; Wirz, J. Spectroscopy and Reactivity of Kekulé Hydrocarbons with Very Small Singlet–Triplet Gaps. *J. Am. Chem. Soc.* **2001**, *123*, 238–246. DOI: <a href="https://doi.org/10.1021/ja0004377">https://doi.org/10.1021/ja0004377</a>
- 406. Horii, K.; Kishi, R.; Nakano, M.; Shiomi, D.; Sato, K.; Takui, T.; Konishi, A.; Yasuda, M. Bis-periazulene (Cyclohepta[*def*]fluorene) as a Nonalternant Isomer of Pyrene: Synthesis and Characterization of Its Triaryl Derivatives. *J. Am. Chem. Soc.* **2022**, *144*, 3370–3375. DOI: <a href="https://doi.org/10.1021/jacs.2c00476">https://doi.org/10.1021/jacs.2c00476</a>
- 407. Shimizu, A.; Morikoshi, T.; Sugisaki, K.; Shiomi, D.; Sato, K.; Takui, T.; Shintani, R. Synthesis and Isolation of a Kekulé Hydrocarbon with a Triplet Ground State. *Angew. Chem. Int. Ed.* **2022**, *61*, e202205729. DOI: <a href="https://doi.org/10.1002/anie.202205729">https://doi.org/10.1002/anie.202205729</a>
- 408. Eliel, E. L.; Wilen, S. H. *Stereochemistry of Organic Compounds*; Wiley-VCH: New York, 1994; Chapter 13, pp 991–1118 (Table 13.2).
- 409. Rajca, A.; Miyasaka, M.; Pink, M.; Wang, H.; Rajca, S. Helically Annelated and Cross-Conjugated Oligothiophenes: Asymmetric Synthesis, Resolution, and Characterization of a Carbon-Sulfur [7]Helicene. *J. Am. Chem. Soc.* **2004**, *126*, 15211–1522. DOI: <a href="https://doi.org/10.1021/ja0462530">https://doi.org/10.1021/ja0462530</a>
- 410. Zhang, S.; Liu, X.; Li, C.; Li, L.; Song, J.; Shi, J.; Morton, M.; Rajca, S.; Rajca, A.; Wang, H. Thiophene-Based Double Helices: Syntheses, X-ray Structures, and Chiroptical Properties. *J. Am. Chem. Soc.* **2016**, *138*, 10002–10010. DOI: https://doi.org/10.1021/jacs.6b05709
- 411. Tsuji, Y.; Hoffmann, R.; Strange, M.; Solomon, G. C. Close relation between quantum interference in molecular conductance and diradical existence. *Proc. Natl. Acad. Sci. U.S.A* **2016**, *113*, E413–E419. DOI: 10.1073/pnas.1518206113
- 412. Baghernejad, M.; Zhao, X.; Baruël Ørnsø, K.; Füeg, M.; Moreno-García, P.; Rudnev, A. V.; Kaliginedi, V.; Vesztergom, S.; Huang, C.; Hong, W.; et al. Electrochemical Control of Single-Molecule Conductance by Fermi-Level Tuning and Conjugation Switching. *J. Am. Chem. Soc.* **2014**, *136*, 17922–17925. DOI: 10.1021/ja510335z

- 413. Mayor, M.; Weber, H. B.; Reichert, J.; Elbing, M.; von Hänisch, C.; Beckmann, D.; Fischer, M. Electric Current through a Molecular Rod—Relevance of the Position of the Anchor Groups. *Angew. Chem., Int. Ed.* **2003**, *42*, 5834–5838. DOI: 10.1002/anie.200352179
- 414. Nowik-Boltyk, E.; Junghoefer, T.; Glaser, M.; Giangrisostomi, E.; Ovsyannikov, R.; Zhang, S.; Shu, C.; Rajca, A.; Calzolari, A.; Casu, M. B. Long-term degradation mechanisms in application-implemented radical thin films. *ACS Appl. Mater. Interfaces* **2023**, *15*, 30935–30943. DOI: <a href="https://doi.org/10.1021/acsami.3c02057">https://doi.org/10.1021/acsami.3c02057</a>
- 415. Weiß, R.; Korczyn, J. Über Triphenylmethane, deren Benzolkerne miteinander verbunden sind I. Trimethylentriphenylmethantriketon. *Monatshefte Chem.* **1925**, *45*, 207–214. DOI: https://doi.org/10.1007/BF01524661

416.

- 417. Holt, C. J.; Wentworth, K. J.; Johnson, R. P. A Short and Efficient Synthesis of the [3]Triangulene Ring System. *Angew. Chem. Int. Ed.* **2019**, *58*, 15793–15796. DOI: https://doi.org/10.1002/anie.201907226
- 418. Mou, Z.; Kertesz, M. Sigma- versus Pi-Dimerization Modes of Triangulene. *Chem. Eur. J.* **2018**, *24*, 6140–6147. DOI: https://doi.org/10.1002/chem.201705763
- 419. Pavlick, N.; Mistry, A.; Majzik, Z.; Moll, N.; Meyer, G.; Fox, D. J.; Gross, L. Synthesis and Characterization of Triangulene. *Nat. Nanotechnol.* **2017**, *12*, 308–312. DOI: <a href="https://doi.org/10.1038/nnano.2016.305">https://doi.org/10.1038/nnano.2016.305</a>
- 420. Wang, T.; Berdonces-Layunta, A.; Friedrich, N.; Vilas-Varela, M.; Calupitan, J. P.; Pascual, J. I.; Peña, D.; Casanova, D.; Corso, M.; Oteyza, D. G. de. Aza-Triangulene: On-Surface Synthesis and Electronic and Magnetic Properties. *J. Am. Chem. Soc.* **2022**, *144*, 4522–4529. DOI: <a href="https://doi.org/10.1021/jacs.1c12618">https://doi.org/10.1021/jacs.1c12618</a>
- 421. Turco, E.; Bernhardt, A.; Krane, N.; Valenta, L.; Fasel, R.; Juríček, M.; Ruffieux, P. Observation of the magnetic ground state of the two smallest triangular nanographenes. *JACS Au* **2023**, *3*, 1358–1364, DOI: https://doi.org/10.1021/jacsau.2c00666
- 422. Inoue, J.; Fukui, K.; Kubo, T.; Nakazawa, S.; Sato, K.; Shiomi, D.; Morita, Y.; Yamamoto, K.; Takui, T.; Nakasuji, K. The First Detection of a Clar's Hydrocarbon, 2,6,10-Tri-*Tert*-Butyltriangulene: A Ground-State Triplet of Non-Kekule Polynuclear Benzenoid Hydrocarbon *J. Am. Chem. Soc.* **2001**, 123, 12702–12703. DOI: <a href="https://doi.org/10.1021/ja016751y">https://doi.org/10.1021/ja016751y</a>
- 423. Valenta, L.; Mayländer, M.; Kappeler, P.; Blacque, O.; Šolomek, T.; Richert, S.; Juríček, M. Trimesityltriangulene: A Persistent Derivative of Clar's Hydrocarbon. *Chem. Commun.* **2022**, *58*, 3019–3022. DOI: https://doi.org/10.1039/D2CC00352J
- 424. Arikawa, S.; Shimizu, A.; Shiomi, D.; Sato, K.; Shintani, R. Synthesis and Isolation of a Kinetically Stabilized Crystalline Triangulene. *J. Am. Chem. Soc.* **2021**, *143*, 19599–19605. DOI: <a href="https://doi.org/10.1021/jacs.1c10151">https://doi.org/10.1021/jacs.1c10151</a>

- 425. Wei, H.; Hou, X.; Xu, T.; Zou, Y.; Li, G.; Wu, S.; Wu, J. Solution-Phase Synthesis and Isolation of An Aza-Triangulene and Its Cation in Crystalline Form. *Angew. Chem. Int. Ed.* **2022**, *61*, e202210386 (1-6). DOI: https://doi.org/10.1002/anie.202210386
- 426. Arikawa, S.; Shimizu, A.; Shiomi, D.; Sato, K.; Takui, T.; Sotome, H.; Miyasaka, H.; Murai, M.; Yamaguchi; S.; Shintani, R. A Kinetically Stabilized Nitrogen-Doped Triangulene Cation: Stable and NIR Fluorescent Diradical Cation with Triplet Ground State. *Angew. Chem. Int. Ed.* **2023**, *62*, e202302714. DOI: <a href="https://doi.org/10.1002/anie.202302714">https://doi.org/10.1002/anie.202302714</a>
- 427. Neese, F. The ORCA program system. *Wiley Interdiscip. Rev.: Comput. Mol. Sci.* **2012**, *2*, 73–78. DOI: https://doi.org/10.1002/wcms.81
- 428. Sinnecker, S.; Neese, F. Spin-Spin Contributions to the Zero-Field Splitting Tensor in Organic Triplets, Carbenes and Biradicals A Density Functional and Ab Initio Study. *J. Phys. Chem. A* **2006**, *110*, 12267–12275. DOI: <a href="https://doi.org/10.1021/jp0643303">https://doi.org/10.1021/jp0643303</a>

### **Biographical sketches**

#### **Chan Shu**

Chan Shu received his B.S. degree in 2016 from University of Science and Technology of China. In 2022, he earned his Ph.D. degree from University of Nebraska-Lincoln under the supervision of Prof. Andrzej Rajca. His research was focused on the design and synthesis of high-spin di- and tri-radicals. Now he is a research chemist in the Toyota Research Institute of North America.

## **Zhimin Yang**

Zhimin Yang was born in China and received her B.S. and M.S. degree from Nanjing Tech University, China. In 2021, she received her Ph.D. degree from University of Nebraska-Lincoln under the guidance of Prof. Andrzej Rajca. Subsequently, she did one-year postdoctoral research with Prof. Andrzej Rajca. Her research was focused on the design and synthesis of stable radicals. Now she is a synthetic chemist in Element Biosciences.

#### Andrzej Rajca

Andrzej Rajca was born in Poland where he graduated from Politechnika Wroclawska in 1981 with M.S. degree. In 1982, he joined Laren Tolbert's group at University of Kentucky (Ph.D. 1985). Subsequently, he did three-year postdoctoral research as a Miller Fellow and Lecturer with Andrew Streitwieser at Berkeley. Now he is a professor at University of Nebraska-Lincoln. Current research in his group is focused on stable radicals and thermally robust high-spin polyradicals with applications ranging from biomedicine and biophysics to organic materials.

## **Table of Content**

# High-spin diradicals

